Fracture Characterization of Clays and Clay-Like Materials Using Flattened Brazilian Test

by

Shehab Sherif Wissa Agaiby

Bachelor of Science in Civil Engineering
Cairo University, Cairo, Egypt (2009)

Master of Science in Soil Mechanics and Foundation Engineering
Cairo University, Cairo, Egypt (2011)

Submitted to the Department of Civil and Environmental Engineering
in Partial Fulfillment of the Requirements for the Degree of

Master of Science in Civil and Environmental Engineering

at the

MASSACHUSETTS INSTITUTE OF TECHNOLOGY

September 2013

Signature of Author................ ....
Department of Civil and Environmental Engineering
August 16, 2013

Certified by................................ ....
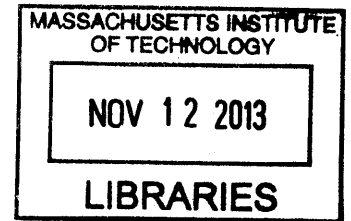John T. Germaine
Senior Research Associate of Civil and Environmental Engineering
Thesis Supervisor

Accepted by..
Heidi M. Nepf
Chair, Departmental Committee for Graduate Students

Fracture Characterization of Clays and Clay-Like Materials Using Flattened Brazilian Test

by

Shehab Sherif Wissa Agaiby

Submitted to the Department of Civil and Environmental Engineering on
August 16th, 2013 in Partial Fulfillment of the Requirements for the Degree of
Master of Science in Civil and Environmental Engineering

ABSTRACT

Fracture mechanics has been used for many years to study the mechanical behavior of brittle and quasi-brittle materials like concrete, rock, wood, and ceramics. To date, the application of fracture mechanics to soils has been limited to dry and partially saturated soils where soil consistency changes due to suction and tends to be harder exhibiting a quasi-brittle behavior. Of late, studying fracture propagation in clays and mudrocks has become of interest as it provides a means to extract oil from oil bearing strata.

While crack initiation in soils can be analyzed using basic soil mechanics theories, development and propagation of a crack is energy driven and requires application of fracture mechanics principles. An essential parameter in Linear Elastic Fracture Mechanics (LEFM), the main analytical tool in studying fracture in rock, is the critical stress intensity factor that defines stress concentration near a crack tip beyond which a fracture would propagate.

The basic mode of crack loading can be obtained by applying a normal stress that has a corresponding opening mode of crack surface displacement, called mode-I (tensile mode), with a critical stress intensity factor termed fracture toughness, denoted by K_{IC}.

In this experimental research, K_{IC} is measured indirectly using a modified Brazilian Test configuration where load is applied normally on flattened Brazilian disk specimens without the need to introduce a flaw into the specimen. Intact natural specimens from four different deposits; Boston Blue clay, San Francisco Bay Mud, Presumpscot Maine clay, and Gulf of Mexico clay; are tested in oven-dried state under atmospheric conditions. In addition, two Clay-like materials; molded Gypsum and Plaster of Paris; have been investigated.

Based on the analysis of the test data, the relation between mode I fracture toughness and tensile strength for the six tested materials agrees to a great extent with reported trends in the literature even for different fracture toughness and tensile strength testing techniques and for wider tested range of soils, rocks, geomaterials, clay-like, and rock-like materials. However, no clear relation between mode I fracture toughness and elastic modulus or any other physical parameter was determined.

Thesis Supervisor: John T. Germaine
Title: Senior Research Associate of Civil and Environmental Engineering

ACKNOWLEDGEMENTS

Dedication
To the most loving and caring parents,
Sherif W.Agaiby and Amani R. Nashed
To my beloved sister,
Shireen W. Agaiby

Thank you for giving me the tools to be successful in life
and the motivation to use them.

TABLE OF CONTENTS

LIST OF TABLES

LIST OF FIGURES

15

18

LIST OF SYMBOLS

$2a$	Crack length
$2a_c$	Critical crack length
2D	Two dimensional
$2L$	Flattened end width
2α	Loading angle
$2\alpha_{max}$	Maximum loading angle
$2\alpha_{min}$	Minimum loading angle
3D	Three dimensional
3PB	Three-point bending
a	Depth of crack
A	Cross-sectional area of specimen
a/R	Relative crack length
ace/R	Critical dimensionless crack length computed from experimental results
acn/R	Critical dimensionless crack length computed from numerical modeling
B	Thickness of specimen
B	Brazilian test
BBC	Boston Blue Clay
BD	Brazilian disc
BDT	Uncracked Brazilian disk test
CB	Chevron bend
CCNBD	Cracked chevron notched Brazilian disc
CNRBT	Circumferentially notched round bar in tension
CNSCB	Chevron notched semi-circular bending
CRS	Constant Rate of Strain
CSTBD	Cracked straight through Brazilian disc
CT	Compact specimen in tension
D	Specimen diameter
DC	Diametric compression
DT	Direct tension
FBD	Flattened Brazilian disc
F_{max}	Maximum tensile force
GS	Specific gravity
HCFBD	Hole-cracked flattened Brazilian disc
HDB	Single edge cracked half disc in three-point bending
IP	Plasticity index
ISRM	International Society for Rock Mechanics
K_I	Mode I stress intensity factor
K_{IC}	Mode I fracture toughness
$K_{IC\ avg}$	Average mode I fracture toughness

$K_{IC\ avg(CCNBD)}$	Average fracture toughness of cracked chevron notched Brazilian disc method
$K_{IC\ avg(FBD)}$	Average fracture toughness of flattened Brazilian disc method
K_{Imax}	Maximum stress intensity factor
LVDT	Linear Variable Differential Transformer
MR	Modified ring
NC	Normally Consolidated
P	Applied load
pa	Atmospheric pressure
Pmin	Minimum local load
R	Specimen radius
r	Coefficient of determination
RBDT	Round bar in direct tension
ReBDT	Rectangular bar in direct tension
S	Effective length of specimen
SC3PB	Single edge straight through cracked rectangular plate in three-point bending
SCB	Semi-circular bending
SCR3PB	Single edge straight through cracked round bar in three-point bending
SD	Standard deviation
SECB	Single edge cracked Brazilian disk
SECBD	Single edge cracked Brazilian disk in diametral compression
SECRBB	Straight edge cracked round bar bend
SENRBB	Single edge notched round bar in bending
SR	Short rod
t	Specimen thickness
W	Width of specimen
WL	Liquid limit
WP	Plastic limit
y/R	Dimensionless vertical distance
α	A proportion coefficient
γ w	Unit weight of water
$\sigma 1$	Maximum principal stress
$\sigma 3$	Minimum principal stress
σG	Dimensionless equivalent stress
σt	Tensile strength
σ_{ys}	Yield stress of material
ϕ	Dimensionless stress intensity factor
ϕc	Dimensionless fracture toughness
ϕmax	Maximum dimensionless stress intensity factor

Chapter (1)

INTRODUCTION

1.1 Background

Since the discovery of the Burgess Shale in the Canadian Rockies of British Columbia in 1909, scientists, engineers, and oil producers have realized the significance of shallow mudrocks to the oil and gas industry. Mudrocks, including clays and shale, are natural gas and petroleum bearing materials that are characterized with low porosity and permeability values. These rocks cover fifty percent of the Earth's sedimentary geological formations and, hence, any economically extracted product from such formations can provide significant quantities. This potential has encouraged researchers to study the properties of these materials and explore, in particular, the potential of recovering natural gas from shallow mudrocks through hydraulic fracturing; a process that is essentially associated with fracture mechanics.

Fracture mechanics has been used in studying the mechanical behavior of brittle and quasi-brittle materials like concrete, rock, wood, and ceramics. To date, the application of fracture mechanics to soils has been limited to dry and partially saturated soils; where the soil consistency changes due to suction. Dried soils tend to be harder and exhibit a quasi-brittle behavior as compared to the saturated material. And while cracks in dry soils / rocks can be analyzed by basic soil mechanics theories, the development and propagation of a crack is energy driven and requires applying fracture mechanics principles. An essential parameter in Linear Elastic Fracture Mechanics (LEFM), main analytical tool in studying fracture in rock, is the critical stress intensity factor that defines stress intensity value near a crack tip beyond which a fracture would propagate.

The basic mode of crack loading can be obtained by applying a normal stress that has a corresponding opening mode of crack surface displacement, called mode-I (tensile mode), with a critical stress intensity factor, named fracture toughness and denoted by K_{IC}.

To date there are no certain reliable standards for testing methods to determine the critical Mode I fracture toughness value, K_{IC}. The International Society for Rock Mechanics has suggested three methods for the determination of fracture toughness mainly for rocks and can

27

be applicable to soils. Despite the suggested standard methods of the ISRM, several other methods, with advantages and disadvantages, were developed and conducted by researchers to better quantify the fracture toughness K_{IC}, however, most reported methods suffer from difficulty in creating the precrack condition and impracticality in specimen preparation, loading method, experimental set-up and equipment.

Hence, a simpler more practical convenient means of determining K_{IC} was needed. With recent advances in fracture mechanics experimental research, the concept of the flattened Brazilian disc (FBD) has developed; which is considered a modification to the conventional Brazilian test. In FBD test, both the top and bottom edges of the circular disc specimen are flattened and are subjected to normal static loading until center crack intimates and the specimen fails. Using the FBD testing approach, three parameters were investigated from the test record of a single specimen; mode I fracture toughness, tensile strength, and the elastic modulus. In the conducted experimental work six different materials have been investigated covering both natural soils and clay-like materials; Boston Blue Clay, San Francisco Bay Mud, Presumpscot Maine Clay, Gulf of Mexico Clay, molded Gypsum, and Plaster of Paris.

1.2 Objectives

The main objectives of performing this research/ experimental study are:
1. Investigating the fracture properties of six different dry clays and clay-like materials.
2. Using a simple convenient means to quantify mode I fracture toughness, tensile strength, and the elastic modulus for different materials.
3. Applying the flattened Brazilian disc (FBD) testing method on new materials besides rock such as: Boston Blue Clay, San Francisco Bay Mud, Presumpscot Maine Clay, Gulf of Mexico Clay, molded Gypsum, and Plaster of Paris.
4. Studying the relation between mode I fracture toughness and the corresponding tensile strength, unit weight, and the elastic modulus. And correlating this empirical relation statistically.
5. Comparing the relation between mode I fracture toughness and tensile strength for the tested materials with the trends reported in the literature for different materials (soils, rocks, geomaterials, shale, clay-like, and rock-like materials) tested using other different techniques.

28

6. Using the tensile strength value as an indirect method to estimate the mode I fracture toughness.

1.3 Organization of Thesis

This thesis is divided into six chapters. Following this introduction, Chapter **2** presents a general review of the literature available on fracture toughness and its significance for rocks and soils. The chapter provides a description of the different modes of loading / fracturing with an illustration to the means of stress intensity factor evaluation and better understanding to the factors affecting its value. The chapter presents a summary of the different experimental methods used to quantify mode I fracture toughness. In addition, the chapter summarizes the relationships between fracture toughness and other physical mechanical parameters with an emphasis on the tensile strength.

Chapter **3** presents a general review of the literature on the Brazilian testing method and provides a summary of the modifications to the Brazilian test including the flattened Brazilian approach. The chapter covers the theory behind the flattened Brazilian test with an emphasis on the stress and displacement distributions within the flattened discs. Then appropriate methods to obtain the maximum stress intensity factor for the flattened discs are discussed. The chapter presents methods to evaluate the mode I fracture toughness, tensile strength, and the modulus of elasticity of the same specimen.

Chapter **4** presents a detailed description of the laboratory testing program performed for this research. First the soils and materials tested are described, including a summary of their origin, index and strength properties. Next, a description of the Flattened Brazilian Disc (FBD) testing equipment is presented, which includes details pertaining to testing device, measuring transducers, specimen preparation technique, and testing procedures.

Chapter **5** presents the results of the experimental study conducted on six different materials; four different natural soils and two clay-like materials; to investigate the relation between mode I fracture toughness, tensile strength, unit weight, and modulus of elasticity using flattened Brazilian disc (FBD) specimens. The chapter provides an explanation to the methodology implemented in interpretation of the results and the governing equations to quantify the parameters of interest. Then a detailed description to the experimental results of the conducted tests is presented for both natural soils and clay-like materials. In addition, an

explanation to the failure modes of FBD specimens is presented. Afterwards, different correlations relating mode I fracture toughness and corresponding tensile strength, unit weight, and elasticity modulus are presented followed by a comparison with data values reported in the literature. Finally concluding all the available data including experimental results of current research into one single equation relating fracture toughness to tensile strength.

Finally, Chapter **6** presents the conclusions drawn from this experimental study as well as recommendations for further areas of research.

Chapter (2)

LITERATURE REVIEW- FRACTURE TOUGHNESS

2.1 Introduction

This chapter presents a general review of the literature available on fracture toughness of rocks and soils. The chapter starts with a background on fracture toughness and introduces fracture mechanics in different fields of science and engineering. Then the significance of fracture toughness in rock/soil fracture mechanics is highlighted, followed by an explanation to some of the topics related to fracture toughness; starting with discontinuities in rocks and rock like materials then the process of fracturing then the types of cracks growth. The chapter also provides a summary on the basis behind fracture toughness evaluation methods by introducing Griffith's theory and linear elastic fracture mechanics (LEFM). Then a description of the different modes of loading / fracturing is reviewed with an illustration to the means of stress intensity factor evaluation and better understanding to the factors affecting its value. Then a review on fracture toughness determination using different experimental methods whether suggested standardized methods or alternative methods from the literature. Finally, the chapter summarizes the relationships between fracture toughness and other physical mechanical parameters with an emphasis on the tensile strength.

2.2 Background

It has been suggested that a material's fracture properties should be characterized in terms of the particle strength, specific breakage energy, and the breakage fragment size distribution of the material (Bourgeois et al., 1992). In this case, the strength is measured in terms of the tensile strength become the particles of brittle materials break in tension under compressive loads due to the pre-existence of natural flaws within the material. However, tensile strength does not fully describe the fracture process as it can only quantify the particle's resistance to an applied load. Tensile strength does not consider inherent flaws present in brittle materials, or the concentration of the stresses around these flaws when the material is loaded, and their effect on the fracture process. Thus, particle strength should be replaced by another, more descriptive measure of a material's ability to withstand fracture (Donovan, 2003). Hence,

fracture toughness is introduced as a means of quantifying and describing the material's resistance to fracturing.

Fracture toughness is an intrinsic material property expressing a material's resistance to crack propagation. It is a measure of the energy required to create a new surface in a material (Donovan, 2003). Fracture toughness is the critical value of the stress intensity factor; which is a quantity characterizing the severity of the crack situation within a material as affected by crack size, stresses near the crack tip, and the geometry of the crack, material specimen, and loading configuration (Dowling, 1999). Providing sound theoretical foundation, evolving from the study of fracture mechanics and Griffith's theory of fracture, fracture toughness can offer a fundamental basis for describing size reduction processes. It is already used as an index for rock fragmentation processes such as tunnel boring and scale model blasting, as a key element in modeling rock cutting and blasting, and in the stability analysis of rock structures (Whittaker et al., 1992).

2.3 Applications of Fracture Mechanics

The occurrence and propagation of a crack or flaw; due to applied load in a structure; can be best described and explained using fracture mechanics. As cracks can occur anywhere, many disciplines of science and engineering study fracture mechanics in their applications such as: Medical Sciences, Petroleum Engineering, Aerospace Engineering, Mechanical Engineering, Civil Engineering, Geological Engineering, and Mining Engineering.

Shi (2006) illustrates an example for the application of fracture mechanics in adhesive joint applications used in material sciences, where discontinuous interfaces are caused in electronic packages when adhesive bonding is used during packaging for electronic devices integration. As the packages arrive under different environmental conditions; influenced by thermal, mechanical, moisture, and electrical loadings; they are subjected to different failures as crack occurrence in the adhesive layer causing damage to the solder joint and the total failure of the whole electronic device. Thus, understanding fracture mechanics principles is essential to prevent further failures.

Another field where fracture mechanics is commonly used is medicine where basic fracture principles are used to determine fracture resistance of bones. Experimental testing similar to ones used in determining the fracture toughness of rocks and metals are used to determine the

fracture toughness of bones. Cook (2005) thoroughly investigated the application of fracture mechanics in medical sciences where he used disc-shaped compact specimens and three-point bending specimens to determine the fracture toughness of cancellous bones.

Fracture mechanics has also been applied in Aerospace engineering where many accidents and planes crashed in the past due to fracture failure and fatigue occurrence. For instance, an Aloha Airlines Boeing 737-200 aircraft lost a major part of its upper fuselage because of the multiple fatigue cracks in 1988.

The applications of fracture mechanics manifest in the different fields of civil engineering such as crack propagation analyses in large concrete structures like dams, weirs, and bridges. Fracture mechanics is also applied in the design and building of asphalt pavements suffering from low temperature cracking as in Northern united states and Canada. Li (2004) presented a standard method to quantify and analyze the cracking resistance of different asphalt mixtures. Also, Othman (2006) studied the fracture resistance of rubber modified asphalt mixtures that are subjected to cycles of high temperature aging.

Other disciplines of science and engineering including petroleum engineering, mining engineering, and geological engineering utilize rock fracture mechanics which is a major branch of fracture mechanics, covering different engineering applications from hydraulic fracturing to rock fragmentation to blasting to rock slope analyses to in-situ stress and strain determination (Alkiliçgil, 2006). Other geological applications applying the principles of fracture mechanics include earthquake mechanics, earthquake prediction, plate tectonics, magmatic intrusions, hot dry rock geothermal energy extraction, fluid transport properties of fracturing rock masses, propagating oceanic rifts, the development of steeply dipping extension fractures that are nearly ubiquitous at the earth's surface and are formed through folding, upwarping and rifting and the modeling of time-dependent rock failure (Atkinson, 1987; Whittaker et al., 1992; and Alkiliçgil, 2006).

2.4 Importance of Fracture Toughness in Rock/Soil Fracture Mechanics

Fracture toughness is considered a very important parameter in different earth sciences and engineering disciplines; it has been used as *a parameter* for rock material classification as in the research studies by Gunsallus and Kulhawy (1984) where fracture toughness was used as a rock classification index. In addition, Bearman (1996) used fracture toughness value to

classify and to estimate comminution behavior. Fracture toughness is not a strength, but independent natural property.

Fracture toughness has also been used as *an index* for tunnel boring and model scale blasting and other fragmentation processes. In a study by Nelson and Fong (1986), they proved the possibility of predicting cutter forces and force penetration relationships by the knowledge of the fracture toughness value. In a more recent study Momber (2006), used fracture toughness value to verify a proposed transition index which was eventually used in the design and execution of non conventional drilling and cutting methods such as hydrodynamic fragmentation, cavitation drilling, and hydrodemolition (Alkiliçgil, 2006).

Moreover, fracture toughness has been used as *a material property* with an application in modeling of rock fragmentation processes such as explosive simulation of gas wells, radial explosive fracturing, hydraulic fracturing, stability analyses, and crater blasting. According to Chen and Chen (1995), fracture toughness has been widely accepted as a criterion for fracture propagation in the simulation of hydraulic fracturing where the fracture is expected to extend and propagate when $K_I >_ K_{IC}$. Chen and Zhang (2002) added that for underground rock materials located at great depths, the fracture toughness value is essential in the simulation of hydraulic fracturing treatments of reservoir pay-zones in the oil and petroleum industries.

Finally, Balme et al. (2004) highlighted the importance of fracture toughness determination to better evaluate the mechanical behavior of rocks under high pressures and temperatures to better model different volcanolgical problems like lava flows and dike emplacement (Alkiliçgil, 2006).

2.5 Concepts Associated with Fractures

2.5.1 Discontinuities in Rocks

Different terminology is often used to describe discontinuities in rocks and in rock-like materials, which causes confusion to the reader as no clear specified meaning is provided. Also various nomenclatures evolve from different fields and applications. Backers (2004) summarized the different discontinuities that can occur; *a crack* can be considered any opening in the material that has one or two dimensions smaller than the third one. According to (Simmons and Richter, 1976) the ratio of width to length in a crack is in the order of 10^{-3} to

10^{-5}.

Cracks can be divided into three subcategories; micro, meso, and macro cracks. A *microcrack* is a planar discontinuity with the largest dimension in the size range of a few grain diameters which according to En-gelder (1987) can reach $1*10^{0} - 1*10^{4}$ microns. And based on the location of its occurrence can be considered either *grain-boundary* crack if located at interface between grains or considered *intra-granular* crack if concentrated within one grain or can be considered *inte-rgranular* crack if the cracks penetrate more than one grain. A *mesocrack* extends and penetrated over more grains than a microcrack, it is usually a result of complicated rupture incidents that finally joins several microcracks. According to Backers (2004) a mesocrack extends hundreds of microns to few milli-metres. Finally a *macrocrack* extends several millimeters to decimeters and can be referred to as a fracture which is the interest of our study. A macrocrack consists of a clear separation and is surrounded by a fracture process zone (FPZ) consisting of a number of micro and meso cracks as illustrated in **Figure 2.1.** The development of a fracture and the fracture process zone under a tensile load perpendicular to a starter notch is shown in **Figure 2.2** where a sketch shows the schematic sequence A to D shows (micro-crack) to (meso-crack) to (macro-crack) development with the load increase.

In other sciences and disciplines such as tectonics and engineering geology, the term joint or fault can be used to describe fractures. According to Pollard and Aydin (1988), a joint is a discontinuity that shows displacement normal to its surface or trace and does not show displacement parallel to its surfaces. While a fault; usually results from shear displacements; which evidently shows displacement parallel to the surface. Figure 2.3 shows a comparison between the lengths of different types of discontinuities starting from a microcrack to a joint.

2.5.2 The Process of Fracturing

Over the years scholars and researchers have studied the process of fracturing in rocks, soils, and rock like materials. This was done for different loading conditions and for different materials, using different observation scales and techniques such as interpretation of mechanical data, microscopy at different scales and detection and interpretation of Acoustic Emission (AE) events (Backers, 2004). A number of classical references and textbooks should also be considered for example Pollard & Aydin (1988), Atkinson (1991), and Dresen

& Guéguen (2004).

Under compressive loading, both tensile and shear stress concentrations develop at preexisting inclined in-homogeneities at both the mesoscopic and macroscopic observation scale. When compressive stresses are applied, tensile cracks will initiate at the tips of the pre-existing fractures. These cracks are called wing cracks and they grow progressively into the direction of the remote major principal stress then stop (Brace and Bombolakis, 1963; Kemeny and Cook, 1987, Petit and Barquins, 1988). At the early stages of crack propagation the growth of the stable wing crack is dominated by the stress field of the originated fracture. As it extends, it starts to interact with neighboring microcracks and this interaction might lead to coalescence and ultimate failure (Backers, 2004).

Depending on the geometry and pattern of the interacting fractures, and also the stress condition, different coalescence behavior can take place. Generally, wing cracks initiate at the fracture tips for uniaxial and low confinement biaxial conditions as illustrated in **Figure 2.4**. Bobet and Einstein (1998) reported that the location of crack initiation moves to the middle of the flaw upon the increase of confining pressure and macro/mesoscopic wing cracks vanish completely for higher confining stresses. Eventually, secondary fractures probably connect with the pre-existing fractures. The secondary fracture follows the direction of shear and was found to be unstable (Sagong & Bobet, 2002). The most preferable geometry for shear fractures to develop in a set-up with two initial fractures as shown in **Figure 2.4** is to organize them co-planar, as well as with no confining pressure (Bobet & Einstein, 1998).

According to Lockner (1995), shearing will take place along surfaces oblique to the maximum principal stress, σ_1, and play an important role in the development of local stress concentrations. The local stresses induced near a fracture tip loaded in shear contain a component of tension as well as shear. This will in general lead to tensile failure before shear failure. It is worth noting, that two mechanisms take place during the loading of fractures under compressive shearing. First mechanism is propagation of extensional cracks decreasing the stress intensity; accordingly, additional deviatoric stresses should be applied to cause further fracture propagation. At some point the extensional crack propagates out of the area of high stress concentration and ceases. The second mechanism is the propagation of diagonal flaws out-of-plane parallel to the major principal stress direction. These flaws are favorably oriented to act as initiation points for shear failure (Backers, 2004). When the flaw density

becomes high enough for crack interaction to occur, arrays of cracks will develop (Costin, 1987; Lockner, 1995). Finally, the stress concentration becomes high enough to initiate shear fractures propagating in plane and being governed by their own stress field.

2.5.3 Fracture Growth

Fracture propagation can be described using two different terminological frames; one frame is function of fracture propagation velocity and the other frame is stress intensity dependent. In the velocity frame, the fracture can be either static or dynamic. While for the stress intensity frame, the fracture can be described as either stable or unstable. The different regimes of fracture propagation are exhibited in **Figure 2.5**.

For crack instability the stress intensity should be equal to the fracture toughness value. (K => K_C, and that $dK/dc > 0$, where c is the crack length) (Lawn, 1993). In other conditions, the crack can be considered *stable*; a *stable* crack extends relatively slow, stopped at any stage, and requires further stress / load application for each increment in the crack growth. On the contrary, an *unstable* crack can be accelerated by excess energy and propagates at speeds approaching a terminal velocity that is governed by the speed of elastic waves (Backers, 2004). In this situation the crack is called *dynamic*. Intermediate conditions for instability can be either achieved by reaching a critical crack length or by impact loading. According to Backers (2004), the term *critical* is used for the onset of unstable crack growth, reflecting the transition from stable to unstable. In terms of stress intensity factor it is called the critical stress intensity factor, K_C. Any fracture propagation taking place at fractions of K_C is referred to as *subcritical* crack growth (Atkinson, 1984); it is governed by several competing mechanisms such as diffusion, dissolution, ion exchange, microplasticity and stress corrosion.

2.6 Griffith's Theory

Griffith is considered one of the earliest scientists conducting research in fracture mechanics where he began his studies around 1920s. He proposed that brittle material failure is a result of the existence and extension of inherent cracks; which eventually yield a new crack surface that consumes the energy applied by work done due to external forces or by the release of internal stored strain energy. Failure takes place when the energy; due to the externally applied force or due to the release of internal strain energy; is more than the energy of new crack surface (Donovan, 2003).

37

According to Griffith's theory for failure to take place in a brittle material the local stress should be high to overcome the molecular cohesive strength of the material. This condition can take place by stress concentrations around cracks or inherent flaws within the material. In addition, sufficient potential energy should be released to overcome the material's crack propagation resistance. This condition can take place when the work done by external forces is high enough.

Griffith utilized the stress analyses of Inglis for an elliptical crack in an infinite plate to develop a relation between crack size and stresses associated with fracturing. The total energy for an infinite plate with an elliptical crack was defined as follows:

$$U = U_t + U_c - W + U_s \qquad (2.1)$$

Where, U_t is the initial elastic strain energy of non cracked plate, U_c is the elastic energy release caused by the introduction of a crack, W is the work done by externally applied forces, and U_s is the change in the elastic surface energy due to new crack surfaces.

Whittaker et al., (1992) used elastic theory expressions and definitions to quantify the energy components in the previous equation which gave the following equation:

$$U = \frac{\sigma^2 A}{2E'} - \frac{\pi\sigma^2 a^2}{E'} - \frac{\sigma\varepsilon A}{2} + 4a\gamma_s \qquad (2.2)$$

Where, A is the infinite area of the plate, E' is the effective Young's modulus for plane stress; and is defined as $(E/ (1-v^2))$ for plane strain where v is Poisson's ratio, ε is the value of strain, γ_s is the specific surface energy, and a is the crack length.

The specific surface energy term γ_s was defined by Griffith as a constant material property which represents the energy needed to induce and create a new crack surface. The crack will propagate when the increase in the crack length does not change the net energy of the plate, which can be expressed as dU/da >= zero. And by differentiating the previous equation with respect to the crack length, the following the relation can be obtained:

$$4\gamma_s - \frac{2\pi\sigma^2 a}{E'} = zero \qquad (2.3)$$

The logical extension from this fundamental concept explained by Griffith yields the energy release rate, G (Irwin, 1958) for a constant applied external stress. The parameter has been denoted G in honor of Griffith.

$$G = \frac{\pi\sigma^2 a}{E'} \qquad (2.4)$$

For crack extension to occur G needs to reach a critical energy release rate value, G_C, which is defined at the failure stress, σ_F.

Though Griffith's Theory was so significant, there have been some limitations on its applications as he only considered elastic, brittle materials where no plastic deformations took place. It was eventually proven that plastic deformation within a material yielded an energy requirement for crack extension and propagation that was ten times more than that predicted by Griffith's original theory.

Orowan (1949) and Irwin (1948) extended Griffith's theory of brittle materials to include ductile materials. Irwin hypothesized that there is a definite limited energy from plastic deformations of ductile materials and this energy needed to be added to the strain energy previously defined by Griffith. However, he realized that the surface energy term for ductile materials is so small that it can be neglected if compared to the remaining energy associated with the plastic deformation.

Irwin (1957) used a stress intensity approach to relate the critical strain energy release rate G_c to the critical stress intensity factor K_c. Rather than follow Griffith's global approach, Irwin considered the crack tip region, which is small compared to the rest of the body but large enough with respect to atomic dimensions such that linear elastic theory applies (Knott, 1972). Irwin determined the work required to close up a small portion of a crack by superimposing tensile forces along the crack surfaces and hypothesized that this work is equal to the energy released when the crack extends (Donovan, 2003). Thus the work required to close a unit length of the crack is the strain energy release rate and, based on the stresses and displacements occurring as a result of the tensile forces, is equal to:

$$G = \frac{(1 - v^2)K^2}{E} \tag{2.5}$$

Since crack propagation occurs when G reaches a critical value, the critical value of stress intensity can be defined as:

$$K_c = \sqrt{\frac{G_c E}{(1 - v^2)}} \tag{2.6}$$

By demonstrating the equivalence of K and G, Irwin provided the basis for the development of Linear Elastic Fracture Mechanics (LEFM). In LEFM the crack tip stresses, strains, and displacements can be characterized by K as long as plastic yielding ahead of the crack tip is

small. The advantage of LEFM is that it provides a universal approach for determining a material's resistance to fracture, as defined by K_c. As long as an explicit function for the stress intensity near a crack tip is known for a given crack geometry and loading configuration, K_c can be measured experimentally (Donovan, 2003).

Then in 1958 Irwin showed the equivalence of energy release rate and stress intensity factors, with the aid of the principle of superposition the relation can be written as follows:

$$G = \frac{K_I^2}{E'} + \frac{K_{II}^2}{E'} + \frac{K_{III}^2 (1 + v)}{E'} \tag{2.7}$$

Where v is Poisson's ratio, K_i stress intensity factor under a specific mode of loading and E' identifies Young's modulus of elasticity (plane stress or plane strain condition).

Later in the 1960s, researchers and scientists started to focus on the plasticity of the crack tips and associated plastic deformations and in 1968, Rice was the first to model the plastic deformation as nonlinear elastic behavior. Moreover, he extended the energy approach to include nonlinear materials. He figured out that the energy release rate G can be expressed as a path-independent line integral, named the J integral. Rice's theory has provided the development of fracture mechanics in United States.

Particle size effect is one major issue related to Griffith's theory that was thoroughly investigated, it has been proven that for a given material, as particle size decreases strength increases. This can be explained due to the distribution of flaws and cracks within the material. Weibull's weakest link theory (1951) suggests that the particle strength is dependent on its most critical flaw. From this critical flaw, fracture initiates independently of all other flaws within the particle. As the size of the particle decreases the existence of such a critical flaw becomes less probable leading to an increase in the strength with the decrease in particle size. Defining a material's fracture resistance should account for the effect of size or be independent of it (Donovan, 2003).

Schoenert (1972) also explained particle size effect using energy considerations. He stated that as the failure of brittle solids takes place when the energy by an externally applied force or by the release of internal stored strain energy is greater than the energy of the new crack surface, then smaller particles will mostly have less capacity for storing elastic energy (Ut is proportional to volume) which indicates that smaller particles will need further work by external forces or higher stresses in order to fracture. Smaller particles also exhibit a more

plastic response than larger ones, which leads to much irreversible deformations when subjected to high stress levels, these plastic deformations alter stress distributions within the particle leading to much coarser fragments upon fracture.

2.7 Linear Elastic Fracture Mechanics

The basics of the Linear Elastic Fracture Mechanics (LEFM) were developed by Irwin in the 1950s; LEFM assumes that the material is isotropic and linear elastic. **Figure 2.6** illustrates a typical stress-strain behavior of an isotropic and linear elastic material. The behavior implies that the material properties are independent of direction and these materials have only two independent elastic constants which are Young's Modulus (E) and Poisson's ratio (υ). Applying the basic principles of the LEFM, the stress field near the crack tip is calculated by considering the theory of elasticity. Moreover, it is applicable to brittle fracture situations where the load-deflection response of the cracked body is essentially linear up to the point of fracture (Alkiliçgil, 2006).

LEFM is only applicable when the plastic (inelastic) deformation is much smaller than the size of the crack. If large zones of plastic deformation develop before the crack propagations, Elastic Plastic Fracture Mechanics (EPFM) should be used instead of LEFM.

The general expression of LEFM equation is presented in the following equation:

$$\sigma_{ij} = \frac{K_I}{\sqrt{2\pi r}} f_{ij}(\theta) + \dots \tag{2.8}$$

Where σ_{ij} is the stress tensor in Cartesian co-ordinates, r and θ are cylindrical coordinates of a point with respect to the crack tip, f_{ij} is a geometric stress factor depending solely on angle θ (for notations see **Figure 2.7**), and K is the stress intensity factor which is a factor depending on the outer boundary conditions (applied loading and geometry). K_I is the *stress intensity factor* that gives the grade of stress concentration at the tip of a crack of length a at a given loading and has the dimension of stress* (length)$^{1/2}$, in units Pa · m$^{1/2}$.

$$K = \sigma \sqrt{\pi * a} = \sigma_{ij} \sqrt{2\pi * r} \; ; \; \theta = zero$$

$$Dimension\ (K) = \frac{F}{L} \sqrt{L} = F * L^{-3/2} = Stress * \sqrt{Length} = Pa\sqrt{m} \tag{2.9}$$

2.8 Rock Fracture Mechanics and Fracture Toughness

The development of fracture mechanics was started after several modifications to Griffith's theory. As earlier mentioned fracture mechanics quantifies fracture initiation and crack propagation and provides both qualitative and quantitative descriptions to the material behavior. As rocks, rock-like materials, and soils contain discontinuities, fractures, and flaws, continuum methods of macroscopic failure like Mohr-Coulomb cannot be used and fracture mechanics principles should be applied. Despite having several critical applications outside rock and soil mechanics, fracture mechanics was primarily developed for geomaterials. Hence, the main differences between the behavior of soils/rocks and other materials including manmade materials such as metals should be highlighted. Whittaker et al. (1992) gave a comprehensive detailed list and explanation of these differences, which can be summarized as:

a) Stress state: Structures are mainly subjected to compressive stresses more than tensile stresses. However, in comminution and crushing the induced stress state is tensile (from point-load compression) and thus tensile fracture is seen in rocks and soils.

b) Rock and soil fracture: Rock materials usually fracture in a brittle or quasi-brittle manner and usually do not exhibit plastic flow.

c) Fracture process zone (FPZ): Plastic behavior ahead of a crack tip in rock takes the form of micro-cracking as opposed to excessive shear strain and the resultant plastic process zone seen in metals. If the size of the FPZ is small, then linear elastic fracture mechanics applies.

d) Crack surface: Crack surfaces in soils and rocks can be non-planar with friction and inter-locking occurrence, but linear elastic fracture mechanics assumes that no forces are transmitted across the surface of a smooth planar crack.

e) Crack propagation: In rocks and rock-like materials there is a tendency for crack propagation to extend along grain boundaries or planes of weakness. The area of newly created surface is then larger than the assumed planar fracture area.

f) Heterogeneity: Changes in local structure and strength ahead of a crack tip affects the continuity of crack growth.

g) Presence of discontinuities: Pre-existing discontinuities affect the local stress states and

crack propagation.

h) Anisotropy: Rocks and soils can be anisotropic affecting measured fracture parameters as a function of crack orientation.

By understanding the previously mentioned differences researchers and scientists were able to develop more reliable, practical and relevant concepts of fracture mechanics with special application to soil and rock behavior. The most fundamental aspect of rock / soil fracture mechanics is establishing a relation between rock / soil fracture strength and the geometry of the flaws that result in fracture (Donovan, 2003). Through this relationship an intrinsic material property that describes a materials' resistance to crack propagation can be measured. This property is called fracture toughness. Fracture toughness represents a critical level above which crack extends and fracture occurs. When individual rock or soil particles are subjected to the applied forces of size reduction, it is most likely that the intrinsic property measured as the fracture toughness will control breakage (Bearman, 1998). Since the amount of energy input into a size reduction process and the amount of size reduction achieved (are related to the type of loading and the crack pattern in the material, there should be a relationship between these parameters and fracture toughness (Donovan, 2003).

2.9 Stress Intensity Factor and Modes of Loading

In fracture mechanics, cracks and fractures can be classified as three basic types, namely Mode I, Mode II and Mode III, from a mostly mathematical viewpoint (Irwin, 1958). The classification is based on the crack surface displacement (Lawn, 1993), or crack tip loading (Engelder, 1987; Whittaker et al., 1992). In the literature, this is indicated as either mode of crack propagation, mode of fracturing or mode of loading. Relating the modes of fracturing to the modes of loading is appropriate for most metals given that the fracture propagates within its own plane (Rao et al., 2003). However, for rocks and soils a specific mode of loading is not necessarily leading to the same mode of fracturing. Unfortunately, the reference of mode regarding the applied loading and fracture propagation is often mixed up in literature. There should be a clear distinction between 'mode of loading' – for the applied boundary stresses – and 'mode of fracturing or failure' – for the mechanical breakdown process defined by relative displacement (Alkiliçgil, 2006).

In terms of crack surface displacement (mode of fracturing), there are three basic modes;

43

Mode I, Mode II, and Mode III, which are displayed in **Figure 2.8.** In *Mode I*, known as the opening (tensile) mode, the crack tip is subjected to displacements perpendicular to the crack plane and the crack propagation is in the crack plane direction. The crack carries no shear traction and no record of shear displacement is visible. In *Mode II*, known as the in-plane sliding mode due to shearing, the crack faces move relatively to each other in the crack plane. Crack propagation is perpendicular to the crack front. Shear traction parallels the plane of the crack. Finally, *Mode III* which is known as the tearing mode or out of plane mode also due to shearing. Shear displacement is acting parallel to the front in the crack plane. Any combination of the three basic modes is referred to as mixed mode. The principle of superposition is sufficient to describe the most general case of crack tip deformation (Atkinson, 1987). Mode I is the most commonly encountered mode in engineering applications and is also the easiest to analyze, produce experimentally on laboratory specimens, and apply (Schmidt and Rossmanith, 1983). In LEFM, most formulas are derived considering these modes by assuming either plane stress or plane strain conditions. Plane Stress Condition can be defined as in the case of a thin plate where the stress through the thickness (σ_{zz}) cannot change noticeably owing to the thin section and it is equal to zero (σ_{zz} = 0). While the Plane Strain Condition can be defined in the case of a thick body where the material is constrained through the thickness and strain in the z-direction is equal to zero (ε_{zz} = 0). Illustration of the two conditions with associated stresses and strains is displayed in **Figure 2.9**.

Each mode is characterized with specific stress symmetry properties near the crack edge (Broberg, 1999) defining the directions for maximized stress intensity. In a Cartesian co-ordinate system, the modes may be specified based on linear elastic calculations as follows: In *Mode I*, the lateral stress component (f_{yy}) and the directional stress component (f_{xx}) are symmetric with respect to the crack trace. The shear stress component (f_{xy}) shows point-symmetry as shown in **Figure 2.10**. In *Mode II*, both the lateral (f_{yy}) and the directional stress components (f_{xx}) are point-symmetric, while the shear stress component (f_{xy}) is the only component to be symmetric with respect to the crack trace as shown in **Figure 2.10**. And in *Mode III*, f_{yz} appears to be symmetric with respect to the crack trace while f_{xz} shows point-symmetry (Backers, 2004).

2.9.1 Evaluating Stress Intensity Factor

Using the theory of elasticity which is known as the stress analysis methods of Muskhelishvili (1963) and Westergaard (1939), the crack tip stress (and hence K) and displacement fields for each mode of loading can be determined (further derivation and explanation can be found in Pook, 2000). The coordinate system measured from the leading edge of a crack as shown in **Figure 2.11**, the Mode I stress components are given according to the following equations:

$$\sigma_x = \frac{K_I}{\sqrt{2\pi r}} \cos\frac{\theta}{2}\left(1 - \sin\frac{\theta}{2}\sin\frac{3\theta}{2}\right) \tag{2.10}$$

$$\sigma_y = \frac{K_I}{\sqrt{2\pi r}} \cos\frac{\theta}{2}\left(1 + \sin\frac{\theta}{2}\sin\frac{3\theta}{2}\right) \tag{2.11}$$

$$\tau_{xy} = \frac{K_I}{\sqrt{2\pi r}} \cos\frac{\theta}{2}\left(\sin\frac{\theta}{2}\cos\frac{3\theta}{2}\right) \tag{2.12}$$

For Plane strain conditions, $\sigma_z = v\left(\sigma_x + \sigma_y\right)$

For Plane stress condition, $\sigma_z = zero$

$$\tau_{xz} = \tau_{yz} = zero \tag{2.13}$$

Where, K_I is the stress intensity factor for Mode I. The displacements at the crack tip can be found by substituting the previous equations into Hooke's Law.

By examining the previous equations, it can be observed that the stresses at the crack tip reach an infinite value when the value of r approaches zero (indicating the crack tip location). Since no value of stress at the crack tip can be given, and all non-zero stresses of the previous equations are proportional to K_I, with the remaining factors varying only with r and θ, the stress field near the crack tip can be determined by giving the value of K_I, which has a formal definition of (Dowling, 1999; Pook, 2000):

$$K_I = \lim_{r,\theta \to 0} \sigma \sqrt{2\pi * r} \tag{2.14}$$

The previous equation can be arranged to account for the crack size, stress condition, and geometry as follows:

$$K_I = F \sigma \sqrt{2\pi * a} \tag{2.15}$$

Where, F is a dimensionless constant dependent on the geometric configuration, σ is the stress averaged over the gross area, and a is the half-crack length.

F is described as a function of loading geometry and (a/w) relation where w is defined as the

maximum possible crack length. When F is determined for a given geometry, the critical value of stress intensity, known as the fracture toughness, can be determined as long as inelastic yielding ahead of the crack tip is small and the conditions for LEFM are met (Donovan, 2003). Equations and values of F for a wide range of crack, specimen, and loading geometries are determined using different analytical, numerical, and experimental methods and have been compiled in various handbooks such as Tada et al., 2000; Murakami, 1987; Rooke and Cartwright, 1976; Sih, 1973.**Figures 2.12 and 2.13** show the stress intensity relationships for some of the more common loading and geometry conditions.

2.10 Determination of Mode I Fracture Toughness

To date there are no certain reliable standards for testing methods to determine the critical Mode I fracture toughness value, K_{IC}. The earliest approach to determine K_{IC} in rock fracture mechanics was employing the ASTM standard method (ASTM-E399) that was primarily used for metals. Initially, ASTM-E399 seemed to be effective and beneficial for rock testing, however, general consensus for rock testing were to develop an ideal methodology that would determine a representative fracture toughness value and yet to be simple and practical, requiring neither pre-cracking, nor crack length and displacement measurements, nor sophisticated complicated evaluation techniques (Ouchterlony, 1989). According to the mentioned requirements ASTM-E399 is neither convenient nor practical, and most testing methods for rock now employ core-based specimens. Accordingly, the International Society of Rock Mechanics (ISRM) has suggested two guidance methods; Chevron Edge Notched Round Bar in Bending (**CB**), the Chevron Notched Short Rod (**SR**); that can be used as standardized tests in order to determine accurate, compatible, and reproducible K_{IC} values for rocks (ISRM, 1988). However, to overcome some of the reported disadvantages of the CB and SR testing methods, the ISRM recommended a third method (ISRM, 1995) for determining the fracture toughness of rock using Cracked Chevron Notched Brazilian Disc (**CCNBD**) specimen. **Figure 2.14** shows the three testing methods that have been introduced by the International Society for Rock Mechanics (ISRM) as Suggested Methods (Ouchterlony, 1988; Fowell, 1995).

According to the ISRM suggested methods, there are a few factors that need to be taken into consideration to be able to determine K_{IC} value accurately. These factors include the crack

requirements, the testing level, the loading rate, and the testing method.

2.10.1 Crack Requirements

To be able to determine the fracture toughness value for any specimen, the specimen should be "cracked". This crack should be representative of a natural crack, a crack that is sharp and free from the effects of residual stresses, specimen boundaries, and pre-fabricated notches (Whittaker et al., 1992 and Donovan, 2003). In the case of testing metals, the specimens are pre-cracked by fatigue to simulate a naturally sharp crack. However, in rocks and clays (soils in general) fatigue pre-cracking is a difficult process as the load requirement for fatigue crack growth is relatively high and special attention and care is required in order to prevent further propagation of the induced pre-crack after it has been initiated.

Over the years researchers and scientists developed more convenient methods to create a pre-cracked rock or soil specimen, the simplest method is utilizing a thin saw-cut. Despite the ease of notching there is evidence that notched specimens tend to underestimate fracture toughness (Donovan, 2003). In their experimental studies Sun and Ouchterlony (1986) showed that apparent fracture toughness values obtained using a notched specimen are evidently lower than those obtained using a pre-cracked specimen, they concluded that the use of notch length in the calculation of K_{IC} ignores micro-crack growth prior to crack extension. Later Fenghui (2000) created a numerical model, based on the size of the fracture process zone (FPZ) and notch radius, that estimates the fracture toughness value based on the measured fracture toughness of a notched specimen as long as the notch radius is not greater than the average grain size of the rock.

The most common and widely accepted method of pre-cracking samples is producing a chevron-notch, which is a V-shaped notch that allows the development of a stable the crack front as the crack propagates. An increase in the applied pressure (load) is needed for further crack propagation and inherent monotonic pre-cracking is produced during testing (Sun and Ouchterlony, 1986). A sharp natural crack is eventually created and the resistance to propagation becomes fully developed after initial crack growth. However, creating a chevron-notch is not an easy procedure if compared to a standard or a straight-through saw-cut notch, and the decision to use one or the other is based on the "level" of testing required which is explained in the following section.

2.10.2 Testing Level

The International Society of Rock Mechanics ISRM (1988) suggested two testing levels to guide researchers and practitioners to decide what combination of screening and accuracy is best for a given application of the measured fracture toughness values. They defined level I testing as the type of testing that can be carried out using portable equipment and requires only the registration of maximum load. The associated estimated value of fracture toughness in this case acts as an index property more so than of a material property. Level I testing is more appropriate for screening purposes or for the rapid estimation and comparison of fracture toughness values.

On the contrary, level II testing requires both load and displacement measurements, and thus is laboratory based and is considered more complicated and sophisticated to perform. This testing level is recommended for the determination of accurate, compatible, and reproducible fracture toughness values.

2.10.3 Loading Rate

Barton (1983) reported that different loading rates have been prescribed for rock fracture testing, ranging from 0.01 to $0.03 MPam^{1/2}/sec$. For the testing methods suggested by the ISRM, loading rate is not supposed to be greater than $0.25 MPam^{1/2}/sec$ or such that failure is recorded within 10 seconds (ISRM, 1988). Although general rock and soil strength properties depend on loading rate and their behavior differ greatly upon changing the loading rate, there is no agreement on whether or not K_{IC} is affected by a change in the loading rate. The size of the FPZ should be affected by the loading rate and whether the load is applied statically or dynamically. In the case of dynamic loading, where fracture would occur before the full development of the FPZ, an underestimated fracture toughness value is expected. Khan and Al-Shayea (2000) reported that by testing in accordance with the suggested recommendations of the ISRM it has been shown that loading rate has a negligible effect on measured fracture toughness value.

2.10.4 Testing Method

The International Society for Rock Mechanics has suggested three methods for the determination of fracture toughness mainly for rocks and can be applicable to soils. These

48

methods are the Chevron Edge Notched Round Bar in Bending (**CB**), the Chevron Notched Short Rod (**SR**), and the Cracked Chevron Notched Brazilian Disc (**CCNBD**). Each method is core based, the only viable specimen alternative as rock is often available in the form of core pieces (Ouchterlony and Sun, 1983).

Despite the suggested standard methods of the ISRM, several other methods, with advantages and disadvantages, were developed and conducted by researchers to better quantify the fracture toughness K_{IC}. Whittaker (et al., 1992) and Chang et al. (2002) provide an exhaustive review of these alternative methods. The alternative methods include the commonly used method of the Semi-Circular Bend (**SCB**) test. The SCB can be prepared from rock cores and is adaptable to small, compact samples (favorable for soils) that require duplicate samples to test parameters that may affect K_{IC} such as loading rate, specimen thickness, and crack length (Karfakis et al., 1986; Chong, 1980; and Chong and Kuruppu, 1984). The Semi-Circular Bend (**SCB**) test is sometimes referred to as single edge Half Disc specimen in three point Bending (**HDB**) test. Other specimen geometries and conditions are used in other alternative methods such as the Chevron Notched Semi-Circular Bend (**CNSCB**) test (Kuruppu, 1997), the uncracked Brazilian Disc (**BD**) test (Guo et al., 1993), Straight Notched Brazilian Disc (**SNBD**) Specimens (Chong and Kuruppu, 1984), the Radial Cracked Ring (**RCR**) test (Shiryaev and Kotkis, 1982), the Modified Ring (**MR**) test (Thiercelin and Roegiers, 1986), Straight Edge Cracked Round Bar Bend (**SECRBB**) method (Ouchterlony 1982), the hollow Pressured Cylinder (**PC**) (Abou-Sayed and Simonson, 1977), the Double Torsion (**DT**) test (Evans, 1972), Punch Through Shear (**PTS**) Tests, Vicker indentation method (Atkinson and Avdis, 1980), Hertzian indentation methods (Lawn and Wilshaw, 1975a; Warren,1978; and Laugier, 1984, 1985), Diametric Compression (**DC**) test (Szendi-Horvath 1980), Cracked Straight Through Brazilian Disc (**CSTBD**) method (Awaji and Sato 1978), Flattened Brazilian Disc (**FBD**) method (Wang and Xing 1999), and Hole Cracked Flattened Brazilian disc (**HCFBD**) method (Zhang and Wang 2006).

In order to choose the simplest fracture testing method with reasonable fracture toughness results, methods can be compared with each other in terms of specimen preparation, loading method, experimental set-up and equipment, and applicability of the method to the mixed mode fracture toughness estimation, this comparison is illustrated in **Table 2.1**. It should be noted that most studies are relevant to mode I (opening mode) with some studies on mode II

(in-plane shear mode) or the mixed-mode.

A brief description of the main testing methods, highlighting the main advantages and disadvantages, is provided in the following section followed by summary tables of reported fracture toughness K_{IC} values from the literature using the different testing techniques in **Table 2.2.**

2.10.5 The ISRM Suggested Methods:

2.10.5.1 Chevron Edge Notched Round Bar in Bending (CB)

Ouchterlony was the first to propose the Chevron Bond specimen configuration in 1988. A chevron bend specimen and test set up are illustrated in **Figure 2.15.**

The test requires a long cylindrical specimen which can be obtained from a rock core or soil Shelby tube, the specimens are cut into the suggested lengths, then with the aid of a rotary saw, two notches which form a v-shaped ligament are achieved in opposite angles. The v-shaped notch, which is called chevron notch, is sawed in the middle of the specimen and perpendicular to the specimen (core) axis. After preparation, the specimen is loaded under three-point bending and the loading and resulted crack/fracture propagation are servo controlled by a clip on gauge that measures the chevron notch opening or what is called crack mouth opening displacement (CMOD). Two roller supports are used for the specimen to rest on and a compressive load is applied to cause crack propagation and transverse splitting of the specimen. A complete review and background of the test are thoroughly described in research by Sun and Ouchterlony (1986), ISRM (1988), Ouchterlony (1989), Ouchterlony (1989a), and Whittaker (et al., 1992).

The following equations can be used to calculate fracture toughness of CB according to the ISRM (1988). For level I testing the following equation should be used:

$$K_{CB} = C_K \, 24.0 \, {F_{max}}/{D^{1.5}} \tag{2.16}$$

Where F_{max} is the load at failure, D is the specimen diameter; C_k is a correction factor to account for size variation of the specimen and can be computed from the following equation:

$$C_K = \left(1 - \frac{0.6W}{D} + \frac{1.4a_o}{D} - 0.01\,\theta\right) \tag{2.17}$$

Where W is the specimen height, a_o is the initial position of the chevron notch apex, and θ is

the chevron notch angle.

For level II testing, the previous two equations can be used to obtain a preliminary value then a correction factor to account for the non linearity should be calculated and applied. By using the readings of a load and crack mouth opening displacement (CMOD) curve (a typical curve is shown in **Figure 2.16** to illustrate terms used in the calculating formulae), the correction factor can be computed as follows:

$$\sqrt{\frac{1+p}{1-p}}$$

Accordingly,

$$K_{CB}^{c} = \sqrt{\frac{1+p}{1-p}} \, K_{CB} \tag{2.18}$$

Where K_{CB}^{c} is critical fracture toughness value according to CB method, K_{CB} is the stress intensity factor obtained from previous equation (Level I testing), and p = Δxo / Δx (definitions of both terms are illustrated in **Figure 2.16**).

The main advantages of the CB method include utilizing core based cylindrical specimens which are convenient in the case of testing rocks or soils, the chevron-notch, stable crack growth, ability to account for non-linearity while calculating the fracture toughness value, and multiple testing levels (Level I and II). However, the specimen geometry and required dimensions and loading configuration are not simple, the chevron notch might appear an easy simple approach yet it is still a rather difficult pre-crack to machine. Furthermore, the advantages of the CB test seem only to be significant in terms of Level II testing. If Level I testing is sufficient then other more straightforward techniques are available for the rapid estimation of fracture toughness (Donovan, 2003).

2.10.5.2 Chevron Notched Short Rod (SR)

The short rod specimen configuration was first developed by Barker (1977), the configuration of an SR specimen and test set up are illustrated in **Figures 2.17** and **2.18.**

The SR specimen utilizes a cylindrical specimen similar to the CB test but in an SR specimen a chevron-notch is cut parallel to the core axis. A tensile load is applied at the notch mouth causing crack growth and lengthwise splitting of the specimen. To obtain a loading surface in tension, a rectangular grip groove is machined in one end of the short rod specimen. After the

grip groove is machined, two slots are cut at opposing angles, forming a triangular ligament which is called the chevron.

For fracture toughness calculation, tensile load and displacement measurements are made at the grip groove. Fracture toughness computation is done by an analytical method which is achieved by ISRM (1988) and a correction factor for the nonlinear behavior of the material is calculated with another equation depending on the Load-CMOD curve of the fracture experiments. There are two levels of testing in SR method. In Level 1 testing, maximum load during bending is recorded and in Level 2 testing, load and displacement measurements are taken into account. For a complete background review and detailed analysis see Barker (1977), Bubsey (et al., 1982), Sun and Ouchterlony (1986), ISRM (1988), Ouchterlony (1989), Ouchterlony (1989a), and Whittaker (et al., 1992).

The following equations can be used to calculate fracture toughness of SR according to the ISRM (1988). For level I testing the following equation should be used:

$$K_{SR} = C_K \, 24.0 \, {}^{F_{max}}\!/_{D^{1.5}} \tag{2.19}$$

Where F_{max} is the load at failure, D is the specimen diameter, C_k is a correction factor to account for size variation of the specimen and can be computed from the following equation:

$$C_K = \left(1 - \frac{0.6W}{D} + \frac{1.4a_o}{D} - 0.01\,\theta\right) \tag{2.20}$$

Where, W is the specimen height, a_o is the initial position of the chevron notch apex, and θ is the chevron notch angle.

For level II testing, the previous two equations can be used to obtain a preliminary value then a correction factor to account for the non linearity should be calculated and applied. By using the readings of a load and crack mouth opening displacement (CMOD) curve (a typical curve is shown in **Figure 2.16** to illustrate terms used in the calculating formulae), the correction factor can be computed as follows:

$$\sqrt{\frac{1+p}{1-p}}$$

Accordingly,

$$K_{SR}^c = \sqrt{\frac{1+p}{1-p}} \, K_{SR} \tag{2.21}$$

Where K_{SR}^c is critical fracture toughness value according to SR method, K_{SR} is the stress intensity facot obtained from previous equation (Level I testing), and p = Δxo / Δx (definitions of both terms are illustrated in **Figure 2.16**)

The advantages of SR testing method are the same as those for the CB test. The SR method uses a shorter length of core sized specimen and according to the ISRM, two SR specimens can be obtained from one fractured CB test (since the length to diameter requirement of the CB test is 4:1 and for the SR it is 1.45:1). This saves material and allows for the measurement of fracture toughness using two crack orientations. However, the disadvantages of the SR testing method are mainly related to specimen preparation, notably the chevron-notch, is difficult to reproduce consistently and that for Level I type testing it is too complex (Alkiliçgil, 2006).

2.10.5.3 Chevron Notched Brazilian Disc (CCNBD)

Shetty et al. (1985) was the first to use Chevron notched Brazilian discs to measure the fracture toughness of ceramics, and applied the stress intensity factor solutions of a cracked straight-through Brazilian disc (CSTBD) with a through notch to the CCNBD by means of the straight-through crack assumption (STCA) method (Donovan, 2003). Afterwards, the ISRM presented the suggested method for determining mode I fracture toughness using a CCNBD specimen as it has many advantages over other methods (Fowell, 1995).

The cracked chevron-notched Brazilian disc (CCNBD) specimen, which is illustrated in **Figure 2.19**, has the same geometry and shape as the conventional Brazilian disc used for measuring the indirect tensile strength of rock, except that the CCNBD specimen has a chevron notch. The chevron notches are machined using slow speed circular saw, where the circular disk is first marked on both sides along the diameter of the disc to show the two extreme points up to which the saw can cut. The marked Brazilian disc is pressed against the rotating circular saw until the saw reached the two marked extreme points. Then the disc is removed and turned and the same procedure is repeated from the other side of the disc as shown in **Figure 2.20**. During the notch-making process, the discs are held manually against the saw, making it difficult to obtain precise dimensions and crack geometry (**Alkiliçgil, 2006**). A strain controlled loading frame is used for the load application. The applied load and load point displacement are obtained using a computerized data logger as displayed in **Figure**

2.21.

Fracture toughness is calculated by an equation which depends on normalized stress intensity factor. Stress intensity factor is computed with numerical methods and an equation can be derived by fitting the numerical results. CNBD specimen is used not only to achieve fracture toughness in Mode I but also fracture toughness in Mode II and mixed modes.

Fracture toughness is calculated by using the following expression as suggested by ISRM (1995):

$$K_{IC} = \frac{P_{max}}{B\sqrt{D}} \; Y^*_{min} \tag{2.22}$$

Where D is the diameter of the Brazilian disc = 2R, B is the thickness of the specimen, P_{max} is the compressive load at failure, and Y_{min}^* is a critical dimensionless stress intensity factor and can be computed as follows:

$$Y^*_{min} = ue^{v\alpha} \tag{2.23}$$

Where u and v are constants determined by $a0$/R and B/R and obtained from a corresponding chart and α is equal to a/R and a is half the notch length.

2.10.5.4 Concluding Remarks on ISRM Suggested Methods

The standardization of the suggested methods aided in obtaining more reliable and representative values of K_{IC} yet with a variation of 20–30% in both the Chevron Bend (**CB**) and Short Rod (**SR**) test values. Researchers have attributed this variation to several factors including the size of specimens, anisotropy of rock or soil being tested, size of fracture process zone near crack tip, micro- and macro-structure of tested material, and moisture conditions of tested specimens (Iqbal and Mohanty, 2007). Indications of specimen size effect were observed to exist in K_{IC} determination in a number of studies, recently Cui et al. (2010) conducted mode I fracture toughness tests on SR specimens of four diameters prepared from weak weathered sandstone cores and it was observed that K_{IC} value for the smallest diameter group was approximately 1.2 times lower than K_{IC} value for largest diameter group. Accordingly, specimen size in addition to anisotropy can be considered as the main reasons for the variation in the calculated values, accordingly a number of improvements had been suggested such as empirical relations to accurately determine the required minimum diameter of the core specimens (Ouchterlony, 1989; Matsuki et al., 1991; Ouchterlony et al., 1991). However, other issues were problematic and were not overcome such as: the relatively low

loads required to initiate fracture (in the order of 1–2 KN) which resulted in less precision in measurements, a large number of specimens is needed to reach the correct testing orientation, complicated inconvenient fixtures for specimen installation and loading, and complex procedure of specimen preparation for the SR method (Fowell and Xu, 1993).

Even after the standardization of the Chevron-Notched Brazilian Disc (**CCNBD**) method in 1995, research on fracture toughness of rock used other similar simpler methods. The main reason behind that is the difficulty of the notch making process in the disc specimen preparation for the CCNBD test. Moreover, experimental research showed that fracture toughness values obtained with the CCNBD test were considerably lower (30–50%) than the values obtained with the CB and SR tests, for the same rock type (Dwivedi et al., 2000). Several reasons have been offered to explain this deviation. These include the critical dimensionless stress intensity factor (SIF) value for the disc specimens used in formula for the CCNBD test, the anisotropy of rock, and the micro- and macro-structure of rock. The stress intensity factor corresponds to the critical state of the specimen when the crack front is somewhere between the initial and the final notch lengths, accordingly the critical crack length and the critical dimensionless SIF values are specimen geometry dependent only (ISRM, 1995; Fowell and Xu, 1993; Xu and Fowell, 1994). The critical dimensionless SIF value has been considered as the major factor for the lower values of fracture toughness obtained with the CCNBD method (Iqbal and Mohanty, 2007).

2.10.6 Alternative Methods from the Literature:

2.10.6.1 Semi Circular Bend (SCB)

The semi circular bend technique was first developed and proposed by Chong and Kuruppu (1984) in order to have a test method that was simple to fabricate and load. Then the technique was advocated by Lim et al. (1994). The pre-crack can be a saw cut notch that is fatigue loaded in order to produce a natural crack, a chevron-notch, or a very thin saw-cut notch. The kinematics of the test are similar to that of the CB test as a vertical compressive load is applied under three-point bending and transverse splitting of the specimen (Akram, 1991). A more detailed description of the test is given by Chong and Kuruppu (1984), Karfakis et al., 1986, Chong (et al., 1987), and Whittaker (et al., 1982).

Testing material cores are obtained then sliced into circular disks, using a high-speed

diamond plated rotary saw. Then the discs are polished to ensure uniform thickness using a sander or similar tools. The disks are cut along the diameter into two equal halves as shown in **Figure 2.22**. Finally, a radial line is marked at the required orientation with respect to the loading direction. Then a notch of the required length is made along this marked line by using a wire saw. It is worth noting that the test is difficult to perform on standard NX core specimens (approximately 50 mm in diameter) and larger diameter specimens are usually required in order to obtain stable loading and crack growth. The specimen geometry and loading configuration of the SCB test are shown in **Figure 2.23**.

A strain-controlled loading frame is then used for load application. The applied load, load point displacement, and crack opening are acquired using a computerized data logger as illustrated in **Figure 2.24**.

Chong et al. (1987) developed a formula for K_{IC} by using both the strain energy release rate method and the elliptical displacement approach.

$$Y_k = \frac{K_I}{\sigma_o \sqrt{\pi a}}$$ (2.24)

Where, Y_k is normalized stress intensity factor, K_I is stress intensity factor under mode I loading, a is the notch or crack length and σ is the applied stress at failure and can be computed as follows:

$$\sigma_o = \frac{P}{2RB}$$ (2.25)

Where P is the load at failure, R is the specimen radius, and B is the specimen thickness.

The normalized dimensionless stress intensity factor, Y_k can be computed as a function of the dimensionless crack length, a/D (where D is the specimen diameter). Y_k can be approximated by a third-order polynomial as follows:

$$Y_K = 4.47 + 7.40 \frac{a}{D} - 106.0 \left(\frac{a}{D}\right)^3 + 433.3 \left(\frac{a}{D}\right)^3$$ (2.26)

By using same equation fracture toughness is calculated with experimental data and normalized stress intensity factor calculated by numerical results.

2.10.6.2 Chevron Notched Semi Circular Bend (CNSCB)

In 1997 Kuruppu carried out numerical 3D finite element analyses to obtain a relation between the crack tip stress intensity factors of a chevron notched semi circular bend

specimen (CNSCB) and the crack length. The shape of the chevron notched SCB specimen is illustrated in **Figure 2.25** According to the reported methodology; an initial crack length a_o of 6 mm and a thickness t of 25 mm are required. All specimens should have a span to radius ratio (S/R) of 0.8 and a chevron notch angle υ of $90°$ (Chang et al., 2002).

The average value of the stress intensity factor determined along the crack front can be normalized as follows:

$$K_{nd} = \frac{K_I}{p} \, t \sqrt{R} \tag{2.27}$$

Where K_{nd} is normalized stress intensity factor, P is the applied load and t and R are the specimen thickness and radius, respectively. The relation between the normalized stress intensity factor and the normalized crack length (a/R) is illustrated in **Figure 2.26.**

The stress intensity factor of the chevron-notched SCB specimen has a minimum value in the same way as other chevron-notched specimens. Initial crack growth in a chevron notch occurs in a stable manner during which the load increases and the specimen fails immediately beyond its maximum load bearing capacity. Therefore, the maximum load was used as the critical fracture load. This value along with the minimum value of the stress intensity factor of *7.269* as shown in **Figure 2.26** was used to determine the mode I fracture toughness.

Hence, the critical mode I fracture toughness can be determined as follows:

$$K_{IC} = \frac{7.269 \, P_{max}}{t \sqrt{R}} \tag{2.28}$$

2.10.6.3 Uncracked Brazilian Disc (BD) Test

An uncracked Brazilian Disc Test (BD) specimen has the same geometry as a conventional Brazilian disc without any notch or crack (Guo et al., 1993). The main advantage of this testing method is lack of requirement of a notch or crack for specimen preparation which makes this method the quickest, the most controlled and the easiest. One of the features of the BD specimen is that it uses the local minimum load as the critical load instead of the maximum load (Chang et al., 2002). The local minimum load is defined as P_{min} in **Figure 2.27**. The behavior of the tested specimen can be divided into three main behaviors; *oa* where

elastic deformation occurs, **ab** where unstable crack propagates and finally **bc** where crushing and secondary cracking occur. The local minimum load utilized in evaluating K_{IC} can be defined at the beginning of **bc** stage. Detailed further explanation of the Brazilian test, its modifications, introduction of the flattened Brazilian disc configuration, and how to obtain the fracture toughness value is covered in **Chapter 3**.

2.10.6.4 Straight Notched Brazilian Disc (SNBD) Specimens

Straight Notched Brazilian disc (SNBD) testing was first developed by Chong and Kuruppu (1984). Specimens are obtained from rock cores or soil Shelby tubes, they are cut into circular discs taking the Brazilian configuration using a high speed diamond plated rotary saw. Then the circular discs are sanded to ensure uniformity and flatness of surfaces. Then a drill bit in a lathe is used to initially create a hole in the center of the disc, the bit penetrates half the thickness of the circular disc then the disc is flipped to drill the remaining thickness half. A wire saw is inserted through the drilled hole and used to machine a straight notch with a specific length (*2a*) in the disc. **Figure 2.28** shows the geometry of the prepared SNBD specimens. The testing equipment and setup are similar to that of CCNBD specimen test discussed earlier.

Fracture toughness is calculated by a mathematical expression. The expression includes the normalized stress intensity factor, which is determined using numerical methods. Atkinson et al. (1982) proposed a mathematical expression to compute the stress intensity factor under Mode I loading as follows:

$$K_{IC} = \frac{P\sqrt{a}}{\sqrt{\pi RB}} N_I \tag{2.29}$$

Where K_{IC} is the critical stress intensity factor under mode I loading, R is the Brazilian disc radius, B is the thickness of the specimen, P is the compressive load at failure, *a* is half the length of machined notch, and N_I is a non-dimensional coefficient which depends on *a*/R.

N_I can be evaluated by the following equation derived by Shetty and Rosenfield (1985) by fitting the numerical results of Atkinson et al. (1982).

$$N_I = 0.99 + 0.141 \left(\frac{a}{R}\right) + 0.863 \left(\frac{a}{R}\right)^2 + 0.886 \left(\frac{a}{R}\right)^3 \tag{2.30}$$

2.10.6.5 Concluding Remarks on Alternative Methods from the Literature:

Krishnan et al. (1997) pointed out the SNBD specimen is the most convenient configuration when the soft sand stone is considered since the SNBD specimen configuration permits the use of the same setup and conditions for mode I, mode II and mixed mode I-II testing with fewer preparations than other type of tests. Also the effect of anisotropy and bedding planes in fracture toughness can be evaluated easily by orienting the notch with respect to the direction of interest (e.g. bedding planes).

Then Khan and Al-Shayea (2000) used SCB specimens under three-point-bending and Brazilian disk specimens under diametrical compression in their mixed mode I-II study to investigate the effect of testing method and specimen geometry such as diameter, thickness, and crack length and type on measured fracture toughness. The results show that specimen diameter and crack type have a substantial influence on the measured fracture toughness; however, loading rate, crack size, and specimen thickness seem to have a negligible effect on the fracture toughness. Mode I fracture toughness is significantly influenced by specimen diameter and crack type. The different specimens (Brazilian disc, and semicircular) can give comparable results only when the proper span to diameter ratio is used. The Brazilian disc with a straight notch was found to be the most convenient geometry to use for fracture toughness determination.

Then in a later study Chang et al. (2002) investigated rock fracture toughness under mixed-mode conditions using the straight through crack assumption (STCA) applied to the CNBD specimen and SCB specimen. Size effects, in terms of specimen thickness, diameter and notch length on fracture toughness, were investigated. The CNBD specimen can be used to measure mixed-mode and mode II fracture toughness values by the STCA method. It is also unnecessary to perform pre-cracking for the CNBD specimen because it uses a chevron notch which induces self-pre-cracking during testing and leads to a stable crack propagation. As a result, it is concluded that the CNBD specimen is the most preferable and versatile among disc-type specimens used in this study. Chang et al. (2002) summarized the main differences between the different testing methods performed on disc type specimens, where they compared between ISRM suggested methods; chevron bending specimens (CB), short rod specimens (SR), and the Chevron Notched Brazilian Disc (CCNBD) and other alternative methods from the literature; semi circular bend specimen (SCB). This summary is presented

in **Table 2.3.**

2.11 Relationship between Fracture Toughness and other Physical Mechanical Parameters

The application of fracture mechanics theory requires the evaluation of fracture toughness of the rock or soil. However, standard sampling techniques are often unable to supply suitable samples for fracture toughness testing (Haberfield and Johnston, 1989). And despite the standardization of fracture toughness testing, its use for rock or soil characterization and indexing purposes is not common mainly due to the lengthy sample preparation time, premature failure of samples and difficulties in obtaining consistent notch dimensions to the tolerances required and other preparation related problems (Zhang, 2002). Hence, a simple alternative method for determining fracture toughness may be required.

Great attempts are being made to predict the fracture toughness of rocks and soils based on their relationship with other mechanical and physical parameters. Gunsallus and Kulhawy (1984) and Bhagat (1985) experimentally found that Mode I fracture toughness K_{IC} of several types of rock and soil is directly proportional to their tensile strengths. Furthermore, Whittaker et al. (1992) obtained some approximate relations between fracture toughness and different index tests such as hardness index, uniaxial tensile strength, uniaxial compressive strength, and elastic modulus. Chen and Chen (1995) performed tentative research on the relevant relationships between the acoustic speed and fracture toughness of rock materials. After that, Brown and Redish (1997) explored an experimental relation between Mode I rock fracture toughness and density, and Bearman (1999) experimentally investigated the relation between Mode I fracture toughness and the point load strength.

2.11.1 Relationship between Fracture Toughness and Tensile Strength

As fracture toughness and tensile strength are material parameters indicating the ability of the specimens to resist failure induced by critical tensile stresses under mode I loading and uniaxial tension conditions, researchers believed that Mode I fracture toughness, the opening mode, should be related to the tensile strength, in which the material is separated by tensile stresses.

The earliest studies were carried out by Gunsallus and Kulhawy (1984) where they investigated the variation in strength for eight lithologically similar, Silurian sedimentary

rock units from the northeastern United States. They carried out fracture toughness, uniaxial compression, point load index and Brazil tensile tests. The tested specimens mainly dolostone, limestone, and sandstone; were obtained from Silurian rock from tunnel projects in Buffalo, Rochester and Chicago. Fracture toughness determination was carried out using the short rod (SR) configuration and strength was obtained using three different mechanisms: uniaxial compressive strength test, point load index test, and Brazil tensile strength test following the suggested methods developed by the ISRM. From their experimental results and regression analyses they were able to obtain the following relations between fracture toughness and uniaxial compressive strength (displayed in **Figure 2.29**):

$$K_{IC} = 0.0044\, Q_u + 1.04, \text{ with a coeffiecient of determination } r^2 = 0.72 \qquad (2.31)$$

And relation between fracture toughness and point load index (displayed in **Figure 2.30**):

$$K_{IC} = 0.0995\, I_{s\,50} + 1.11, \text{ with a coeffiecient of determination } r^2 = 0.67 \qquad (2.32)$$

And relation between fracture toughness and Brazil tensile strength (displayed in **Figure 2.31**):

$$K_{IC} = 0.0736\, \sigma_t + 0.76, \text{ with a coeffiecient of determination } r^2 = 0.73 \qquad (2.33)$$

Similar studies were carried out by Haberfield and Johnston (1989) where they argued that there are many situations in foundation engineering, especially in the case of weak and weathered rocks / soils, where tensile failure governs behavior. In such cases, tensile failure should be considered using fracture mechanics theory. Accordingly, they investigated the relation between tensile strength and Mode-I fracture toughness for a wide variety of rocks and soils, such as Melbourne mudstone; which is a soft rock, Johnstone; which is a synthetic rock developed to minimize the scatter in the behavior and simulates natural soft rocks. They also investigated oil shale, granite, marble, micrite, basalt, syenite, and clay. Fracture toughness was experimentally determined using three point loading of single edge cracked beams (SECB) and the tensile strength was determined using three or four point bend tests on un-notched prismatic specimens (Haberfield, 1987). The results of their tests are summarized and plotted with other values from the literature is shown in **Figure 2.32.** The results indicated that a strong correlation between fracture toughness and tensile strength exists regardless the wide range of strengths, mineral compositions and formation methods. A linear correlation can be used to express the results of the used data points as follows:

$K_{IC} = 0.0761 \, \sigma_t$, with a coeffiecient of determination $r^2 = 0.80$ (2.34)

It is worth noting that Haberfield and Johnston included a single reference from the literature for the behavior of clays as studied by Lee et al. (1982). They observed that clay lies above the extrapolated curve of the remaining rocks behavior which indicates the relatively higher ductility of clay if compared to rocks.

Over the years much experimental work was carried out to investigate the relation between the fracture toughness and the tensile strength. Whittaker et al. (1992) carried out an experimental research and concluded that the relation between Mode I fracture toughness and tensile strength of various types of rock including coal can be expressed as follows:

$\sigma_t = 9.35 \, K_{IC} - 2.53$, with a coeffiecient of determination $r^2 = 0.62$ (2.35)

More details on the testing method used to determine each quantity are illustrated in **Table 2.4.**

However, the previous equation was questionable as it indicated that at zero tensile strength the material still had a certain value for fracture resistance which is certainly not the case for soils and rocks. Accordingly, Zhang et al. (1998) changed the format of the relation to a power law regression instead of a linear relation. Making use of their own experimental data they obtained a relation between Mode I fracture toughness and the tensile strength for several rock types as follows:

$\sigma_t = 8.88 \, K_{IC}^{0.62}$, with a coeffiecient of determination $r^2 = 0.94$ (2.36)

Further details on the testing method used to determine each quantity are illustrated in **Table 2.4.**

Other researchers investigated the behavior of soils and weak rock, Harison et al. (1994) experimentally obtained a strong correlation between Mode I fracture toughness and tensile strength of soils using the ring test. He also considered the dependency of the tensile strength value on the testing method so he converted the tensile strength values obtained earlier by Haberfield and Johnston (1989) to equivalent splitting tensile strengths that would agree with his testing methodology using ring tests. The obtained results were expressed in the following format:

$\sigma_t = a_o \, K_{IC}$ (2.37)

where a_o is a constant, they concluded that a_o is equal to 15.4 for soils and a_o is equal to 13.6

for soft rocks. For the tested cohesive soils using ring tests, the relation between K_{IC} (in MPa.m$^{0.5}$) and tensile strength (in MPa) can be expressed as follows:

$$K_{IC} = 0.022 \left(\frac{Pa}{\gamma_w}\right)^{0.5} \sigma_t, \quad \text{With a coeffiecient of determination } r^2 = 0.93 \qquad (2.38)$$

Where Pa is the atmospheric pressure and γw is the unit weight of water. Since the atmospheric pressure and the unit weight of water can be considered constant, then the previous equation can be written as follows:

$$K_{IC} = 0.0706 \, \sigma_t, \text{ with a coeffiecient of determination } r^2 = 0.88 \qquad (2.39)$$

Then Li and Zhu (2002) used conventional three point bending fracture test on soil beams and uniaxial tensile strength test on soil columns from frozen Lanzhou (city in Western China) loess. From their results they concluded that the relationship between the two parameters can also be regarded as linearly correlated as expressed below:

$$K_{IC} = 0.1456 \, \sigma_t, \text{ with a coeffiecient of determination } r^2 = 0.63 \qquad (2.40)$$

The correlation of the two parameters (expressed in MPa.m$^{0.5}$ and in MPa) and detailed testing data from both Harison et al. (1994) and Li and Zhu (2002) can be shown in **Figure 2.33**. By comparing the two studies, it can be concluded that the main reason behind the difference in the proportionality coefficients is the difference of the tested soils and the test methods.

Then in 2002 Zhang compiled all the reported tensile strength (in MPa) and fracture toughness (in MPa.m$^{0.5}$) data from experimental research by Whittaker et al. (1992), Zhang et al. (1998), Nordlund et al. (1999), Khan and Al-Shayea (2000), and Yu (2001). The compiled data is plotted in **Figure 2.34**, and an empirical correlation was developed as follows:

$$\sigma_t = 6.88 \, K_{IC}, \text{ with a coeffiecient of determination } r^2 = 0.94 \qquad (2.41)$$

Or for convenience can be written as: $\quad K_{IC} = 0.1453 \, \sigma_t \qquad (2.42)$

More details on the testing method used to determine each quantity are illustrated in **Table 2.4.**

Figure 2.35 compares the results of Haberfield and Johnston (1989) and Zhang (2002), it is found that the values of proportionality coefficient and the coefficient of determination in the empirical relationship differ due to the difference in the tested rock and the adopted testing

method.

Finally, in 2007 Wang et al. investigated the fracture toughness of a specific clay type in Western China using single edge cracked soil beams loaded using an improved three point bending beam loading assembly which minimized the influence of specimen's weight. The Tensile strength was determined using uniaxial tension loading assembly on cylindrical compacted specimens. Based on the testing data (shown in **Figure 2.36**), a linear empirical relationship between the two parameters of the tested clay was suggested as follows:

$$K_{IC} = 0.3546 \, \sigma_t \, , \text{with a coeffiecient of determination } r^2 = 0.88 \tag{2.43}$$

2.11.2 Relationship between Fracture Toughness and Confining Pressure

In a recent study by Zhenfeng and Mian (2006), fracture toughness experiments were performed for fabricated specimens with clay content of 60% and 30%, under confining pressure conditions and at room temperature. In their study the fracture toughness value was calculated with the help of the finite element model established by Chen and Zhang (2004). Using statistical methods, the relationship between the fracture toughness K_{IC} and confining pressure Pc is regressed as shown in **Figure 2.37**.

From their analyses it can be seen that the fracture toughness is directly proportional to the confining pressure, and the toughness under zero confining pressure may be far below those under confining pressure conditions, especially in the case of high confining pressures. Hence, the fracture toughness under confining pressures should be used in practical engineering, rather than the ones under zero confining condition (Zhenfeng and Mian, 2006).

2.11.3 Relationship between Fracture Toughness and other Physical Mechanical Parameters

In the same study by Zhenfeng and Mian (2006), other mechanical and physical parameters were investigated and correlated with the fracture toughness value. In their study they included compressive wave velocity v_P, shear wave velocity v_S, density p, uni-axial compressive strength, and modulus of elasticity. The acoustic velocities were measured using a conventional acoustic velocity apparatus, uni-axial compressive strength and the static modulus of elasticity were measured using an MTS system, and the dynamic modulus of elasticity was calculated from the measured acoustic velocity. The relationship between the

previously mentioned parameters and the mode I fracture toughness is shown in **Figure 2.38**.

From their analyses, it can be observed that statistic results obtained with the least square method that fracture toughness increases linearly with acoustic velocities, dynamic and static moduli of elasticity, and uni-axial compressive strength, but it decreases linearly with the clay content. In practice, density, different acoustic velocities, and clay content can be determined from logging data. Then fracture toughness can be predicted with acoustic logging data, density logging data and gamma logging data.

Similar findings were reported in an experimental study by Chang et al. (2002), where rock fracture toughness was determined using disc-type specimens. Keochang Granite and Yeosan Marble produced in Korea were the main rock types that were used for testing. Rock fracture toughness under mixed-mode, mode I and mode II conditions were measured by using the straight through crack assumption (STCA) applied to the cracked chevron-notched Brazilian disc (CCNBD) specimen and the semicircular bend (SCB) specimen. **Figure 2.39** presents a summary of the relationship between mode I fracture toughness and other parameters including acoustic wave velocity, uni-axial compressive strength, Young's modulus of elasticity, Poisson's ratio, specific gravity, and porosity.

From the previous studies, it can be concluded that the value of proportionality coefficient and the coefficient of determination in the empirical relationships is soil or rock type dependent. The value is also dependent on the testing method used and the accompanying loading / testing conditions.

Table 2.1 Comparison between different fracture testing methods

(after Keles and Tutluoglu, 2011)

Method	Notch Type			Loading Method	Set up and equipment	Precrack	Mixed Mode Evaluation
	Straight		Chevron				
	Rotary Saw	Wire Saw	Rotary Saw				
CB	–	–	Yes	Bending	Complex	–	No
SR	–	–	Yes	Tensile	Complex	–	No
CCNBD	–	–	Yes	Compressive	Simple	–	Yes
BD	–	–	–	Compressive	Simple	–	No
FBD	–	–	–	Compressive	Simple	–	No
HCFBD	Yes	–	–	Compressive	Simple	–	No
MR	–	–	–	Compressive	Simple	–	No
CSTBD	–	Yes	–	Compressive	Simple	Yes	Yes
DC	Yes	–	–	Compressive	Simple	Yes	No
SECRBB	Yes	–	–	Bending	Simple	Yes	Yes
SCB	Yes	–	–	Bending	Simple	Yes	Yes
CNSCB	–	–	Yes	Bending	Simple	–	Yes

Table 2.2: Summary of Fracture Toughness Values for Different Geomaterials.

Tested Material		Experimental Testing Method	Mode I Fracture Toughness Value (K_{IC}) ($MPa.m^{1/2}$)	Reference
Sandstone	Coarse grained	SCB	0.35	Singh & Sun, 1990
	Fine grained	SCB	0.28	Singh & Sun, 1990
	Fine grained	SC3PB	0.56	Whittaker, 1992
	Fine grained	CCBD	0.62	Fowell & Chen, 1990
		BDT	0.67	Whittaker, 1992
	Ruhr	CB	1.03	Müller & Rummel, 1984
	Ryefield	SECBD	1.04	Whittaker, 1992
	Flechtingen	CB	1.15	Backers et al., 2003
	Montcliffe	CB	1.18	Bearman, 1999
	Grimsby	SR	1.47	Gunsallus & Kulhawy, 1984
	Alvdalen	SR	1.91	Ouchterlony, 1987
	Alvdalen	CB	0.73	Ouchterlony, 1987
	Pennant	CB	2.1	Bearman, 1999
	Pennant	SR	2.56	Meredith, 1983
		CB	1.67	Rao et al.,2003
		CB and SR	0.67 – 2.56	Guo, 1990; Ouchterlony, 1988; Meredith, 1983
	P = 0.1MPa	CB	1.08	Muller, 1984
	P = 40MPa	CB	2.21	Muller, 1984
	P = 80MPa	CB	2.54	Muller, 1984
	Coarse-grained	HDB	0.28	Whittaker et al, 1992. Zhang et al, 1998. Zhang, 2002.
	Fine-grained	HDB	0.38	Whittaker et al, 1992. Zhang et al, 1998. Zhang, 2002.
	Fine-grained	SC3PB	0.56	Whittaker et al, 1992. Zhang et al, 1998. Zhang, 2002.
Diorite	Aspo	CB	3.21	Staub et al., 2003
		CB	2.22 - 2.57	Bearman et al. , 1989
	Bolton hill	CB	2.22	Bearman, 1999

Tested Material		Experimental Testing Method	Mode I Fracture Toughness Value (K_{IC}) (MPa.m$^{1/2}$)	Reference
	Aspo	SENRBB	3.21	Nordlund et al., 1999
	Cliffe hill	CB	2.77	Bearman, 1999
Dolostone		SR	0.81 - 2.57	Gunsallus & Kulhawy, 1984
	Falkirk	SR	1.66	Gunsallus & Kulhawy, 1984
	Kankakee	SR	1.66	Gunsallus & Kulhawy, 1984
	Oatka	SR	1.78	Gunsallus & Kulhawy, 1984
	Markgraf	SR	1.8	Gunsallus & Kulhawy, 1984
	Romeo	SR	2.47	Gunsallus & Kulhawy, 1984
Granite		CB	1.88	Rao et al., 2003
		CB	0.65 - 2.47	Muller & Rummel, 1984, Ouchterlony, 1988 Ouchterlony & Sun, 1983
		SECBD	1.65	Whittaker, 1992
	Utinga (Rift plane)	CNBD	0.6	Almeida et al., 2006
	Falkenberg	CB	0.65	Müller & Rummel, 1984
	Utinga (Grain plane)	CNBD	0.73	Almeida et al., 2006
	Utinga (Hardway	CNBD	0.82	Almeida, et al., 2006
	Favela (Grain plane)	CNBD	0.9	Almeida et al., 2006
	Favela (Rift pla ne)	CNBD	0.97	Almeida et al., 2006
	Iidate	SR	1.12	Takahashi et al., 1986
	Favela (Hardway	CNBD	1.16	Almeida et al., 2006
	Daejeon	BDT	1.18	Yoon & Jeon, 2004
	Cornwall	CB	1.32	Müller & Rummel, 1984
	Bohus	CB	1.42	Ouchterlony, 1987
	Falkenberg	CB	1.52	Müller & Rummel, 1984

Tested Material		Experimental Testing Method	Mode I Fracture Toughness Value (K_{IC}) (MPa.m$^{1/2}$)	Reference
	Newhurst	SCB	1.72	Whittaker, 1992
	Iidate	CB	1.73	Müller & Rummel, 1984
	Epprechtstein	CB	1.74	Müller & Rummel, 1984
	Stripa	SECRBB	1.74	Sun & Ouchterlony, 1986
	Merrivale	SR	1.8	Meredith, 1983
	Westerly	SR	1.82	Meredith, 1983
	Penryn	CB	1.83	Bearman, 1999
	Pink	SR	2.03	Meredith, 1983
	TGP	SENRBB	2.08	Yu, 2001
	Krakemala	CB	2.16	Ouchterlony, 1987
	Straht Halladale	SR	2.19	Meredith, 1983
	Krakemala	SR	2.22	Ouchterlony, 1987
	Iidate	CB	2.26	Takahashi et al, 1986
	Westerly	SR	2.27	Ouchterlony, 1987
	Stripa	SR	2.36	Sun & Ouchterlony, 1986
	Bohus	SR	2.4	Ouchterlony, 1987
	Stripa	SR	2.7	Ouchterlony, 1987
	Westerly	CT	2.7	Schmidt & Lutz, 1979
	Westerly	CT	2.7	Sun & Ouchterlony, 1986
	Rasjö	SR	2.8	Ouchterlony, 1987
	D = 75 mm	CCNDB	1.3509	Chang et al., 2002
	D = 54 mm	CCNDB	1.3376	Chang et al., 2002
		SCB	0.6836	Chang et al., 2002
		BDT	1.2894	Chang et al., 2002
		CNSCB	1.3932	Chang et al., 2002
	Stripa	SCR3PB	2.15	Zhang et al., 1998
Limestone		CB	0.82 - 2.21	Bearman et al., 1989, Guo (1990)1, Ouchterlony & Sun (1983)
	P = 0.1MPa	CCBD	0.42	Al-Shayea et al., 2000
	P = 28MPa	CCBD	1.57	Al-Shayea et al., 2001

Tested Material		Experimental Testing Method	Mode I Fracture Toughness Value (K_{IC}) (MPa.m$^{1/2}$)	Reference
	Middleton	CB	0.73	Bearman, 1999
	Harrycroft	CB	0.82	Bearman, 1999
	Welsh	SCB	0.85	Singh & Sun, 1990
	Indiana	SECB	0.97	Ingraffea & Schmidt, 1979
	Indiana	CCP	0.97	Sun & Ouchterlony, 1986
	Indiana	SC3PB	0.99	Whittaker, 1992
	Irondequoit	SR	1.36	Gunsallus & Kulhawy, 1984
	White	BDT	1.38	Whittaker, 1992
	Shelly	SR	1.44	Meredith, 1983
	Grey	BDT	1.58	Whittaker, 1992
	Wredon	CB	1.7	Bearman, 1999
	Klinthagen	SR	1.87	Ouchterlony, 1987
	Reynales	SR	2.06	Gunsallus & Kulhawy, 1984
	Saudi Arabia	SENRBB	0.39	Khan & Al-Shayea, 2000
Marble		CB	2.21	Rao et al., 2003
		CB	0.46 - 2.25	Muller & Rummel, 1984
		SR	0.46 - 2.26	Ouchterlony, 1988
		CB	0.46 - 2.27	Guo 1990
	Fine grained	BDT	1	Whittaker, 1992
	Coarse grained	BDT	1.12	Whittaker, 1992
	Carrara	CB	1.38	Müller & Rummel, 1984
	Treuchtlingen	CB	1.7	Müller & Rummel, 1984
	Ekeberg	CB	1.76	Ouchterlony, 1987
	Ekeberg	SR	2.25	Ouchterlony, 1987
	D = 75 mm	CCNDB	1.0605	Chong et al., 2002
	D = 54 mm	CCNDB	1.815	Chong et al., 2002
		SCB	0.8711	Chong et al., 2002
		BDT	0.9865	Chong et al., 2002
	FS—Fangshan	SR	0.21 - 1.13	Zhang et al., 1998
	FS—Fangshan	CNRBT	0.36	Zhang et al., 1998
	FS—Fangshan	CNSCB	1.1133	Chong et al., 2002

Tested Material		Experimental Testing Method	Mode I Fracture Toughness Value (K_{IC}) (MPa.m$^{1/2}$)	Reference
Basalt		SECBD	1.8	Whittaker, 1992
		SC3PB	2.27	Whittaker, 1992
		BDT	3.01	Whittaker, 1992
Coal		SC3PB	0.03 - 0.27	Whittaker et al, 1992. Zhang et al, 1998. Zhang, 2002.
Oil shale	Anvil points D-80 PB	SC3PB	1.08	Whittaker et al, 1992. Zhang et al, 1998. Zhang, 2002.
	Anvil points D-80 PB	SC3PB	0.98	Whittaker et al, 1992. Zhang et al, 1998. Zhang, 2002.
	Anvil points D-160 PB	SC3PB	0.67	Whittaker et al, 1992. Zhang et al, 1998. Zhang, 2002.
	Anvil points D-160 PB	SC3PB	0.6	Whittaker et al, 1992. Zhang et al, 1998. Zhang, 2002.
	Anvil points D-160 VB	SC3PB	0.37	Whittaker et al, 1992. Zhang et al, 1998. Zhang, 2002.
	Colorado	SCB	1.02	Chong et al., 1987
Siltstone		SECBD	0.8	Whittaker, 1992
Syenite	Dark grey	SC3PB	1.55 - 1.93	Whittaker et al, 1992. Zhang et al, 1998. Zhang, 2002.
	Greyish white	SC3PB	1.21 - 1.51	Whittaker et al, 1992. Zhang et al, 1998. Zhang, 2002.
Johnstone	w =18%	SECB	0.05	Harberfield & Johnstone, 1990
	w =18%	SCB	0.06	Harberfield & Johnstone, 1990
Andesite	Tampomas	CB	1.26 - 1.68	Abrahamsson et al, 1987
	Ankara andesite	MR	1.59	Şener, 2002
	Whitwick	CB	2.17	Bearman, 1999
Greywacke	Ingleton	CB	2.38	Bearman, 1999

Tested Material		Experimental Testing Method	Mode I Fracture Toughness Value (K_{IC}) ($MPa.m^{1/2}$)	Reference
	Cornish	CB	3.15	Bearman, 1999
Gabbro	Kallax	SR	2.58	Yi, 1987
	Kallax	SR	3.23	Yi, 1987
	FS—Fangshan	SR	0.34	Zhang et al., 1998
	FS—Fangshan	CNRBT	0.58	Zhang et al., 1998
Tuff	Ogino	SR	1.06	Matsuki et al, 1987
	Ogino	CB	1.08	Matsuki et al, 1987
	Göynük	SR	1.29	Şantay, 1990
Norite	Grey	SR	2.69	Meredith, 1983
Dolerite	Whin Sill	SR	3.26	Meredith, 1983

CNRBT: Circumferentially notched round bar in tension, **CT**: Compact specimen in tension, **HDB**: Single edge cracked half disc in three-point bending, **RBDT**: Round bar in direct tension, **ReBDT**: Rectangular bar in direct tension, **SC3PB**: Single edge straight through cracked rectangular plate in three-point bending, **SCR3PB**: Single edge straight through cracked round bar in three-point bending, **SECBD**: Single edge cracked Brazilian disk in diametral compression, **SENRBB**: Single edge notched round bar in bending, **SR**: Short rod.

Table 2.3 Comparison between fracture toughness testing methods for disc type specimens

(after Fowell and Chen, 1990; Lim et al., 1994b; and Chang et al., 2002)

Item of comparison	CCNBD	SCB	CB	SR
Method of obtaining mixed-mode conditions	Rotate specimen	Vary notch angle	None	None
Size of specimen	Small	Small	Long	Small
Preparation apparatus	Simple	Simple	Simple	Complex
Set-up of equipment	Simple	Simple	Complex	Complex
Loading machines	Compressive	Compressive	Compressive	Tensile
Loading method	Compressive	Three-point	Three-point	Tensile
Reproducible data	Excellent	Excellent	Reasonable	Reasonable
Requirement of testing	Ordinary	Ordinary	High	High

Table 2.4: Summary of Fracture Toughness and Corresponding Tensile Strength for Different Soils and Rocks.

Tested Material		Fracture Toughness Testing Method	K_{IC} (MPa.m$^{1/2}$)	Tensile Strength Testing Method	σt (MPa)	Reference
Coal		SC3PB	0.03	ReBDT	0.12	Bhagat, 1985
		SC3PB	0.06	ReBDT	0.22	Bhagat, 1985
		SC3PB	0.05	ReBDT	0.12	Bhagat, 1985
		SC3PB	0.27	ReBDT	0.93	Bhagat, 1985
		SC3PB	0.12	ReBDT	0.36	Bhagat, 1985
Dolostone	Falkirk	SR	1.66	B	13.3	Gunsallus KL, Kulhawy FH, 1984
	Kankakee	SR	1.66	B	16.4	Gunsallus KL, Kulhawy FH, 1985
	Markgraf	SR	1.8	B	12.1	Gunsallus KL, Kulhawy FH, 1986
	Oatka	SR	1.78	B	13	Gunsallus KL, Kulhawy FH, 1987
	Remeo	SR	2.47	B	17	Gunsallus KL, Kulhawy FH, 1988
Limestone	Irondequoit	SR	1.36	B	11.9	Gunsallus KL, Kulhawy FH, 1989
	Reynales	SR	2.06	B	15	Gunsallus KL, Kulhawy FH, 1990
	Saudi Arabia	SENRBB	0.39	B	2.31	Khan and Al-Shayea [11]
Sandstone	Grimsby	SR	1.47	B	10.1	Gunsallus KL, Kulhawy FH, 1991
Oil shale	Anvil points D-80 PB	SC3PB	1.08	DT	17	Schmidt RA, 1977
	Anvil points D-80 PB	SC3PB	0.98	DT	17	Schmidt RA, 1977

Tested Material		Fracture Toughness Testing Method	K_{IC} (MPa.m$^{1/2}$)	Tensile Strength Testing Method	σt (MPa)	Reference
	Anvil points D-160 PB	SC3PB	0.67	DT	12.5	Schmidt RA, 1977
	Anvil points D-160 PB	SC3PB	0.6	DT	12.5	Schmidt RA, 1977
	Anvil points D-160 VB	SC3PB	0.37	DT	3.3	Schmidt RA, 1977
			0.63		3	Haberfield and Johnston, 1989
			0.63		12	Haberfield and Johnston, 1989
Gabbro	FS—Fangshan	CNRBT	0.58	RBDT	6.2	Zhang et al. 1998
Diorite		SENRBB	3.21	B	14.7	Nordlund et al. [13]
Granite			0.95		4.5	Haberfield and Johnston, 1989
			0.95		5.5	Haberfield and Johnston, 1989
			2.53		37	Haberfield and Johnston, 1989
	Stripa	SCR3PB	2.15	B	15.4	Zhang et al. 1998
	TGP	SENRBB	2.08	B	9.5	Yu, 2001
Micrite			0.95		4	Haberfield and Johnston, 1989
Syenite			1.11		7.5	Haberfield and Johnston, 1989
			1.26		12	Haberfield and Johnston, 1989
Marble		SECB	0.63	3PB	18	Haberfield and Johnston, 1989
		SECB	0.95	3PB	22	Haberfield and Johnston, 1989
		SECB	1.26	3PB	17	Haberfield and

Tested Material		Fracture Toughness Testing Method	K_{IC} (MPa.m$^{1/2}$)	Tensile Strength Testing Method	σt (MPa)	Reference
						Johnston, 1989
		SECB	1.64	3PB	15	Haberfield and Johnston, 1989
	FS—Fangshan	SR	2.68	B	17.3	Zhang et al. 1998
	FS—Fangshan	SR	1.13	B	7.3	Zhang et al. 1998
	FS—Fangshan	SR	0.21	B	3.5	Zhang et al. 1998
Basalt		SECB	2.09	3PB	22	Haberfield and Johnston, 1989
Mudstone	Melbourne	SECB	0.019 - 0.17	3PB	0.2 - 1.3	Haberfield and Johnston, 1989
Johnstone		SECB	0.044 - 0.079	3PB	0.2 - 0.58	Haberfield and Johnston, 1989

3PB: Three-point bending, **B:** Brazilian test, **BDT:** Uncracked Brazilian disk test, **CNRBT:** Circumferentially notched round bar in tension, **DT:** Direct tension, **ReBDT:** Rectangular bar in direct tension, **SC3PB:** Single edge straight through cracked rectangular plate in three-point bending, **SCR3PB:** Single edge straight through cracked round bar in three-point bending, **SECB:** Single edge cracked Brazilian disk, **SENRBB:** Single edge notched round bar in bending, **SR:** Short rod.
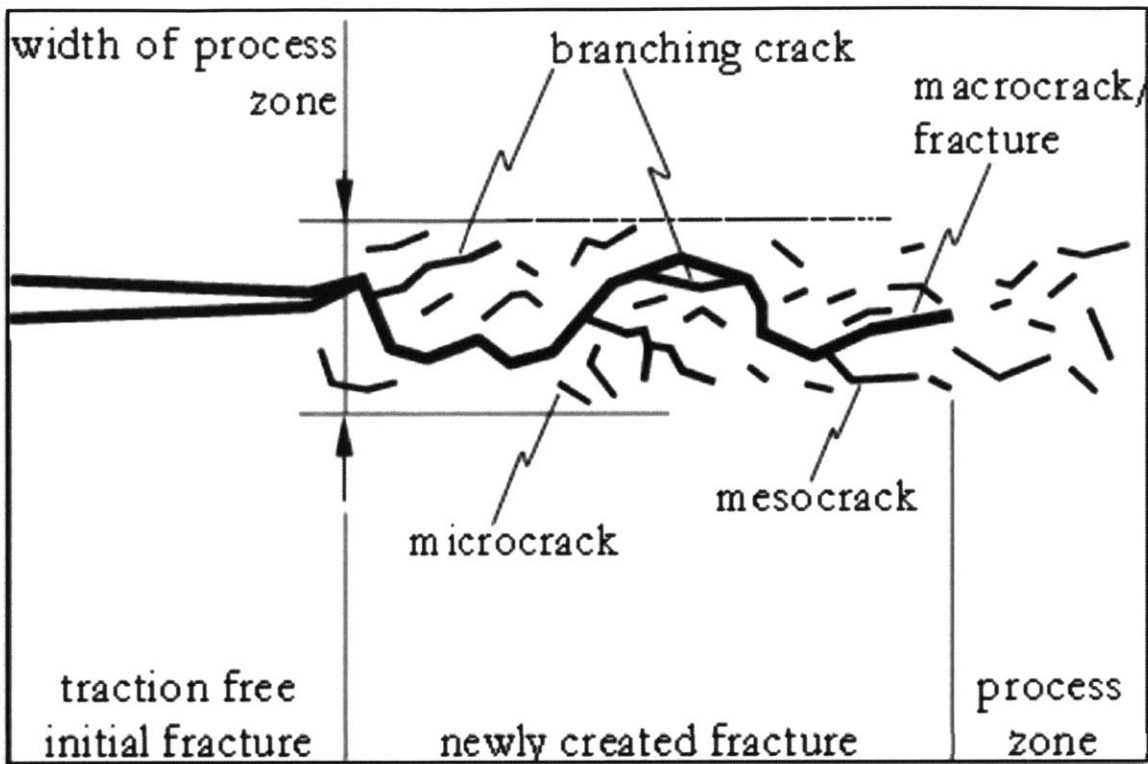
Figure 2.1: The nomenclature of a fracture system; fracture with surrounding fracture process zone (FPZ). The process zone consists of micro- and mesocracks. (After Backers, 2004 and Modified from Liu et al., 2000)
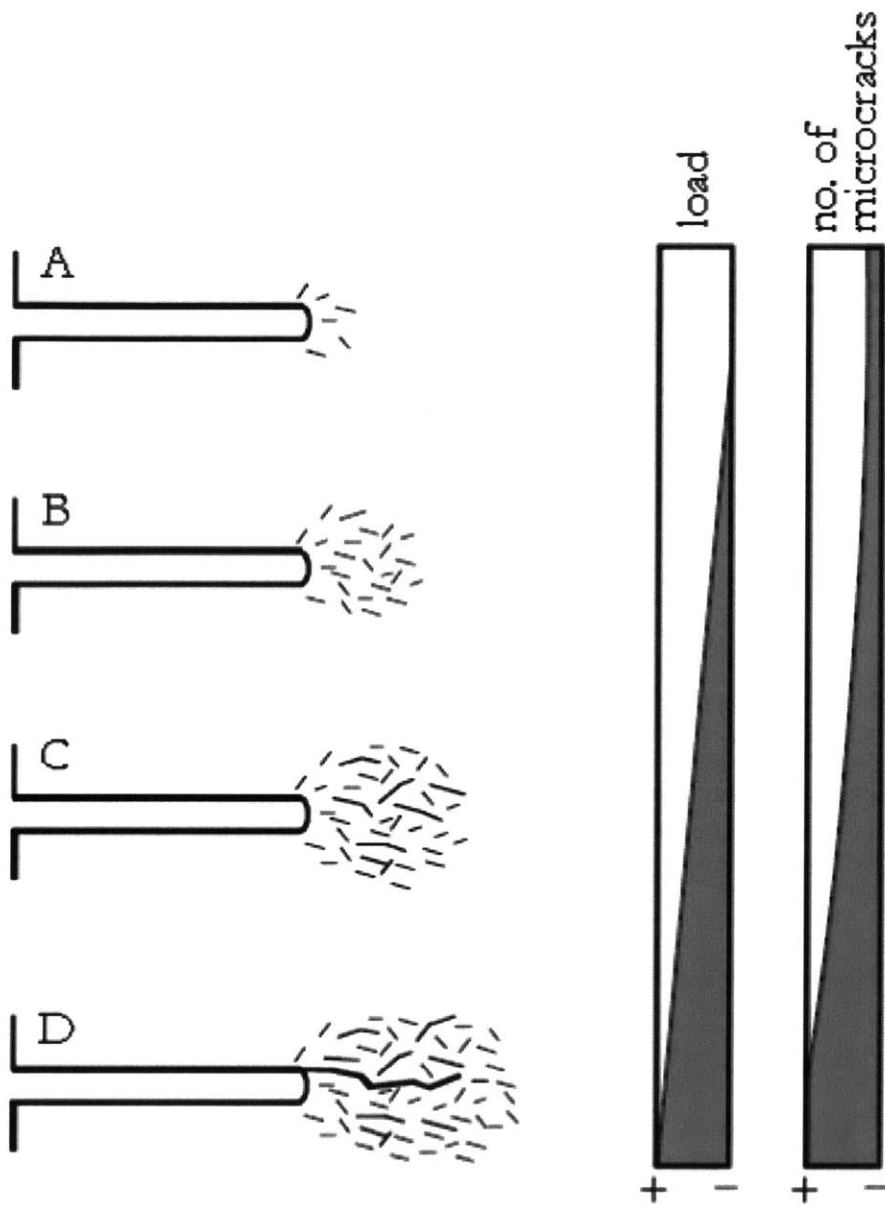
Figure 2.2: The development of a fracture and fracture process zone under a tensile load perpendicular to a starter notch. The schematic sequence A to D shows (micro-crack) to (meso-crack) to (macro-crack) development with load increase. (After Backers, 2004 and Modified from Hoagland at al., 1973)
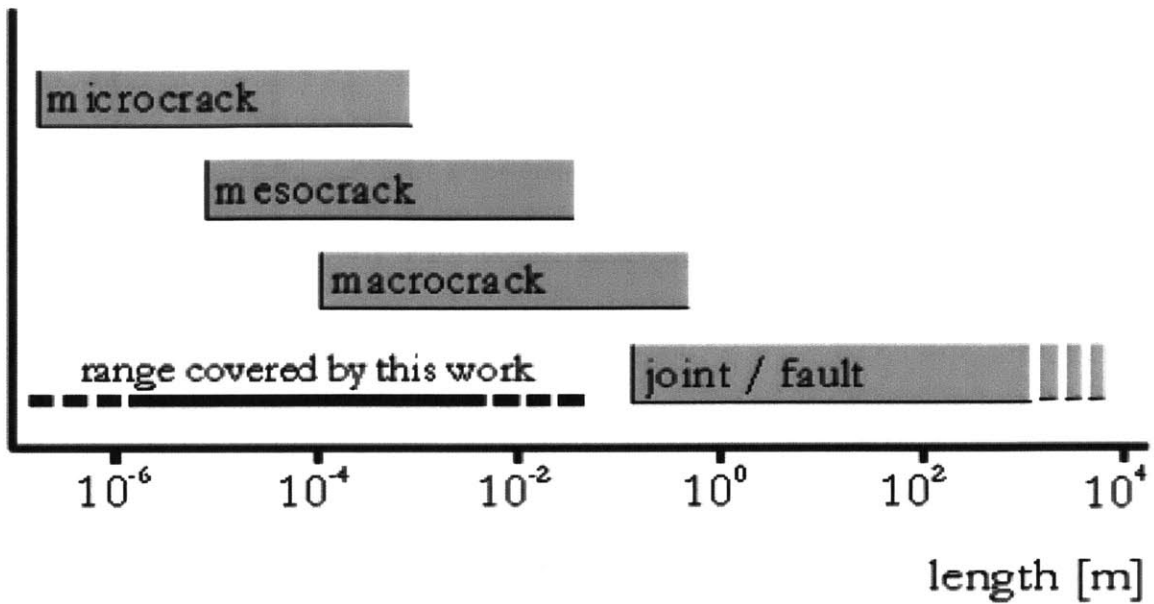
Figure 2.3: Length range of different types of discontinuities in rock (After Backers, 2004)
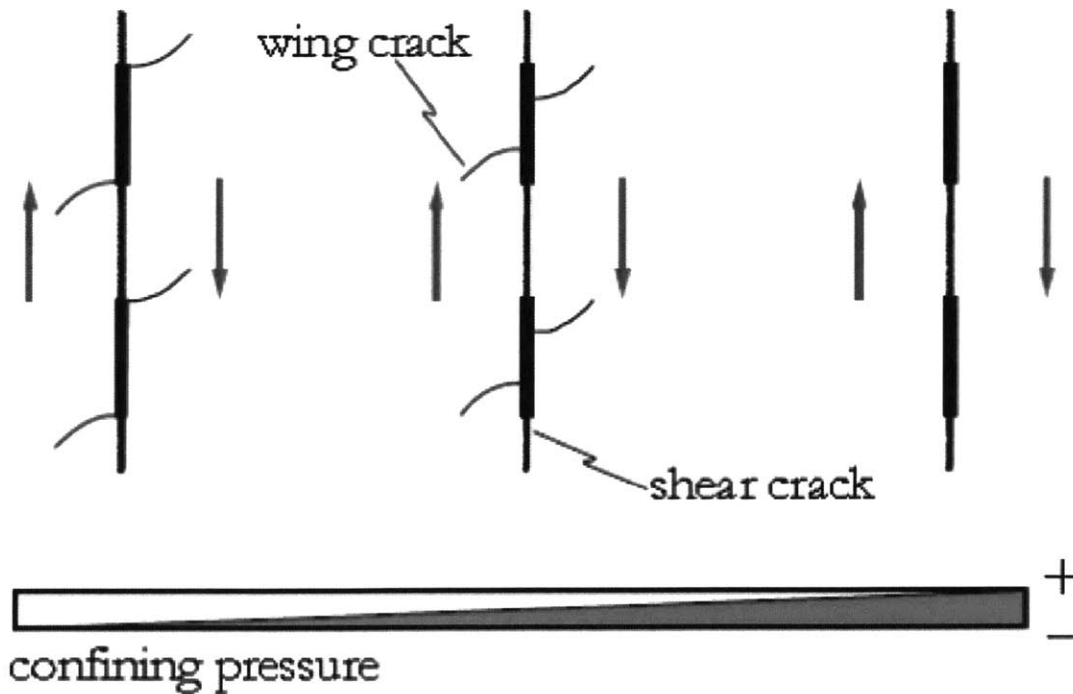
Figure 2.4: Set-up for fracture coalescence in shear and the influence of confining pressure on the fracture pattern as described by Bobet and Einstein (1998). (Backers, 2004)
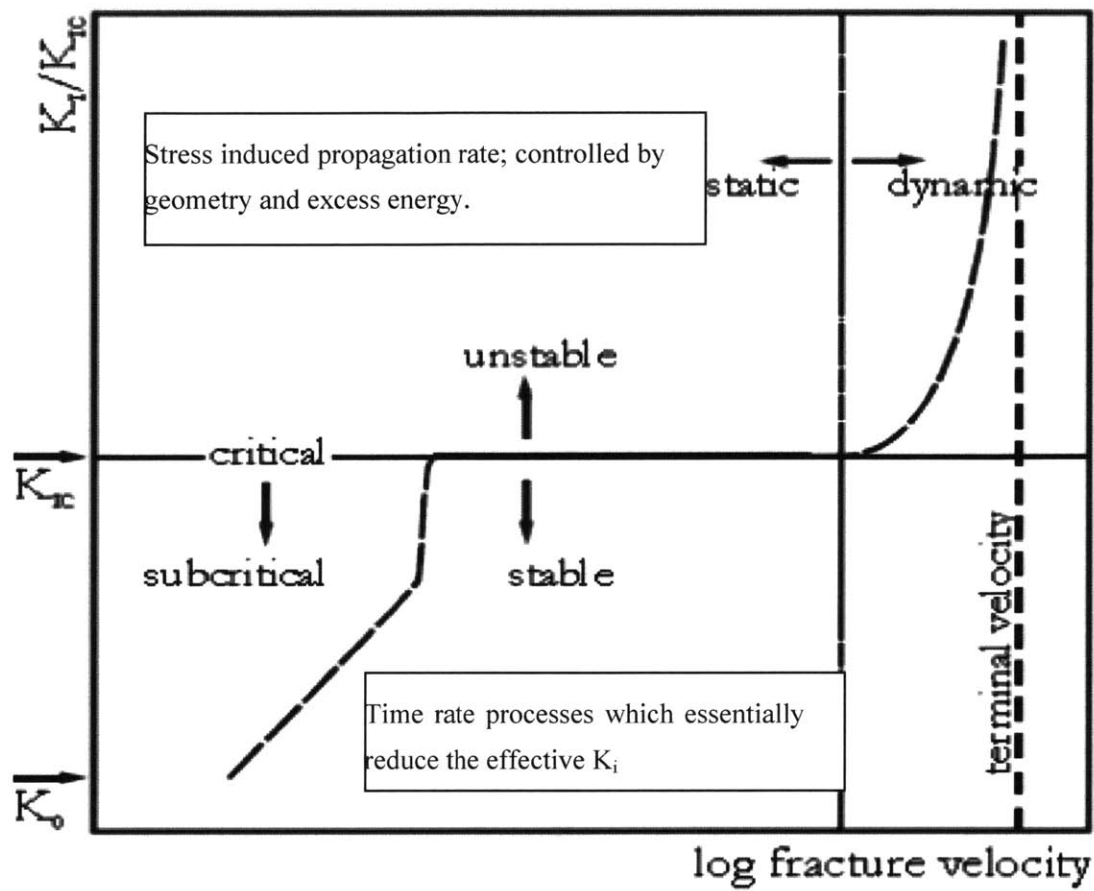
Figure 2.5: Static-dynamic versus stable-subcritical-critical-unstable fracture growth. Schematic plot of K vs. fracture velocity of Mode I. (After Backers, 2004, Zhang et al., 1999, and Atkinson, 1984)
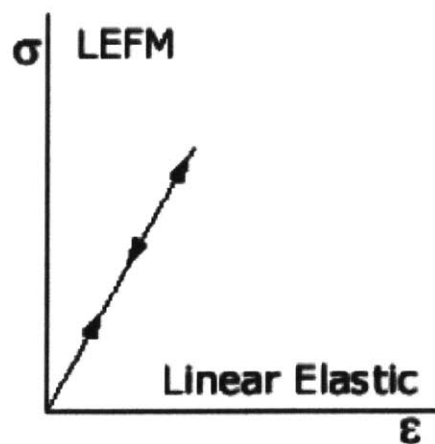
Figure 2.6: Stress – strain curve of the LEFM (after Alkiliçgil, 2006)
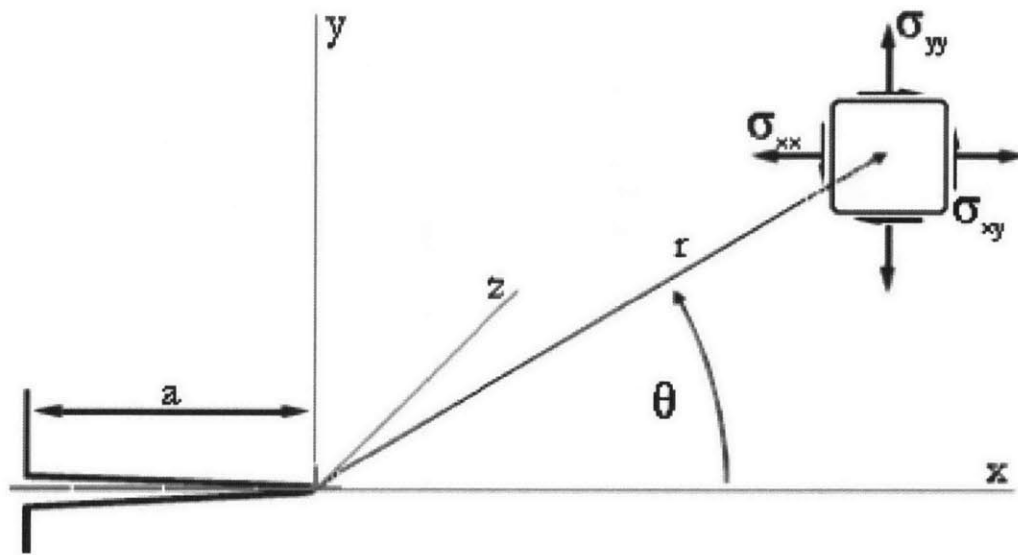
Figure 2.7: Notations within Cartesian co-ordinate system for stress tensor (After Backers, 2004)
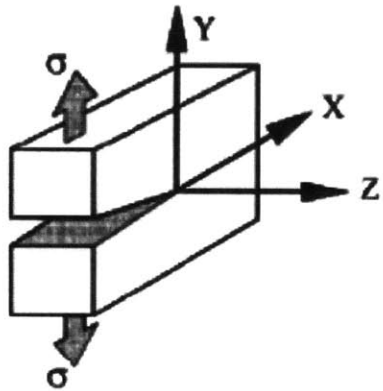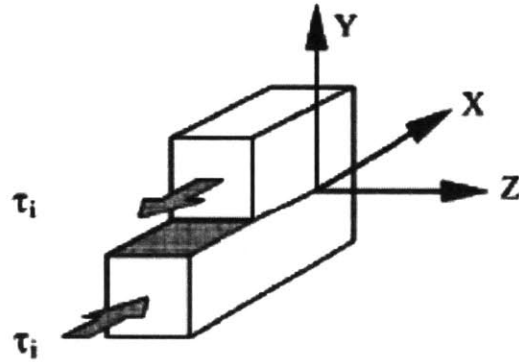
Mode-I: Opening mode   Mode-II: Sliding mode   Mode-III: Tearing mode
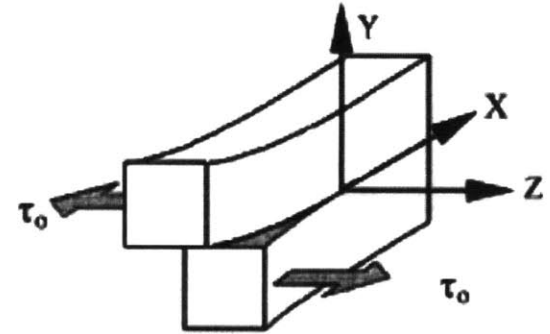
Figure 2.8: Modes of displacement for a crack surface corresponding to three basic modes of loading for a crack
(Whittaker at al., 1992)
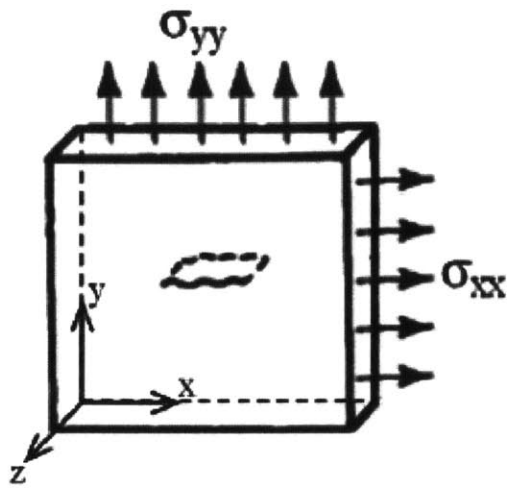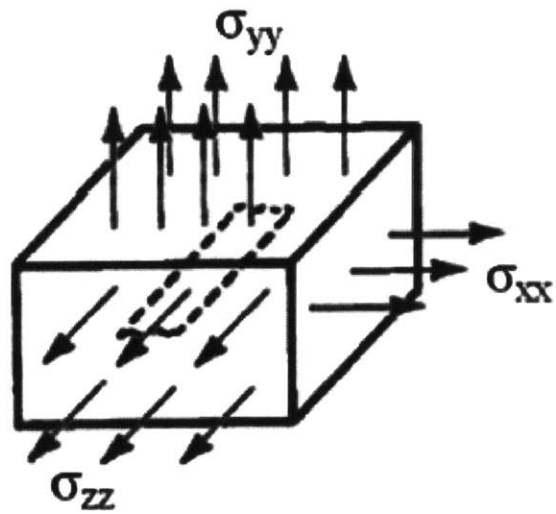
Figure 2.9: Plane stress and plane strain conditions for plates under biaxial tensile stresses (after Alkiliçgil, 2006)
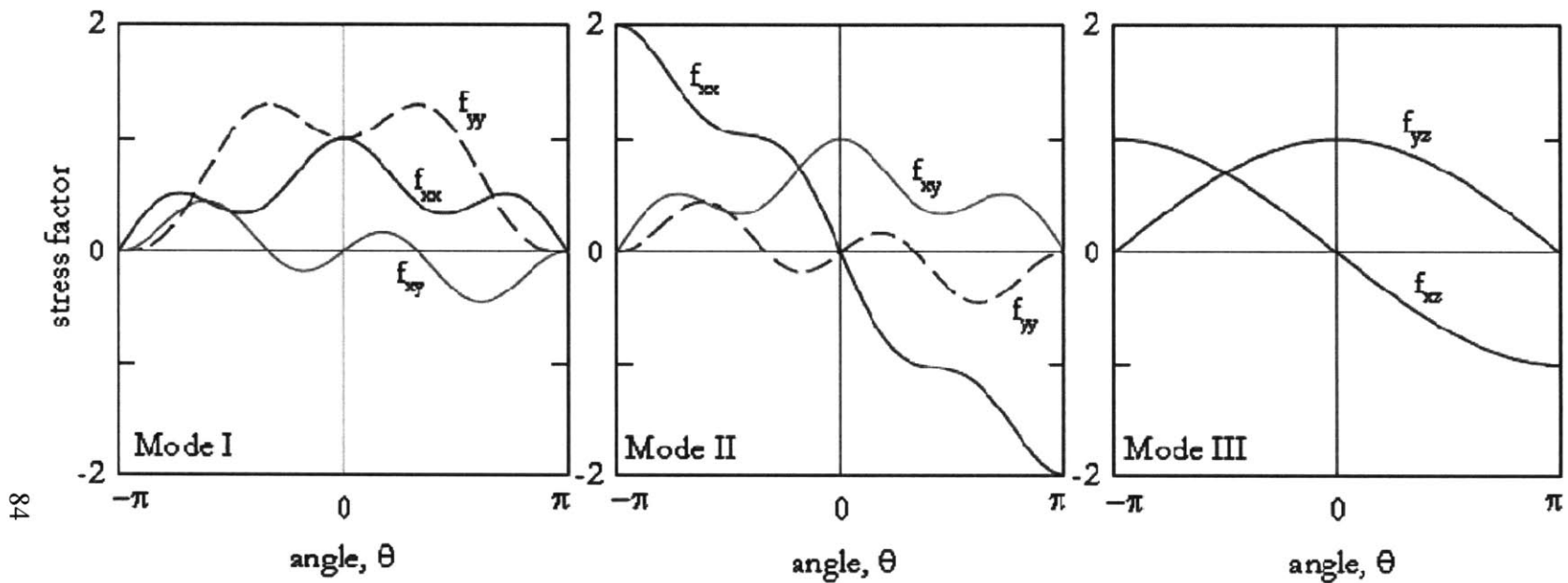
Figure 2.10: Stress distribution in terms of stress factor (f$_{ij}$) around crack trip for different pure modes of loading based on linear elastic calculations (After Backers, 2004 and Broberg, 1999)
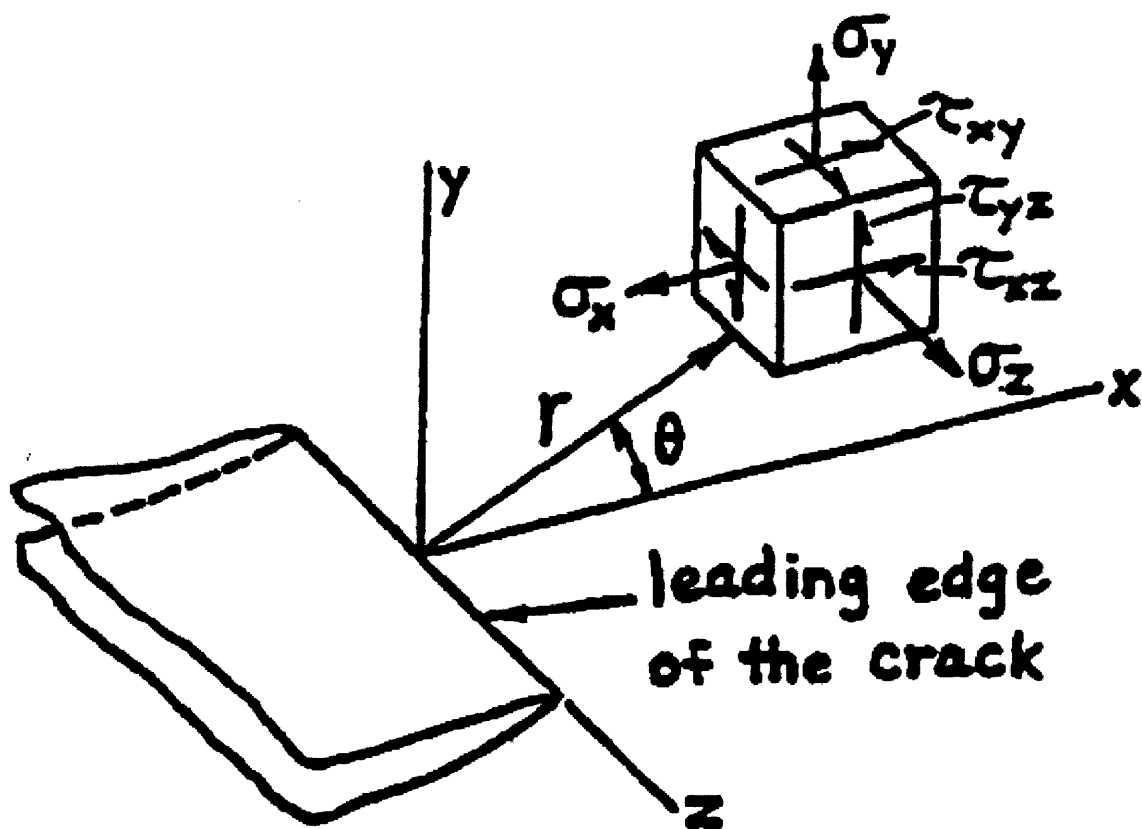
Figure 2.11: Coordinate system for a crack tip (after Tada el al., 2000)

$$K_I = \sigma\sqrt{\pi a}$$

(a)

$$K_I = 1.12\sigma\sqrt{\pi a}$$

(b)

$$K_I = \sigma\sqrt{\pi a}\left[1 + 2.365\left(\frac{R}{R+a}\right)^{2.4}\right]$$

(c)

$$K_I = \sigma\sqrt{\pi a}\left[\frac{2w}{\pi a}\tan\left(\frac{a}{2w}\right)\right]^{1/2}$$

(d)
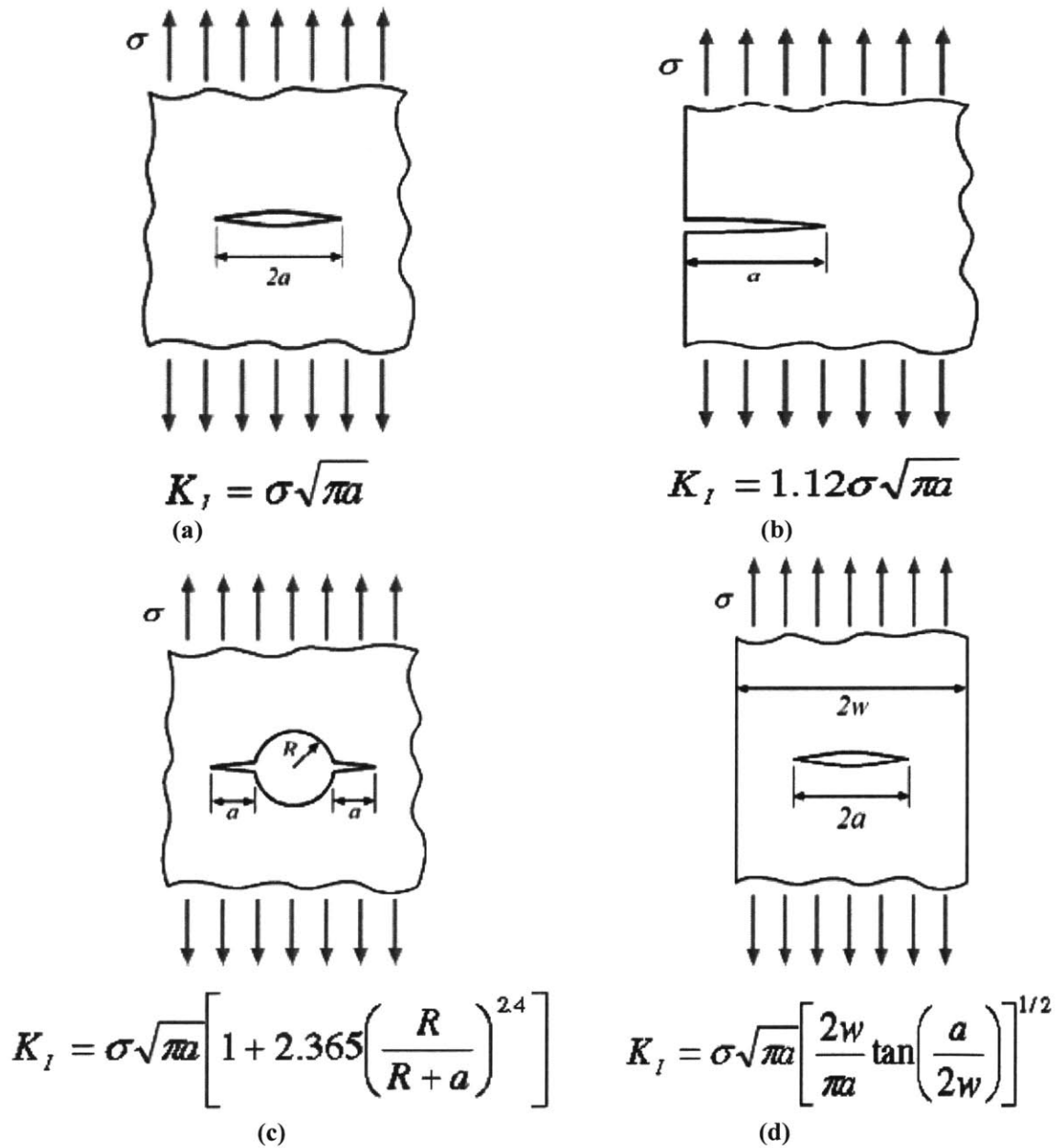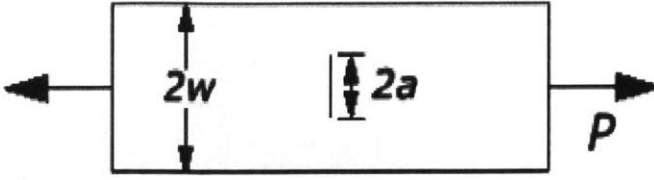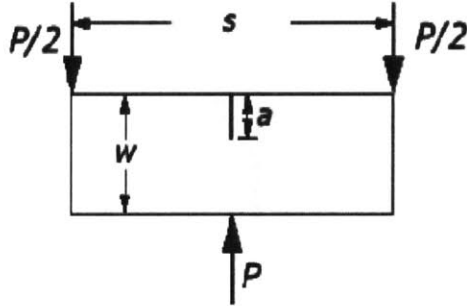
Figure 2.12: K_I **calculations for common loading conditions; a: Semi-infinite plate with a center through crack under tension, b: Semi-infinite plate with an edge through crack under tension, c: Infinite plate with a hole and symmetric double through cracks under tension d: Semi-infinite plate with an edge through crack under tension, (after Alkiliçgil, 2006)**

$$K_I = \frac{P}{B\sqrt{w}}\left\{\sqrt{\frac{\pi a}{2w}\sec\left(\frac{\pi a}{2w}\right)}\left[1 - 0.025\left(\frac{a}{w}\right)^2 + 0.06\left(\frac{a}{w}\right)^4\right]\right\}$$

(e)

$$K_I = \frac{P}{B\sqrt{w}}\left\{\frac{3\frac{s}{w}\sqrt{\frac{a}{w}}}{2\left(1+2\frac{a}{w}\right)\left(1-\frac{a}{w}\right)^{\frac{3}{2}}}\left\{1.99 - \frac{a}{w}\left(1-\frac{a}{w}\right)\left[2.15 - 3.93\frac{a}{w} + 2.7\left(\frac{a}{w}\right)^2\right]\right\}\right\}$$

(f)

Figure 2.13: K_I calculations for common loading conditions; e: Center cracked specimen under tension, f: Single edge notched specimen under bending (after Alkiliçgil, 2006)
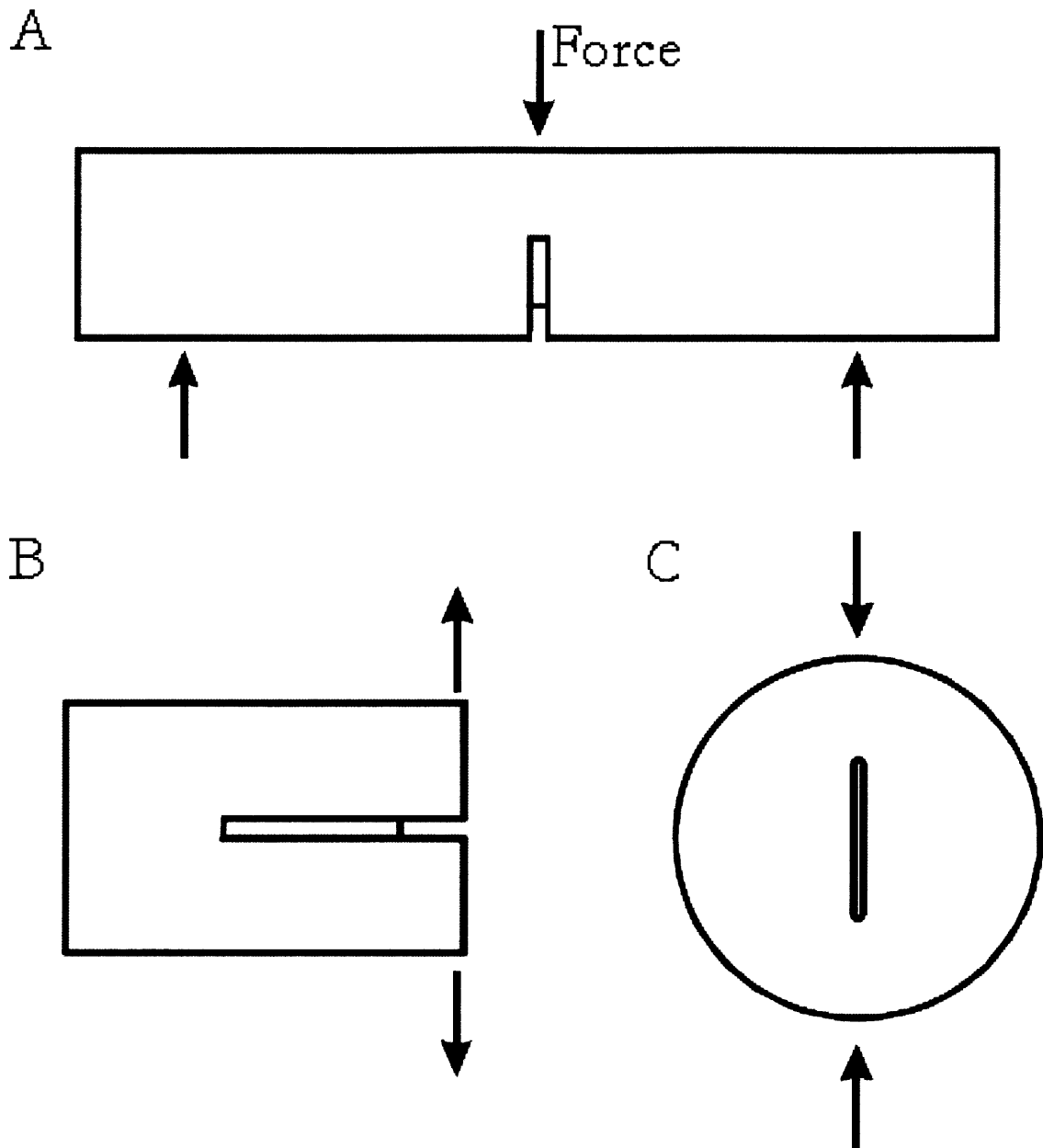
Figure 2.14: ISRM Suggested Methods for determination of Mode I fracture toughness; A: Chevron Bend Method by Ouchrerlony, 1988 (CB), B: Short Rod Method by Ouchrerlony, 1988 (SR), and C: Cracked Chevron Notched Brazilian Disc Method by Fowell, 1995 (CCNBD) (After Backers, 2004)
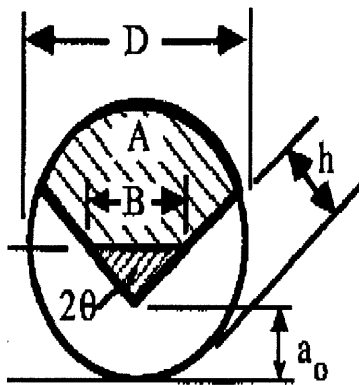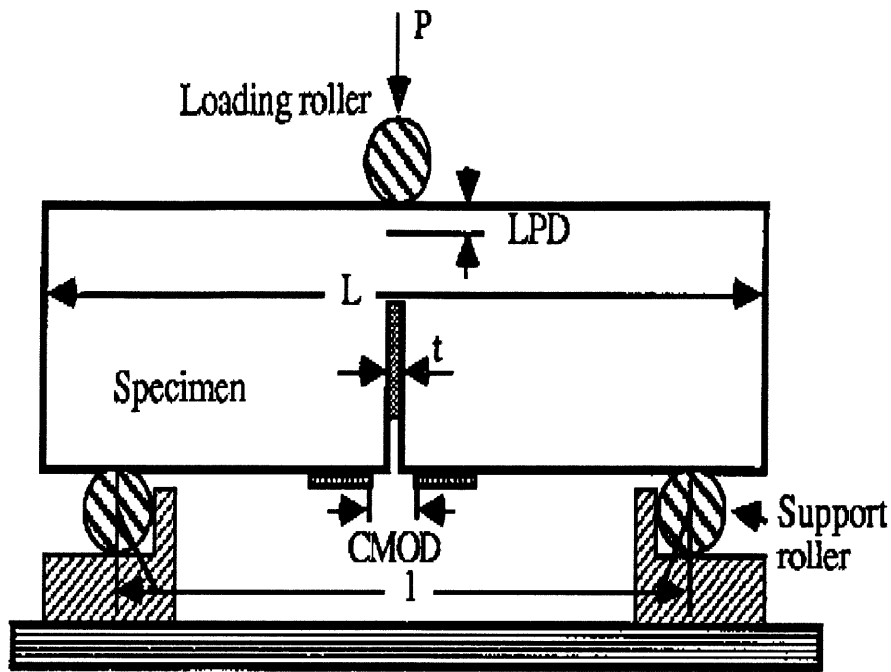
Notations:

A = Ligament area
D = Specimen diameter
l = Loading span, 3.33D
a = Crack length
a_0 = Chevron tip distance from specimen surface, 0.15D
h = Depth of cut in notch flank
B = Crack front width
t = Notch width
L = Specimen length
P = Applied load
2θ = Chevron angle, 90°

Figure 2.15: The CB specimen and testing configuration (after ISRM, 1980; Whittaker et al., 1992; and Donovan, 2003)

89
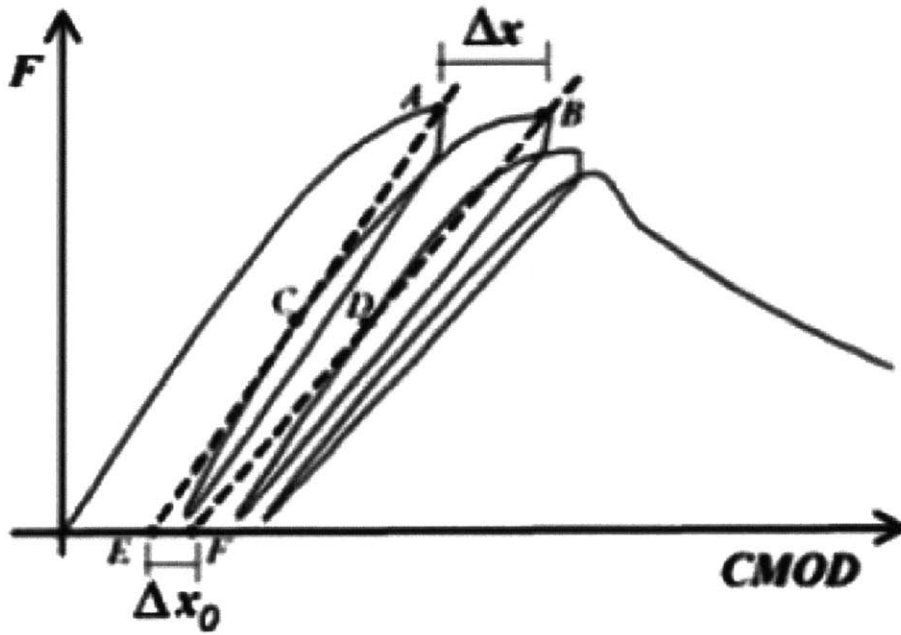
Figure 2.16: Definitions for computation of correction factor based on load and crack mouth opening displacement (CMOD) curve (after Sousa and Bittencourt, 2001)
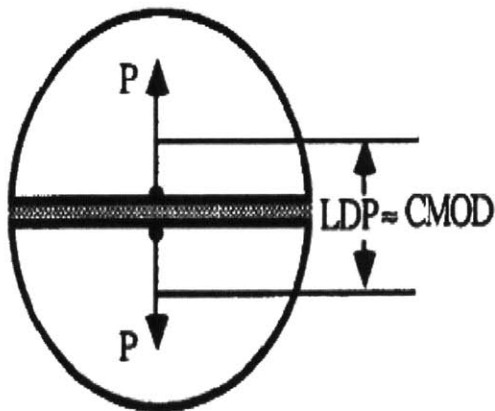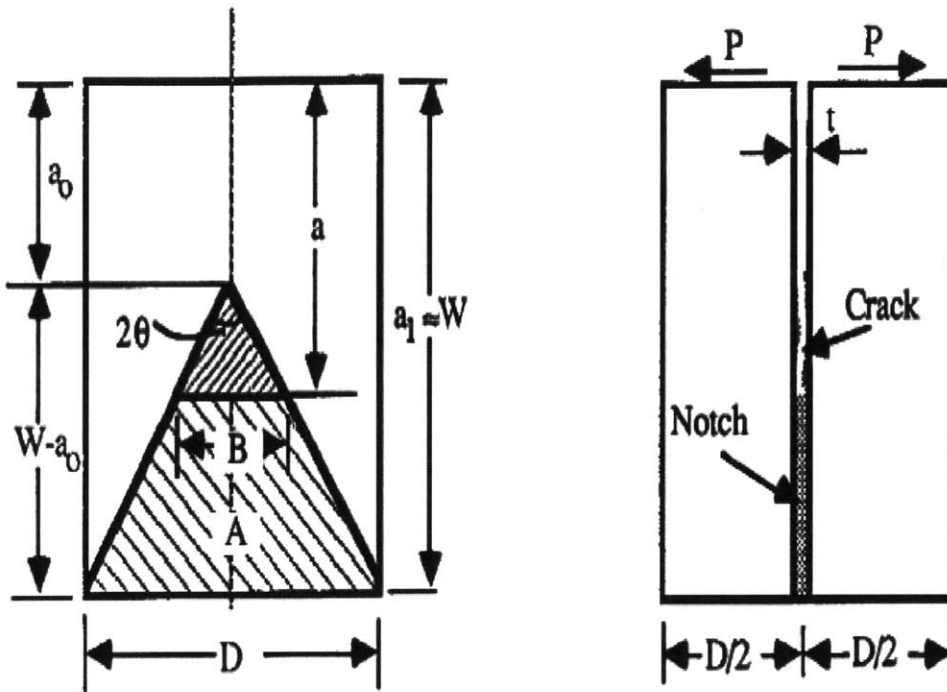
Notations:

A = Ligament area
D = Specimen diameter
a = Crack length
a_0 = Chevron tip distance from load line, 0.48D
a_1 = Maximum depth of chevron flanks, $a_1 \approx$ W
B = Crack front width
t = Notch width
W = Specimen height
P = Applied load at the notch mouth
2θ = Chevron angle, 54.6°

Figure 2.17: The SR specimen and test configuration (after ISRM, 1988; Whittaker et al., 1992; and Donovan, 2003)

91
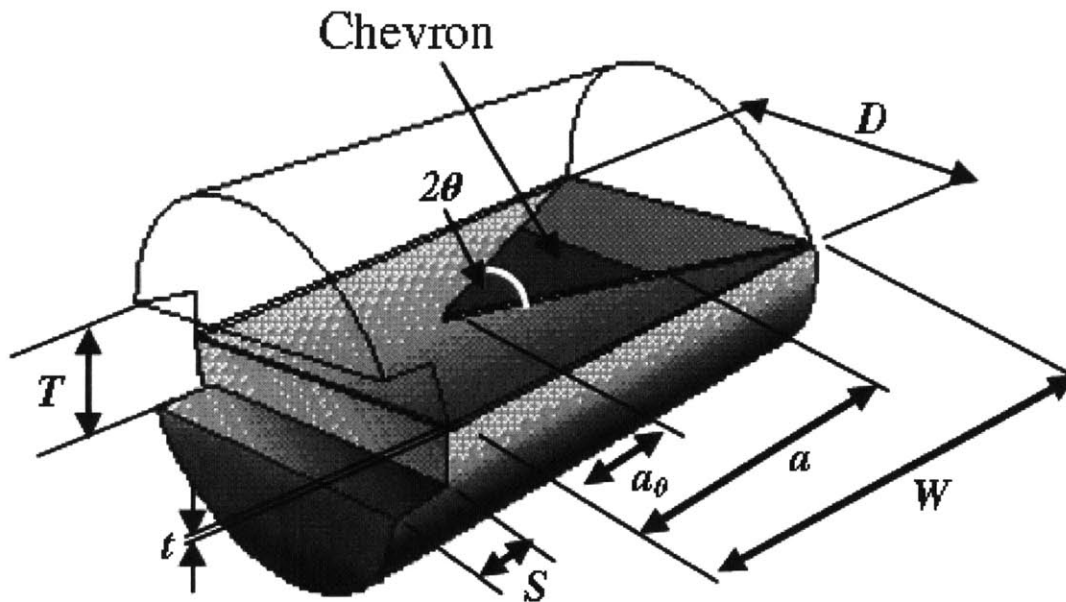
Figure 2.18: Short rod specimen dimensions (after Alkiliçgil, 2006)
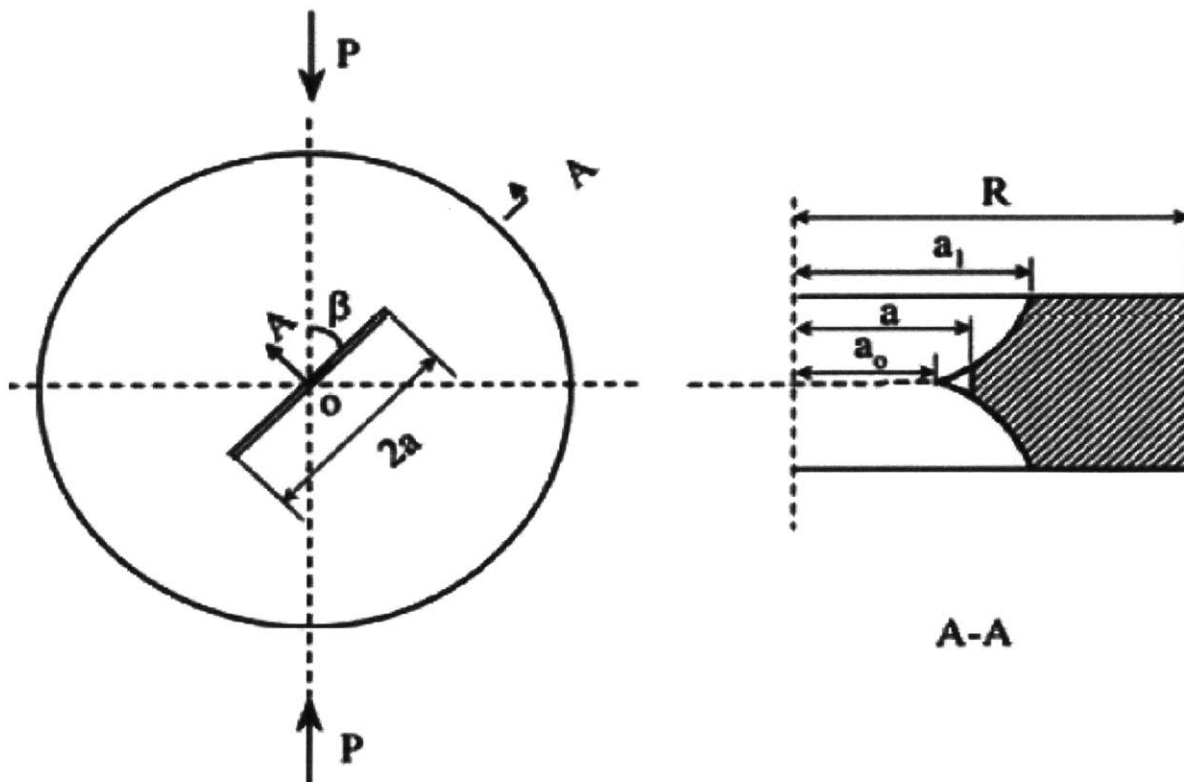
Figure 2.19: CCNBD under diametrical compression (after Khan and Al-Shayea, 2000 and Alkiliçgil, 2006)

(a) First cut

h_c

CCNBD Disc

(b) second cut

D

B

D_s

Diamond saw
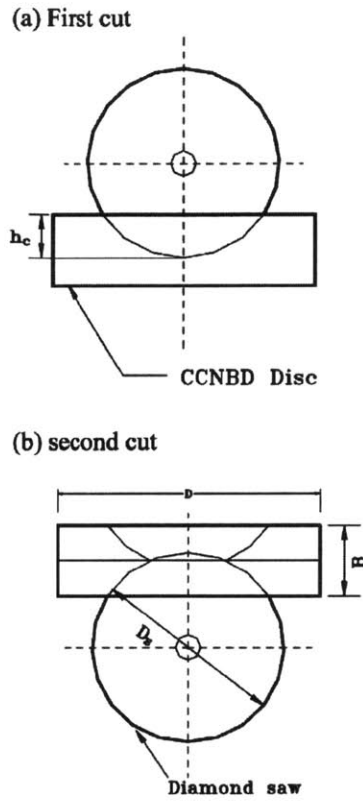
D_c: Saw diameter

Figure 2.20: Cutting Procedure of CCNBD specimen (after Chang et al., 2002)

Load cell

Specimen

R   β

2l

LVDT

Data Logger   PC
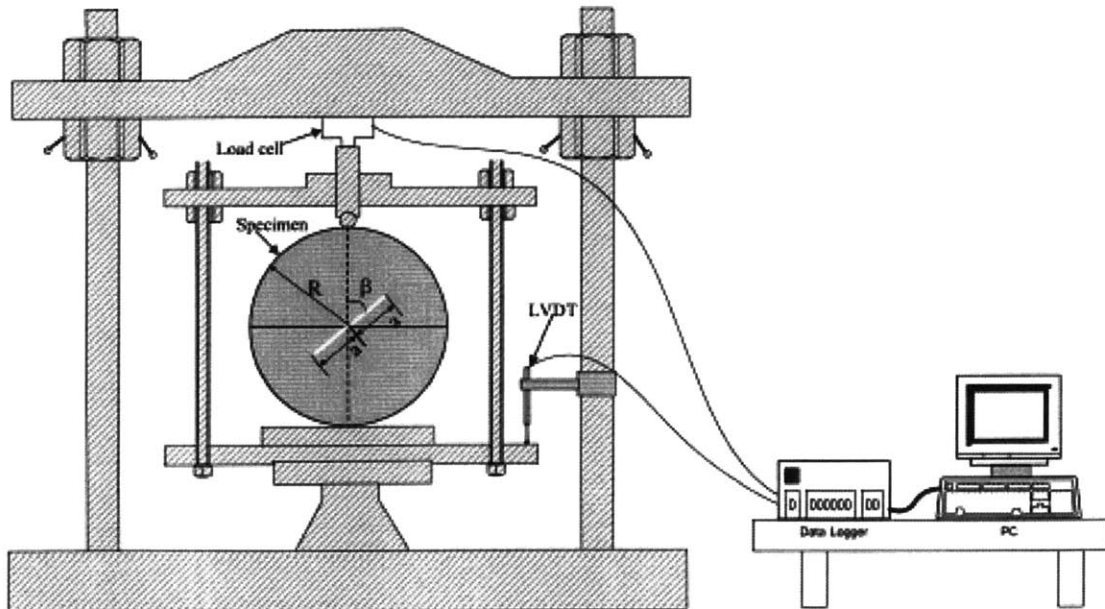
Figure 2.21: Loading setup for fracture testing on CCNBD specimen (after Khan and Al-Shayea, 2000 and Alkiliçgil, 2006)

93
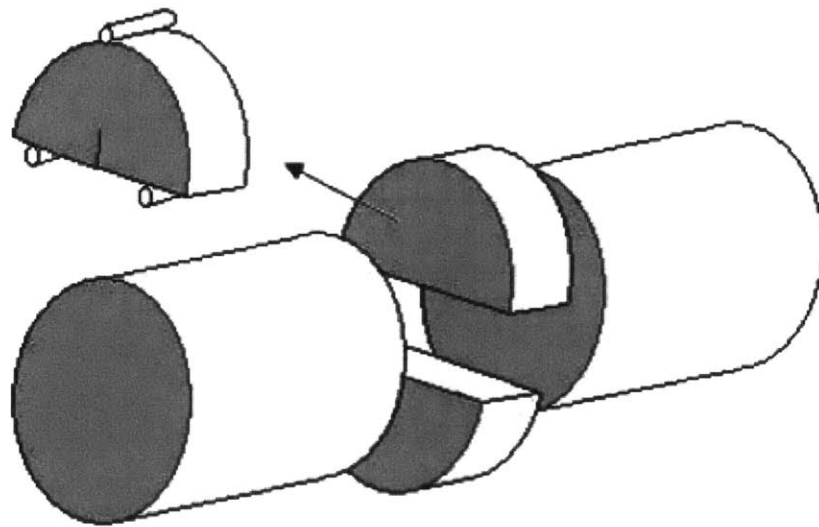
Figure 2.22: Cutting of Semi circular bend (SCB) specimens (after Alkiliçgil, 2006)
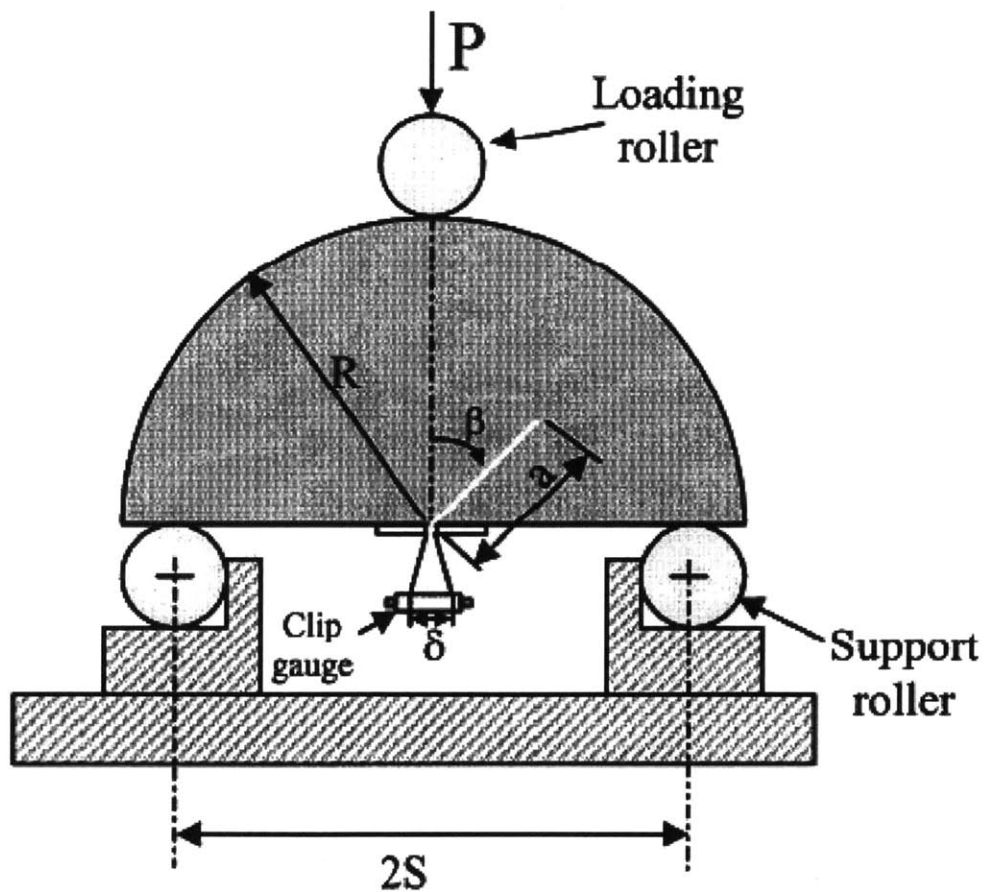
Figure 2.23: A semi circular specimen containing an angled edge crack under three point bending loading (after Khan and Al-Shayea, 2000 and Alkiliçgil, 2006)
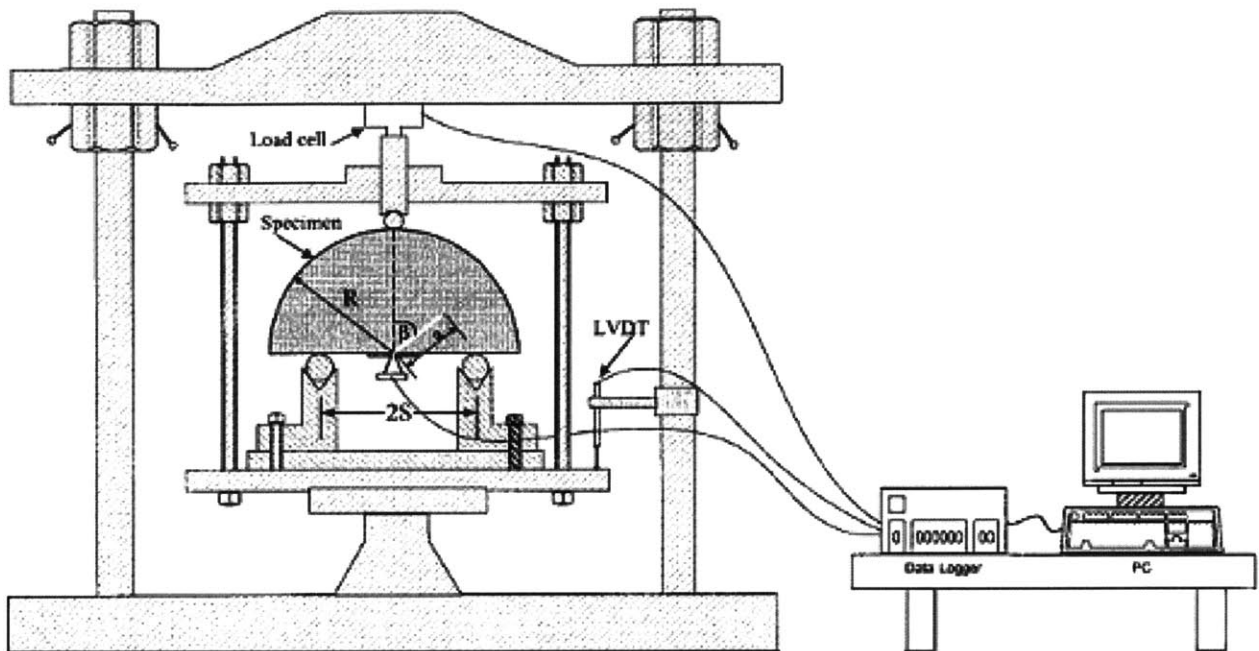
Figure 2.24: Loading setup for fracture testing on SCB specimen (after Khan and Al-Shayea, 2000 and Alkiliçgil, 2006)
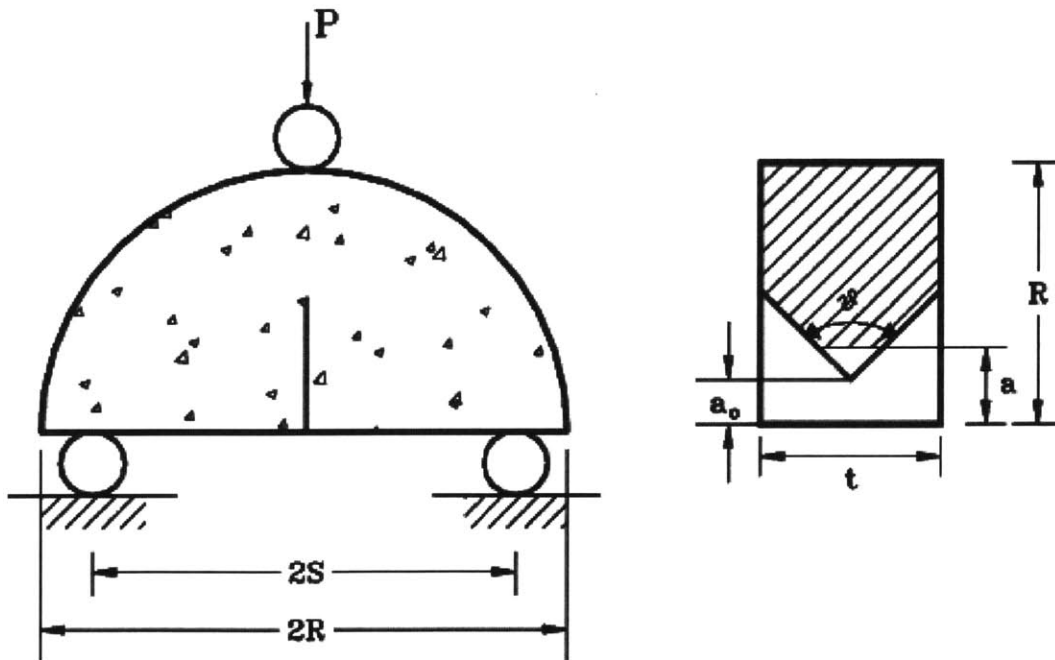
Figure 2.25: The Chevron Notched Semi Circular Bend (CNSCB) Specimen (Chang et al., 2002)
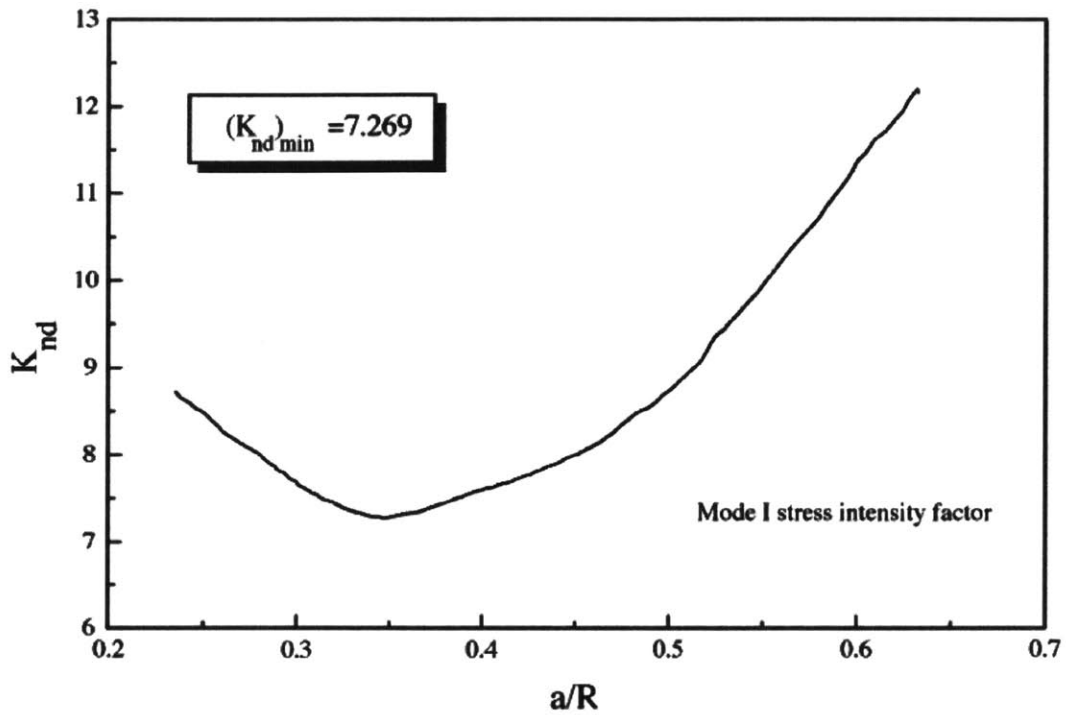
Figure 2.26: Normalized mode-I stress intensity factor for CNSCB specimen (Chang et al., 2002)
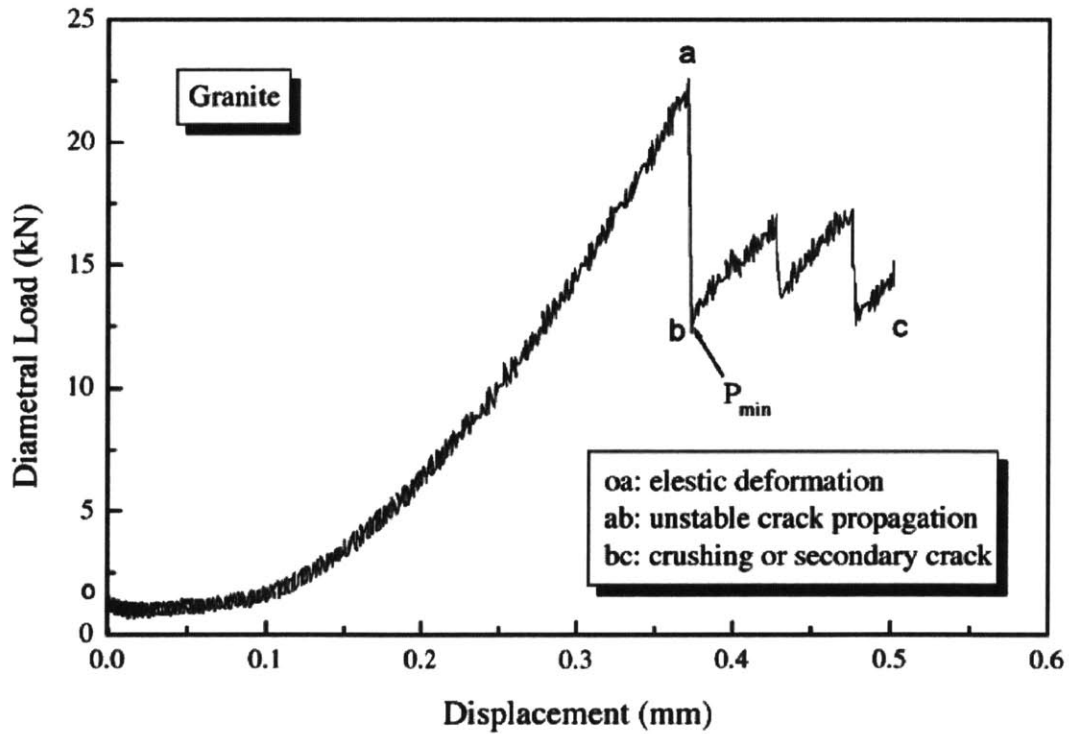
Figure 2.27: Typical failure curve for a BD specimen (after Chang et al., 2002)
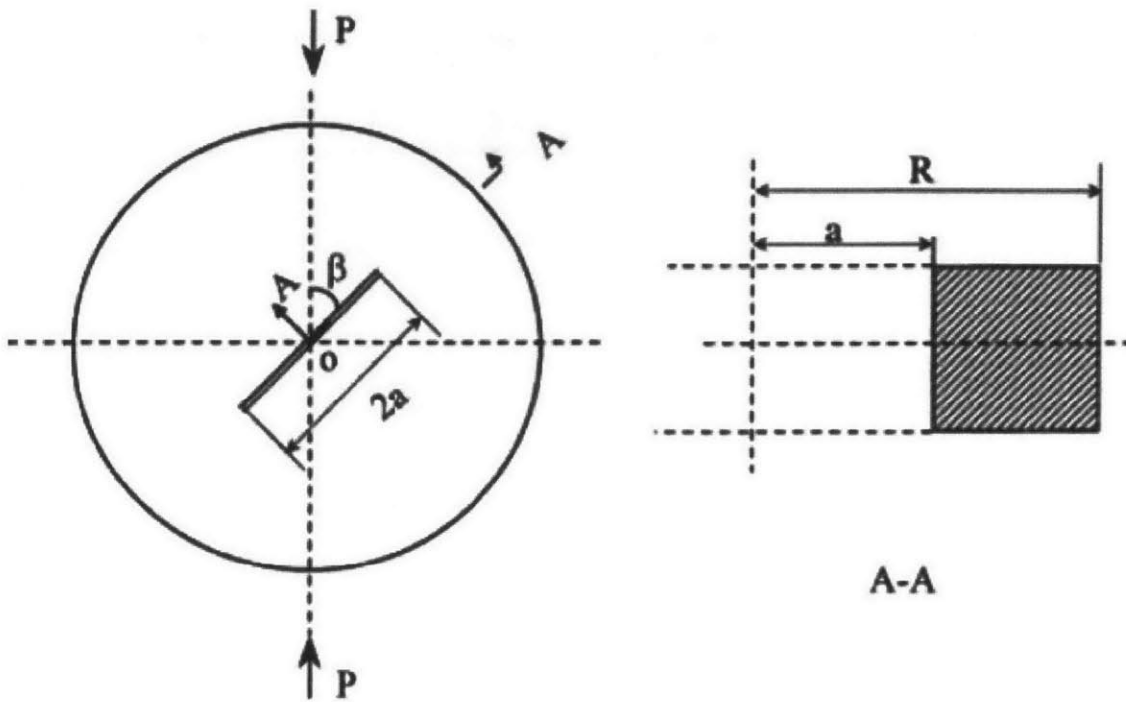
Figure 2.28: SNBD under diametrical compression (after Khan and Al-Shayea, 2000 and Alkiliçgil, 2006)
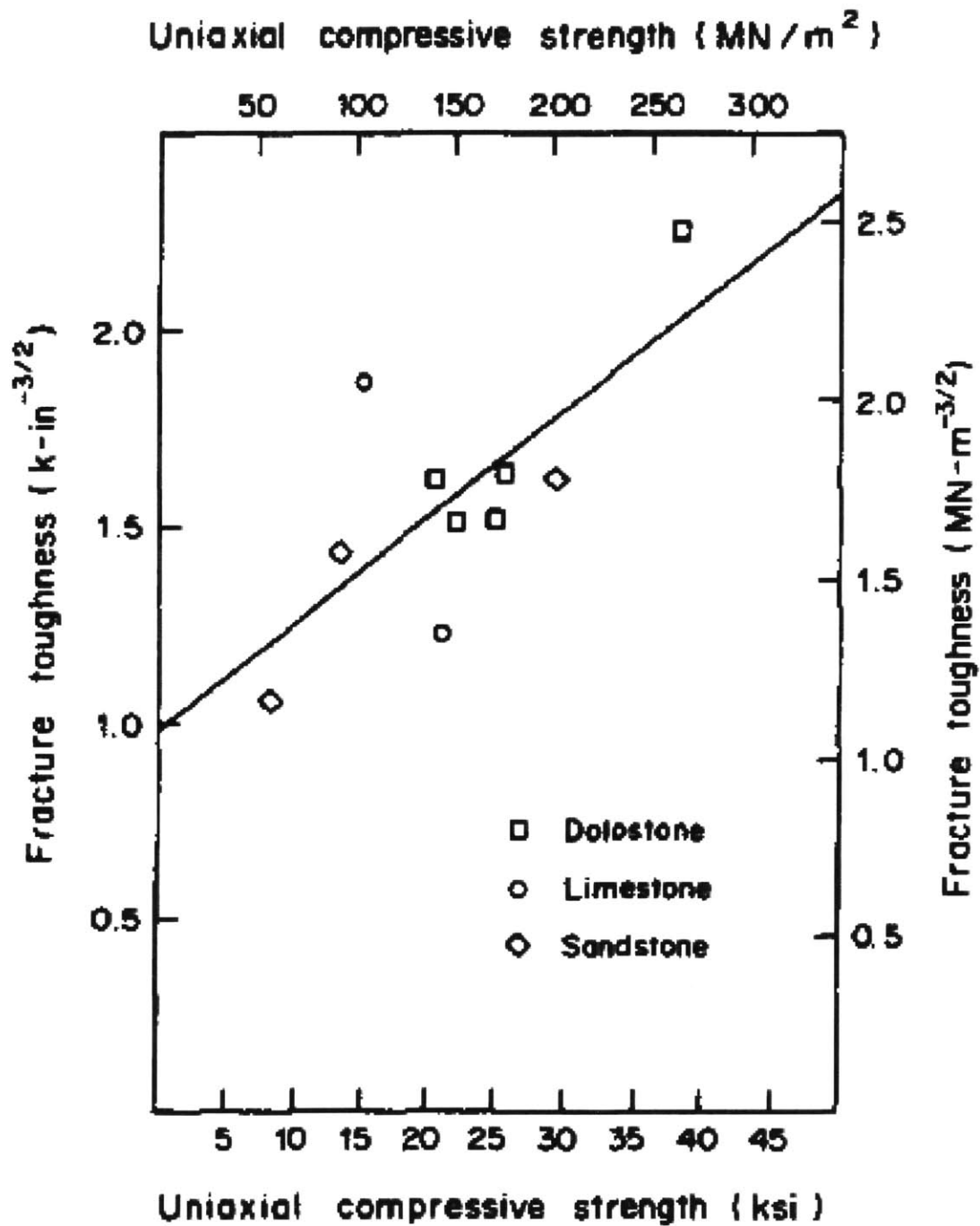
Figure 2.29: Fracture toughness versus uniaxial compressive strength of Dolostone, Limestone, and Sandstone (Gunsallus and Kulhawy, 1984)
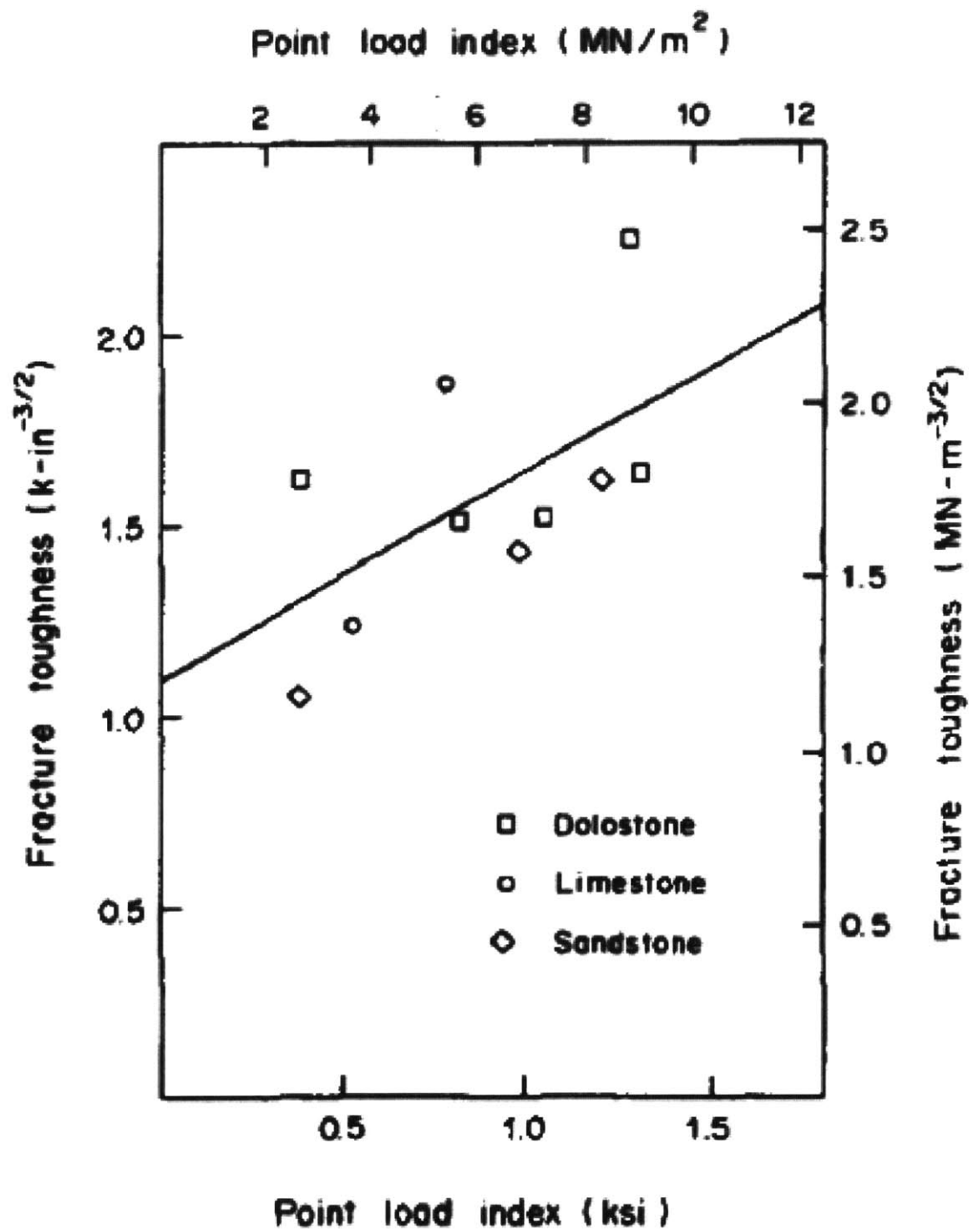
Figure 2.30: Fracture toughness versus point load index of Dolostone, Limestone, and Sandstone (Gunsallus and Kulhawy, 1984)

99
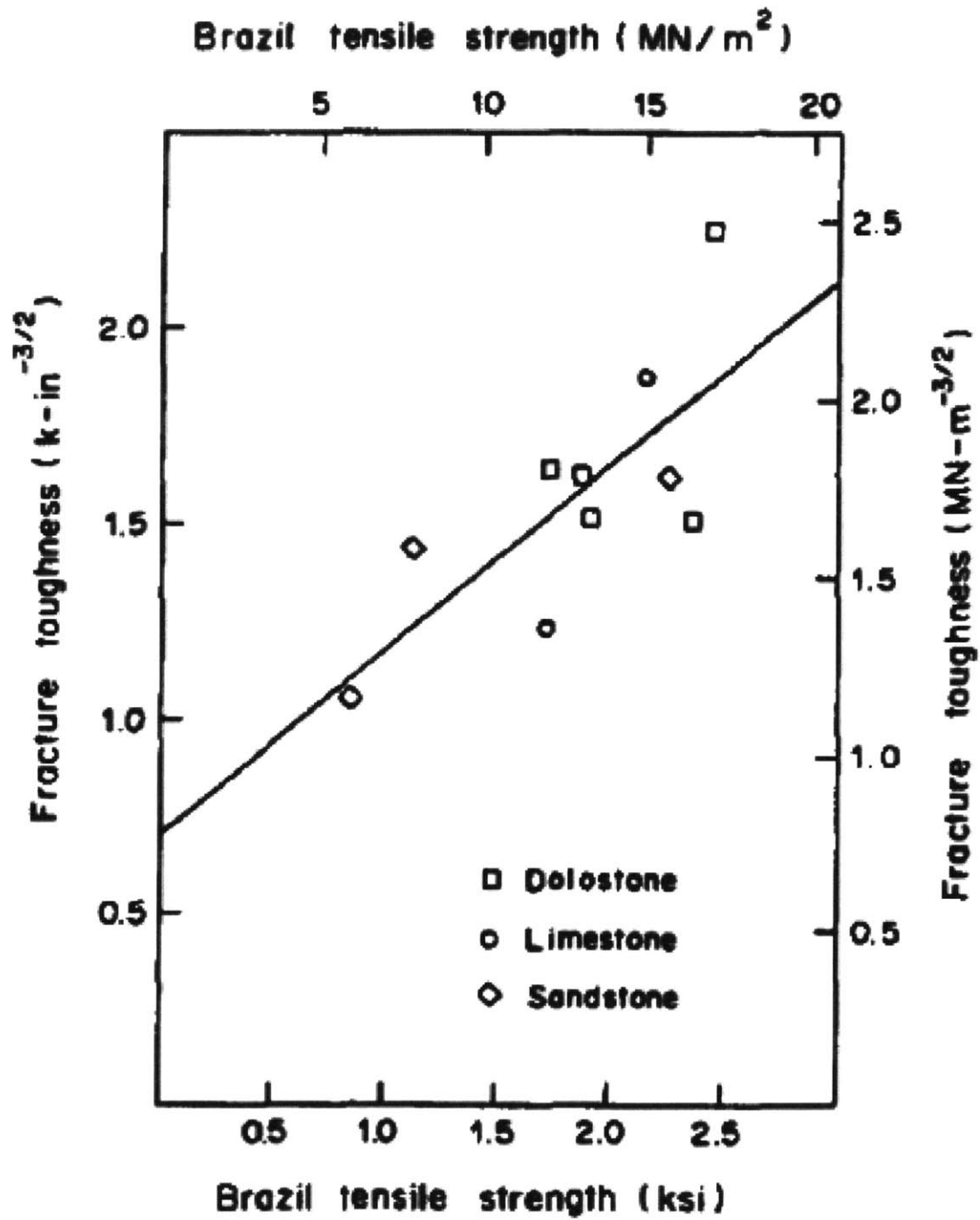
Figure 2.31: Fracture toughness versus Brazil tensile strength of Dolostone, Limestone, and Sandstone (Gunsallus and Kulhawy, 1984)
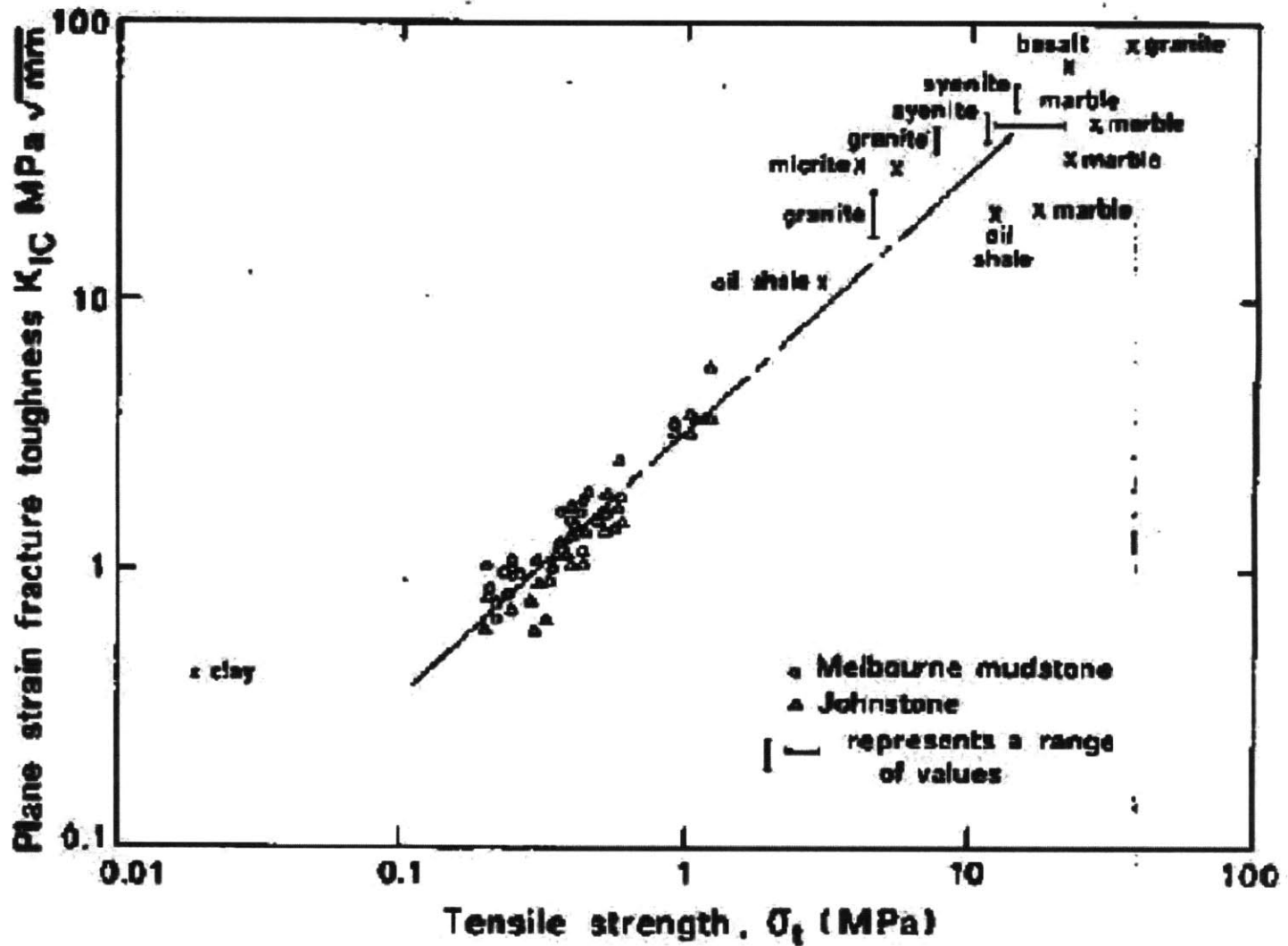
Figure 2.32: Relationship between plane strain fracture toughness and tensile strength for some rocks and soils (Haberfield and Johnston, 1989)
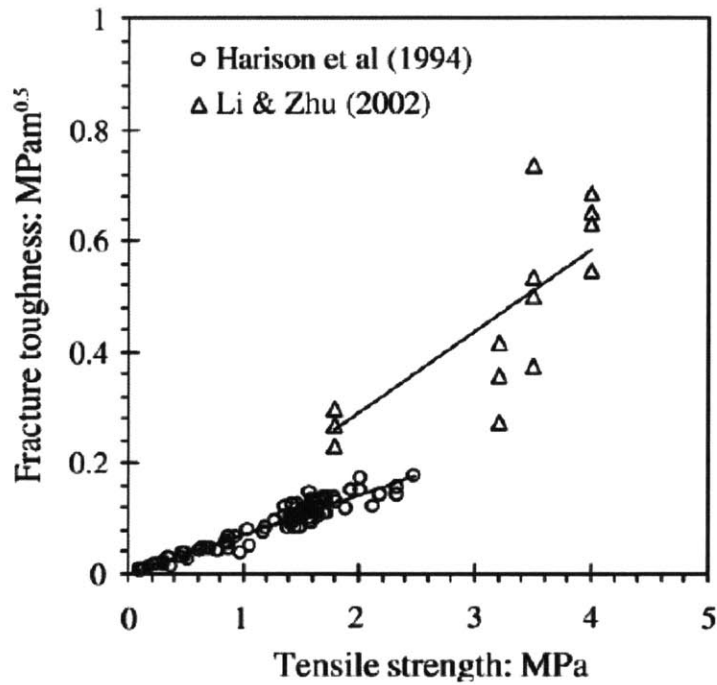
Figure 2.33: Relationship between K_{IC} and sigma t of different soils in literature (Wang et al., 2007)
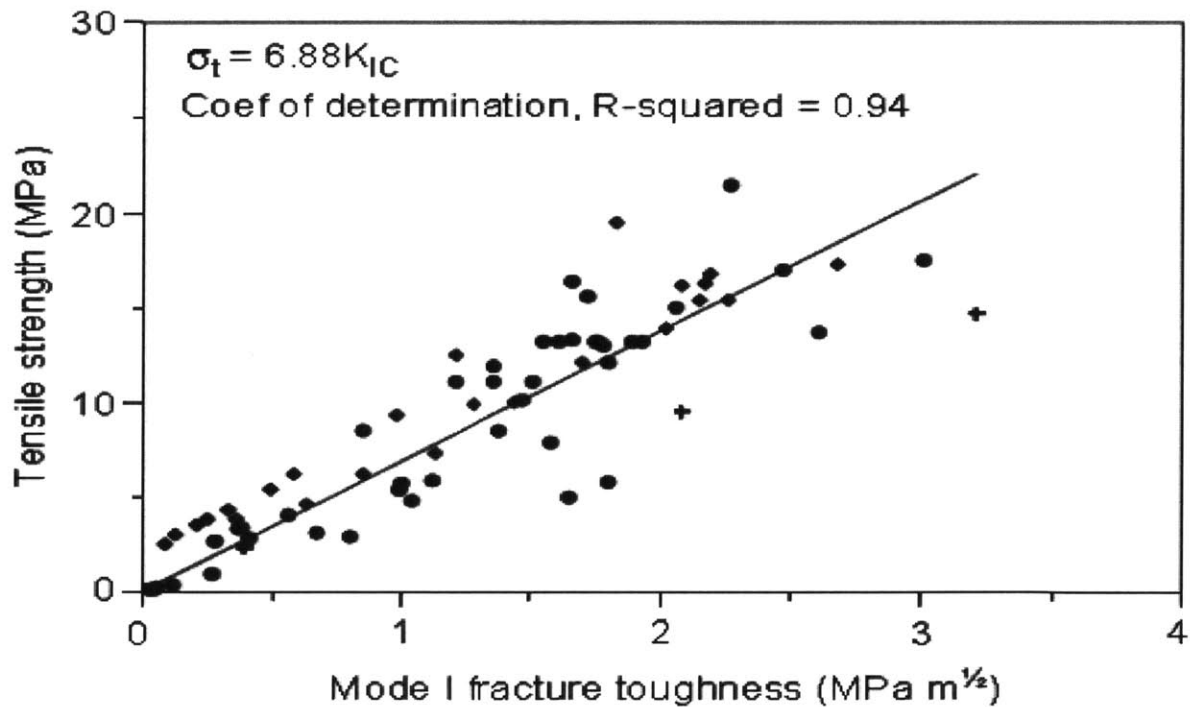
Figure 2.34: Empirical relation between fracture toughness and tensile strength of rocks (After Whittaker et., 1992; Zhang et al., 1998; Nordlund et al., 1999; Khan and Al-Shayea, 2000; Yu, 2001; and Zhang, 2002)
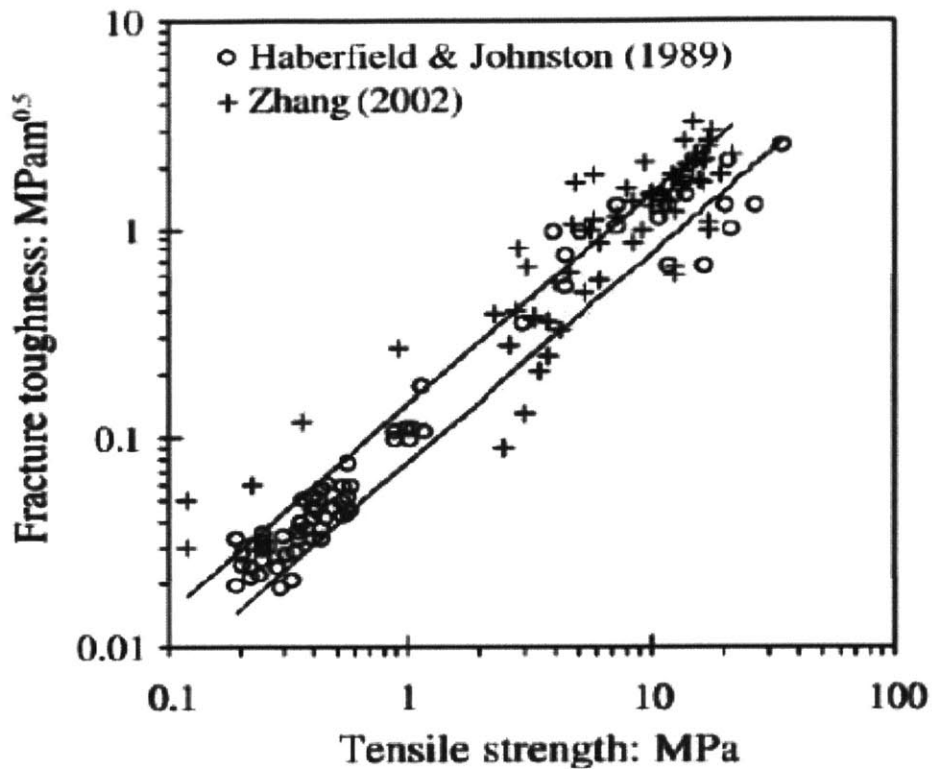
Figure 2.35: Relationship between K_{IC} and sigma t of different rocks in the literature (Wang et al., 2007)
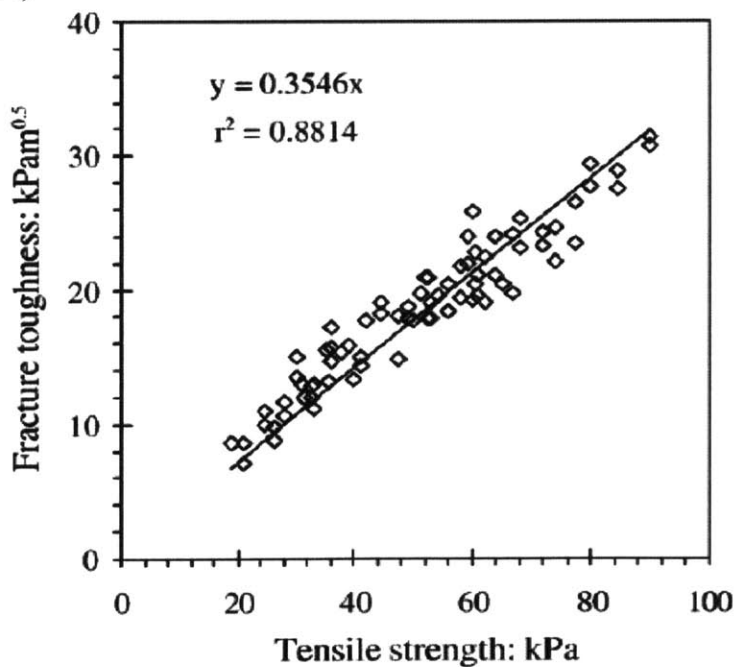
Figure 2.36: Relationship between K_{IC} and sigma t of Western China clay (Wang et al., 2007)
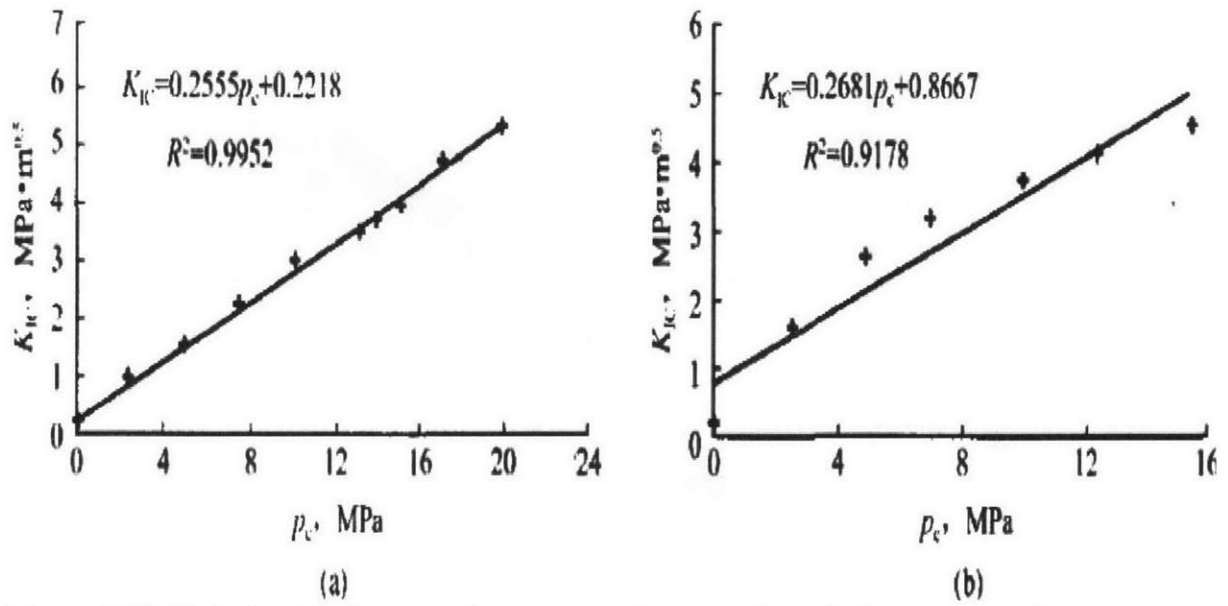
Figure 2.37: Relationship between fracture toughness and confining pressure for specimens with a clay content (a) 60% and (b) 30% (after Zhenfeng and Mian, 2006)
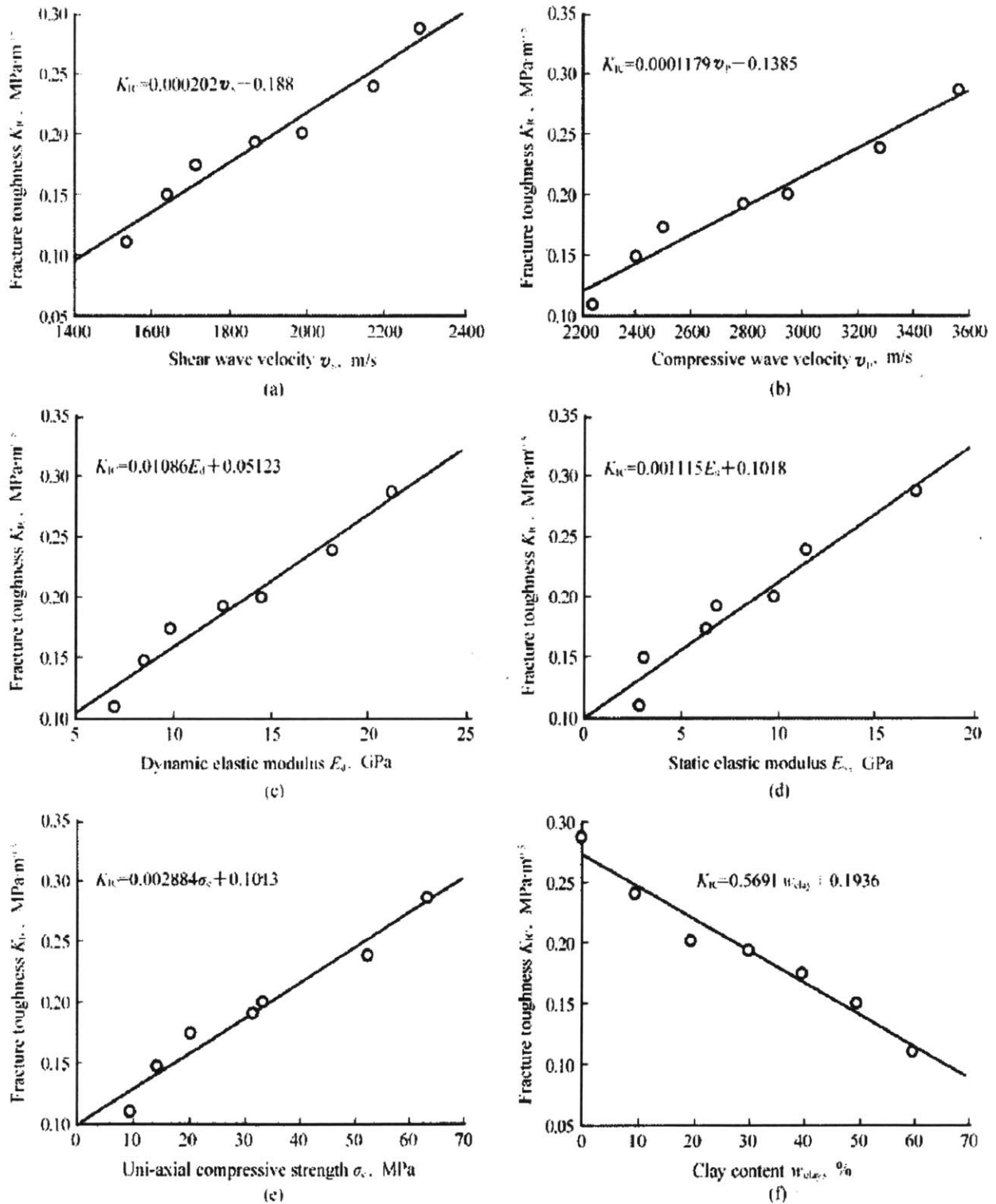
Figure 2.38: Fracture toughness versus physical mechanical properties: (a) Shear Wave Velocity, (b) Compressive Wave Velocity, (c) Dynamic Elastic Modulus, (d) Static Elastic Modulus , (e) Uniaxial Compressive Strength, (f) Clay Content (Zhenfeng and Mian, 2006)
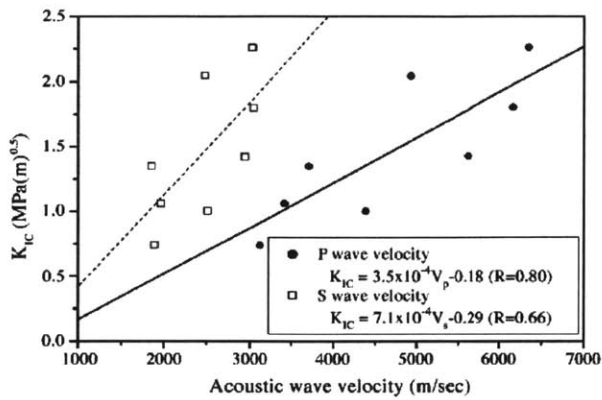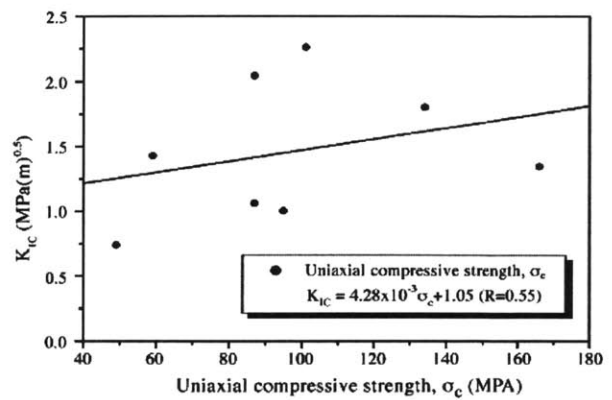
105

(a) Acoustic wave velocity

(b) Uniaxial compressive strength
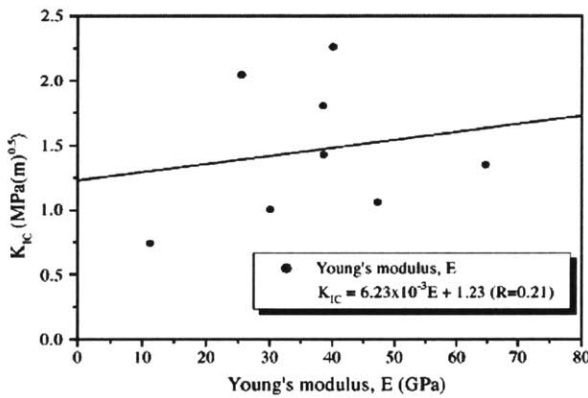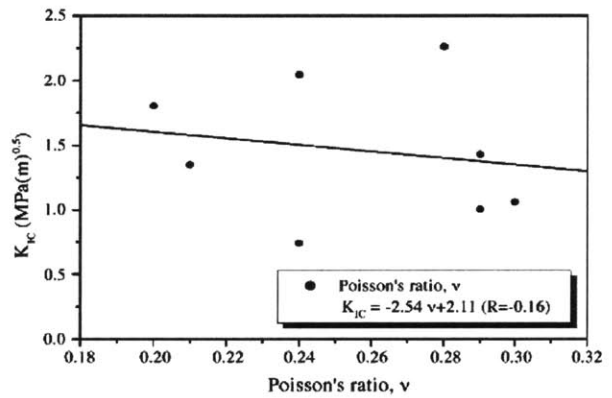
(c) Young's modulus
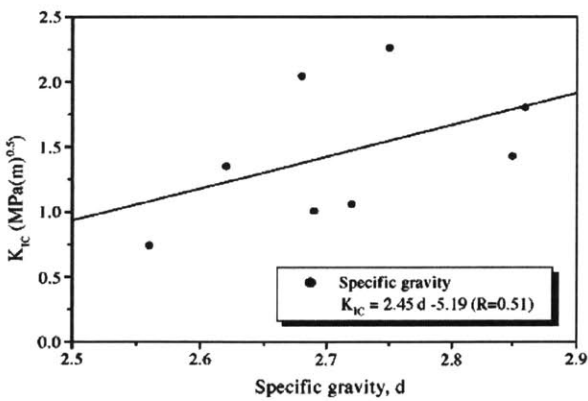
(d) Poisson's ratio
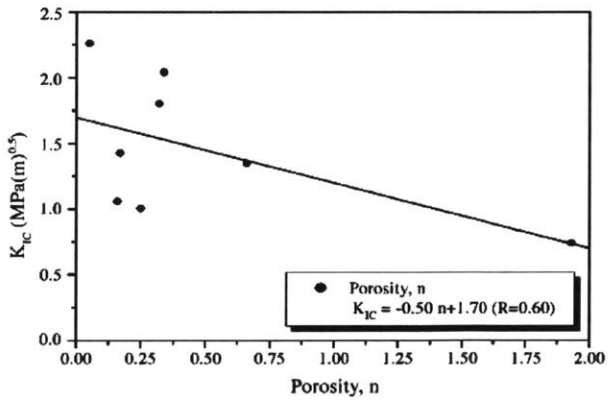
(e) Specific gravity

(f) Porosity

Figure 2.39: Relationships between physic-mechanical properties and fracture toughness of rock (a)Acoustic Wave Velocity, (b)Uniaxial Compressive Strength, (c) Young's Modulus, (d) Poisson's Ratio, (e) Specific Gravity, (f) Porosity (Chang et al., 2002)

Chapter (3)
LITERATURE REVIEW- FLATTENED BRAZILIAN TEST

3.1 Introduction

This chapter presents a general review of the literature available on the Brazilian testing method and provides a summary of the modifications to the Brazilian test over the years including the flattened Brazilian approach. The flattened Brazilian disc test is adopted as a convenient simple means for fracture toughness determination. The chapter covers the theory behind the flattened Brazilian test with an emphasis on the stress and displacement distributions within the flattened discs. Then appropriate methods to obtain the maximum stress intensity factor for the flattened discs are discussed. The chapter presents methods to evaluate the mode I fracture toughness, tensile strength, and the modulus of elasticity of the same specimen. In addition, some limitations on the results of the testing method are discussed.

3.2 Background on the Brazilian Test

The Brazilian test; sometimes known as the splitting tension test; is a simple indirect testing method mainly used to obtain the tensile strength of brittle material such as concrete, rock, soils and rock-like materials. In the test, a thin circular disc is diametrically compressed to failure (Li and Wong, 2013). Four typical loading configurations used in testing are shown in **Figure 3.1**. Since it was introduced in the 1940s by Brazilian and Japanese scholars (Carneiro and Akazawa, 1943; Carneiro and Barcellos, 1953; Akazawa, 1953; and Fairbairn and Ulm 2002) the test method has been popular for determining tensile strength indirectly for rocks and concrete materials. Based on the history of research on the Brazilian test by analytical, experimental, and numerical approaches, three main research stages have been identified: the 1st stage before 1978 (the stage of groundwork for the preparation of the standard suggested Brazilian test method for rock and rock-like materials), the 2nd stage between 1979–1991; widespread application of the Brazilian test in rock mechanics, and the 3rd stage from 1992 to present; the stage of application, modification, and improvement of the Brazilian test in rock mechanics). Li and Wong (2013) summarized the developmental timeline of the Brazilian test from 1943 to 2012. The summary; shown in **Table 3.1**; focuses on the various milestones and

the research approaches over the past 70 years.

Hertz (1883) was the first to develop a stress solution that was used as a theoretical foundation for the Brazilian test. It was then improved by J. H. Michell. Since then researchers and scientists have invested so much in the development of the Brazilian test, its validity, its credibility, and its applications. In 1959, Hondros developed an experimental approach to measure the modulus of elasticity and Poisson's ratio of different geomaterials with an emphasis on concrete using the Brazilian disc. However, additional strain gauge measurements were required, making the process complicated and difficult. Hondros (1959) also formulated a complete stress solution for the case of a radial load distributed over finite circular arcs of the disc, which was considered as a better method of load application when compared to the original concentrated (line) load; however, the derived approximate expressions for the stress components did not provide sufficient explanation and in-depth error analyses making the credibility of the solution questionable. In addition, it was difficult to ensure the required uniform and radial load distributed over a pair of arcs in real experiment (Wang et al., 2004).

In 1964, Fairhurst was the first to discuss the validity of the Brazilian test. He stated that "failure may occur away from the centre of the test disc for small angles of loading contact area". Then in 1971, Mellor and Hawkes reviewed the opposed strip load, and discussed the contact stresses under the applied loads, and designed a new load application method using a test jig with curved platens or jaws (an examples is illustrated in **Figure 3.1**). However, the manufacture of the curved jaws is not an easy job and is dependent on the curvature of the specimens being tested. Furthermore, contact force distributions between the jigs and the specimen are questionable (Wang et al., 2004). Hudson et al. (1972) conducted experimental research and realized that, 'In the Brazilian test, it was found that failure always initiated directly under the loading points if flat steel platens (also illustrated in **Figure 3.1**) only were used to load the specimen in a servo-controlled testing machine". They concluded that neither the Brazilian test nor the ring test could be recommended as a proper method for measuring the "tensile strength" as a material property. In 1978, the Brazilian test was officially proposed by the International Society for Rock Mechanics (ISRM) as a suggested method for determining the tensile strength of rock and rock-like materials. The American Society for Testing and Materials (ASTM) also standardized the Brazilian test for obtaining

the tensile strength of concrete materials in 1984.

In 1993, Guo et al. modified the conventional Brazilian test application and proposed a simple method to determine the opening mode (mode-I) fracture toughness K_{IC} using a circular disc. In their method the diametrical load is assumed to be uniformly distributed on an arc of angle 2α as illustrated in **Figure 3.2**. In their study, tests were conducted on six Australian rocks; typical specimens' failure after testing is shown in **Figure 3.3**. The main advantage of the proposed method is its convenience in specimen preparation; where the specimen does not need any pre cracking or notch drilling in its configuration, the crack by the specimen is required to be initiated and extended automatically during testing. In addition, the critical point used in the quantification of the fracture toughness can be determined easily from a simple test record between the point load and the vertical displacement without any crack length measurements. Accordingly, Guo's method can be considered the simplest, easiest, and most economic method for the determination of fracture toughness of rocks, soils, and other brittle materials (Wang and Xing, 1999).

However, a number of issues were not addressed in Guo's method; they did not explain how to guarantee the crack initiation at the center of the disk specimen and then its propagation. In addition, they did not address how the load angle (2α) variation affects location and behavior of the crack initiation. According to the analyses by Satoh (1987), whose work was based on the fracture criterion by Grifith and stress solution for the Brazilian disk by Hondoros (1959), the angle sustained by the load arc strongly affects the position of crack initiation. Wang and Xing (1999) proved that when the load angle satisfies the condition $2\alpha > 19.58$, a center crack initiation can be guaranteed for the Brazilian disk specimen under uniform distributed diametrical loading. Detailed analyses and explanation can be found in the research by Wang and Xing (1999).

Moreover, Guo's solution for the stress intensity factor (SIF) for center cracked disk was not entirely correct as they used Green's function for infinite plate to treat the finite domain problem in the disk (Wang and Xing, 1999). Finally, the arc loading of the disc specimen as shown in **Figure 3.2** is practically hard to satisfy exactly, and the stress distribution on the loaded arc can never be uniform; however, it was assumed to be uniform in Guo's analyses.

3.3 Introducing the Flattened Brazilian Test

Wang and Xing in 1999 proposed a modification to the Brazilian disk specimen for fracture toughness testing. They pointed out that the key issue with the Brazilian test is primary crack initiation at the centre region of the disc during the test which needed proper solution. Hence, the main modifications were introducing two parallel planes of equal width to the Brazilian disc for load bearing as illustrated in **Figure 3.4**. The flatness facilitates the load application to the specimen and can be considered better than the original line loading of the Brazilian test as it avoids local cracking, breakage or yielding around the loading point due to stress concentration, and can be considered better than other loading schemes like arc or strip loading, which use complex curved loading block or load strips stuck to specimen (Wang et al., 2004). The amount of work needed to prepare and machine the flattened Brazilian specimen is much less if compared to other testing methods such as the ISRM suggested cracked chevron notched Brazilian disc (CCNBD), as the only effort focuses on the flatness and parallelism of the two flat ends.

After verifying the formulae obtained by Wang et al. using finite element results and comparing measured values with other suggested experimental procedures, the formulae can be used for the determination of modulus of elasticity, E; with the information obtained from the slope of the load displacement record before reaching maximum load. Accordingly, the flattened Brazilian test can be used for determination of three material parameters; modulus of elasticity, tensile strength, and fracture toughness from different sections of a complete load displacement test record. It is worth noting, that since two parallel flat ends are introduced to the circular disc, the original formulae used for tensile strength determination in un-flattened discs need to be modified (Wang et al., 2004).

3.4 Displacement Analyses for the Flattened Brazilian Disc

In the literature there is no elastic displacement solution for circular un-flattened Brazilian discs subjected to compressive loading whether line load or concentric arc load, hence, other approximate solutions are needed. Wang et al. (2004) used software ANSYS to preform finite element analyses and approximate elastic solutions to study the radial; σ_r and tangential normal; σ_t stresses and the compression displacement; Δw of the loaded flattened disc. Wang et al (2004) obtained an approximate analytical formula for the elastic displacement solution

after introducing the parallel flat loading ends. Their formula was based on the research of Cauwellaert in 1994 on uniformly and parallel distributed load applied on a section of a circular arc. The main difference between the two studies; Cauwellaert used a circular arc while Wang et al. used two flat ends.

After modifying the formulae of Cauwellaert, Wang et al. were able to provide an approximate displacement solution for the flat end region in the flattened Brazilian specimen:

$$\Delta w = \frac{2P}{\pi Et} \left\{ (1 - \mu) - ln \left(1 + \frac{4}{sin^2 \alpha} \right) \right\} \frac{\alpha}{sin \alpha} \qquad (3.1)$$

Where P is the resultant of the uniformly distributed force applied through the flattened ends, t is the specimen thickness, D is the specimen diameter, E is the elastic modulus, sin α = 2b/D; 2b is the width of the flat end, and μ is Poisson's ratio.

Wang et al. (2004) modified Cauwellaert's formula for the isotropic case by removing an α term and adding α / sin α factor to consider the difference between flattened end and the circular arc. The accuracy of the previous equation was verified by comparison with finite element analyses; Wang et al concluded that the error of the previous equation is less than 5.8%, as compared with the ANSYS results. The comparison between the two methods is displayed in **Table 3.2**.

By following the previous equation, the modulus of elasticity; E can be determined from the slope of the section of load displacement record; this section is just before maximum failure load to avoid contact problems.

3.5 Stress Analyses for the Flattened Brazilian Disc

For a complete circular Brazilian disc, Timoshenko and Goodier (1970) provided an exact solution for the stress distribution on the loading diameter within nearly the inner 80% of its length as follows:

$$\sigma_\theta = \frac{2P}{\pi D t} \qquad (3.2)$$

$$\sigma_r = \frac{2P}{\pi D t} \left(1 - \frac{4D^2}{D^2 - 4r^2} \right) \qquad (3.3)$$

Where P is the total applied force, t is the specimen thickness, D is the diameter, r is the distance to the disc centre, σ_θ is tangential normal stress, and σ_r is radial normal stress.

However, no similar exact elastic solution is available for the flattened Brazilian disc configuration. Hence, Wang et al. (2004) used numerical analyses (ANSYS software) to

111

calculate the stresses for various cases. An illustration for their numerical analyses for stress evaluation in the case of $2\alpha = 30°$ is shown in **Figure 3.5**.

To determine crack initiation location along the diametral line, Griffith strength criterion (Griffith 1924) was applied as in the studies of Wang and Xing (1999); Wang and Wu (2004); Wang et al. (2004a) and Kaklis et al. (2005). Analytical expression of the Griffith's classical fracture theory is as mentioned below (Griffith 1924; Chang 1974; Clausing 1959). In Brazilian test, crack initiates at the center when $3\sigma1 + \sigma3 = 0$ and when this condition is satisfied, according to Griffith's theory, tensile strength is, $\sigma G = \sigma1$ for original Brazilian test. However, when the Brazilian disc is flattened, stress conditions at the center change and $3\sigma1 + \sigma3 < 0$ inequality condition governs the tensile crack initiation. Then for σG estimation, governing expression involving both $\sigma1$ and $\sigma3$ becomes:

When $3\sigma_1 + \sigma_3 \geq 0$

Then $\sigma_G = \sigma_1$;

When $3\sigma_1 + \sigma_3 < 0$,

$$\text{Then } \sigma_G = -\frac{(\sigma_1 - \sigma_3)^2}{8\,(\sigma_1 + \sigma_3)} \tag{3.4}$$

Where, σ_1, σ_3, and σ_G are maximum principal stress, minimum principal stress, and tensile strength, respectively. Left hand side of this equation is also called equivalent stress σ_G, and for Brazilian tensile strength test $\sigma_G = \sigma_t = 2 P / (\pi D t)$.

In a more recent study by Keles and Tutluoglu (2011), they showed the distribution of σG for various loading angles against the vertical distance from center to the flattened end of the specimen, (y/ R) for specimen models having a diameter of 75 mm as shown in **Figure 3.6**. In the figure, the horizontal scale is dimensionless equivalent stress $\bar{\sigma}_G$. This was set by normalizing σG with the stress perpendicular to the crack plane which is $2 P/ (\pi D t)$.

They concluded that crack initiation takes place when the equivalent stress reaches its maximum value along the y/R. For instance as displayed in Figure 3.6, equivalent stress is around 1.13 for $2\alpha = 10°$ and 1.03 for $2\alpha = 12°$ curves around $y/R = 0.77$ and $y/R = 0.70$, respectively. This means that crack initiation is expected to start along the diametrical plane, but out of the center for such 2α values. When 2α values become more than $14°$ maximum $\bar{\sigma}_G$ location stays right at the center of the disc specimens with values lower than one for increasing 2α values. (Keles and Tutluoglu, 2011).

Nearly the same findings were obtained in similar work including interpretation of the crack

initiation location on Brazilian discs conducted by Wang and Xing (1999); Wang and Wu (2004); Wang et al. (2004a) and Kaklis et al. (2005). By using boundary element method, critical 2α was found to be greater than 19.5° (Wang and Xing 1999); where they carried out comparative stress analyses between the flattened Brazilian disk and the original Brazilian disk, the result is shown in **Table 3.3**, from which it can be seen that the stress distribution along the loading diameter for the two cases is almost identical, thus the condition for crack initiation at the center of the specimen, i.e., $2\alpha > 19.5°$, which was initially derived for the original Brazilian disk can also be applied to the flattened Brazilian disk specimen. This angle was found to be equal to 15° in Kaklis et al. (2005) by finite element methods, and equal to 20° in Wang and Wu (2004) and Wang et al. (2004a) where they concluded that when $2\alpha > 20°$ the disc center has a larger value of σ_G than any point elsewhere as shown in **Figure 3.7**; it also means that a crack is most likely to initiate at the center.

Keles and Tutluoglu (2011) generalized the relation between principal stresses at the center of the specimens and the loading angle 2α, where they varied the loading angle 2α from 15° to 60° which corresponds to dimensionless distance between $y/R = 0.966$ and 0.5, respectively. Dimensionless principal stresses normalized by dividing them to the σt equation 2 P /(π Dt) of Brazilian test are given in **Figure 3.8**. By curve fitting for 2α values between 15° and 60°, dimensionless principal stresses at the center of the specimens in terms of α are:

$$\bar{\sigma}_1 = \frac{\sigma_1}{2P/(\pi Dt)} = 0.94 \cos \alpha + 0.04 \tag{3.5}$$

$$\bar{\sigma}_3 = \frac{\sigma_3}{2P/(\pi Dt)} = -1.08 \cos \alpha - 1.92 \tag{3.6}$$

Horizontal stress which is used to estimate σt in Brazilian test is equal to the $\sigma 1$, while vertical stress is equal to the $\sigma 3$. By using the previous two equations, σG can be expressed as a function of the loading angle α as follows:

$$\bar{\sigma}_G = \frac{\sigma_G}{2P/(\pi Dt)} = 0.83 \cos \alpha + 0.15 \tag{3.7}$$

The previous equation can be used as a geometrical factor in σt estimation with flattened Brazilian disc specimens, where the factor is valid for 2α values between 15° and 60°. Dimensionless equivalent stresses normalized by dividing them to the σt equation 2 P /(π Dt) of Brazilian test are given in **Figure 3.9**.

A similar approach was developed by Wang et al. (2004), where after choosing the

appropriate loading angle 2α greater than 20°, the tensile strength σ_t can be determined as follows:

$$\sigma_t = k \, \frac{2 \, P_c}{\pi D t} \tag{3.8}$$

Where, Pc is the critical load applied on the flat ends; which is equivalent to the maximum load during testing, D is the specimen diameter, t is the specimen thickness, and k is the coefficient which is dependent on the loading angle. For the given value of 2α; k can be determined by finite element analyses. According to the Griffith criterion at failure $\sigma_t = \sigma_G$; hence:

$$k = \frac{\sigma_G}{2P/\pi D t} \tag{3.9}$$

Based on finite-element results obtained by Wang et al. (2004), then the value of k is obtained: when $2\alpha = 20^\circ$; k = 0.9644; when $2\alpha = 30^\circ$; k = 0.9205. An approximate formula for determining the k value based on the loading angle can be obtained as follows:

$$k = \frac{(\, 2 \cos^3 \alpha + \cos \alpha + \sin \alpha / \alpha \,)^{\,2}}{8 \, (\cos \alpha + \sin \alpha / \alpha \,)} * \frac{\alpha}{\sin \alpha} \tag{3.10}$$

When α = zero, k is equal to 1 which is the case of the conventional Brazilian test. Wang et al. (2004) compared the results obtained from the approximate analytical formula with the results using ANSYS and both methods agreed to a great extent as shown in **Figure 3.10.** hence, the previous equation can be used for determining the K factor which is used to evaluate the tensile strength of the flattened Brazilian discs with central loading angle > 20°.

3.6 Fracture Toughness Analyses for the Flattened Brazilian Disc

According to the study of Wang and Xing (1999), when $2\alpha > 19.5°$, a crack initiation at the center of the specimen can be expected, then the crack extends along the diameter. They provided a schematic diagram for the trend of the stress intensity factor- SIF (ϕ) as shown in **Figure 3.11**, the value of the SIF gradually increases from zero, represented by point a, which corresponds to the crack initiation, to the maximum value, represented by point b, where ϕmax is obtained, after which ϕ decreases until final breakage of the disk, represented by point c. According to Wang and Xing (1999), in the first region (ab), dimensionless SIF ϕ increases with increment of relative crack length a/R, this region is characterized by unstable crack growth, as the crack will go on extending even if the applied load is held constant. On the contrary, in the second region (bc), after reaching a maximum ϕ value at point b, ϕ

114

decreases with the increment of relative crack length a/R, this region is characterized by stable crack growth, as the crack will stop extension if the load is not increased, only when the applied load is increased can the crack extend further. Point b is the turning point between unstable and stable regions, this point b corresponds to the local minimum load immediately succeeding the peak maximum load, and this point is chosen as the critical point, which will be identified easily in a test record. According to Wang and Xing (1990), the reason for this choice can be explained as follows: for brittle materials such as rock or dried soils, fracture toughness K_{IC} can be considered to be a material constant accordingly, any point during crack extension can be used to determine fracture toughness given that the current load and the crack length are known. Accordingly, it is more convenient to select point b as the critical point, as this point has maximum value which can be determined beforehand for any prescribed specimen geometry, hence, there will be no necessity to measure the critical crack length, also the determination of the critical load is relatively convenient, which is the local minimum load occurring right after the peak load as illustrated in **Figure 3.12**.

Figure 3.12 can be considered a typical test record of the load–vertical total diametrical displacement behavior of the flattened Brazilian specimen. From the behavior, it can be noticed that the loading process can be divided into three stages: stage 1 (oa) representing elastic non linear deformation of the flattened disk, this stage ends with the peak load, which is point a. The non linear initial behavior can be due to compression of existed porosity and micro-cracking of the specimen or due to seating at contact surfaces. Then a linear ascending behavior can be observed until the load reaches its maximum value. Then stage 2 (ab) representing unstable crack extension, at the peak load of point a, the crack initiates at the center of the specimen, then the crack develops unstably until the load drops to the local minimum which is represented by point b; point b is the turning point, which separates the unstable and stable region; this point b is chosen as the critical point in the test which corresponds to the critical crack length ac/R. This critical crack length can be determined analytically and it corresponds to ϕmax and there is no need for its measurement. Finally, stage 3 (bc) representing stable crack extension, beginning from point b, the load must increase for further crack growth until complete breakage of the specimen which marks the failure of the specimen. The fluctuating behavior of the test might be due to sub crack formation near the contact area; these irregularities should not affect test results, as the

115

critical point b is in advance of their happening (Wang and Xing, 1999). The behavior can be summarized as unstable initial extension for the crack then it turns to arrest at a critical point followed by stable crack development. This behavior is very unique and advantageous for the determination of the fracture toughness. The formula to evaluate fracture toughness K_{IC} using local minimum load as the critical point is as follows:

$$K_{IC} = \frac{P_{min}}{\sqrt{Rt}} \, \emptyset_{max} \tag{3.11}$$

Where, Pmin is the local minimum load which can be identified directly from the test record, R and t are radius and thickness of the specimen, respectively and ϕ max is the maximum dimensionless SIF, which is determined as explained in the following section.

3.7 Maximum Stress Intensity Factor Computations for the Flattened Brazilian Disc

Analytical solution for the stress intensity factor (SIF) of cracked Brazilian discs was first given by Guo et al. (1993) when they developed the SIF solution in an infinite plate as the Green's function. Their solution was questionable and not reliable and cannot be applied to the flattened Brazilian disc configuration. Hence, researchers and scholars used different numerical methods to obtain approximate acceptable SIF values. Wang and Xing (1999) were the first to address this issue for the flattened Brazilian configuration, as they stated that the load angle should satisfy the condition $2\alpha > 19.5°$, then they selected two random convenient central angles ($2\alpha = 20°$ and $2\alpha = 30°$) and used boundary element method to quantify the SIF. The SIF solution is put into a dimensionless form and fitted into a polynomial form as follows. For the load angle $2\alpha=20°$, the dimensionless SIF flattened Brazilian disk is:

$$\emptyset \left(\frac{a}{R}\right) = K_I \sqrt{R}\frac{t}{P} = 4.2897 \left(\frac{a}{R}\right)^7 - 26.6765 \left(\frac{a}{R}\right)^6 + 84.9054 \left(\frac{a}{R}\right)^5 - 93.0870 \left(\frac{a}{R}\right)^4$$
$$+ 50.7763 \left(\frac{a}{R}\right)^3 - 14.3776 \left(\frac{a}{R}\right)^2 + 2.4708 \left(\frac{a}{R}\right) \tag{3.12}$$

And for the load angle $2\alpha = 30°$, the dimensionless SIF of flattened Brazilian disk is:

$$\emptyset \left(\frac{a}{R}\right) = K_I \sqrt{R}\frac{t}{P} = -33.9811 \left(\frac{a}{R}\right)^7 - 128.5613 \left(\frac{a}{R}\right)^6 + 189.8983 \left(\frac{a}{R}\right)^5 - 146.3809 \left(\frac{a}{R}\right)^4$$
$$+ 64.0804 \left(\frac{a}{R}\right)^3 - 15.7996 \left(\frac{a}{R}\right)^2 + 2.7115 \left(\frac{a}{R}\right) \tag{3.13}$$

Where ϕ is dimensionless SIF, a/R is the relative crack length, a is half the crack length, R is the radius of the disk, t is the thickness, P is the total load (summation of distributed load), KI

116

is mode-I SIF. Wang and Xing (1999) confirmed that the error of curve fitting for these two formulas is less than 0.5%.

The trend of SIF solutions for the studied two load angles is similar to the shape of a bell; the numerical trend ascends to a maximum value then descends. The maximum value of the dimensionless SIF solution is of the main concern as it will be used in the formula for the fracture toughness test. Wang and Xing (1999) derived by the numerical calculation that for $2\alpha=20°$, when a/R = 0.80, ϕ reaches its maximum value ϕ of 0.78; and for $2\alpha=30°$, when a/R = 0.73, ϕmax=0.58.

Wang and Wu (2004) used the finite element method for specimens with 58, 87, 91 and 108 mm diameter values to verify the accuracy of the computed SIF (ϕ) for central angles of 20 and 30 degrees. Their computation provided the ϕ ~a/R curve which is expressed in a plot between dimensionless stress intensity factor ϕ versus dimensionless crack length a/R as shown in **Figure 3.13**. Since the relation between the fracture toughness, loading angle, applied load, and specimen dimensions can be written in the following format:

$$K_I = \frac{P}{\sqrt{Rt}} \, \emptyset\left(\alpha, \frac{a}{R}\right) \tag{3.14}$$

Then for the two loading angles under the study of Wang et al. (2004), combining Pmin and ϕmax and substituting them into the previous equation, the fracture toughness can be computed using the following equations:

$$K_{IC} = \frac{P_{min}}{\sqrt{Rt}} \, \emptyset_{max}, \quad \emptyset_{max} = 0.7997 \ldots \ldots \ldots \ldots for\ 2\alpha = 20° \tag{3.15}$$

$$K_{IC} = \frac{P_{min}}{\sqrt{Rt}} \, \emptyset_{max}, \quad \emptyset_{max} = 0.5895 \ldots \ldots \ldots \ldots for\ 2\alpha = 30° \tag{3.16}$$

As the previous solutions provided maximum stress intensity factors for two loading angle values only (20 and 30) then the work carried by Wang and Xing (1999) and by Wang et al. (2004) needed further development to cover a wider range of loading. Keles and Tutluoglu (2011) extended the work carried on the flattened Brazilian test, KI computations were carried out by ABAQUS finite element program. ABAQUS program uses J-integral method in KI computations. A circular (for 2D models) or cylindrical (for 3D models) contour integral region is defined around the crack tip and the program computes an average stress intensity factor value for this crack tip.

Modeling results of Keles and Tutluoglu (2011) showed that K_{Imax} is inversely proportional to

117

the thickness t and the square root of the radius R, and directly proportional to the load P, as in Wang and Xing (1999). From K_{Imax} computed in the modeling work, ϕmax can be found by using the following equation:

$$\emptyset_{max} = K_{I\,max}\,\frac{\sqrt{R}\,t}{P}$$

(3.17)

The crack length where the maximum KI value is determined can be called a_{cn} critical crack length and is computed numerically. By fitting a sixth order polynomial to KI versus a/R distribution, Keles and Tutluoglu (2011) set an equation. Maximum stress intensity factor was found by setting the derivative of this equation to zero and finding its roots. One of the roots was equal to the dimensionless critical crack length (acn / R), and this was used in finding the K_{Ima} result of a particular model. ϕmax versus acn / R values of the model are illustrated in **Figure 3.14** for specimens having 54, 75, 100, and 125 mm diameters and 2α values between 15° and 50°.ϕ_{max} values can be calculated by using the fitted expression below:

$$\emptyset_{max} = 0.039 \exp 15.239\,(a_{cn}/R)$$

(3.18)

Keles and Tutluoglu (2011) also determined ϕ_{max} values at the onset of stable crack propagation corresponding to the P_{min} points for various 2α values between 15° and 50° for specimens having 54, 75, 100, and 125 mm diameters. ϕ_{max} values computed for different 2α values were plotted in **Figure 3.15**. Using a curve fitting program for the interpretation of the numerical modeling results, following expression for variation of ϕ_{max} with α can be obtained:

$$\emptyset_{max}(\alpha) = \frac{1}{43.31 - 15.63 \exp(\cos \alpha)}$$

(3.19)

It is worth noting that although the previous equation is valid for ϕ_{max} estimations of disc models with 2α between 6° and 50°, 2α must be greater than 20° to impose central crack initiation. The previous equation gives a flexibility and chance to determine ϕ_{max} applicable to particular experimental conditions over a wider range of loading angles.

3.8 limitations on the Flattened Brazilian Test

According to the experimental work of Wang and Wu (2004), for a valid flattened Brazilian disc method test (as shown in **Figure 3.16**), the load after the crack propagation should not exceed the maximum load achieved at the end of the elastic deformation. Otherwise, secondary cracks may play the leading role instead of primary crack considered in the computation process, and the disc may be broken into four pieces instead of two halves.

Wang and Wu (2004) defined validity criteria for the flattened Brazilian test as follows: 1. After elastic deformation, the crack initiates from the central region of the disc and the initiation of the crack corresponds to the maximum load; 2. The crack propagates to its critical point, this fracture process is characterized by the load descending and ascending in turn, however the ascending load does not surpass the preceding maximum load. Accordingly, the validity of the test based on the shape of the load–displacement record is emphasized.

In their research they provided two examples of invalid test results as the ones shown in **Figure 3.17** and **3.18**. In an invalid test record (**Figure 3.17**), the load Pe at the end of elastic deformation is not the maximum load of the test, the immediately subsequent local minimum load is only slightly lower than Pe , which implies that the primary crack does not extend to the critical point and the secondary cracks play the leading role for the rest of the record. However if the primary crack plays the leading role, the mechanism for the determination of σt and K IC is completed, then the formation of the secondary cracks does not violate the principle for their determination, the test is still considered valid (Wang and Wu, 2004).

Another kind of invalid test is shown in **Figure 3.18**, where upon reaching the maximum load there is a drastic sudden load fall, demonstrating that the test is unstable, which occurs when the disc has no flat ends or their width is not sufficient so this is a total failure of specimen.

Table 3.1: Developmental timeline of the Brazilian test on rocks and rock-like materials over the period from 1943 to 2011 (Extracted from Li and Wong, 2013)

Authors (year)	Contributions	Remarks	
	~~Methods~~		
Carneiro (1943)	Proposing a testing method and giving an evaluation formula to calculate the tensile strength from the elastic tensile strength limit	Inventing the "Brazilian testing method" to obtain the tensile strength of concrete	[E]
Akazawa (1943)	Presenting a method similar to the Brazilian test independently in Japan almost at the same time as Carneiro (1943) (firstly published in Japanese only 2 months later than that by Carneiro, and republished in French in 1953)	Presenting the work without any communication with overseas researchers (Brazil and Japan were on opposite sides in World War II)	[E]
Hondros (1959)	Giving a complete stress solution for the case when the load is distributed over finite arcs with diametral compression, valid for conditions of both plane stress (discs) and plane strain (cylinders)	Assuming that the material is homogeneous, isotropic, and linearly elastic	[A]
Hobbs (1964, 1965, 1967)	Using the diametrical compression of a disk with a central hole (ring test) as a technique for determining the tensile strength of rocks, and comparing with Brazilian test results	Considering the influence of laminations on the tensile strength of rocks	[E]
Fairhurst (1964)	Indicating that failure may occur away from the center of the test disc for small angles of loading contact area with materials of low compression–tension ratios. Pointing out that the "tensile strength" as calculated from the Brazilian test results is lower than the true value. A parameter called stress severity S was defined and used	Generalizing a Griffith-type fracture criterion to analyze the failure of Brazilian test specimens. The applied loading was assumed to have a uniform radial distribution	[A]
Hiramatsu and Oka (1966)	Analyzing the stress in an irregular test piece subjected to a pair of concentrated loads by three-dimensional photoelastic experiments as well as by mathematical analysis, and presenting a new method to test the tensile strength of rocks	This testing method was not perfect because the stress state in the test piece was not simple and uniform, and was affected by the nature of the rock	[A] + [E]
Colback (1966)	Using the modified Griffith fracture theory to predict fracture initiation in a Brazilian loaded disc. Pointing out that failure must originate at the center of the disc if the test is to be a valid tensile test.	High-speed photography of the photoelastic patterns induced in birefringent layers was used to determine the fracture initiation point and study its subsequent propagation	[A] + [E]
Jaeger and Hoskins (1966b), Jaeger (1967)	Comparing three different cases of measurement to obtain the tensile strength of rocks both theoretically and experimentally. Finding that the calculated maximum tensile stress was of the order of the uniaxial tensile strength of the material	Based on the tensile stress calculation	[A] + [E]
Hudson (1969)	Comparing two indirect testing methods, the Brazilian test and the ring test, for obtaining tensile strength.	The tensile strength was concluded to be an experimental property and not a material property	[E]
Mellor and Hawkes (1971)	tensile strength by diametral compression of Brazilian discs and annuli for Griffith-type materials. Designing a curved-jaw loading jig to reduce the stress concentration at the loading points.	Pointing out that the Brazilian test was capable of giving a good measure of uniaxial tensile strength	[A] + [E]
Hudson et al. (1972)	Observing that failure always initiated directly under the loading points in the Brazilian test if only flat steel platens were used in a closed-loop servo-controlled machine.	Some scanning electron photomicrographs of a crack were included to study crack propagation in the Brazilian test	[E]
Barla and Innaurato (1973) Measuring	Experimentally and numerically investigating the suitability of indirect tensile tests (the Brazilian test and the ring test) on anisotropic rocks	Two types of anisotropic rocks were tested under different orientations along the axes of anisotropy	[E] + [N-2D]

120

Table 1 continued

Authors (year)	Contributions	Remarks	Methods
Vutukuri (1974)	Using the ring test to determine the tensile strength of limestone and discussing the effect of liquids on the tensile strength of limestone. Finding that, as the dielectric constant and surface tension of the liquid increased, the tensile strength of the limestone decreased	Using Hobbs' equation to calculate the tensile strength of a ring specimen.	[E]
Wijk (1978)	Showing that the three-dimensional "correction" to the two-dimensional theoretical solution was considerable, even for rather thin samples in the case of the Brazilian test. Discussing the influence of Poisson's number in Brazilian tests and point load tests	The three-dimensional stress distribution was considered rather than the plane stress or plane strain problem	[A]
Yanagidani et al. (1978)	Observing that the crack was not initiated from the loading point but from the tensile stress zone in the Brazilian disc by using strain gages for crack detection	A transient recorder (TR) was used to record the strain variation on the surface of the Brazilian specimen	[E]
ISRM (1978)	Suggesting a standard Brazilian testing method to determine the indirect tensile strength of rocks. Meanwhile, the uniaxial tension test was put forward as a method for determining the direct tensile strength of rock	Formula to calculate tensile strength	[E]
Lajtai (1980)	The tensile strength determined by point load testing and as calculated by the Frocht formula was found to be consistently lower than that obtained by the Brazilian test	The Brazilian test seemed to yield a more accurate definition of both the tensile strength and its variation with direction	[E]
Sundaram and Corrales (1980)	Pointing out that the assumption of the same elastic properties in both tension and compression could overestimate the Brazilian tensile strength of rocks	Considering the difference of elastic properties of rocks under tension and under compression	[N-2D]
Pandey and Singh (1986)	Finding that the Brazilian tensile strength was almost double, and the corrected bending tensile strength was three times the value obtained in uniaxial tension. Discussing the deformation characteristics of rocks under tensile stress	Arguing that tensile strength was an experimental property rather than a material property	[E]
Newman and Bennett (1990)	Carrying out statistical experimental studies on the effect of specimen geometry and stress rate on the determination of the tensile strength of sandstone by the Brazilian test	Confirming that the length-to-diameter ratio of the specimen has a significant effect on the tensile strength	[E]
Andreev (1991a, b)	Reviewing two aspects of the Brazilian test for rock tensile strength determination: calculation formula and contact conditions. Pointing out that the Brazilian test was valid for materials which exhibit brittle failure	Arguing that the experimental result should be abandoned if the failure initiates under the loading devices	[A] + [N-2D] + [E] [A]
Guo et al. (1993)	Proposing a calculation formula and a testing method to measure the fracture toughness of rocks by fracture mechanics analyses of the intact Brazilian disc test	Assuming that the tensile crack initiated from the center to the outside along the compressive diameter	+ [E] [N-
Malan et al. (1994)	Investigating the influence of an interface on crack initiation and propagation in the Brazilian test. Using a computer program to simulate the failure process based on the displacement discontinuity method	Mohr–Coulomb failure criterion with a tension cutoff was used in the two-dimensional numerical simulation	2D]
Chen et al. (1998)	Presenting a combination of analytical and experimental methods to determine the tensile strength and elastic constants of transversely isotropic rocks by the Brazilian test	The solution is implicit, and the mathematical computation procedure is complex	[A] + [E]
Rocco et al. (1999a, b)	Experimentally and theoretically studying the size effect and boundary conditions in the Brazilian test	A cohesive crack model was used for the theoretical analysis	[E] + [N-2D]

Table 1 continued

Authors (year)	Contributions	Remarks	Methods
Exadaktylos and Kaklis (2001)	Presenting explicit expressions for the stresses and strains at any point of an anisotropic circular disc compressed diametrically	Discussing the strain distributions of the anisotropic Brazilian disc	[A] + [E]
Claesson and Bohloli (2002)	Deriving an explicit solution and giving the stress charts for the tensile principal stress for anisotropic (transversely isotropic) rock, particularly the principal tensile stress at the center of a disc due to opposing normal point loads	Stress-based analysis on the effect of anisotropy of rocks. The proposed approximate formula reduces to Eq. (1) for isotropic rocks	[A]
Lavrov and Vervoort (2002)	Analyzing the influence of the friction force applied over two opposite arcs on the stress distribution of the Brazilian test theoretically. Pointing out that the stress distribution inside the sample is only marginally affected by the effects of the frictional conditions at the boundary	Both inward and outward friction forces acting on the Brazilian specimen are taken into consideration	[A]
Lavrov et al. (2002)	Presenting an analysis of the Kaiser effect degradation with increasing deviation of the principal stress between loading cycles in Brazilian tests. Using the displacement discontinuity method to confirm these experimental results	Acoustic emission was monitored during the Brazilian test, and a two-dimensional (2D) displacement discontinuity numerical method was introduced	[N-2D] + [E]
Yue et al. (2003)	Presenting a digital image processing-based finite-element method for two-dimensional mechanical analysis of geomaterials, taking into account material inhomogeneities and microstructures	The inhomogeneities of the material have significant effects on the tensile stress distribution along the loading axis of Brazilian specimens	[N-2D] + [E]
Wang et al. (2004)	Proposing a flattened Brazilian disc test to determine the elastic modulus E, tensile strength r_t, and opening mode fracture toughness K_{IC} for brittle rocks in one test	2D stress-based analysis of a flattened Brazilian disc specimen using FEM code ANSYS	[A] + [N-2D]
Van De Steen et al. (2005)	Proposing that fracturing in the Brazilian test initiated in shear in the vicinity of one of the platens, subsequently growing in tension	A boundary element code DIGS was used in the numerical simulations of the experiments	[N-2D] + [E]
Coviello et al. (2005)	Presenting a critical assessment of some widely used laboratory techniques on the basis of experimental data from the literature and their own investigations. Performing various types of tests for determining the tensile strength of soft rocks, including the uniaxial, Brazilian, ring, three- and four-point bending, and Luong tests	Experimental results indicate that the tensile strength is strongly dependent on the specific test used for its evaluation	[E]
Aydin and Basu (2006)	Proposing an indicator of weathering and accompanying microstructural weakening of igneous rocks by using the diametral stress–strain curves in the Brazilian tension test	A 2-cm-long strain gage was placed in a Brazilian test specimen along its horizontal diametral plane	[E]
Yu et al. (2006)	Pointing out that the formula for the indirect tensile strength is inaccurate when the Brazilian disc has significant thickness. A 3D FEM stress analysis showed that size/shape effects existed in the Brazilian test when the disc thickness was increased	Stress analysis based on a 3D FEM program was used, and the influence of specimen thickness was considered	[N-3D]
Zhu and Tang (2006)	Studying the deformation and failure process of a Brazilian disk of heterogeneous rock subjected to static and dynamic loading conditions by numerical simulation based on rock failure process analysis (RFPA)	Considering rock heterogeneity by assuming that the material properties of elements conform to a Weibull distribution	[N-2D]
Ye et al. (2009)	Presenting an analytical formula and an experimental method to obtain the tensile elastic modulus (E_t) of rock by using strain gages in the Brazilian splitting test	The ratios of E_t to E_c for marble, sandstone, limestone, and granite were about 60–90 %, where E_c is the compressive elastic modulus	[A] + [E]
Lanaro et al. (2009)	Discussing the influence of initiated cracks on the stress distribution, and modeling the crack initiation and propagation of Brazilian rock specimens subjected to indirect tensile loading	A boundary element method (BEM) code (FRACOD2D) was used to model the Brazilian tests	[N-2D]

Table 1 continued

Authors (year)	Contributions	Remarks	Methods
Yu et al. (2009)	Presenting a modified Brazilian disk test by using two special spacers at the loading points to reduce the stress concentrations. Pointing out that the traditional Brazilian test seriously underestimates the tensile strength of the tested material	3D FEM stress analysis was adopted by assuming that the test material is a continuous, isotropic, and homogeneous elastic body	[N-3D] + [E]
Tavallali and Vervoort (2010a, b)	Presenting the effects of layer orientation (anisotropy) on the Brazilian tensile strength and failure patterns in the Brazilian test. The influences of microscale parameters on the macroscale behavior were discussed	Three different fracture types were observed for the particular layered sandstone, namely layer activation, central fractures, and noncentral fractures	[E]
Markides et al. (2010, 2011)	Obtaining closed full-field solutions for the stresses and displacements in a Brazilian disk under uniformly distributed radial load and considering the influence of a uniform distribution of friction stress at the loading rims. Pointing out that the fracture may start at the edge of the load contact points rather than at the specimen center	Assuming that the material of the disk is homogeneous, isotropic, and linear elastic. A plane stress problem is assumed for the analytical analysis	[A] + [E]
Markides and Kourkoulis (2012)	Giving analytic full-field formulae for the components of the stress field developed in a Brazilian disc under four types of loading distribution on the actual contact length	Based on the linear elasticity assumption and ignoring the friction at the loading rims	[A] + [E]
Erarslan and Williams (2011)	Presenting experimental results for an investigation of the stress–strain characteristics of Brisbane tuff disc specimens under diametral compressive cyclic loading	The reduction in indirect tensile strength of tuff was found to be 33–37 % for cyclic loading conditions under the Brazilian test	[E]
Erarslan et al. (2011)	Investigating the difference between standard Brazilian jaws and various loading arc angles for the Brazilian test on Brisbane tuff by experimental and numerical studies	The best loading geometry for indirect tensile testing of rock material was found to be from $2a = 20°$ to $30°$ based on loading arc simulations	[E] + [N-2D]

Classification of study approaches: Analytical (A); experimental (E); numerical (N). The numerical studies are further classified into two-dimensional numerical (N-2D) and three-dimensional numerical (N-3D) analyses.

a Where W is load, a is the ratio of the internal radius (a) to the external radius (b), and t is thickness

123

Table 3.2: A comparison between analytical and numerical solution for the diametrical compression displacement ΔW of the flattened Brazilian disc (Wang et al., 2004)

2α (°)	ΔWEπt / 2P Analytical	ΔWEπt / 2P ANSYS	Error - (Analytical - ANSYS / ANSYS) %
5	6.954	7.208	-3.52
10	5.575	5.839	-4.52
15	4.777	5.026	-4.95
20	4.217	4.472	-5.70
30	3.445	3.656	-5.77

Table 3.3: Comparison between stress distribution on the loading diameter between arc loading (Brazilian Disc) and plane loading (Flattened Brazilian Disc) for load angle=20 (Wang and Xing, 1999)

r/R	σθ/(P/Rt)		σr/(P/Rt)	
	Arc Loading	Plane Loading	Arc Loading	Plane Loading
0.9	-3.086	-3.076	-8.864	-8.846
0.8	-0.457	-0.454	-7.336	-7.357
0.7	0.403	0.404	-5.839	-5.859
0.6	0.709	0.713	-4.801	-4.819
0.5	0.839	0.843	-4.101	-4.117
0.4	0.900	0.904	-3.627	-3.642
0.3	0.931	0.935	-3.309	-3.324
0.2	0.948	0.952	-3.107	-3.121
0.1	0.957	0.960	-2.997	-3.011
0.0	0.963	0.967	-2.961	-2.975
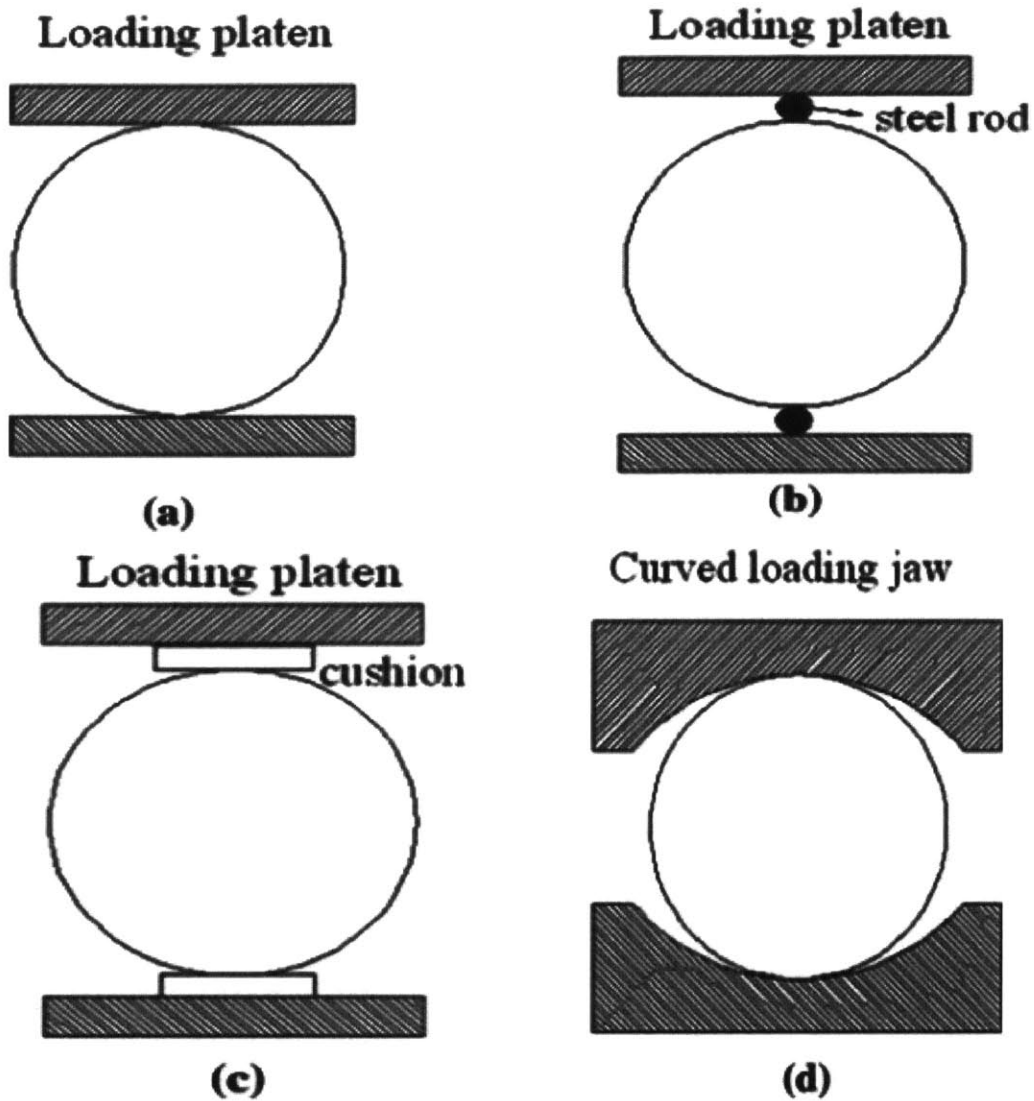
Figure 3.1: Typical Brazilian tensile test loading configurations: (a) Flat loading platens, (b) Flat loading platens with two small diameter steel rods, (c) Flat loading platens with cushion, (d) Curved loading jaws (Li and Wong, 2013)
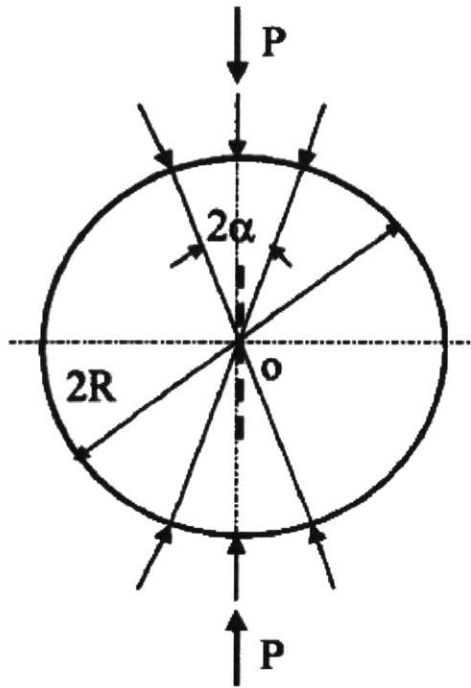
Figure 3.2: The Brazilian disk specimen under uniformly distributed diametrical load; the dashed line representing the crack induced upon loading, P is the summation of the distributed load. (Wang and Xing, 1999)
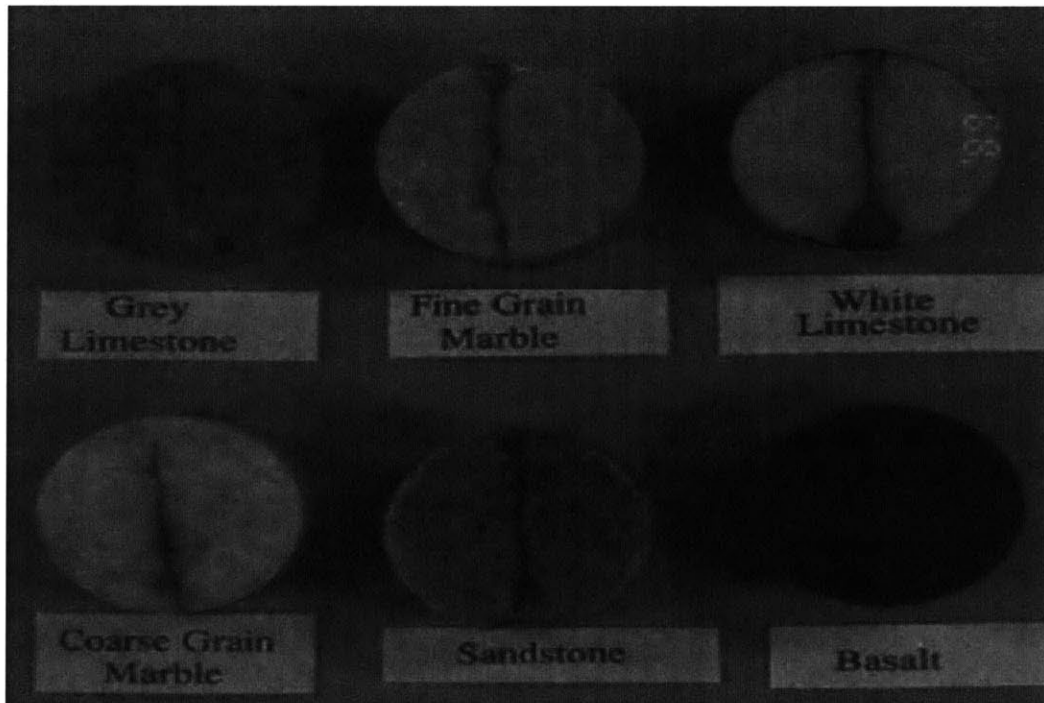
Figure 3.3: The fractured specimens of Australian rocks after Brazilian tests (Guo et al., 1993)
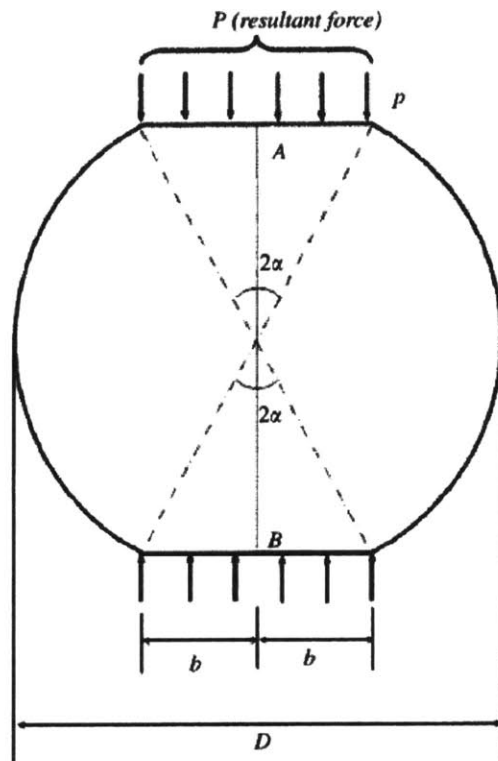
Figure 3.4: The flattened Brazilian disk specimen with two parallel flat ends (Wang et al., 2004)
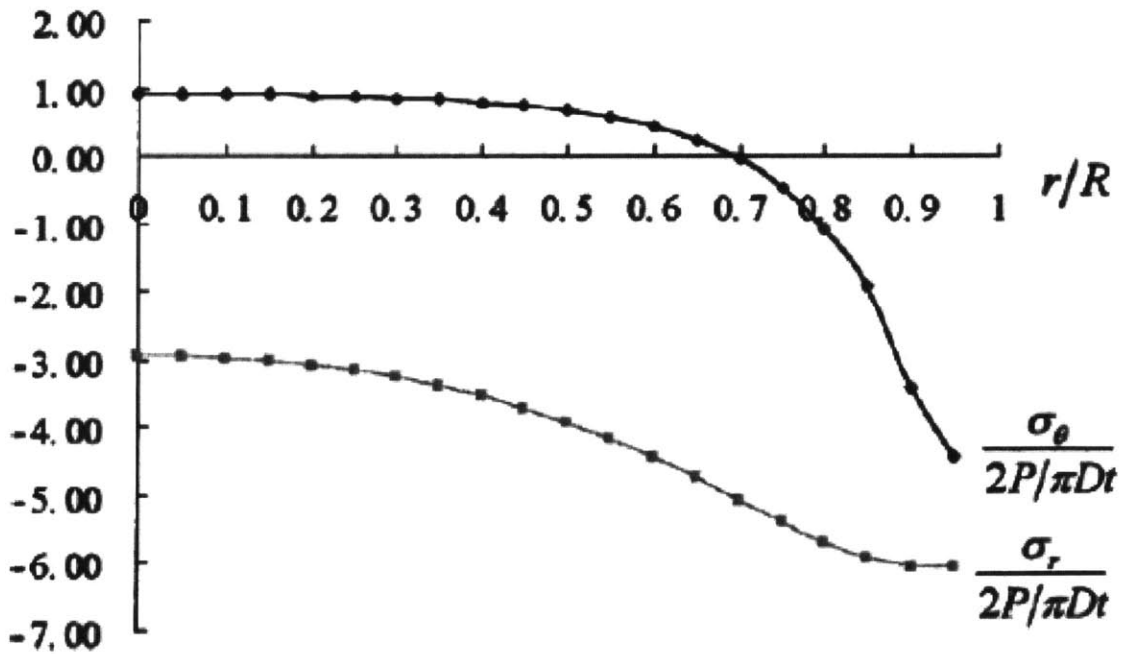
Figure 3.5: Radial and tangential stresses along the vertical diameter of the flattened Brazilian disc calculated using ANSYS for $2\alpha = 30°$. (Wang et al., 2004)

127
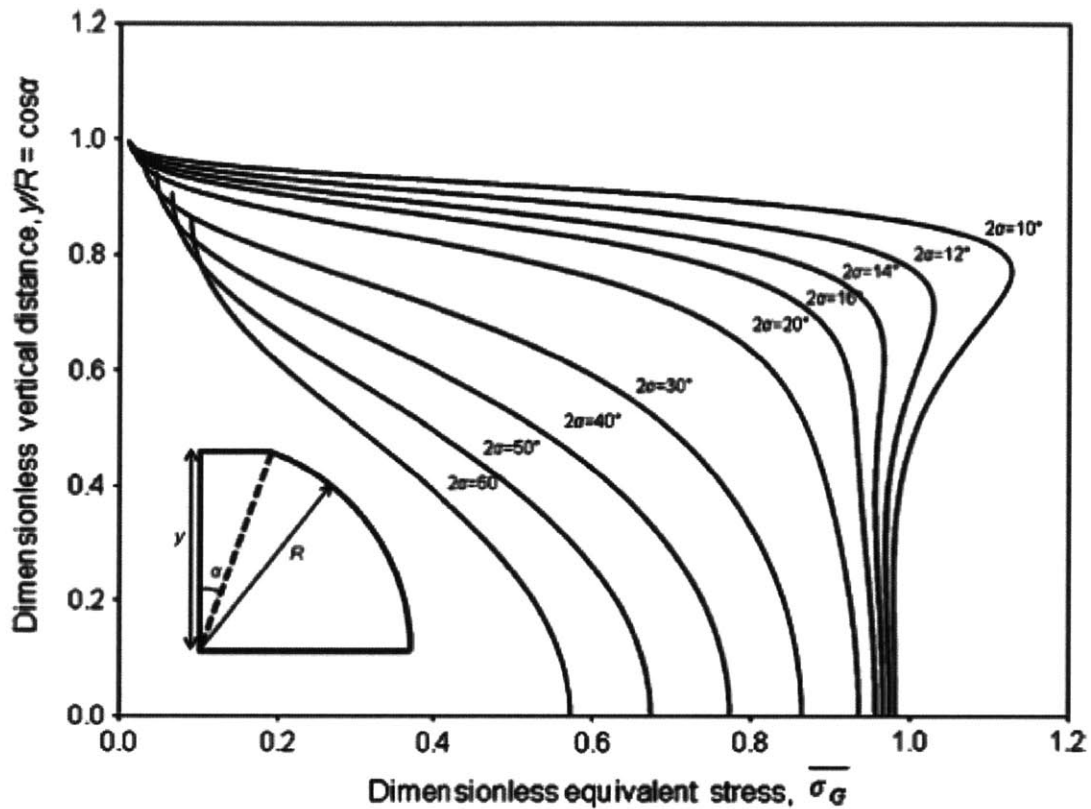
Figure 3.6: Variation of the dimensionless equivalent stress through the dimensionless vertical distance for specimens with 75 mm diameter (Keles and Tutluoglu, 2011)
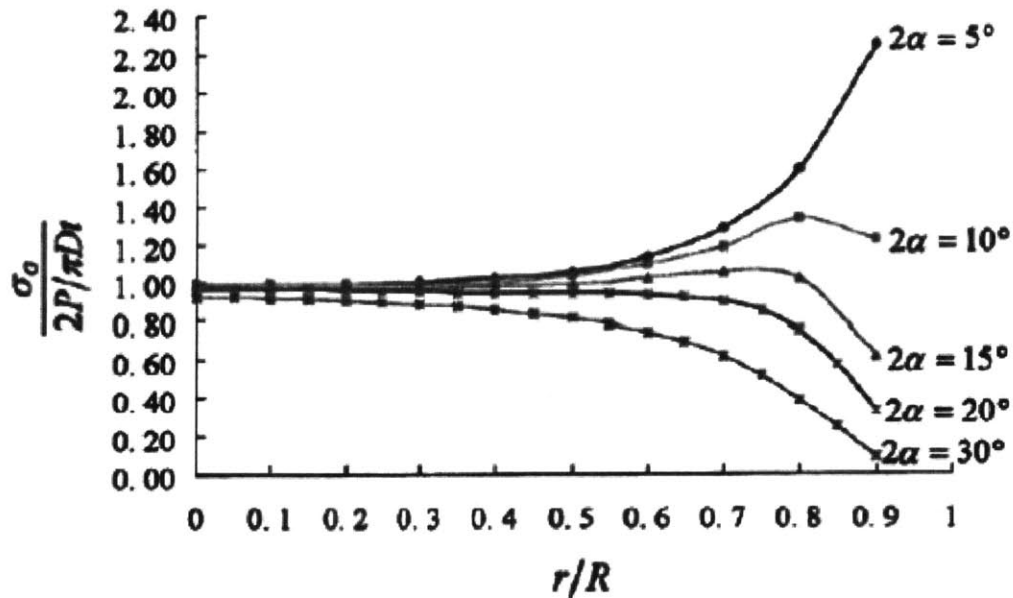
Figure 3.7: Variation of the dimensionless equivalent stress with the dimensionless vertical distance using numerical analyses software ANSYS (Wang et al., 2004)

128
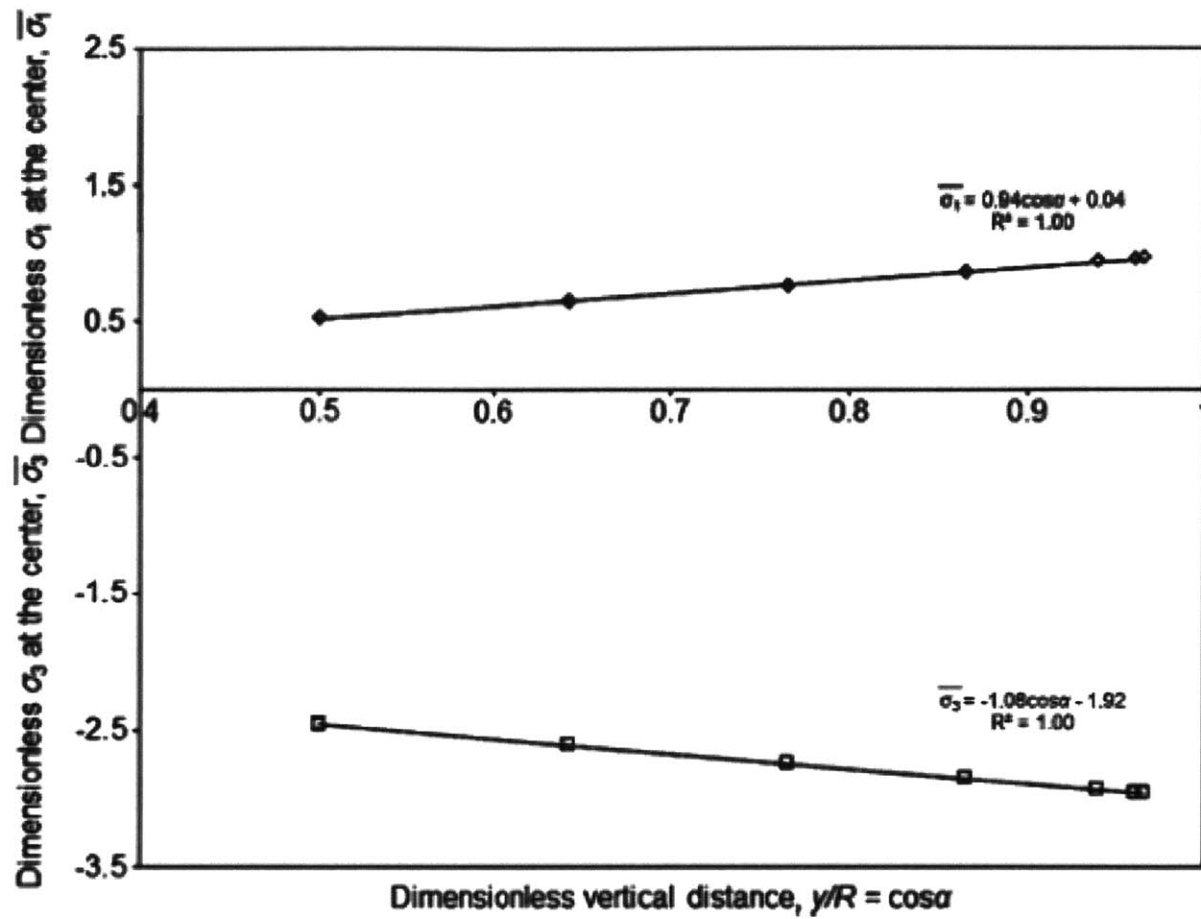
Figure 3.8: Dimensionless principal stresses versus dimensionless vertical distance plot (Keles and Tutluoglu, 2011)
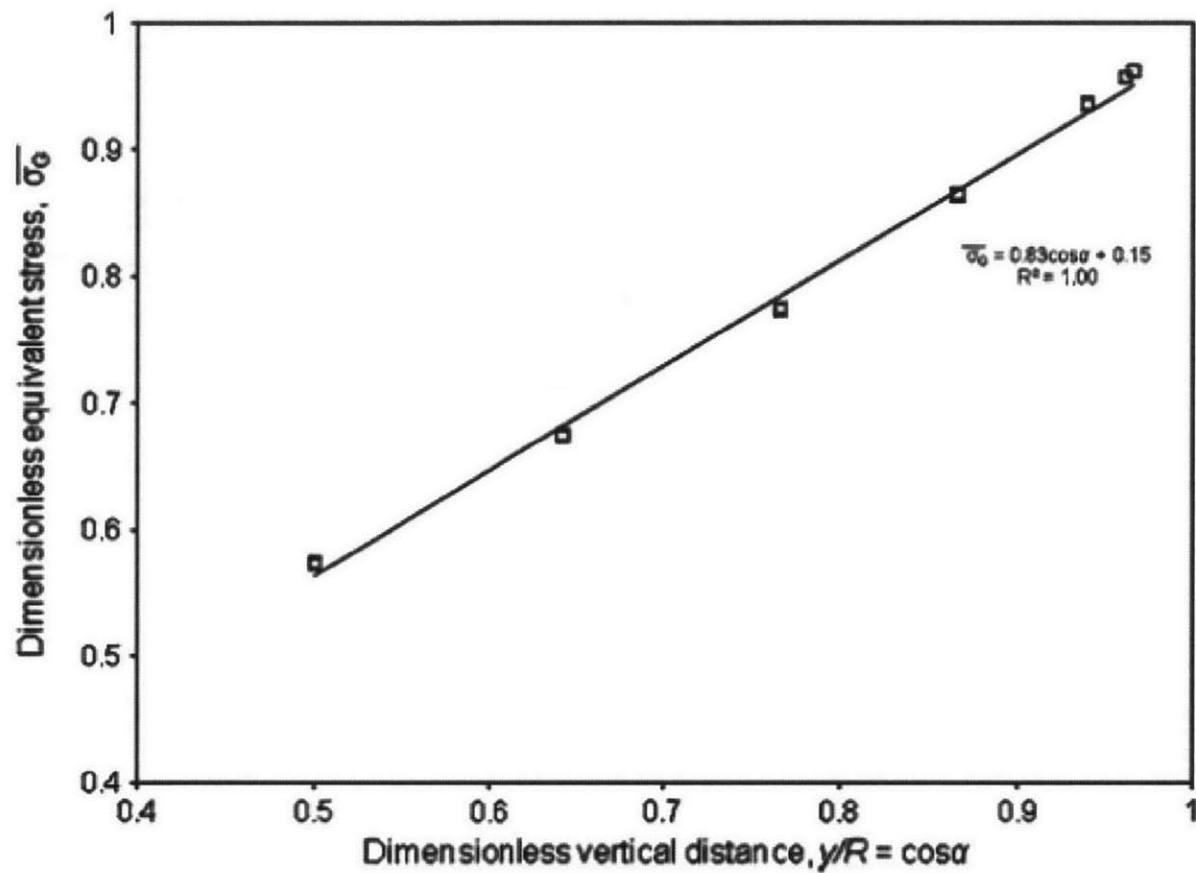
Figure 3.9: Dimensionless equivalent stresses versus dimensionless vertical distance plot (Keles and Tutluoglu, 2011)
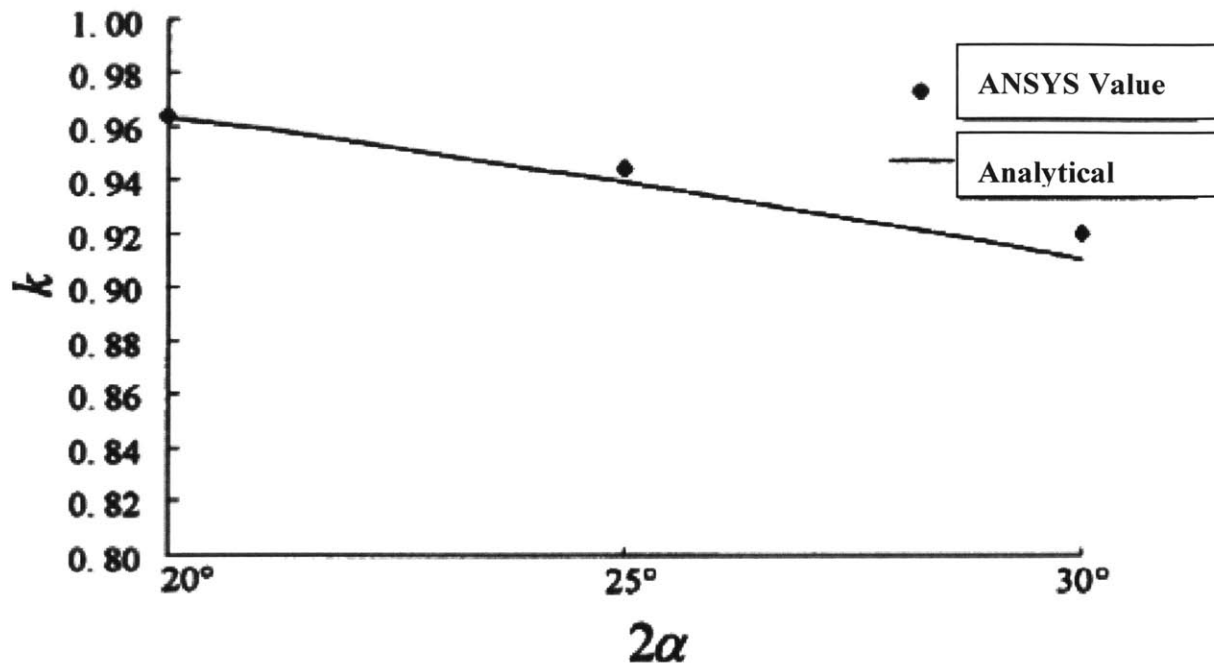
Figure 3.10: Determination of the *k* value in the tensile strength equation using approximate analytical formula and comparing it to ANSYS (Wang et al., 2004)
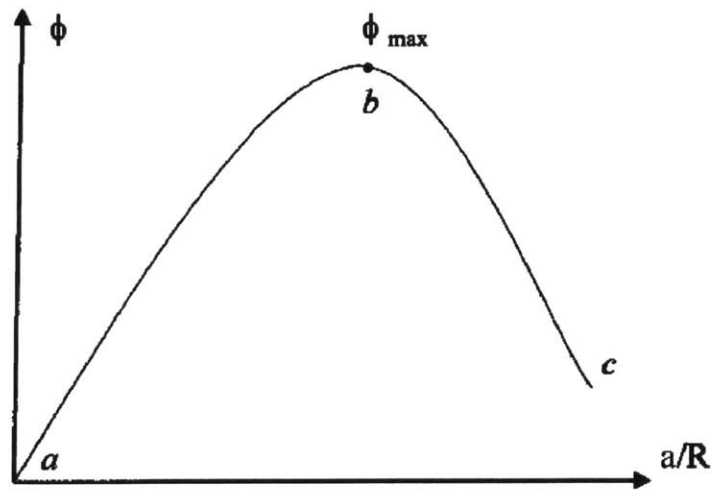
Figure 3.11: A schematic presentation for the dimensionless SIF ϕ vs. dimensionless crack length a/R (Wang and Xing, 1999)
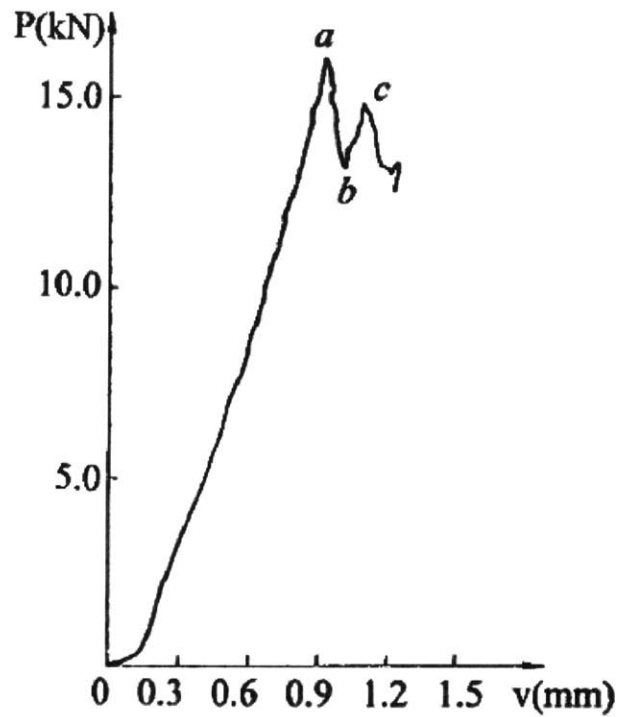
Figure 3.12: A typical test record of load P versus displacement using the Flattened Brazilian Disc Specimen (Wang and Xing, 1999)
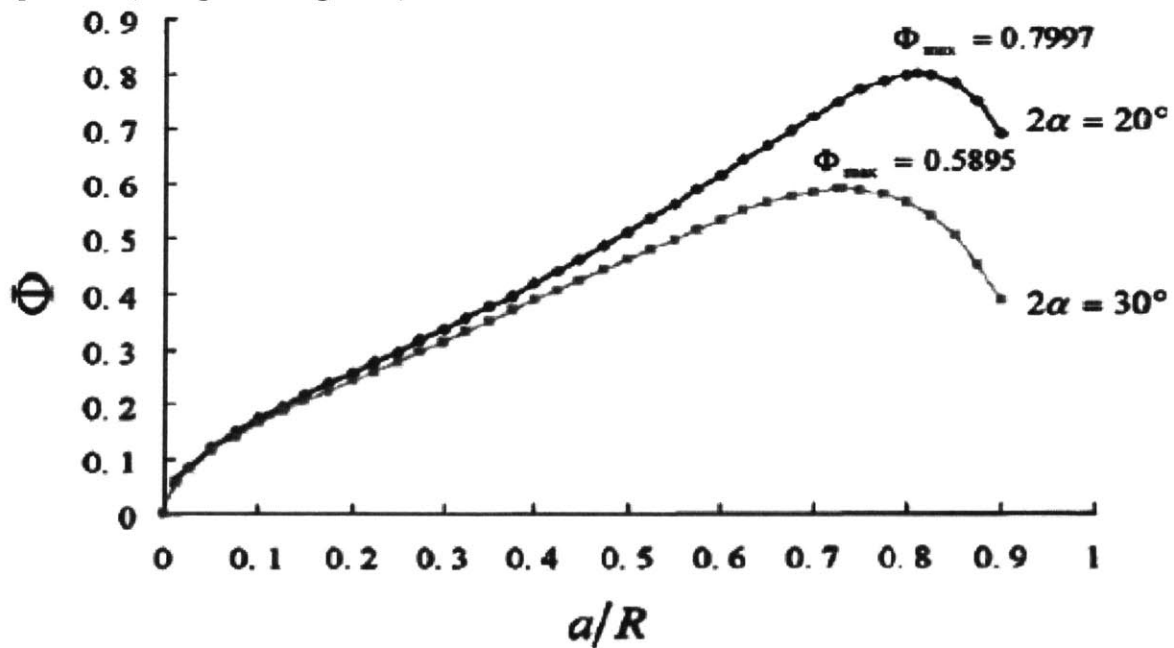
Figure 3.13: The dimensionless SIF versus dimensionless crack length for the flattened Brazilian disc with a central straight through crack (Wang et al., 2004)

132
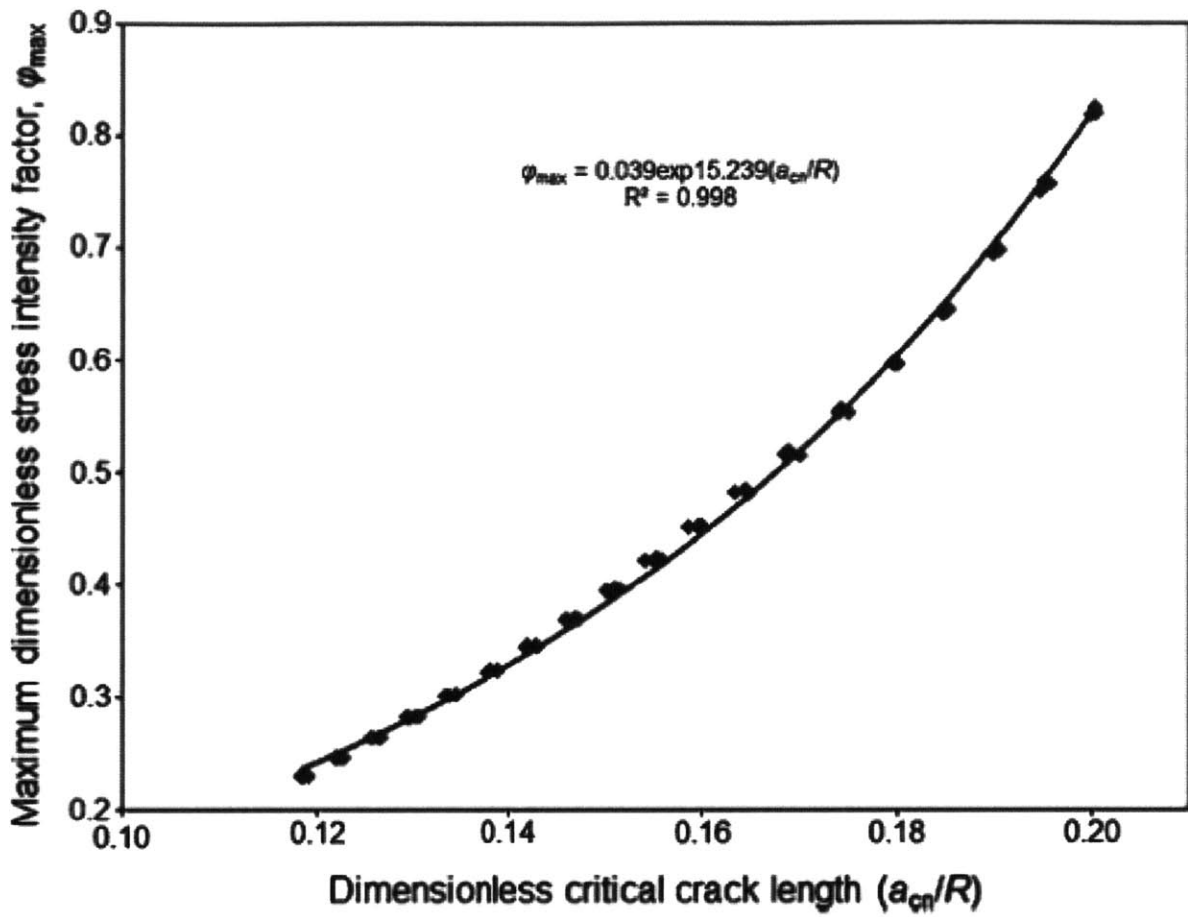
Figure 3.14: Variation of maximum dimensionless stress intensity factor with dimensionless critical crack length for flattened Brazilian disc models (Keles and Tutluoglu, 2011)

$$\varphi_{max} = 1/(43.32 - 15.63 \exp(\cos\alpha))$$
$$R^2 = 0.98$$
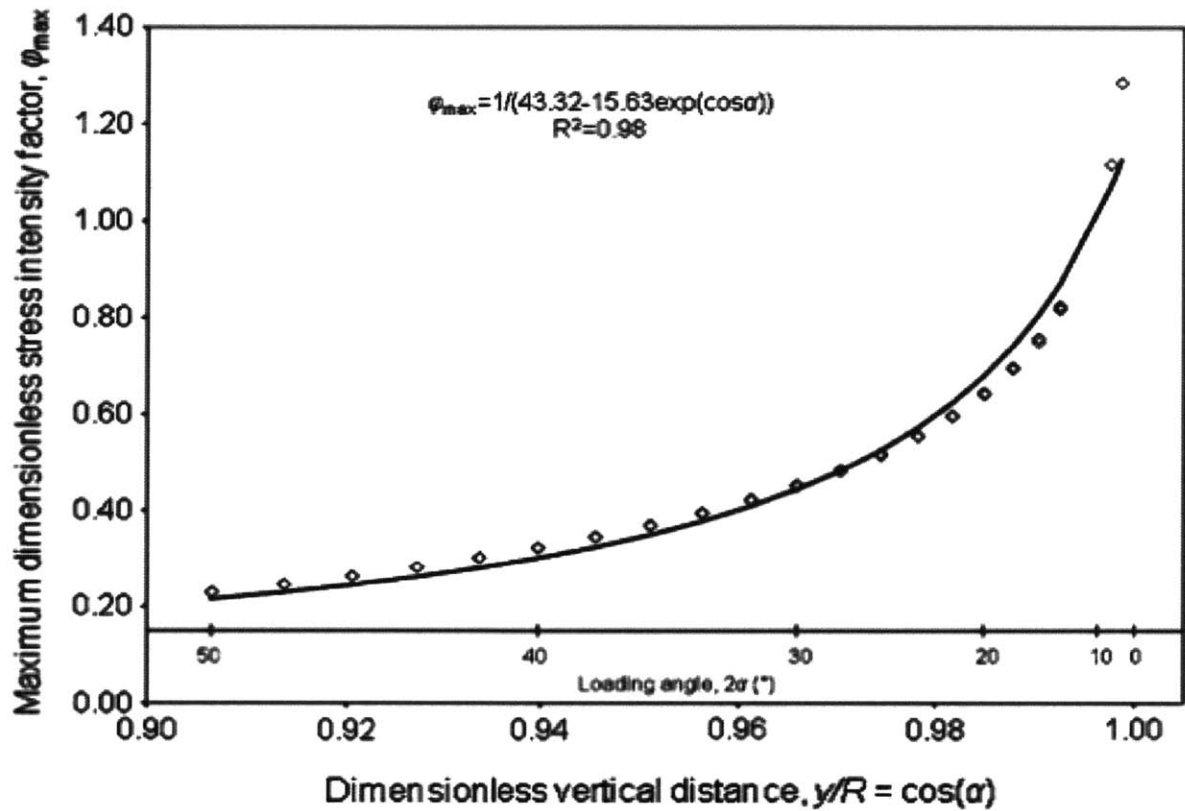
Figure 3.15: Variation of maximum dimensionless stress intensity factor with loading angle for flattened Brazilian disc specimens (Keles and Tutluoglu, 2011)
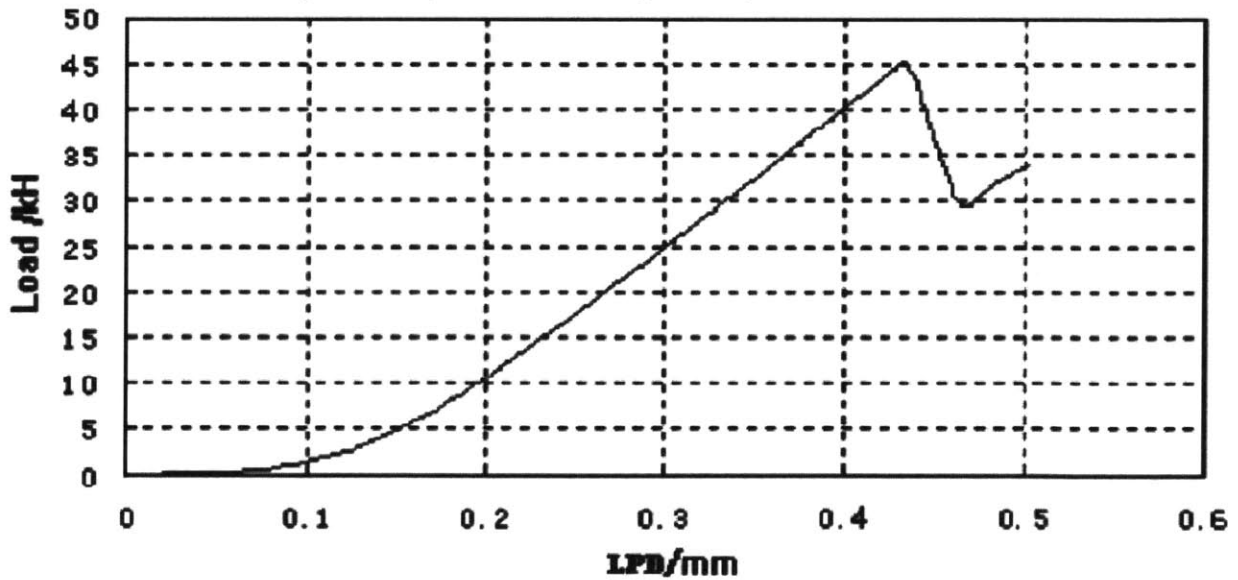
Figure 3.16: Load – load point displacement record for a valid test of marble using the flattened Brazilian configuration (Wang and Wu, 2004)
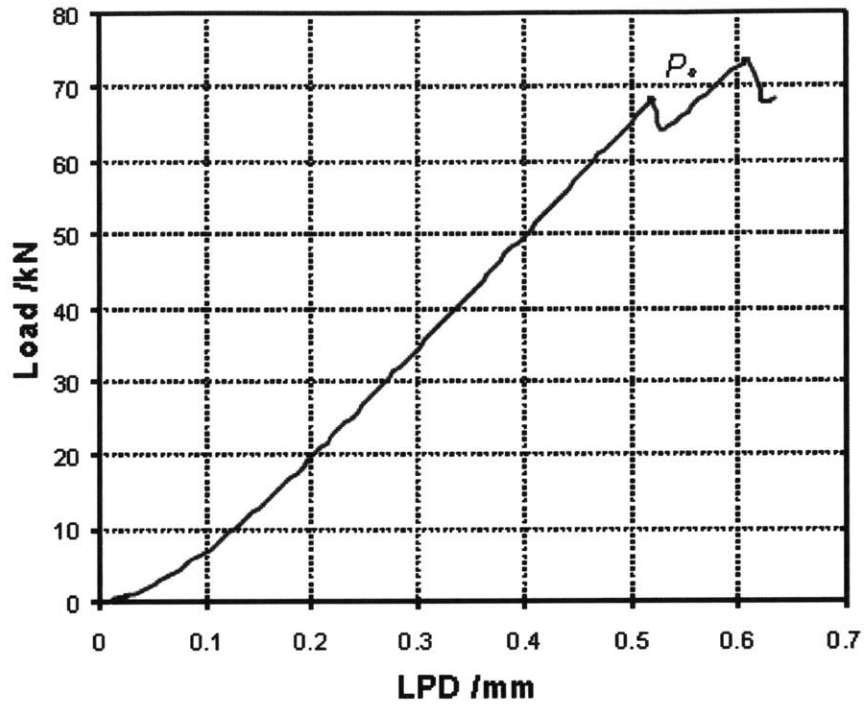
Figure 3.17: An invalid load – Load point displacement record for the flattened Brazilian disc configuration (Wang and Wu, 2004)
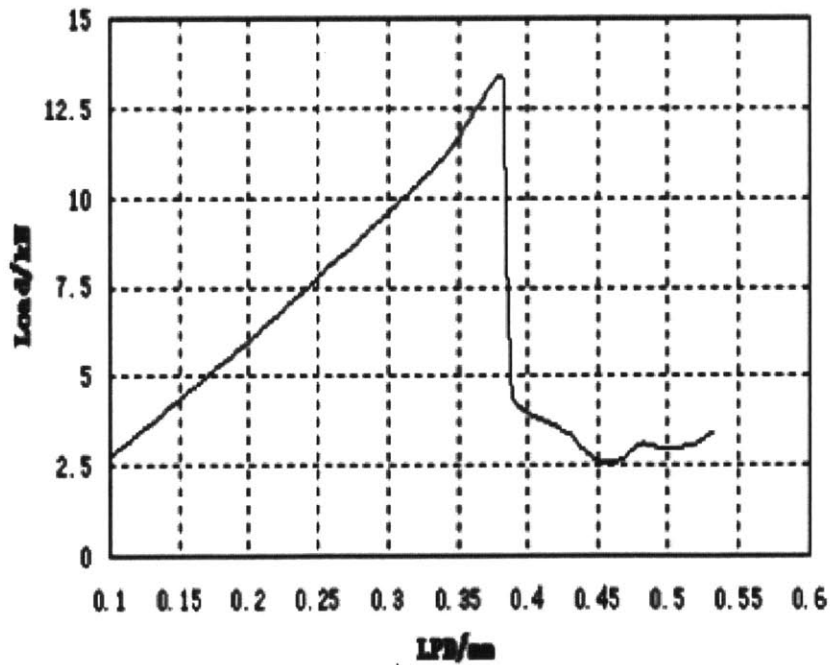
Figure 3.18: Another invalid load – Load point displacement record for the flattened Brazilian disc configuration (Wang and Wu, 2004)

Chapter (4)

EXPERIMENTAL WORK

4.1 Introduction

This chapter presents a detailed description of the laboratory testing program performed for this research. First the soils and materials tested are described, including a summary of their origin, index and strength properties. Next, a description of the Flattened Brazilian Disc (FBD) testing equipment used for determination of mode I fracture toughness, tensile strength, and modulus of elasticity is presented, which includes details pertaining to testing device, measuring transducers, specimen preparation technique, and testing procedures.

4.2 Materials Used in Testing Program

In the conducted flattened Brazilian disc experiments six different materials were under study; four of which are natural intact soils which came from different regions over the world: natural clay from Bangladesh, San Francisco Bay mud from the west coast in the United States, Boston Blue Clay, and Presumpscot Maine Clay both from the eastern coast of the United States. In addition, two clay-like fabricated materials were investigated: Plaster of Paris and molded gypsum. These two materials were chosen as model materials giving nearly uniform repeatable behavior which minimizes the heterogeneity found while testing natural intact soils.

4.2.1 Natural Soils

Based on the availability of natural soils within the laboratory facilities and feasibility of obtaining new specimens, four natural intact soils were investigated in this experimental study. In the following section, a brief description of each soil is provided with details on its origin, its mineralogy, and its basic mechanical and physical properties as reported in the literature.

4.2.1.1 Bangladesh Clay

Generally, Bangladesh clay is tropical residual reddish brown of intermediate to high plasticity inorganic (CI to CH) clay. It is mainly composed of illite, kaolinite, chlorite and some non-clay minerals mainly quarts and feldspar. It contains ferruginous cements, concretions and iron nodules (Alam et al., 1990; Monsur, 1995). It was observed that these Bangladesh sods showed a

random open micro fabric of silt and clay. There was also some evidence that alumina silicates, iron compounds and silica formed bonds between and within the grains. It is established that the tropical clay soils of Bangladesh are bonded. Bonding has an influence on the development of stress-strain and stiffness of the soils. An apparent pre-consolidation pressure of 170 kPa to 250 kPa was estimated for the natural soils, which is likely to be due to the bonded structure of the soils. Under undrained shearing, specimen initially showed peak positive values of excess pore water pressure followed by negative values at higher strains due to the tendency of the samples to dilate. No negative pore water pressures were observed at high confining pressures. Only a few samples at low confining pressures reach the critical state at very large strains approximately in excess of 20%. High confining pressure samples may not have reached the critical state due to the formations of distinct shear surfaces. After a final yield, soils' behavior is controlled only by friction. Generally, the compressibility of the soils is very low to medium (Monsur, 1995).

Bangladesh can be divided into three major physiographic units, namely, (i) the tertiary hill formations, (ii) the Pleistocene terrace, and (iii) the recent flood plains. On the southern tip of a Pleistocene Terrace lie the city of Dhaka, where two characteristics units cover the city and surroundings: Madhupur clay of Pleistocene age and alluvial deposits of recent age. In the current experimental research, clay samples were obtained from a rice field located in Bashailbhog village which lies in the Munshiganj district of Bangladesh, which is roughly 30 km south of Dhaka and 7 km north of the Ganges River (Neumann, 2010). **Figure 4.1** shows an approximate location of the site under study.

According to Neumann (2010), a specific gravity value of 2.78 was assumed, this value was determined from the mineralogy of a groundwater-irrigated rice soil in West Bengal (Norra et al. 2005). The soil contained 33% quartz which has a specific gravity of 2.65, 8% calcite with a specific gravity value of 2.71, 2% dolomite with a specific gravity value of 2.85, 14% feldspar with a specific gravity value of 2.76, 15% illite with a specific gravity value of 2.9, 10% kaolinite with a specific gravity value of 2.7, 18% other phylosillicates, which based on the work of Polizzotto et al. (2006) for the field site under study, are likely biotite or hornblede with a specific gravity value of 3.0. This mineral composition results in a bulk specific gravity of 2.78. However, there is uncertainty in this value mainly due to the fact that many of the minerals, including illite, feldspar, kaolinite and biotite, actually have a range of specific gravities due to natural mineral variations and mineralogical composition of Munshiganj rice field may be

different than that in the studied West Bengal field (Norra et al. 2005).

For the rice field clay specimens used in the current research, data from the tests carried out by Newmann (2010) can be summarized as follows for the in-situ conditions: the initial void ratio e_o, ranged from 0.847 to 1.110, the initial water content, w_c ranged from 29.78% to 32.97%, the porosity n, ranged from 0.46 to 0.53, initial degree of saturation, S ranged from 82.53% to 97.73%, the bulk density, γ_{bulk} ranged from 1.751 g/cm^3 to 1.953 g/cm^3, and the dry density, γ_{dry} ranged from 1.317 g/cm^3 to 1.505 g/cm^3.

Neumann (2010) determined the hydraulic conductivity, void ratio and bulk density of sections of the collected rice field cores; for her PhD research; following the protocol outlined in the ASTM standard for the constant rate of strain test (ASTM 2006). From the carried out test the relationship between the hydraulic conductivity and void ratio can be determined from the stabilized portion of the test which is shown in pink (Neumann, 2010). The in-situ hydraulic conductivity was calculated from this relationship using the initial void ratio of the specimen. A typical CRS test result for the Bangladesh clay tested is shown in **Figure 4.2**.

4.2.1.2 San Francisco Bay Mud

San Francisco Bay is a shallow estuary that forms water drain from approximately 40% of California for three major cities: San Francisco, Oakland and San Jose. It geologically dates back to early Pleistocene or to Pliocene. The bay occupies a depression between two uplifted areas: the Berkeley Hills on the east and the Montara and other mountains on the west. It is affected by two active faults that parallel the uplifted areas, each about 10 miles from the center of the bay: the San Andreas fault, which passes through the central part of the mountains to the west, and the Hayward fault, along the base of the Berkeley Hills to the east. The bedrock east of the Hayward fault is almost entirely Tertiary sandstone and shale. West of the fault most of the bedrock belongs to the Franciscan formation (Jurassic), except for a small area of sandstone and shale, of Merced age (Pliocene), south of the city limits of San Francisco. As the present bay was being formed, the rocks on the adjoining uplifted areas were eroded, and four sedimentary formations deposited in the bay: Bay Mud, Merritt sand, San Antonio formation, and Alameda formation (Lawson, 1914; Louderback, 1939 & 1951; Trask and Rolston, 1965).

The generalized geology near the edge of San Francisco Bay consists of a surface layer of younger bay mud covering older bay sediments, which extend to bedrock. The younger Bay Mud, which consists of more than 50 per cent water, is soft, low shear- strength, compressible

assemblage. The older bay sediments beneath the younger Bay Mud are unconsolidated sediments of late Pliocene to Holocene age deposited by alluvial processes when sea level rose. The older bay sediments vary greatly in composition and properties but are everywhere more compressed than the younger bay mud (Treasher, 1963).

Use of Bay Mud and clay for foundations demands careful engineering design to avoid shear failure and differential settlement problems. These problems are related to high content of both water and the swelling clay mineral, montmorillonite, which together cause low shear strengths, high void ratio, low specific gravity, high consolidation under load and high drying shrinkage. Generally shearing strength varies between 100-1200 pound/square foot.

The upper soil layer (Bay Mud) has up to 100 feet thickness. It is soft mud, becoming firmer with depth; consists of silty clay containing grains of wind-blown sand. In some areas, the upper part of the formation includes thin layers of fine- to medium-grained sand alternating with silty clay. In places, shells and plant fragments are found. Bay Mud usually has stiff crust of desiccated clay (Trask and Rolston, 1965).

The measured index properties for typical San Francisco Bay Mud (SFBM) as investigated by Kontopoulos (2012) are as follows: average liquid limit (LL) of 73%, average plastic limit (PL) of 44%, average plasticity index (PI) of 19%, average clay fraction of 47% and an average specific gravity of 2.69. For the specimens used in the current research SFBM has an average unit weight, γt of 16.59 kN/m^3, an average water content, w_c of 58.48%, and an average tore vane shear strength (T_v) of 0.45 kg/cm^2. According to Germaine (2010) SFBM has an average organic content value of 5.03%. San Francisco Bay Mud is considered grey elastic silt with a Unified Soil Classification System (USCS) classification of silt with high plasticity (MH). A typical gradation curve of San Francisco Bay Mud is exhibited in **Figure 4.3**.

Germaine (2001) determined the hydraulic conductivity, void ratio, coefficient of consolidation, and compressibility of sections of the San Francisco Bay Mud cores used in the current research; following the protocol outlined in the ASTM standard for the constant rate of strain test. From the carried out tests the compression behavior of San Francisco Bay Mud can be determined in addition to the relationship between the hydraulic conductivity and void ratio. A typical CRS test result for the San Francisco Bay Mud used in this research is shown in **Figures 4.4, 4.5, and 4.6**.

4.2.1.3 Boston Blue Clay

Much of the greater Boston area is underlain by thick deposits of glaico-marine illitic clay, locally known as Boston Blue Clay (BBC). Boston Blue Clay has a low plasticity index (Ip ranging from 20-25%) and is moderately sensitive. Engineering properties of both natural and re-sedimented BBC have been extensively studied. Pestana (1994) summarized the average index properties of Boston Blue Clay as follows: Mineralogy composed of Illite as a major component and Quartz as a minor component, the origin of BBC is Marine, the Unified Soil Classification System (USCS) classification of BBC is clay with low plasticity (CL), average specific gravity of 2.77, average liquid limit (LL) of 42%, average plastic limit (PL) of 21%, average plasticity index (PI) of 21%, average liquidity index (I_l) of 95%, clay fraction (C) 53 ± 5%, and activity of 0.42. Intact normally-consolidated BBC has an S shaped (double curvature) compression curve.

Typical triaxial compression behavior of reconstituted Boston blue clay at OCR of 1, 2, 4, and 8 shows that, normally consolidated clay (NC) shows a peak at small strains followed by development of large positive pore pressures that cause a significant decrease in *p'* and significant post-peak softening, while over-consolidated clay (OC) shows a decrease in the peak value of strength, in strain softening and in the development of excess negative pore pressure (Santagata, 1994). The undrained stress-strain lines of over-consolidated (OC) samples of Boston blue clay present flat peaks.

Boston Blue Clay (BBC) has low consolidation time, low swelling behavior, and does not exhibit extreme behavior in any parameter, thus making it good representative clay (Marjanovic, 2012). The soil's salt concentration is observed to vary between 5 and 20 g/l, with a decrease in salt content with increasing depth. Berman (1993) reported typical values of compression index of 0.179±0.038, K_o of 0.51-0.60.

For the current research Boston Blue Clay was obtained from three different locations at the MIT campus in Cambridge, Massachusetts. The intact specimens have average total unit weight, γt of 19.18 kN/m^3, average wet unit weight γw of 18.85 kN/m^3, average water content, w_c of 34.22%, average initial degree of saturation, Si of 99.94%, average initial void ration, e_i of 0.98, and average tore vane shear strength (T_v) of 0.67 kg/cm^2.

Boston Blue clay properties are known to vary spatially as well as by depth (Johnson, 1989). An

example for this variation; at one of tested Boston Blue Clay locations under study in the current research; is illustrated in **Figure 4.7.**

Germaine (2001) determined the hydraulic conductivity, void ratio, coefficient of consolidation, and compressibility of sections of the Boston Blue Clay cores used in the current research; following the protocol outlined in the ASTM standard for the constant rate of strain test. From the carried out tests the compression behavior of Boston Blue Clay can be determined in addition to the relationship between the hydraulic conductivity and void ratio. A typical CRS test result for the Boston Blue Clay used in this research is shown in **Figures 4.8, 4.9, and 4.10.**

4.2.1.4 Presumpscot Maine Clay

The Presumpscot Formation is a glaciomarine silty clay found in the coastal lowlands of Maine and extending inland along the Penobscot and Kennebec River valleys (Thompson, 1987). As the ice sheet margin receded, isostatic crustal rebound resulted in the relative uplift of the Presumpscot sediments above the marine limit. The depositional environment and subsequent uplift have had considerable effects on the geotechnical properties of the Presumpscot formation. For the soft Presumpscot clay, most all shear strength values for design are obtained from the field vane shear test rather than by laboratory testing as is common practice for many clay deposits elsewhere. Typical values of the peak undrained shear strength measured by the vane test for the Presumpscot Formation range from 170 to 2400 psf. Typical examples of Presumpscot strengths have been published by Poulos et al. (1982), MSHC (1969) and Sandford and Amos (1987). Undrained shear strength implies that shearing occurs rapidly enough to preclude drainage and the dissipation of excess pore water pressures generated during shear. According to Adams (2011), the mineralogy of Maine clay resembles that of natural Boston Blue Clay. Presumpscot Maine clay has an average specific gravity value of 2.78. The clay fraction is approximately 30% though this may vary spatially and by depth (Vargas, 2013). Reynolds (1991) reports typical Atterberg limits of Presumpscot Maine clays as 30 % as liquid limit, 20 % as plastic limit, and 10% as plasticity index. The Unified Soil Classification System USCS classification is low plasticity clay, CL.

Germaine (2002) determined the hydraulic conductivity, void ratio, coefficient of consolidation, and compressibility of sections of the Presumpscot Maine clay cores used in the current research; following the protocol outlined in the ASTM standard for the constant rate of strain test. From the carried out tests the compression behavior of Presumpscot Maine clay can be determined in

addition to the relationship between the hydraulic conductivity and void ratio. A typical CRS test result for the Presumpscot Maine clay used in this research is shown in **Figures 4.11, 4.12, and 4.13**.

4.2.2 Clay-like Brittle/Semi-brittle Materials

Some of the first experimental tests on fracturing in brittle materials were conducted by Brace & Bombolakis (1963). Since then researchers have conducted experimental studies to investigate the cracking processes in various natural and composite brittle materials (Morgan, 2011). In the current experimental study two composite clay-like brittle materials were investigated: *Plaster of Paris* which was previously studied by Lajtai (1970) and Nesetova and Lajtai (1973) and *Molded Gypsum* which was extensively investigated in MIT by Reyes (1991); Reyes and Einstein (1991); Shen et al. (1995); Bobet (1997); Bobet and Einstein (1998); Sagong (2001); Sagong and Bobet (2002); Wong and Einstein (2009); and finally Morgan (2011).

4.2.2.1 Plaster of Paris

Plaster of Paris is a brittle, porous solid, easy to shape, which has potential as a model material for the study of brittle, porous, solids such as ceramics, dried clays, rocks and cement (Vekinis et al., 1993). Plaster of Paris, a chemically hydrated calcium sulphate, is a brittle solid with fracture properties that resemble to a great extent those of cement, sandstone, and other porous ceramics. Plaster of Paris is calcium sulphate hemihydrate, $CaSO4 \cdot \frac{1}{2}H2\,0$. It can be prepared by heating gypsum between 120 and 160°c. the following equation expresses the chemical changes during the formation of Plaster of Paris:

$$CaSO4 \cdot 2H_2O \leftrightarrow CaSO4 . \frac{1}{2}H_2O + 1\frac{1}{2}H_2O \tag{4.1}$$

When plaster of Paris is mixed with water the reverse reaction takes place where water is reabsorbed by the formation of gypsum. The reaction is exothermic and results in a coherent mass of interlocking needle-shaped gypsum crystals (Vekinis et al., 1993). The chemistry of the reaction requires only 18.6% by weight water for rehydration, but in practice much more is used to give the fluidity needed for casting. The excess water evaporates leaving considerable porosity. According to Vekinis et al. (1993), true density of the hemihydrate is about 2750 kg/m^3 and of the dihydrate is about 2320 kg/m^3, so contraction on setting would be expected but the arrangement of the crystals is such that setting results in a slight expansion (about 0.5%). Generally, the mechanical properties of Plaster of Paris depend on powder-to-water ratio, curing

time, temperature and pressure, and on post-cure heat treatment. Using Environmental Scanning Electro Microprobe (ESEM) micrograph it can be observed that Plaster of Paris samples may contain small spherical pores as illustrated in **Figure 4.14**. The presence of these pores is probably due to trapped water during casting, which decrease in size with increasing bulk density of the material (Vekinis et al., 1993).

A number of mechanical and physical properties for plaster of Paris have been investigated over the years. According to experimental studies carried by Vekinis et al. (1993), Plaster of Paris has an average density of 1.170 g/cm^3, an average total porosity of 51 (%), an average modulus of elasticity determined by four-point bending, E_{bend} of 4.5 ± 0.1 GPa and determined by uniaxial compression, E_{comp} of 4.6 ± 0.3 GPa, an average modulus of rupture determined under four point bending of 5.8 ± 0.6 MPa, an average fracture toughness, K_{IC}, determined by four-point straight edge notched beam (SENB) of 0.14 ± 0.015 $MPa.m^{0.5}$, an average uniaxial compressive strength of 14.6 ± 0.9 MPa, an average compressive strength under hydrostatic conditions of 19.2 ± 1.4 MPa, and finally an average uniaxial tensile strength of 3.2 ± 0.6 MPa.

4.2.2.2 Molded Gypsum

Molded gypsum has been extensively used as a model rock at the rock mechanics research group at MIT in the past forty years, researchers and scholars included Nelson (1968), Einstein et al. (1969), Motoyama and Hirschfeld (1971), Einstein and Hirschdeld (1973), Reyes and Einstein (1991), Shen et al. (1995), Bobet and Einstein (1998), Ko et al. (2006), Wong (2008), and Morgan (2011).

The molded gypsum (CaSO4·2H2O) is obtained by mixing commercially available gypsum powder (HYDROCAL B-11™) with water. The formed gypsum powder is actually hemihydrate (CaSO4·½H2O). Nelson (1968) noted that hemihydrate is obtained by purifying and heating natural hydrated gypsum:

$$CaSO4 \cdot 2H2O \rightarrow CaSO4 \cdot \tfrac{1}{2}H2O + 1\tfrac{1}{2}H2O \tag{4.2}$$

When the hemihydrate is mixed with water in the laboratory, hydrated gypsum is reformed (CaSO4 · ½H2O + 1½ H2O → CaSO4 · 2H2O). (4.3)

The gypsum specimens are then stored in a 40° oven to remove any excessive water after fabrication, but the water of crystallization ($2H_2O$) associated with CaSO4 is still retained (Wong, 2008).

A number of mechanical and physical properties for molded gypsum have been investigated over

the years. According to experimental studies carried by Wong (2008), the average density, ρ is 1.54 g/cm^3 and the average uniaxial compressive strength, σc is 33.85 MPa and in a more recent study by Janeiro and Einstein (2010), the compressive strength of Hydrocal was found 37.2 MPa. And according to earlier studies the average uniaxial tensile strength, σ_T ranged from 2.4 MPa as reported by Nelson (1968) and 3.2 MPa as reported by Bobet (1997). Bobet (1997) also reported the average Young's modulus of elasticity, E to be 5960 MPa and average Poisson's ratio, v is 0.15 which is less than the value reported by Nelson (1968) of 0.24. According to Morgan (2011), the correct Hydrocal mix should be composed of 85% by weight Portland cement, 10% by weight hemihydrate ($CaSO4 \cdot \frac{1}{2}H2O$), and 5% by weight crystalline silica.

Wong (2008) carried out environmental scanning electro microprobe (ESEM) images that revealed that average gypsum crystals are of a plate to needle shape 5 μm long and 2 μm wide. In-between the plates, small inter-connected pores with approximately 1 to 5 μm size which are exhibited in **Figure 4.15**.

4.3 Material Processing

4.3.1 Natural Soils

The specimen preparation of natural soils (intact materials) involves two main stages: 1st stage involves the material inspection, extrusion, cutting into circular discs while the 2nd stage involves oven drying, trimming, sanding, and obtaining two parallel flat ends. The FBD tests are performed on specimens that were first used for constant rate of strain (CRS) testing and have been compressed in the end to the normally consolidated (NC) range.

The first stage can be summarized as follows: Intact materials; in our research Bangladesh Clay, San Francisco Bay Mud, Boston Blue Clay, and Presumpscot Maine Clay; are obtained from standard push tube samples. These tubes are usually 2.8" diameter galvanized steel or brass and are capped and sealed at each end.

Then the tubes are x-rayed according to the protocol suggested by Germaine and Germaine (2009) where the radiographs as the ones shown in **Figure 4.16** are used to determine least favorable locations of poor sample quality which are not suitable for further testing. Once a suitable specimen is determined, the section is cut from the tube with a band saw located in the

trimming room shown in **Figure 4.17**. Then cut edges of the sample tube are smoothed and processed to remove metal burs for safety reasons as illustrated in **Figure 4.18** (Adams, 2011).

The soil adjacent to the cut portions is disturbed from the cutting process and often contains metal fragments which are removed via scraping shown in **Figure 4.19**. The remaining portions of the sample tube not containing the specimen to be tested are sealed with wax to retain moisture and taped back together for later use and a log sheet is used to record the location of the cut section and the testing performed for future guidance (Germaine and Germaine, 2009).

The specimen is extruded from the tube section first by cutting along the inner circumference of the sample tube with a piece of piano wire as illustrated in **Figure 4.20**. And the specimen is pushed out of the tube by placing it against an elevated circular object of equal diameter as illustrated in Figure **4.21** and pushing the specimen tube down. After the specimen is fully extruded it is transferred to a plate to prepare for trimming, a partially extruded specimen is shown in **Figure 4.22**.

The first stage in trimming involves obtaining a circular disc which is achieved using the cutting ring technique. A schematic of the technique is displayed in **Figure 4.23**.

Germaine and Germaine (2009) provide detailed instructions for performing the cutting ring technique which can be summarized as follows: The ends of the section perpendicular to the axis of the sample should be squared, then ensure that the section of soil has at sufficient thickness on all surfaces to allow for trimming. Then place the soil section on a rigid plate covered with a piece of wax paper. Then place the cutting ring on the soil, as shown in **Figure 4.23**.

In the procedure followed the soil and the ring were put in a trimming frame as shown in **Figure 4.24** to maintain alignment and to provide stability during the trimming process. The majority of the cutting should be performed using a spatula or knife in advance of the cutting ring. The spatula is used to cut a taper leading up to the cutting ring. Next, the assembly is advanced in small increments such that the soil cut away does not cover the beveled portion of the cutting tool. When trimming the soil away, trim in front of the blade to avoid cutting into the specimen.

The cutting procedure is continued until the cutting ring has advanced into the soil a sufficient depth to create a specimen a few millimeters thicker than that required for the test.

The cutting ring and soil are removed from the alignment device and a rigid plate is placed (without wax paper) on the soil and cut off the excess material with a wire saw. While cutting the surface, a small force is applied to the plate to keep the material in compression and a wire is

used to saw back and forth using the ring surface as a guide. The process is repeated until the soil is lifted up and released for testing. After this step the circular disc specimen may be used in any kind of testing requiring circular specimens like constant rate of strain (CRS) test or direct simple shear (DSS) test then the un-cracked intact specimen is oven dried and this is when the second stage of preparation starts.

The second stage of specimen preparation starts with oven drying the specimen at a temperature of 100° C for at least 48 hours to achieve complete drying of any moisture within the specimen. The drying process results in large suction which may draw the particles together internally. The excess negative pore pressure generated upon suction may be much larger than the effective preconsolidation pressure the specimen has witnessed in its stress history. However, the negative pore pressure acts on a limited area and its effect on erasing the specimen's stress history is dependent on the magnitude of the maximum effective stress the specimen s subjected to in the CRS test.

After oven drying, the specimen is cooled in a humidity controlled container then the desired dimensions of the finished flattened disc are marked on the specimen using a pencil and a ruler. The width of top and bottom flat edges is marked to define the loading angle (2α) of the finished specimen. After marking, the circular oven dried disc is trimmed using a sharp edged blade and a miter box, the purpose of this stage is to initiate the removal of the curvature of the top and bottom edges of the circular disc. After careful sawing back and forth with the blade, no further curvature of the circular edges is observed. The specimen is then hand sanded before machine sanding to remove any sharp edges that can be broken off by the belt sander. Some specimens may have sharp pieces on the edges and flaws that cause larger pieces to be broken off if they are directly sanded with the orbital sander.

Then the partially trimmed no-longer circular disc is brought to a sanding machine like the one shown in **Figure 4.25**, for the purpose of these experiments a 6" width belt sander; manufactured by Delta model No. 31-730; located in the rock mechanics laboratory was used. The top and bottom edges of the specimen are carefully sanded using the belt sander machine and provided guides until approaching the initially marked top and bottom flat widths. The guides are used to maintain parallel flat edges while sanding. After obtaining the desired width for the flat top and bottom edges, the flattened specimen is hand sanded again to ensure creation of smooth flat ends. To ensure the parallelism of the top and bottom flat edges, the vertical distance between the top

147

and bottom edges is measured at several locations within the flattened edge and at each location it is measured at least three times. Another means to ensure the flatness and parallelism of the finished flattened surfaces is using a bubble level.

Afterwards, the specimen's final top and bottom flat widths are measured and the central loading angle (2α) is separately measured to be used in calculation formulas of fracture toughness and tensile strength. Hence, the specimen is ready for flattened Brazilian testing. **Figures 4.26 and 4.27** show a typical flattened Brazilian disc before and after the specimen sanding and preparation.

4.3.2 Clay–like Materials

Gypsum and Plaster of Paris specimens were prepared and artificially molded following the same procedures as in previous studies in the rock mechanics group at MIT such as Reyes and Einstein, 1991, Shen, et al., 1995, Bobet and Einstein, 1998, Ko, et al., 2006, Wong, 2008, and Morgan, 2011. Wong (2008) gave detailed instructions on specimen's fabrication which will be summarized in this section.

The gypsum specimens were cast from a mixture of Hydrocal B-11 powder, celite powder and water at mass ratios of 700:8:280. The addition of celite powder reduced the amount of bleeding (migration of water to the top of the fluid mix). In the beginning, measure 6.4 grams of celite powder, 560 grams hydrocal B-11 (gypsum) powder, and 224 milliliters of water. The celite powder is poured into the mixing bowl followed by the water then the bowl is placed into a mixer which will be operated for about 20 seconds. Afterwards, the bowl is removed from the mixer and the gypsum powder is gently poured over the beaten celite and water mix. Then the bowl is returned to the mixer which will be operated for four minutes to ensure proper mixing to the gypsum mix, as shown in **Figure 4.28**. The bowl is removed from the mixer and the beaten paste is poured from the bowl into cylindrical 3 inches plastic molds slightly greased using WD-40 with the aid of a rubber spatula. The mold is brought to a vibrator for two minutes to minimize the trapped air bubbles in the paste. The gypsum molds are placed covered to dry and set on top of a horizontal bench, as shown in **Figure 4.29.**

Afterwards, the specimen is removed from the mold and cleaned using a damp cloth to remove any excess grease. The mass of the specimen is measured and it is placed into an oven set at

40°C. The mass of the specimen is monitored periodically until it reaches a constant value which usually takes from 5 to 7 days. **Figure 4.30** shows an example for a dried extracted gypsum specimen.

After obtaining constant mass, the cylindrical specimen is cut into a number of uniform circular discs using a band saw located in the rock mechanics laboratory. Afterwards, we have circular discs / rings resembling the intact soils described in the previous section. Using the same procedures of pre-defining top and bottom flattened widths with a central loading angle followed by hand and machine sanding the circular gypsum specimens are converted to non- circular flattened Brazilian discs which are ready for testing.

For the Plaster of Paris specimens, nearly the same procedure is followed but with different components and ratios. For the plaster of Paris specimens conducted in this research, a number of plaster powder to water ratios were evaluated and it was found that the optimum powder to water ratio is 1.75: 1. Hence, for specimen preparation 700 grams of plaster powder and 400 milliliters of water were measured then they were poured into the mixing bowl and were mixed for under 2 minutes (the author faced difficulties in dealing with the paste if mixed more than 2 minutes as it solidifies and hardens quickly). The mixture is poured into the same plastic molds as gypsum then vibrated for a couple of minutes then left to set and dry for nearly two hours. The extracted cylindrical specimen is oven dried at 40°C as well and kept in the oven until reaching a constant mass value. The cylinder is cut using the same band saw followed by the same sanding procedure to obtain flattened Brazilian discs ready for testing.

4.4 Testing Equipment

4.4.1 Loading Frame

In the current experimental research two load frames were used to perform the experiments; an off the shelf mini load frame (shown in **Figure 4.31**) manufactured by Wykeham Farrance and has model number: T56B. This mini load frame was mainly used to test the four natural soil types which did not require high loading capacities. This particular load frame has five different displacement rates ranging from 0.0037 to 46 cm/hour. For the conducted experiments average displacement rate of 0.2 mm/min was chosen for testing after trying several different loading rates. There are two main disadvantages when using this load frame; it is a purely mechanical device with no electronic interaction with no computer readout, and no computer control to halt

the device once a certain stress is achieved which means it is entirely operator dependent and must be operated by an on/off switch. The second disadvantage is that it can only apply a constant rate of strain and not a constant level of stress.

The second load frame used in testing the clay-like materials (gypsum and plaster of Paris) requiring higher loading capacities was manufactured by MTS with loading capacity of 110 kips and has model number: 311.21. This particular load frame is equipped with hydraulic lifts, hydraulic locks and controls. It is also provided with MTS 35KIP, 3000 PSI Actuator, Model 204.64, S/N 129, with 4" Stroke, LVDT and area = 12.54 sq. in. In addition, it has an MTS Line Tamer, an MTS 55KIP Fatigue Load Cell, two MTS servo valves, MTS 55KIP 3000 PSI Hydraulic Grips, Model 641.36 with inserts for 3.88" wide flat specimens, and finally MTS 3000 PSI Hydraulic Grip Control Unit.

4.4.2 Overall Test Configuration

Figure 4.32 presents a schematic diagram for the loading setup of the flattened Brazilian disc specimens, where the flattened specimen is bound between two flat surfaces (top and bottom) for load application where the top flat surface is connected to the load cell using a ball for uniform pressure distribution and minimizing stress concentrations. The clip on extensometers are attached to the specimen's surface using the wing attachments and rubber bands, in addition, an attachment is used to hold the linear voltage displacement (LVDT) transducer which is touching a flat stiff surface beneath the loaded specimen to measure the overall machine/specimen vertical displacement. **Figure 4.33** shows the loading setup for a flattened Brazilian disc tested in the mini load frame followed by **Figure 4.34** which presents a close up on the configuration of the used LVDT while testing, and **Figure 4.35** presents an example for the loading setup using the MTS high capacity load frame.

4.4.3 Load Cell

The load cell used in the Flattened Brazilian Disc load frame is a Data Instruments Model JP 500 load cell with a capacity of 500 lb (2.225 kN). The load cell; which was used to determine axial force applied on the flattened Brazilian discs; uses a shear beam geometry to concentrate stains in an instrumented section. Strains are measured with strain gauges whose output voltage can be related to the applied load using a calibration relationship. For the load cell used during the experimental procedures the calibration factor was 6770.033951 (kg/ (V/V)) with a resolution of

150

0.05 N (0.001 mV) and stability of 0.1 N (0.002 mV). **Figure 4.36** shows a photo of a 500 lb capacity load cell like the one used in testing.

4.4.4 Axial Displacement Transducers

The axial deformation of the flattened Brazilian disc is preliminarily measured using a Linear Variable Differential Transformers (LVDT) manufactured by Trans-Tek Inc. The linear range is approximately 2.5 cm. Adams (2011), gives a brief description for the LVDT used during testing which is comprised of three coils including one primary coil in the centre and two secondary coils on either side. An electric current passing in the primary coil creates a magnetic field which induces a voltage in each of the two secondary coils, and this voltage is proportional to the mutual inductance with the primary coil. When the ferrous core moves through the centre of the coils, the mutual inductance is altered, changing the voltage response. A slight movement of the core produces a nearly linear change in the differential voltage output between the two secondary coils. This differential voltage can be related to the displacement using the calibration factor. For the LVDT used during the experimental progress the calibration factor was 1.6444 (cm/ (V/V)) with a resolution of ±0.0001 cm (0.1 mV) and stability of ±0.0003 cm (0.3 mV). **Figure 4.37** shows a photo of an LVDT similar to the one used in testing.

4.4.5 Extensometers

A pair of extensometers has been used to provide more accurate reliable measurements. The extensometers are considered the final means of measuring the moduli of a material where they have been used to measure the displacement over a fixed gauge length within the specimen then converted to axial strain to compute Young's modulus of elasticity during uniaxial loading. An extensometer measures small deformations associated with applied stress. Using the stress-strain relationship during loading, the elastic modulus can be approximated from the slope of the initial portion of the curve (Marjanovic, 2012). The contact extensometer used in this research was the Instron Industrial Products series 2620-826 item. These extensometers contain strain gauge units arranged in a Wheatstone bridge circuit and have the ability to measure dynamic testing up to ±20% strain with an input voltage of 4V which is different from the 5.5 input voltages of remaining transducers. The differential voltage can be related to the displacement using a calibration factor. For the extensometers used during the experimental progress the calibration

factors were 805.3 (mm/ (V/V)) and 865.4 (mm/ (V/V)).

The extensometers measure the displacement that occurs during loading of the specimen over the length of the gauge section. When calculating the percent of strain, the measured displacement is taken with respect to the gauge section. In the case of the extensometers used in this research, the gauge length for the intact clays was 1'' = 25.4mm and for the clay-like materials (gypsum and plaster of Paris) was 2'' = 50.8 mm.

To attach the extensometers to the specimen, a pair of wing attachments was used to provide wider coverage to the surface of the circular disc for better holding, as shown in **Figure 4.38**. In addition, four rubber bands were used to wrap around and bind one extensometer on either side of the specimen, as shown in **Figure 4.39**. While the extensometers are attached, two pins are engaged to hold the gauge length, as shown in **Figure 4.40**. Before loading, the pins are withdrawn, which allows the extensometer to be in range when initializing the experiment to measure the displacement. The main advantage of using the extensometers is that it avoids the seating/contact deformation associated with loading, hence can be considered more precise. However, in the current application there is slight error as the strain is not uniform.

4.4.6 Data Acquisition System

A centralized computer based data acquisition system is used in the MIT Geotechnical laboratory to provide a single location for collection and storage of all transducer measurements (Grennan, 2010). The computerized system is flexible allowing users to specify customized and sometimes complicated transducer recording schedules based on experimental needs; multiple schedules can be run simultaneously. A centralized data acquisition system is a cost effective and efficient means of recording digital data in large laboratories and is heavily relied upon at MIT. **Figure 4.41** presents a schematic drawing of the central data acquisition system which can be sub divided into four main categories according to Adams (2011):

1) The laboratory testing device, such as the Flattened Brazilian Disc load frame, which includes the transducers, power supply, junction box, voltmeter and ground.

2) A switching mechanism which allows the data acquisition mechanism to connect to a particular transducer to make a measurement.

3) An Analog to Digital (A/D) converter that converts the voltage output from each transducer and the power supply to a digital word which can be read by a computer.

152

4) A computer which controls the process and components and performs all administrative and computational tasks associated with collecting and archiving the measurements associated with all programmed tasks.

The MIT Geotechnical data acquisition system uses a personal computer equipped with an Intel 486 microprocessor and driven by Microsoft's Windows XP operating system. This computer is interfaced with an expanded channel Hewlett Packard HP3497A data acquisition unit equipped with a very low noise 5.5 digit integrating analogue to digital converter with auto ranging amplification capabilities to four voltage scales (0.1, 1, 10 and 100V). The system is currently configured to simultaneously monitor 140 channels distributed throughout the laboratory while providing analogue to digital conversion and data storage capabilities at speeds of up to 1 Hertz (Adams, 2011).

4.5 Testing Procedures

After finishing with the specimen preparation procedure, the process of flattening the top and bottom edges of the Brazilian discs, and ensuring the flatness and parallelism of the two surfaces, the specimens are kept in a 40 degree oven to maintain dry until the testing procedure starts. Initially, the specimen dimensions are measured at least three times and at different locations and the specimen is scaled several times to record its mass, these measurements are eventually used to determine the dry unit weight of the specimen.

Afterwards the specimen is setup in the appropriate load frame, zero readings of the different transducers (load cell, LVDT, and two extensometers) are recorded, a data acquisition file is initiated to record at least 500 readings at a rate of reading per 2 seconds, then the load frame is turned on at the chosen displacement rate which in our study is 0.2 mm/min. The pins of the extensometers are removed prior loading after the top flat surface touches the loading platen. Voltage readings of the load, machine displacement, and specimen displacements are recorded and the value of the load is monitored. The test advances until an increase in the load voltage to a maximum value followed by a sudden drop in the voltage indicating the critical loading point which defines the transition stage between the unstable and stable crack growth phases. After this stage the test is manually terminated and the loading frame is turned off where a central crack splitting the flattened specimen into two halves (semi-circles) is observed with a popping sound indicating the initiation of the crack implying the failure of the specimen.
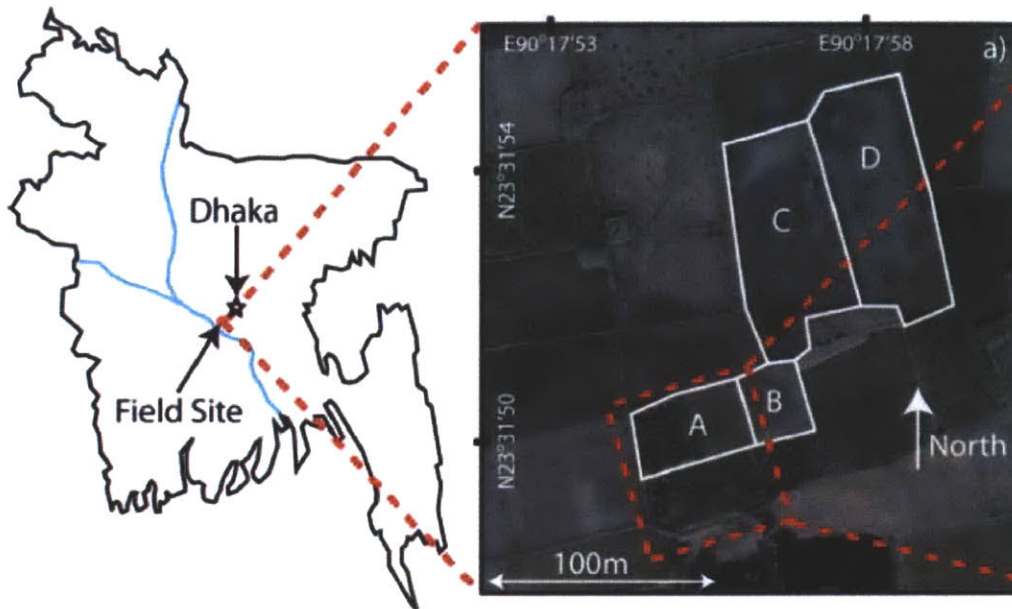
Figure 4.1: Plan view of rice field site in Bashailbhog village, Bangladesh (Neumann, 2010)
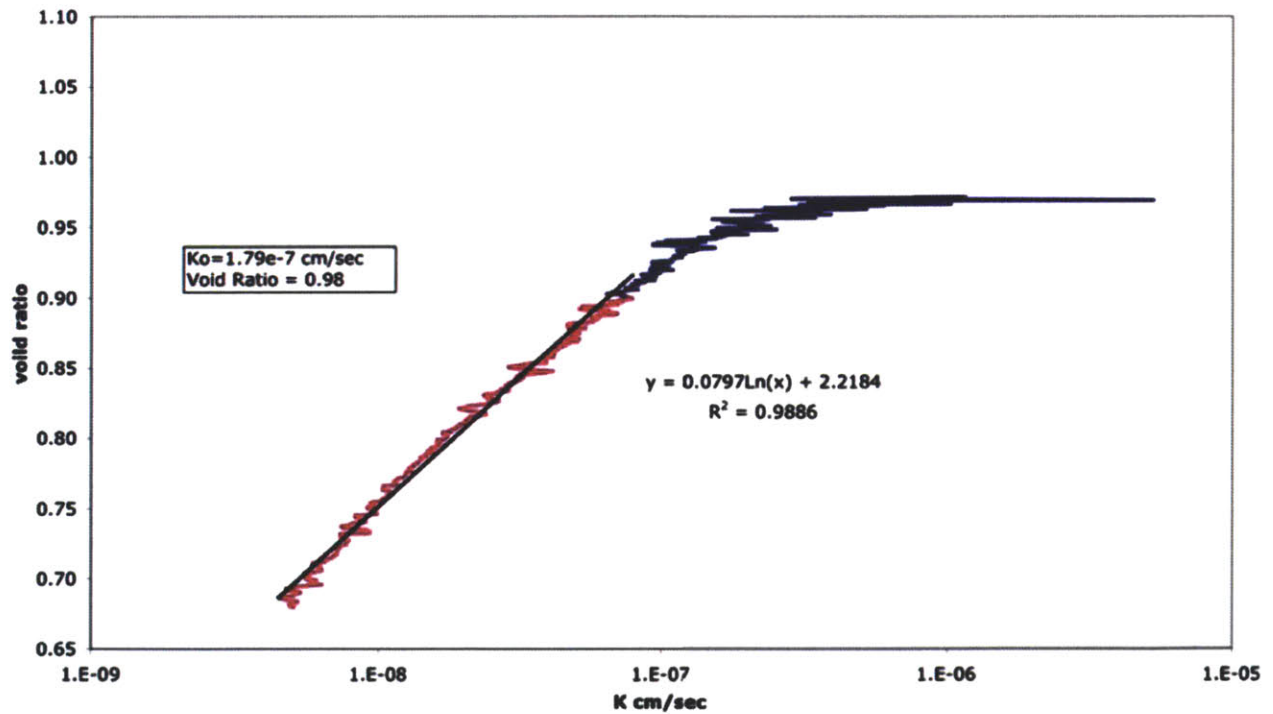
Figure 4.2: Typical CRS test result showing the relation between void ratio and hydraulic conductivity of Bangladesh clay (Nuemann, 2010)
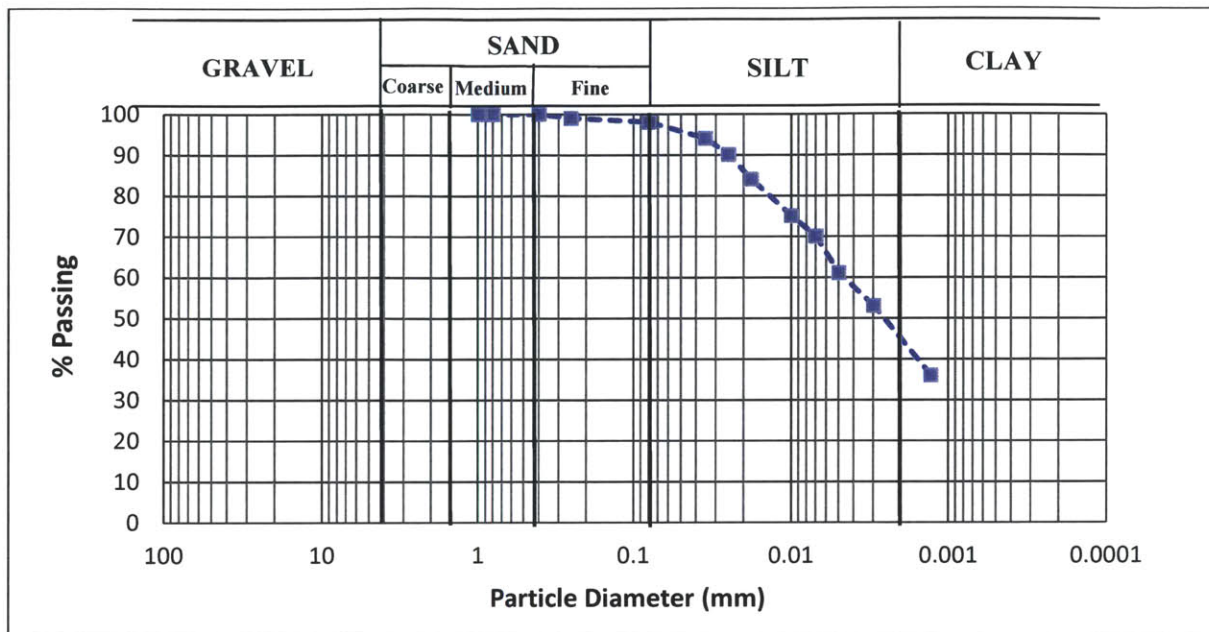
Figure 4.3: San Francisco Bay Mud typical Grain Size Distribution Curve
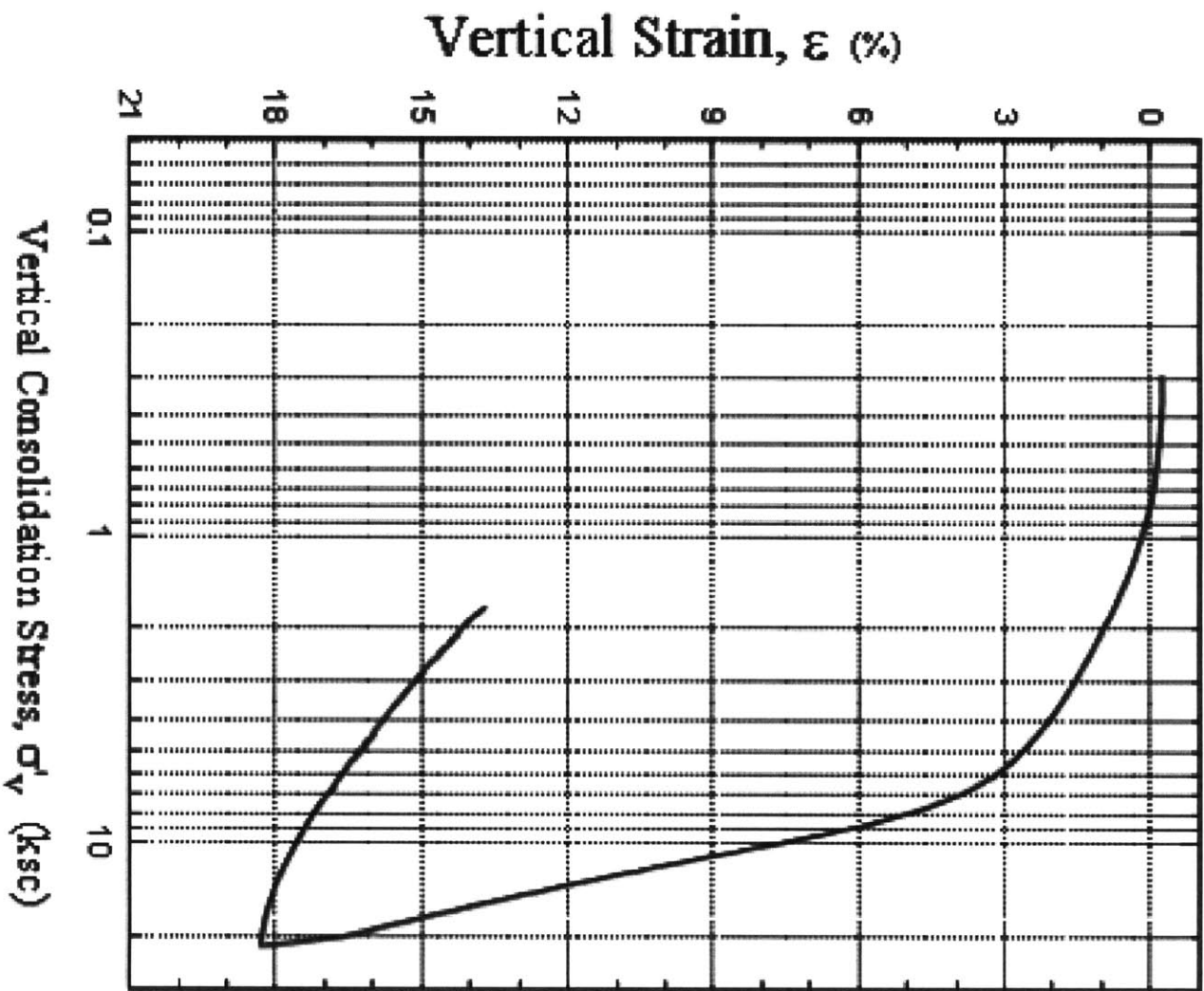
Figure 4.4: Typical CRS test result showing the stress strain relation of San Francisco Bay Mud (Germaine, 2001)
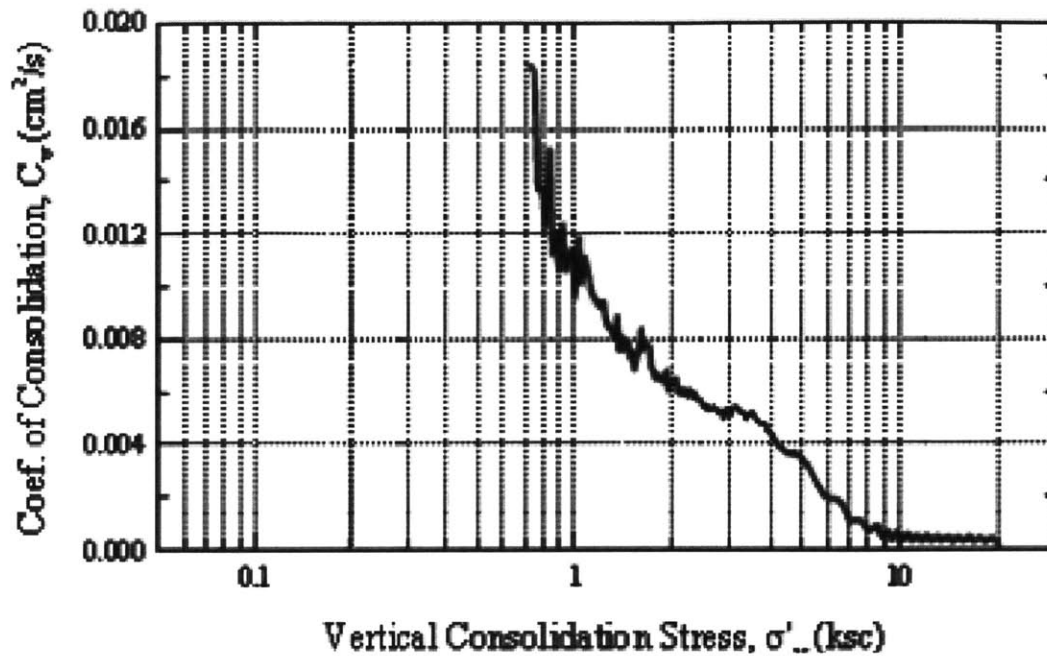
Figure 4.5: Typical CRS test result showing the coefficient of consolidation and effective vertical stress relation of San Francisco Bay Mud (Germaine, 2001)
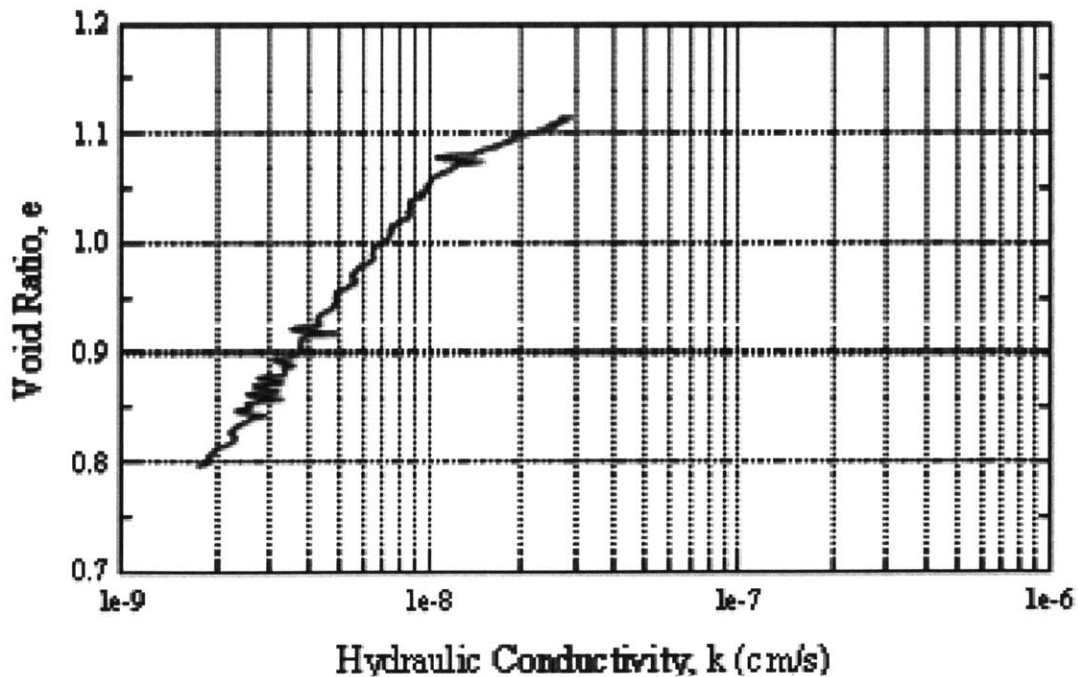
Figure 4.6: Typical CRS test result showing the void ratio and hydraulic conductivity relation of San Francisco Bay Mud (Germaine, 2001)

157
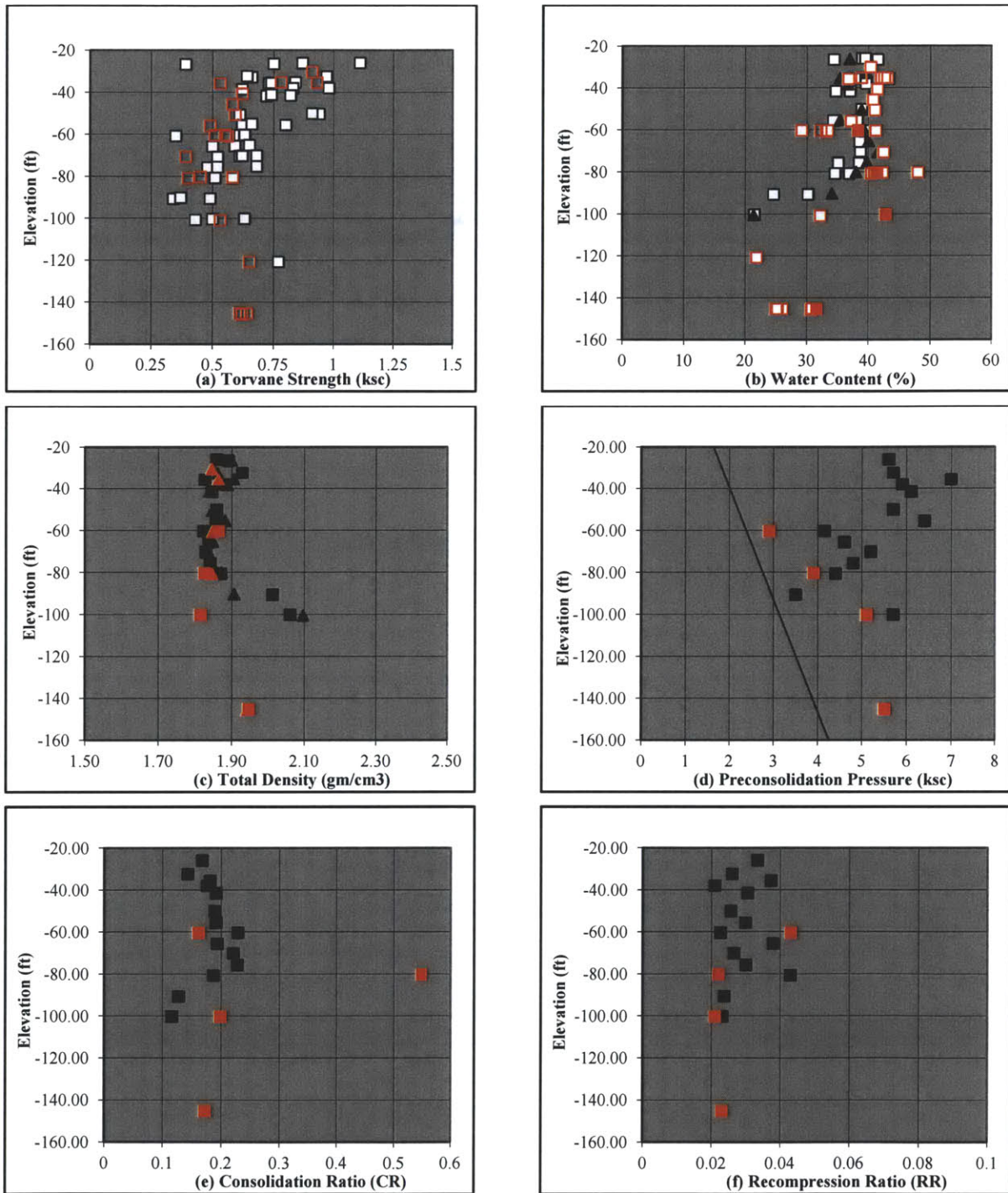
Figure 4.7: Variation of Boston Blue clay properties by depth (a) Tore Vane Strength, (b) Water Content, (c) Total Density, (d) Preconsolidation Pressure, (e) Consolidation Ratio, (f) Recompression Ratio.
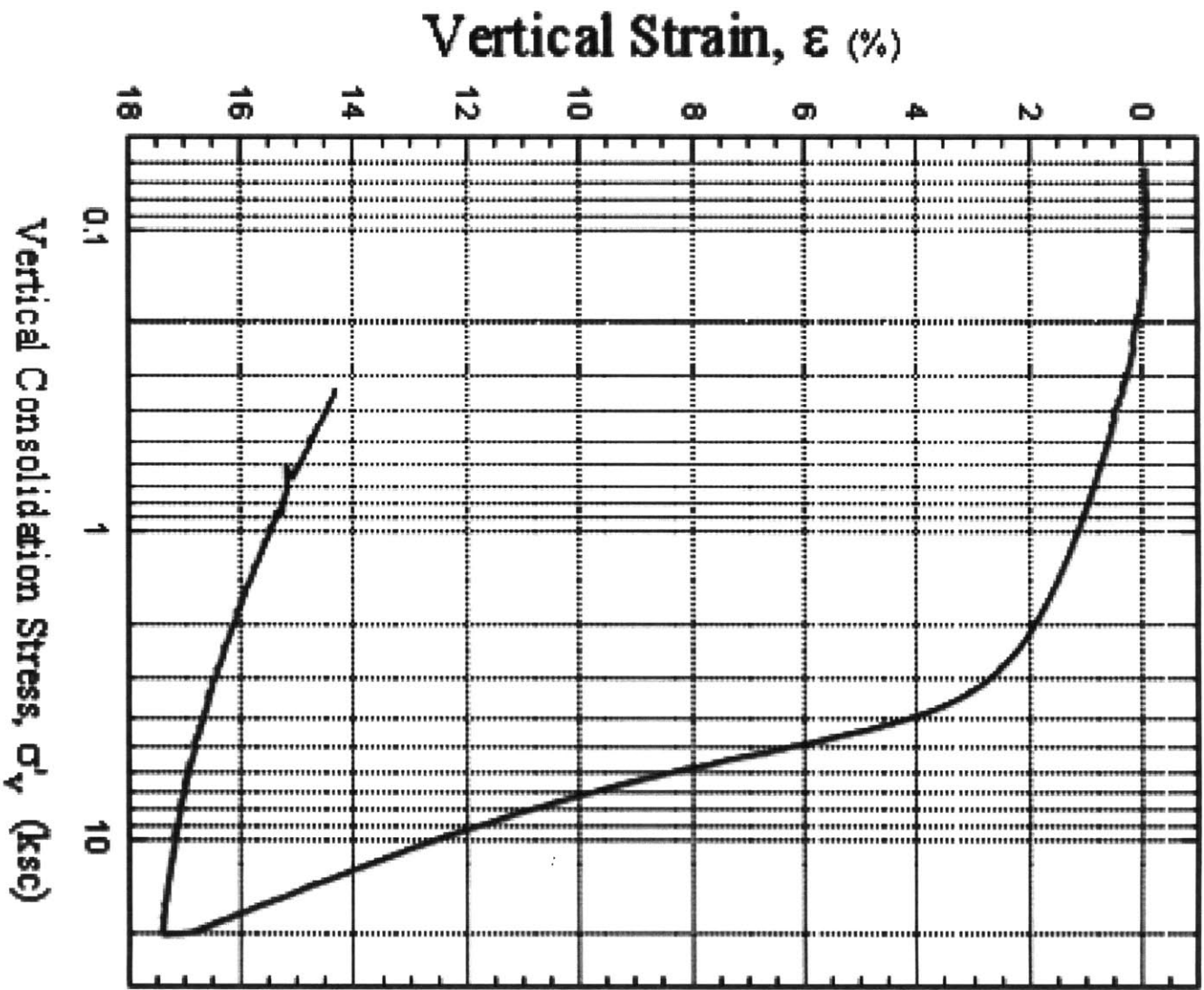
Figure 4.8: Typical CRS test result showing the stress strain relation of Boston Blue Clay (Germaine, 2001)
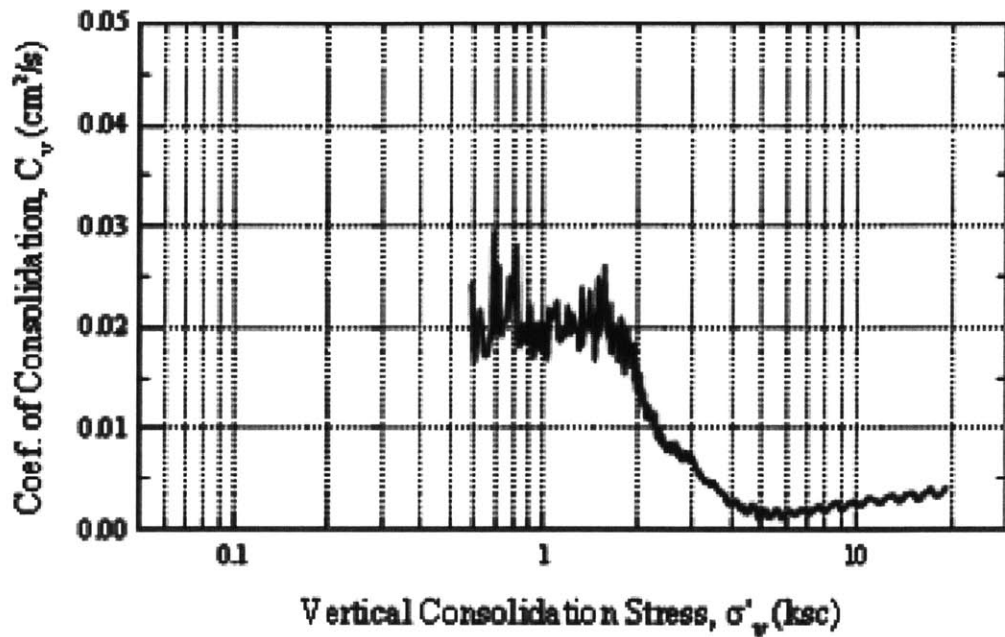
Figure 4.9: Typical CRS test result showing the coefficient of consolidation and effective vertical stress relation of Boston Blue Clay (Germaine, 2001)
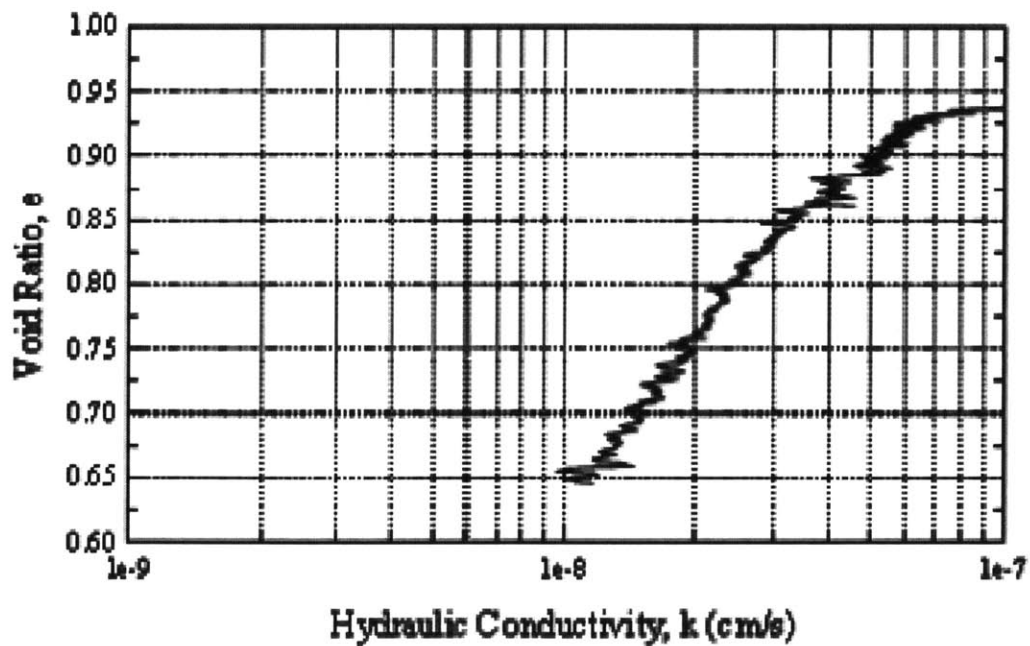
Figure 4.10: Typical CRS test result showing the void ratio and hydraulic conductivity relation of Boston Blue Clay (Germaine, 2001)

160
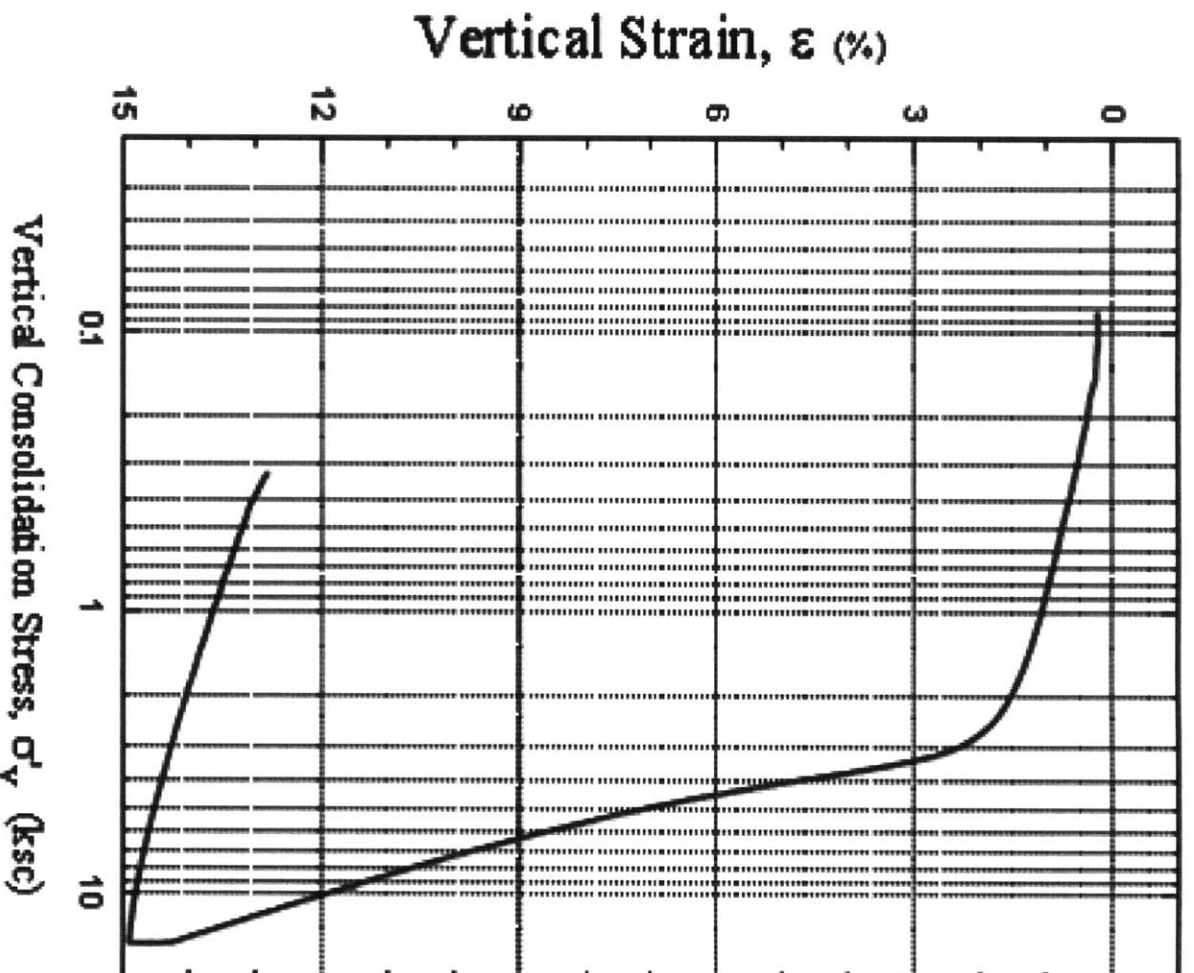
Figure 4.11: Typical CRS test result showing the stress strain relation of Presumpscot Maine Clay (Germaine, 2002)
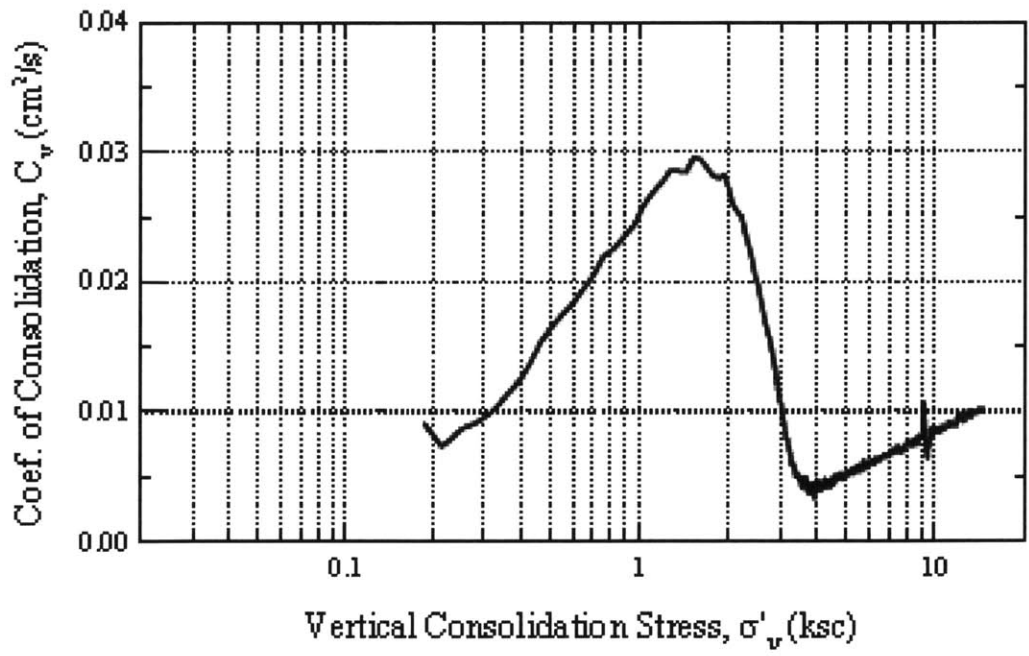
Figure 4.12: Typical CRS test result showing the coefficient of consolidation and effective vertical stress relation of Presumpscot Maine Clay (Germaine, 2002)
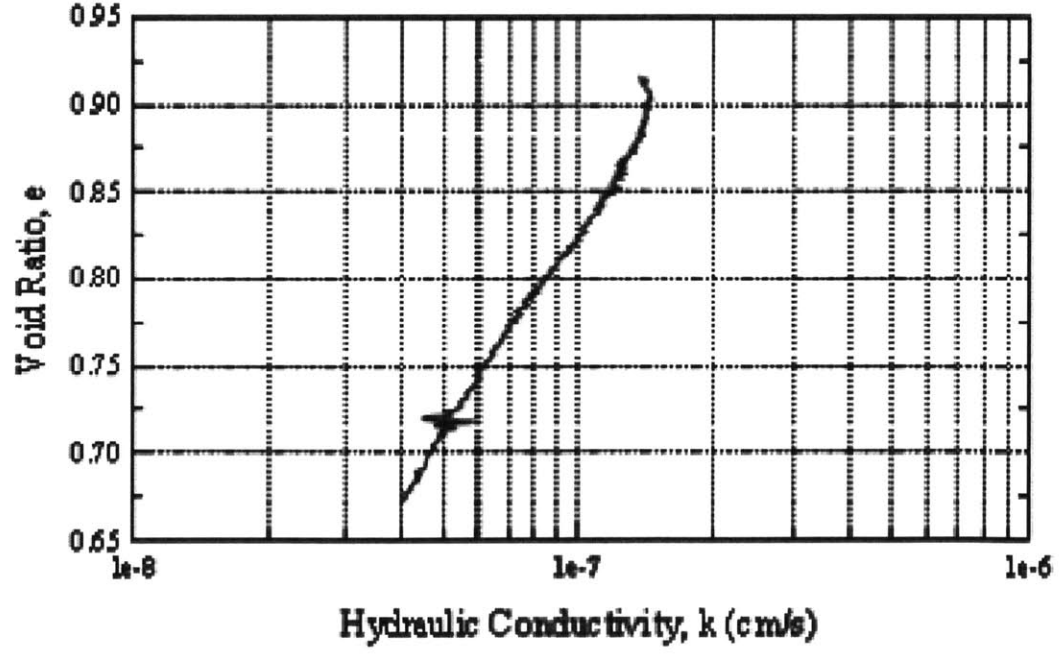
Figure 4.13: Typical CRS test result showing the void ratio and hydraulic conductivity relation of Presumpscot Maine Clay (Germaine, 2002)
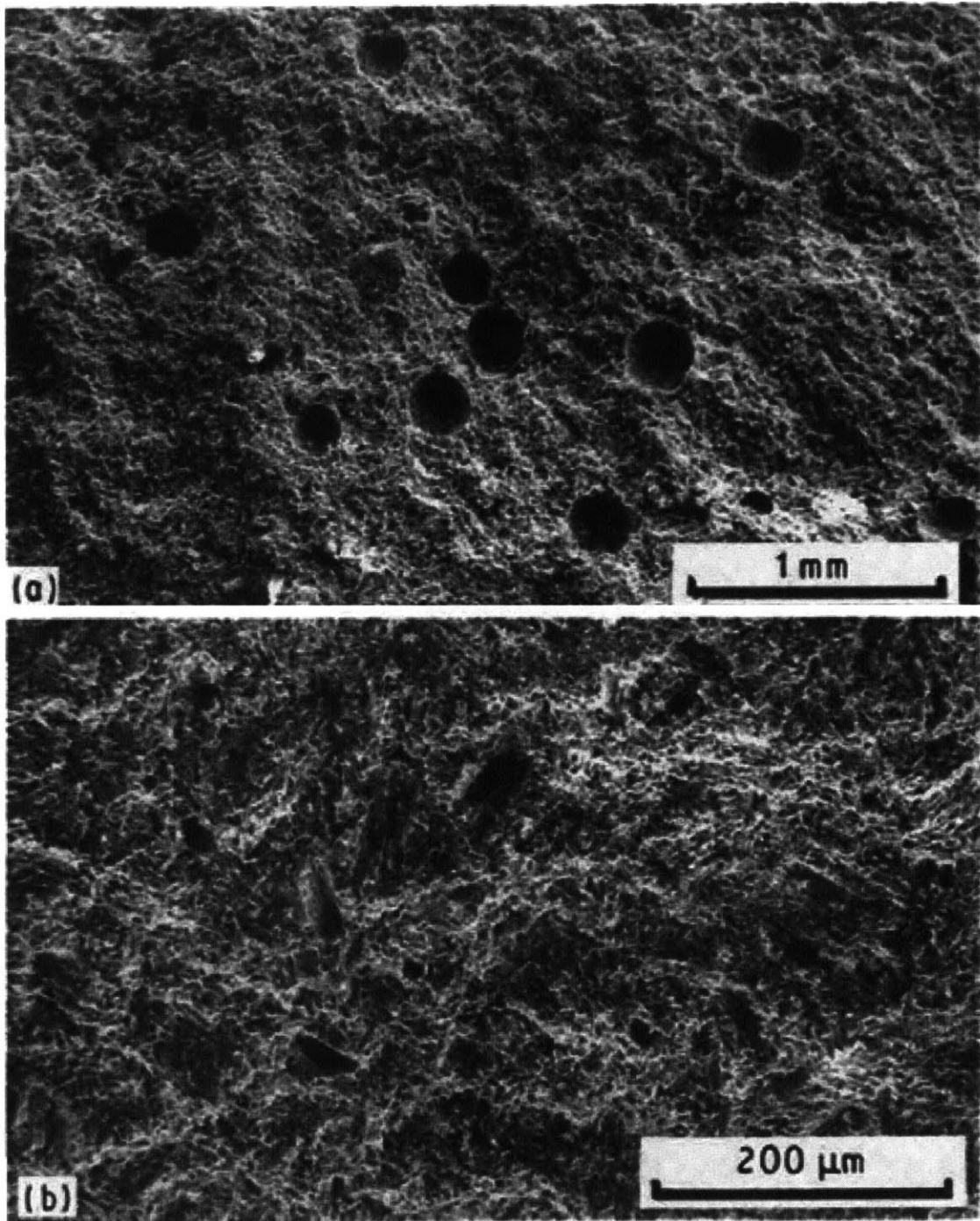
Figure 4.14: Environmental Scanning Electro Microprobe (ESEM) micrograph showing the structure of Plaster of Paris (a) 50% relative density, (b) 70% relative density specimens (Vekinis et al., 1993).
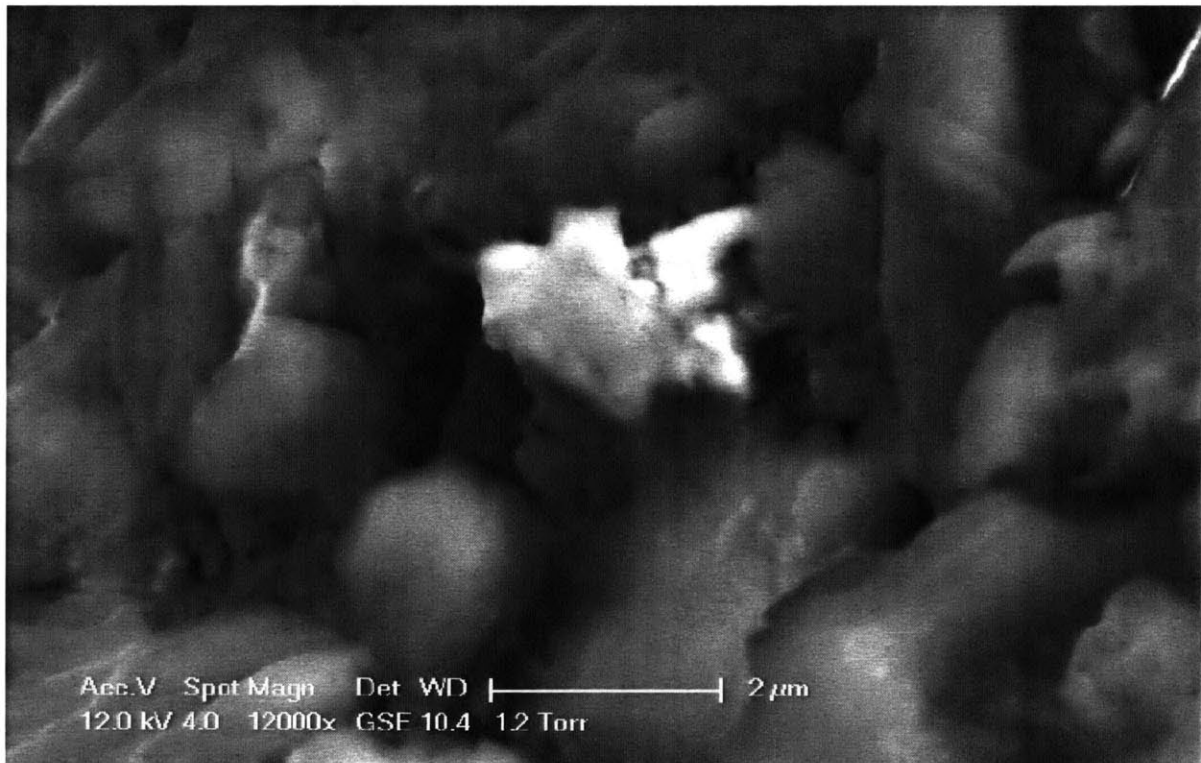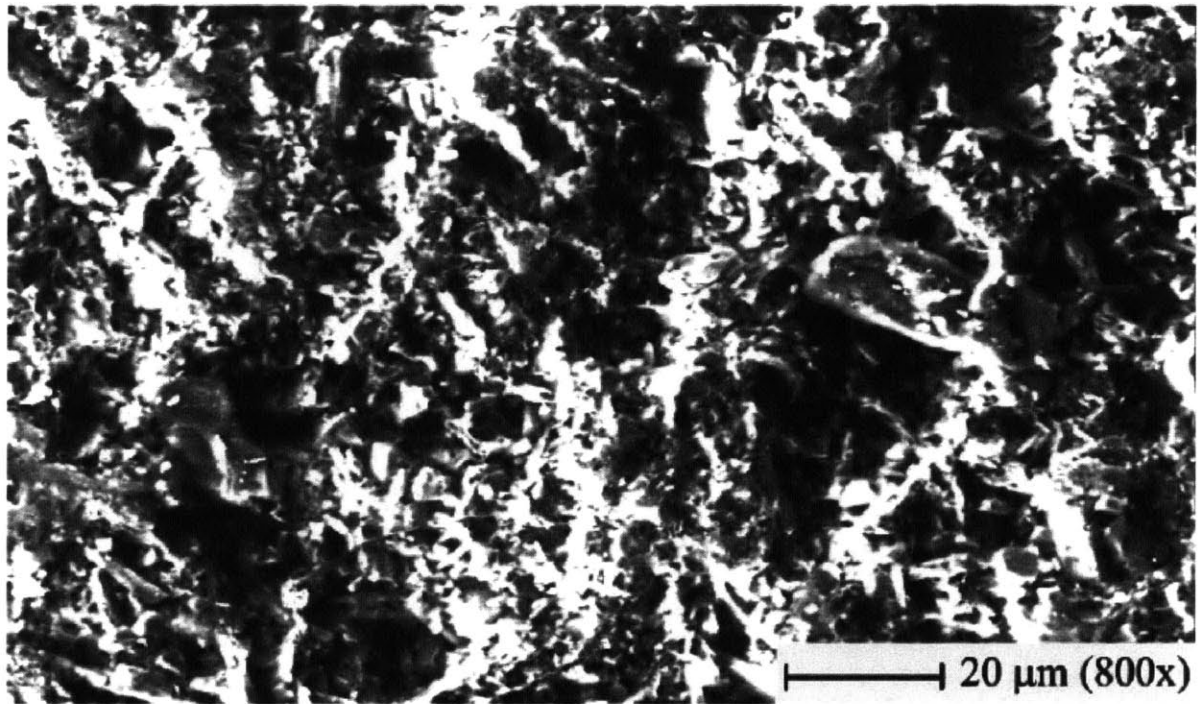
Figure 4.15: Environmental Scanning Electro Microprobe (ESEM) micrograph of molded gypsum (a) magnification of 800x, (b) magnification of 12,000x (Wong, 2008)
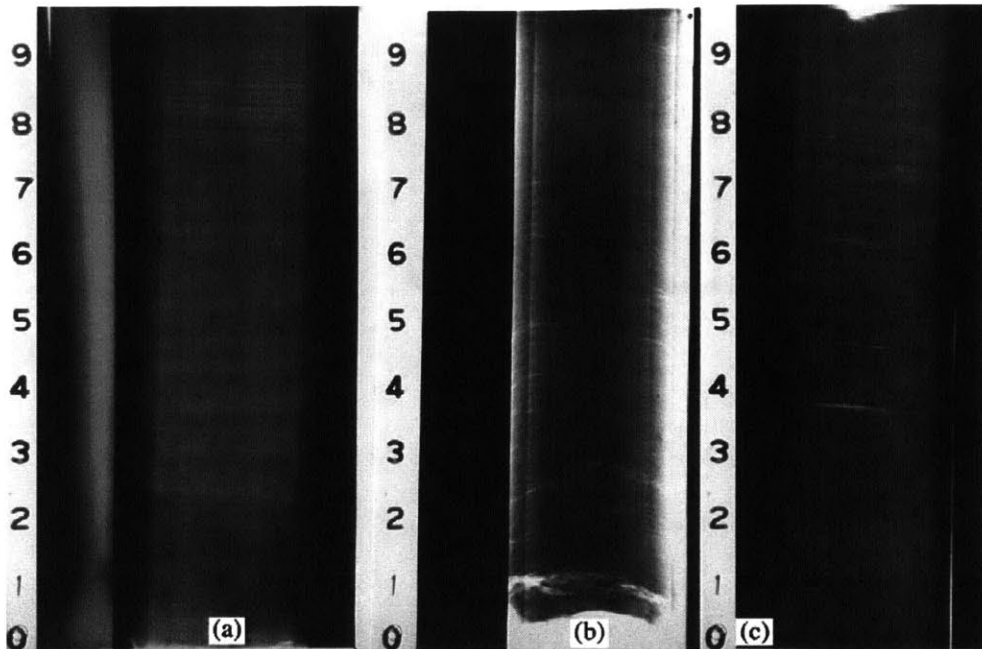
Figure 4.16: Three examples of sample radiographs: a) layering in sedimentary clay deposit; b) significant shear distortion; c) isolated testable material in a generally disturbed sample (Germaine and Germaine, 2009)
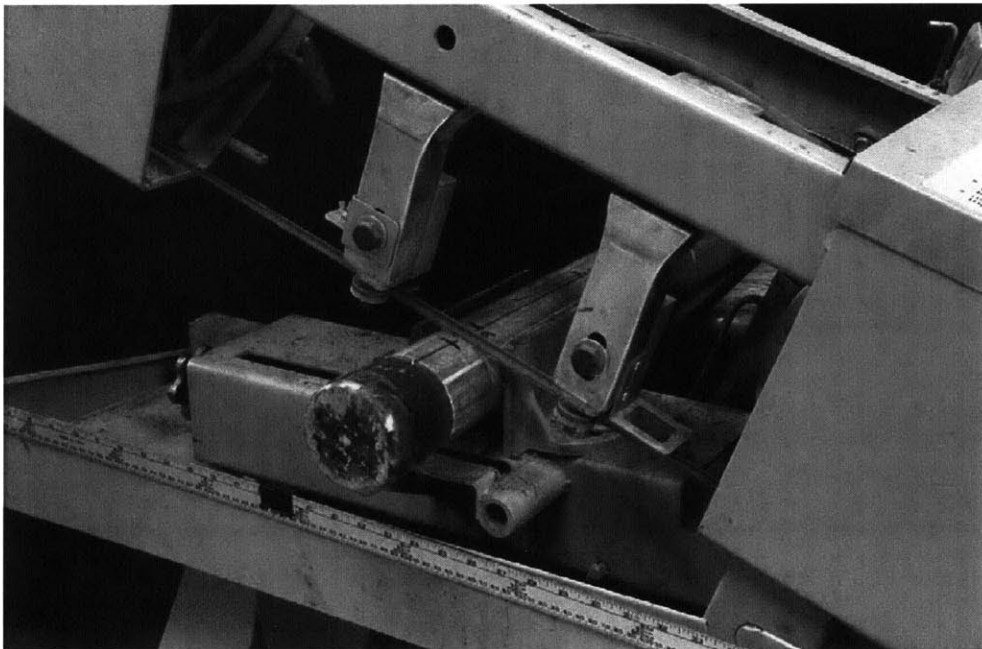
Figure 4.17: Tube set up in band saw for tube cutting (Germaine and Germaine, 2009)
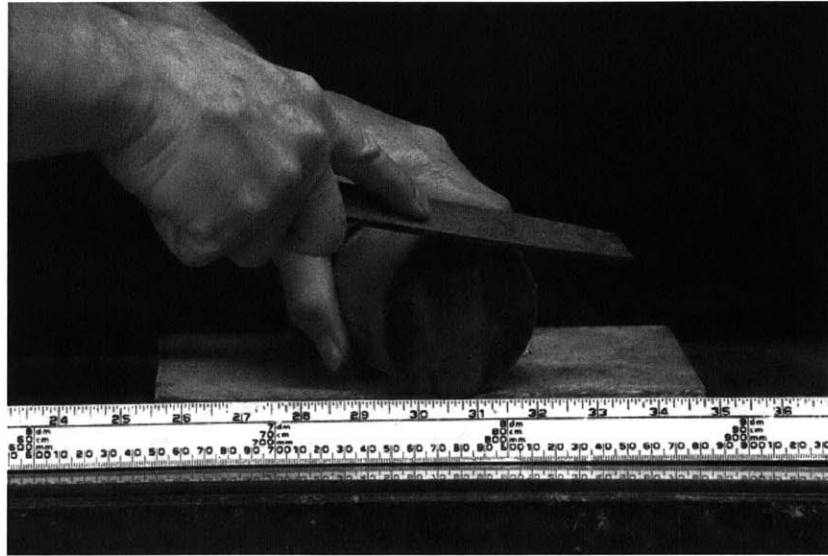
Figure 4.18: Metal file smoothing the outside edge of the cut tube section for safety (Germaine and Germaine, 2009).

Figure 4.19: A straight edge is used to remove soil and debris from the surface to create a level and clean soil surface (Germaine and Germaine, 2009).
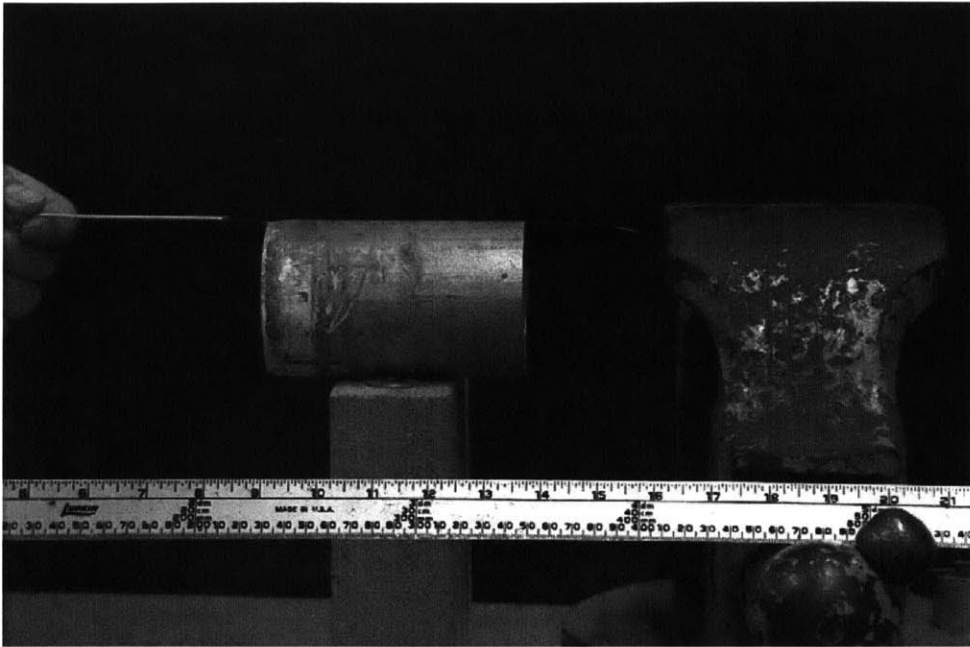
Figure 4.20: Tube section after piano wire has been threaded (Germaine and Germaine, 2009).
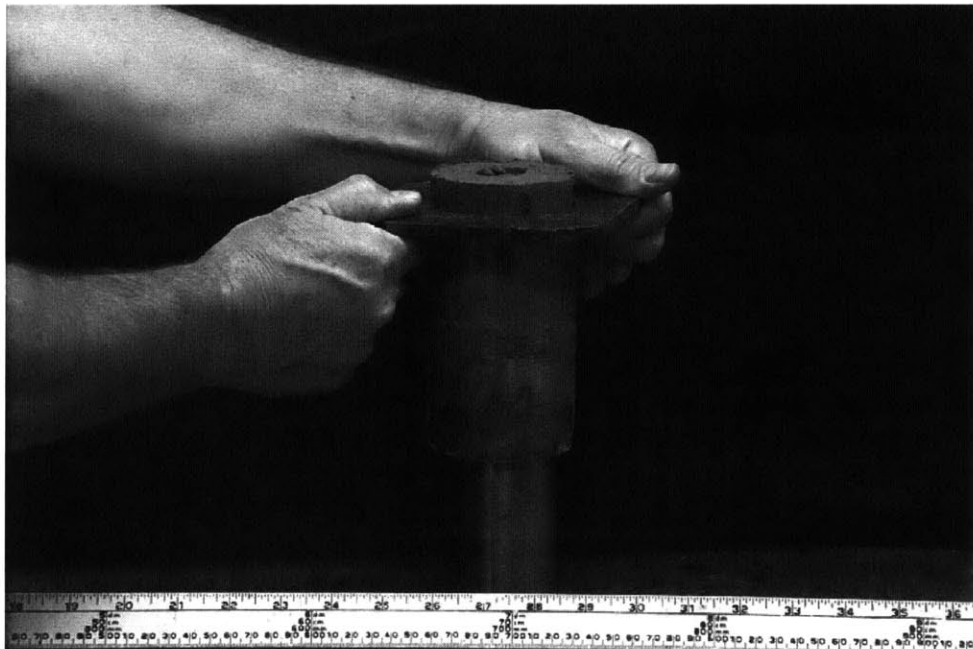
Figure 4.21: Tube section placed on a cylindrical base and the soil pushed out of the tube (Germaine and Germaine, 2009).
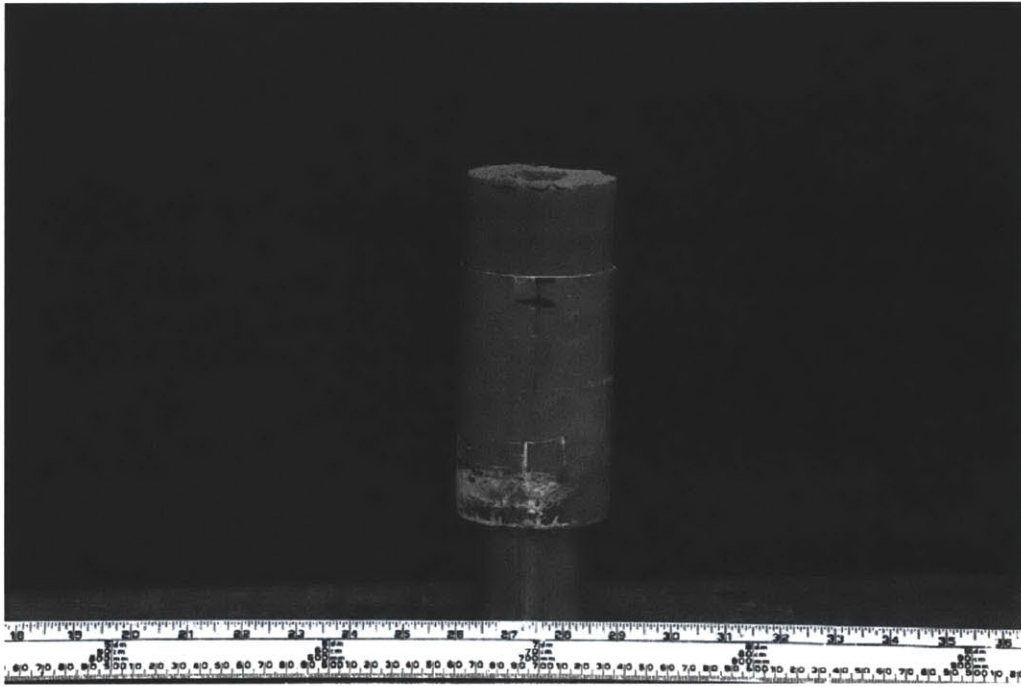
Figure 4.22: Soil is being extruded from the tube (Germaine and Germaine, 2009).
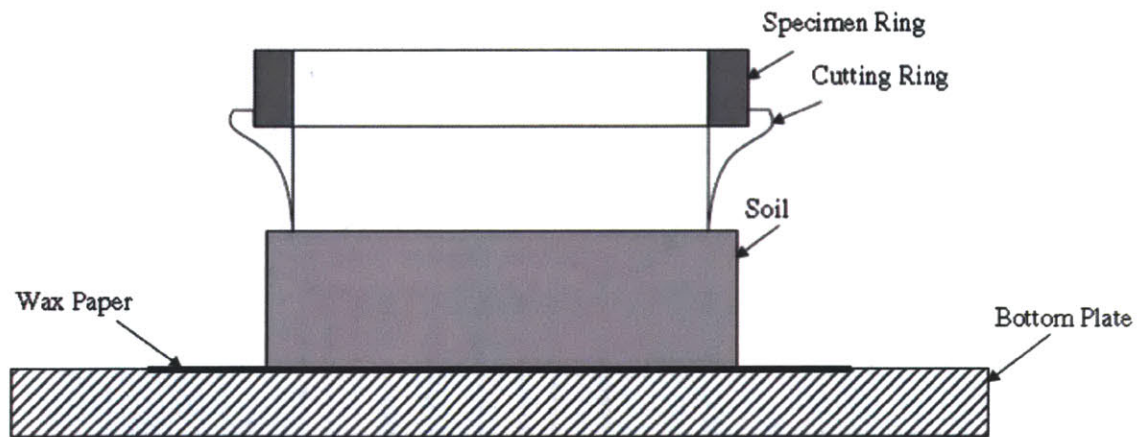
Figure 4.23: The cutting ring technique of trimming a sample (Germaine and Germaine, 2009).
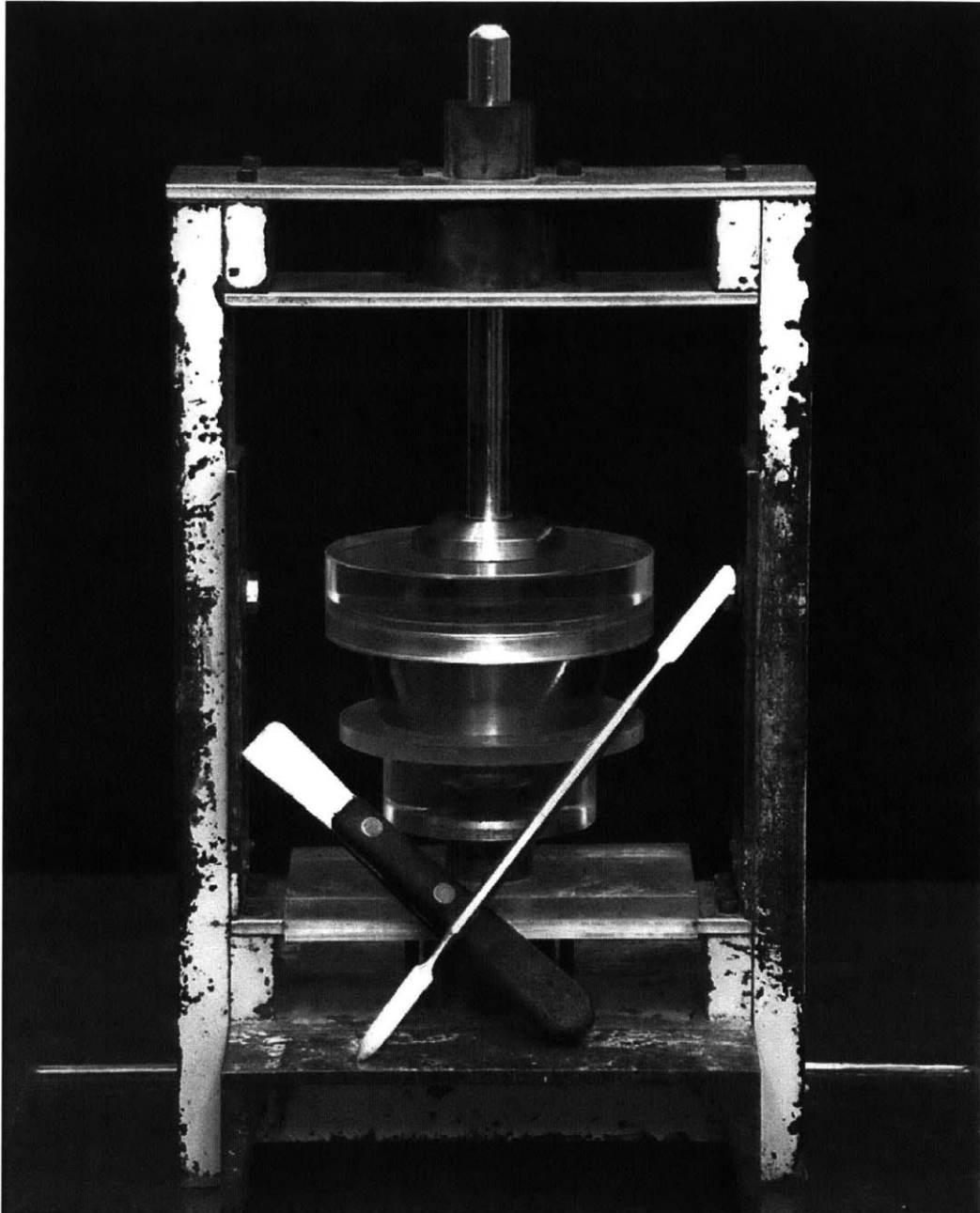
Figure 4.24: Alignment device to aid in trimming a specimen into a ring (Germaine and Germaine, 2009).
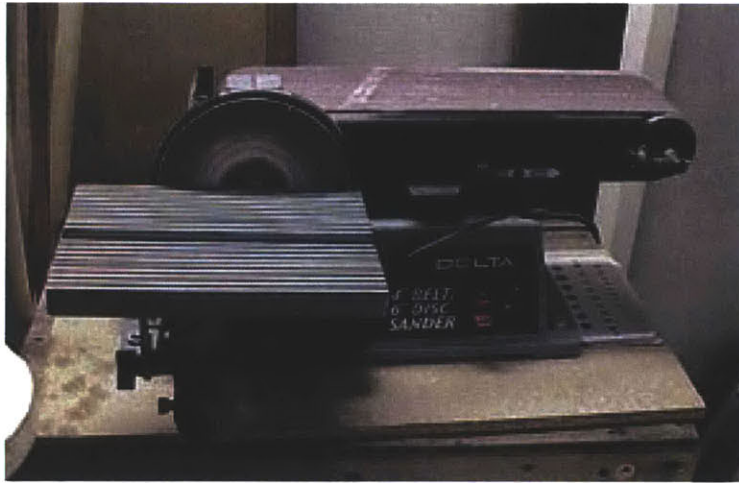
Figure 4.25: 6" width belt sander used in flattened specimen preparation
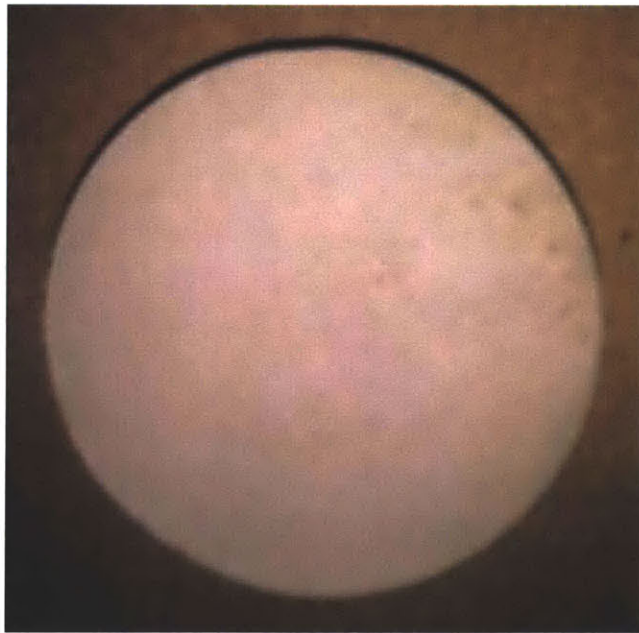
Figure 4.26: Typical oven dried clay circular specimen before flattening
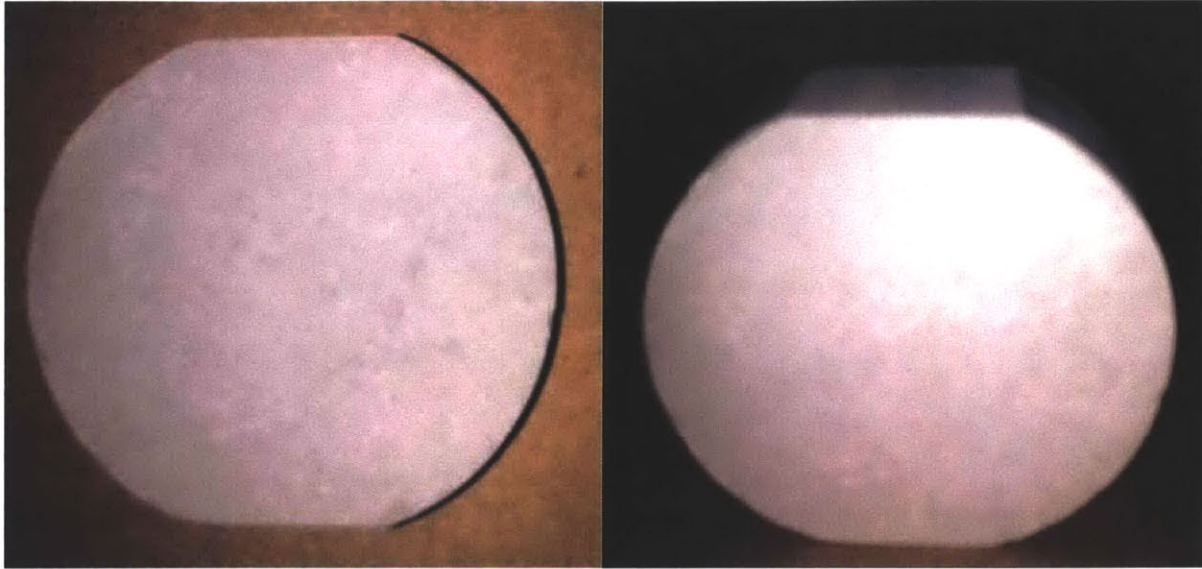
Figure 4.27: Typical oven dried clay specimen after flattening top and bottom edges

Figure 4.28: Mixer and mixing instrument used for gypsum fabrication (Morgan, 2011)

Figure 4.29: 3" Cylindrical plastic mold filled with gypsum mixture

Figure 4.30: Cylindrical Gypsum specimens after drying and releasing from molds
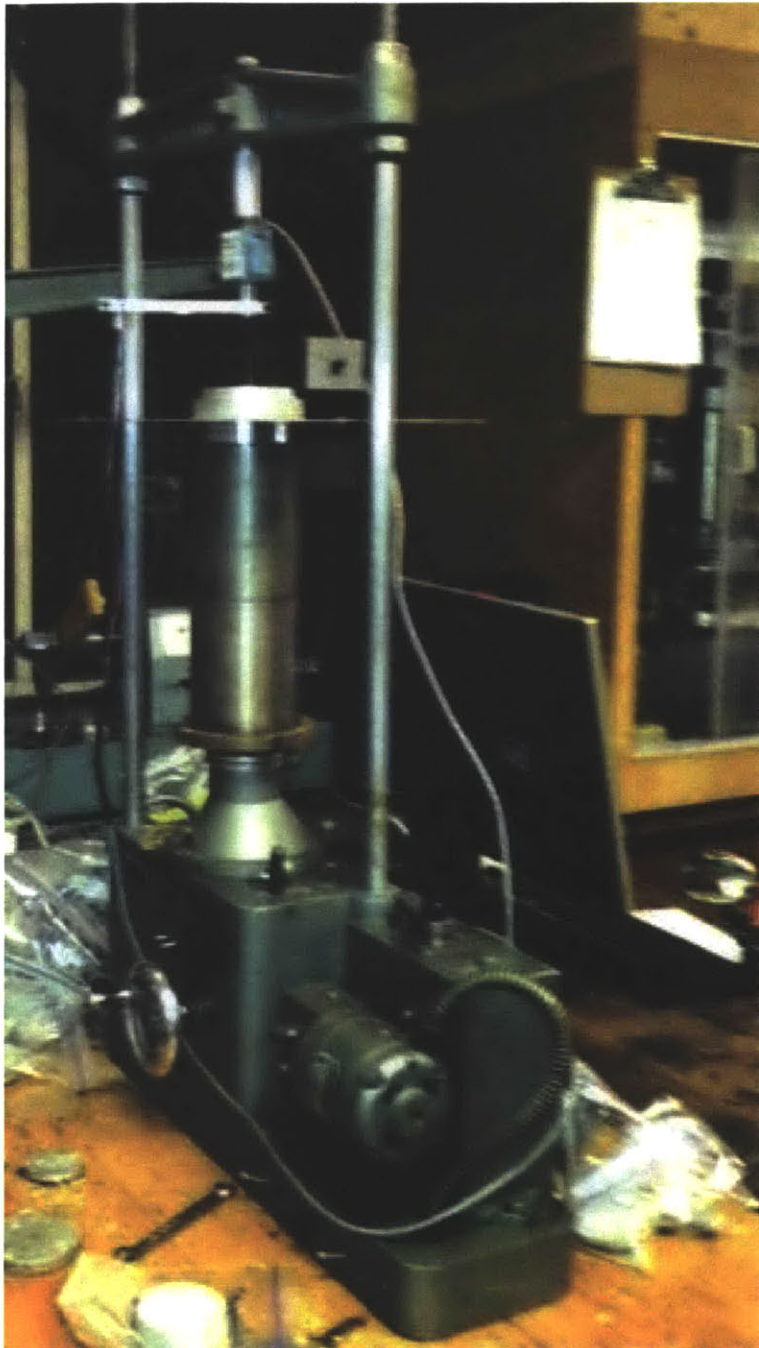
Figure 4.31: Off the shelf mini load frame manufactured by Wykeham Farrance

Load Frame

Load Cell

Flat Platten

Flattened Specimen

LVDT

Extensometer

Wing Attachment

Flat Platten

D 00000 00

Data Acquistion System

PC

174
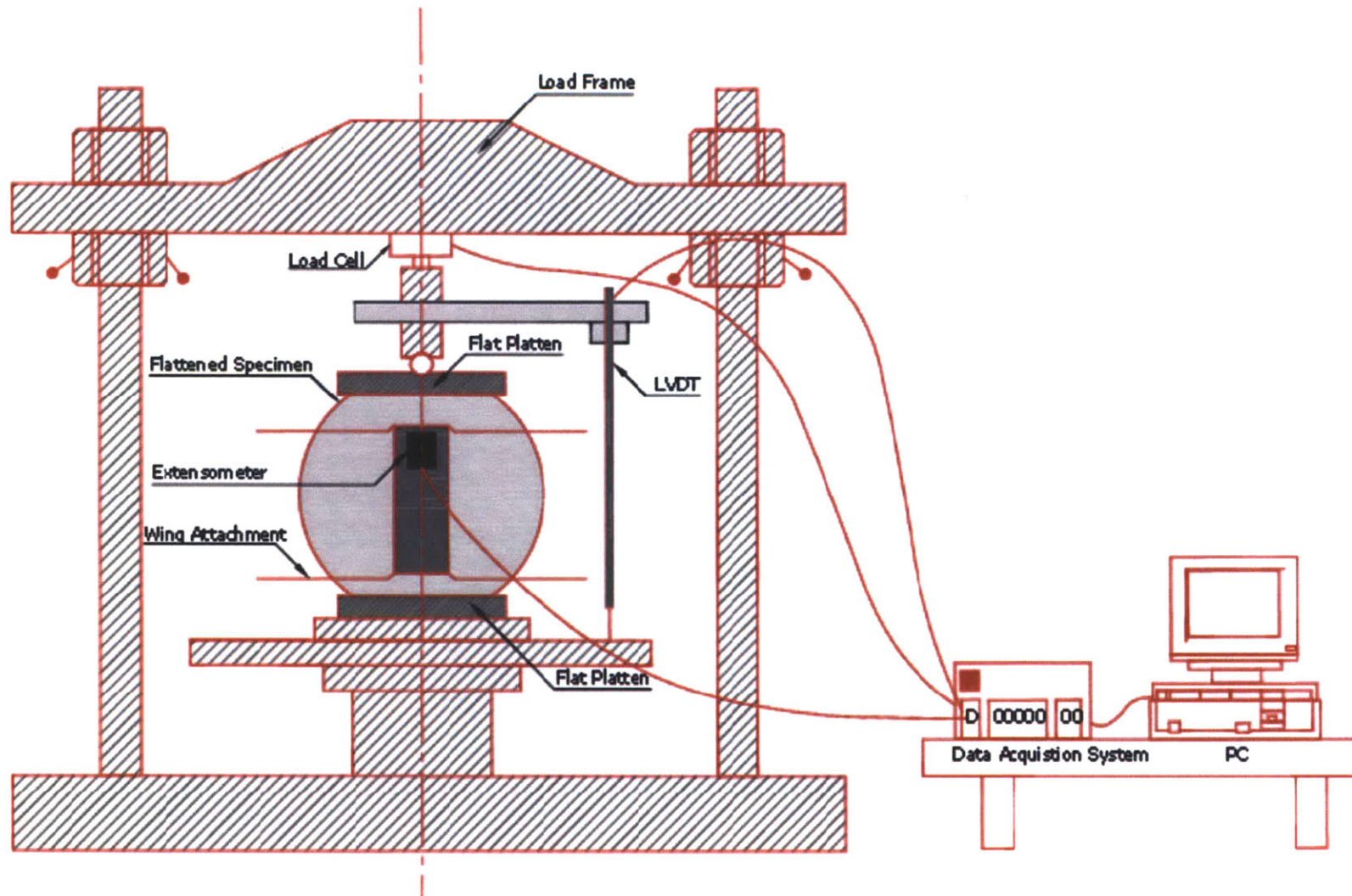
Figure 4.32: Schematic diagram for lading setup for fracture testing on Flattened Brazilian Disc specimen
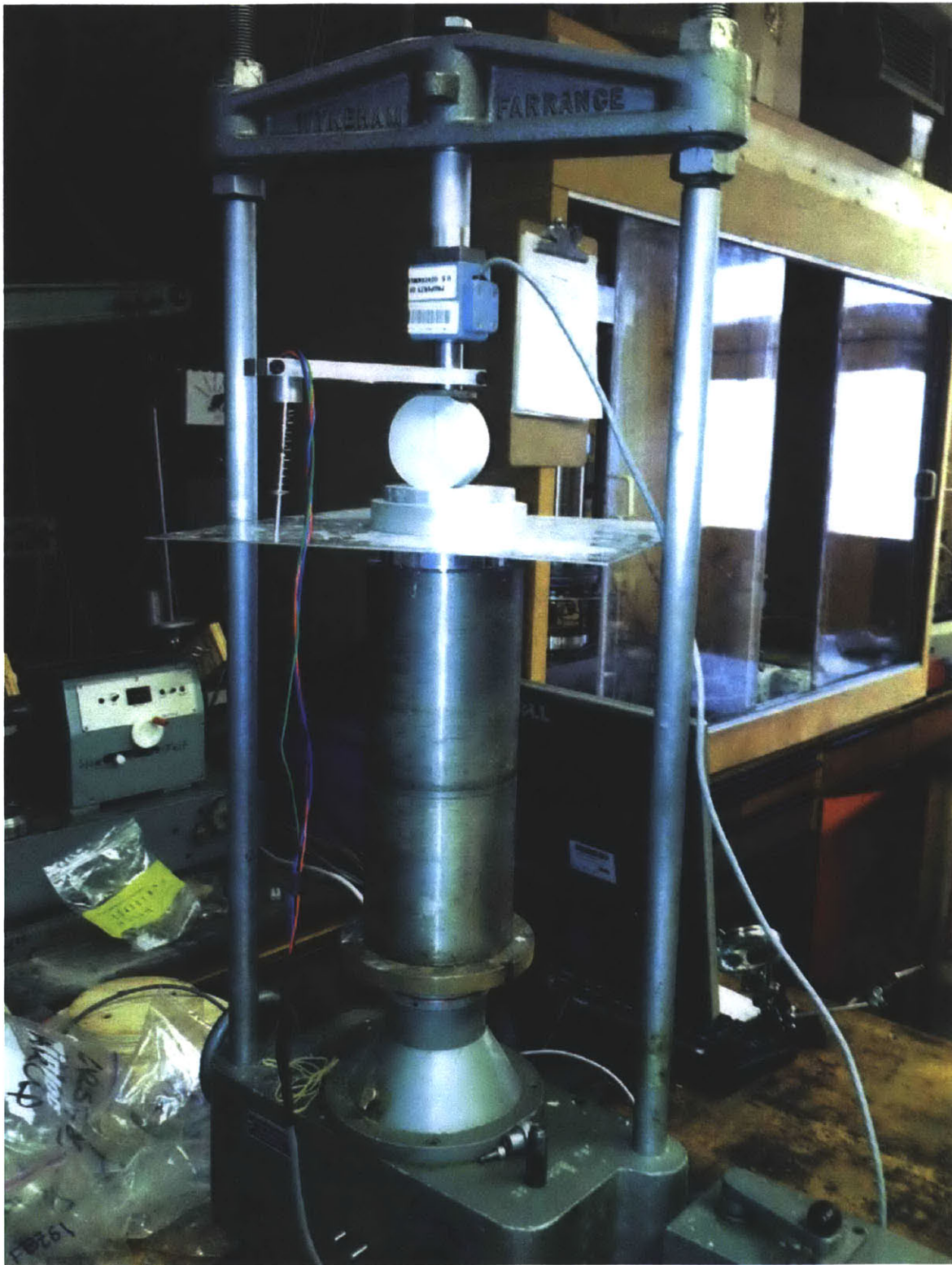
Figure 4.33: Loading setup for specimens in mini load frame by Wykeham Farrance
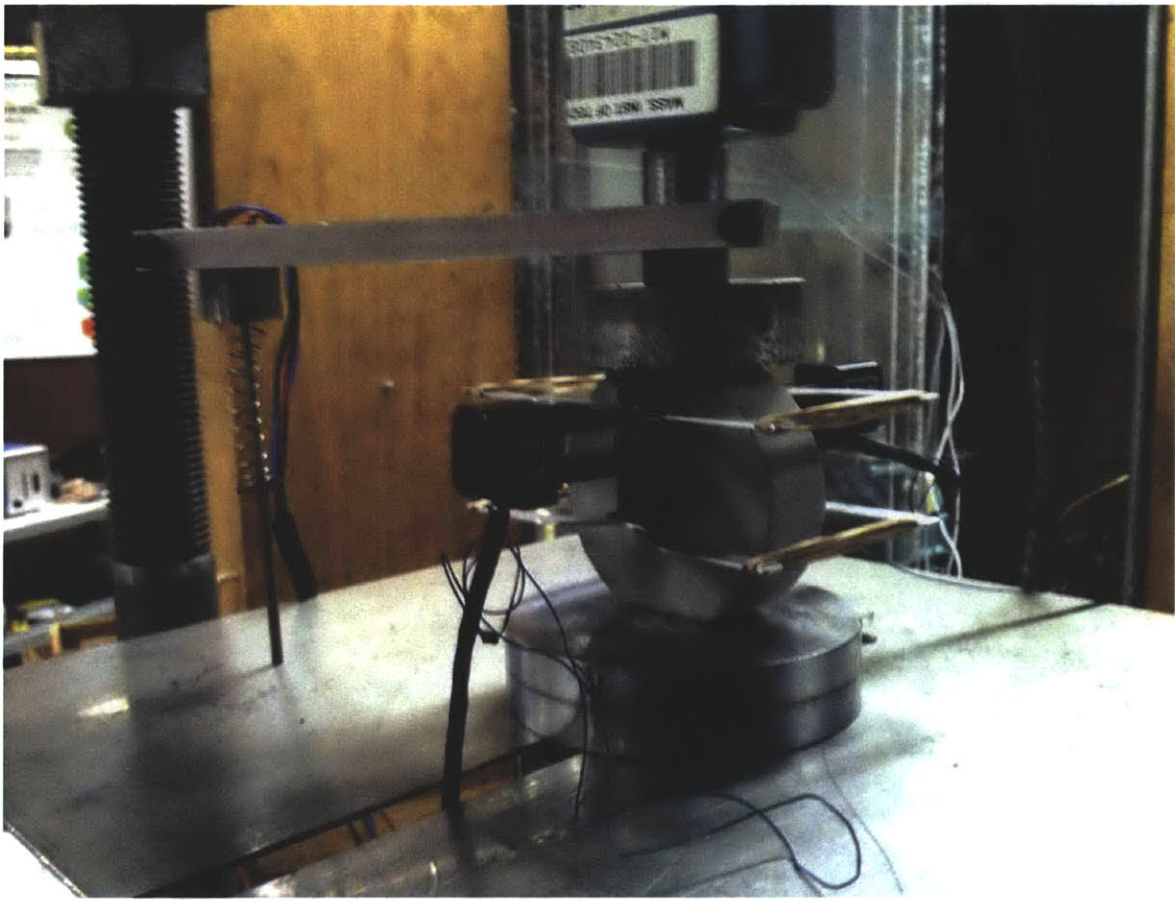
Figure 4.34: A close up on the LVDT configuration while testing
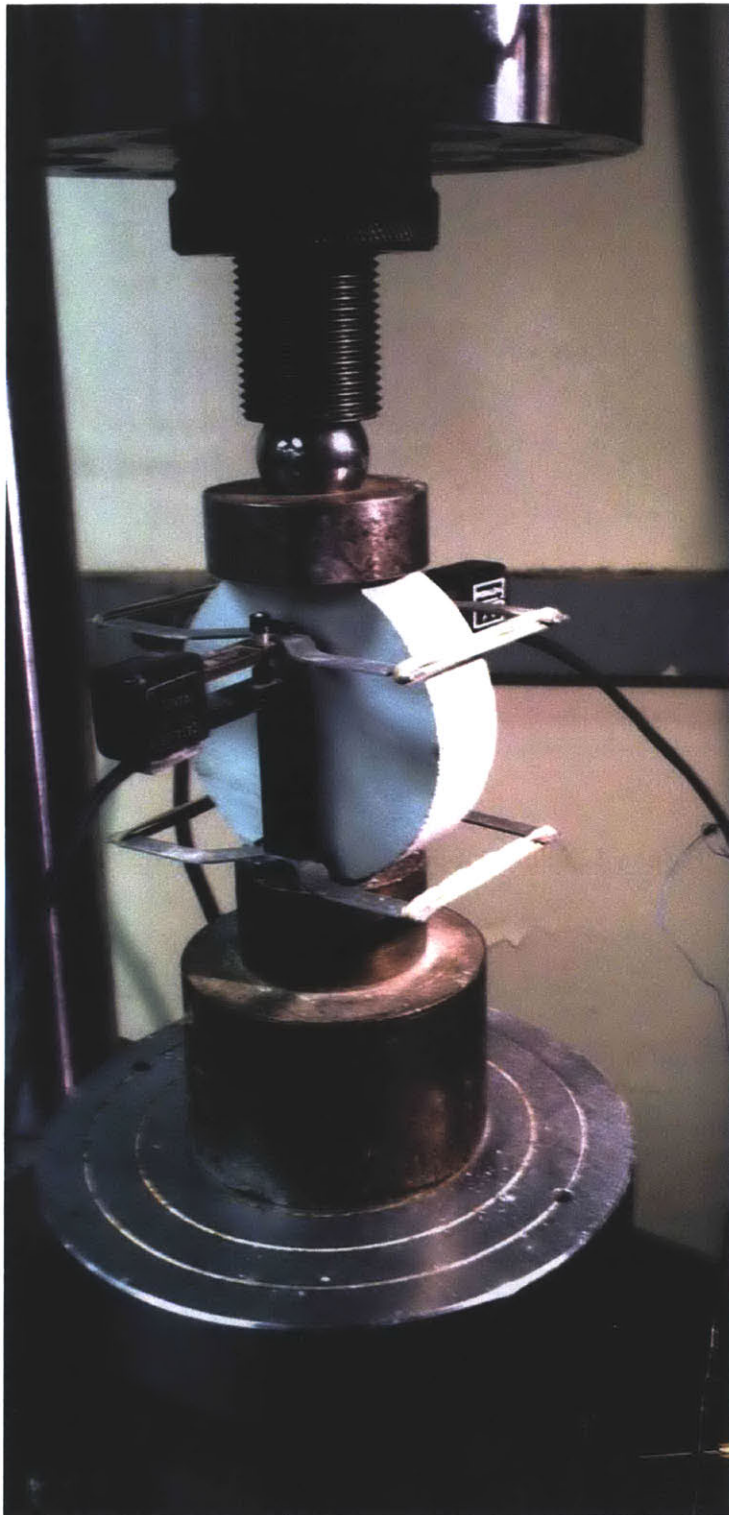
Figure 4.35: Loading setup for specimens in high capacity load frame by MTS

Figure 4.36: JP 500 load cell with a capacity of 500 lb

Figure 4.37: Trans Tek 2.5 cm LVDT
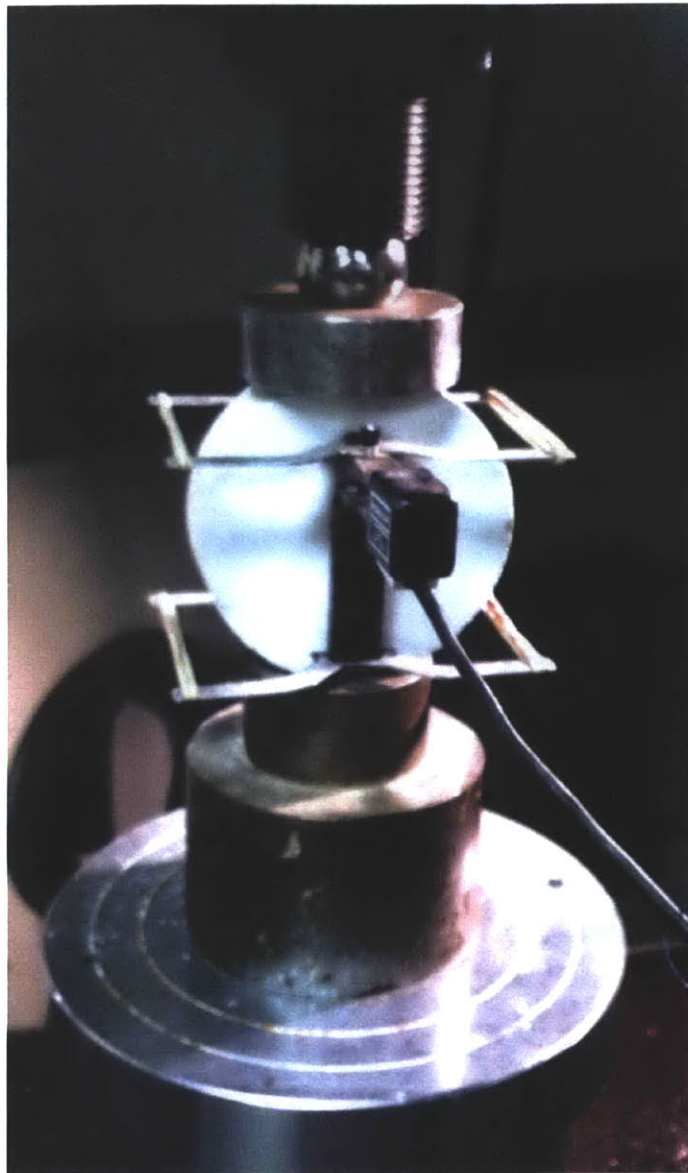
Figure 4.38: A pair of wing attachments to provide a wider coverage over the specimen surface
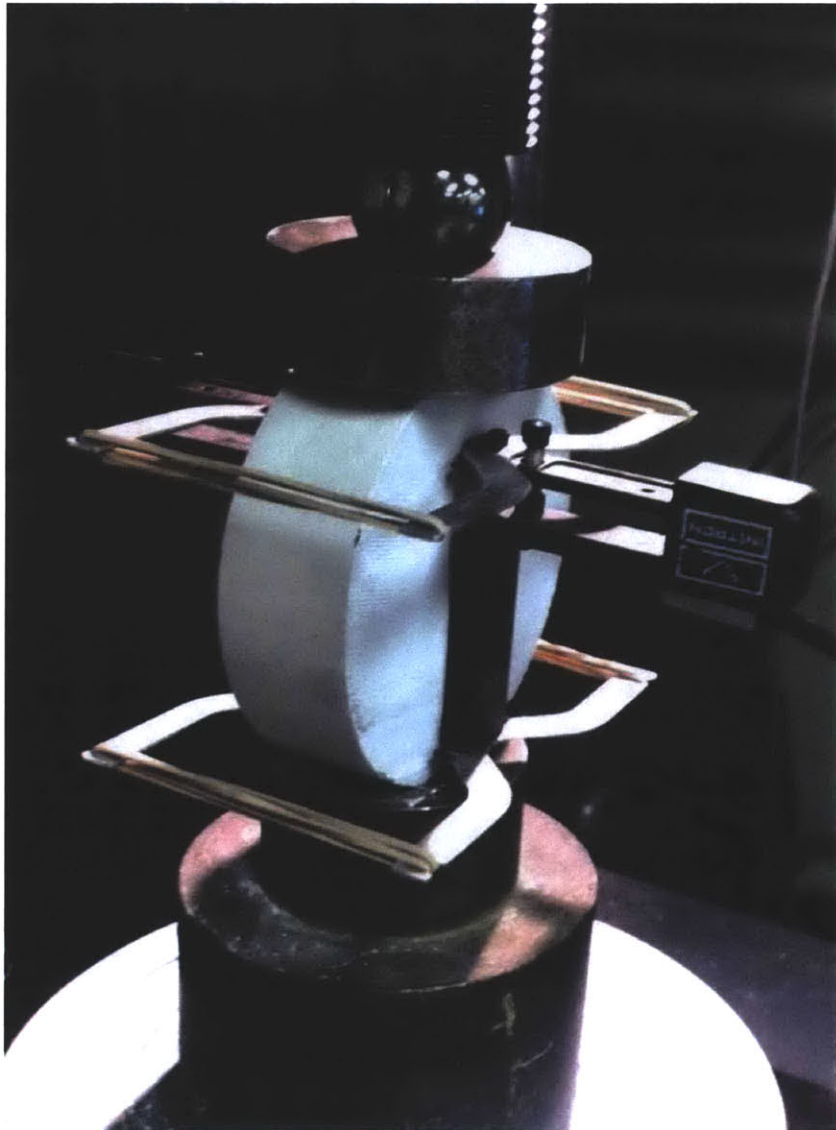
Figure 4.39: Four rubber bands to wrap around and bind one extensometer on either side of the specimen
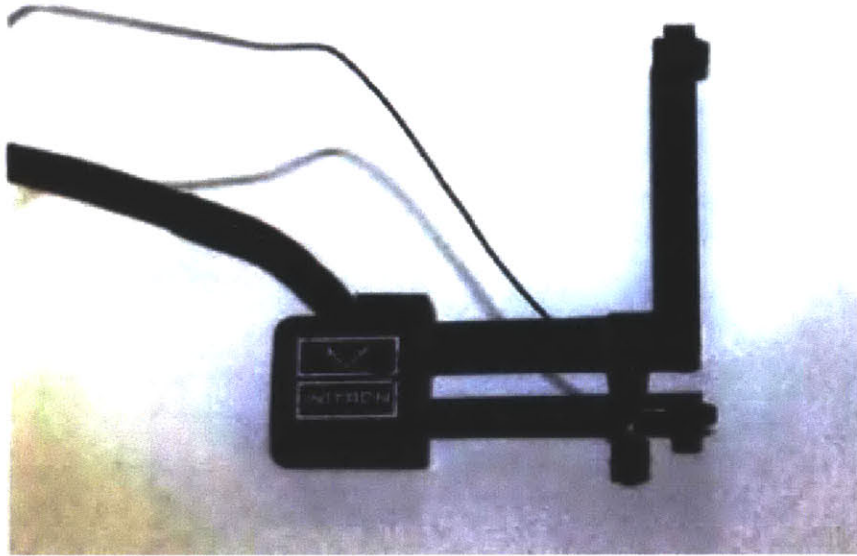
Figure 4.40: One of the extensometers used with an engaged pin for the starting position before starting a test (Marjanovic, 2012)
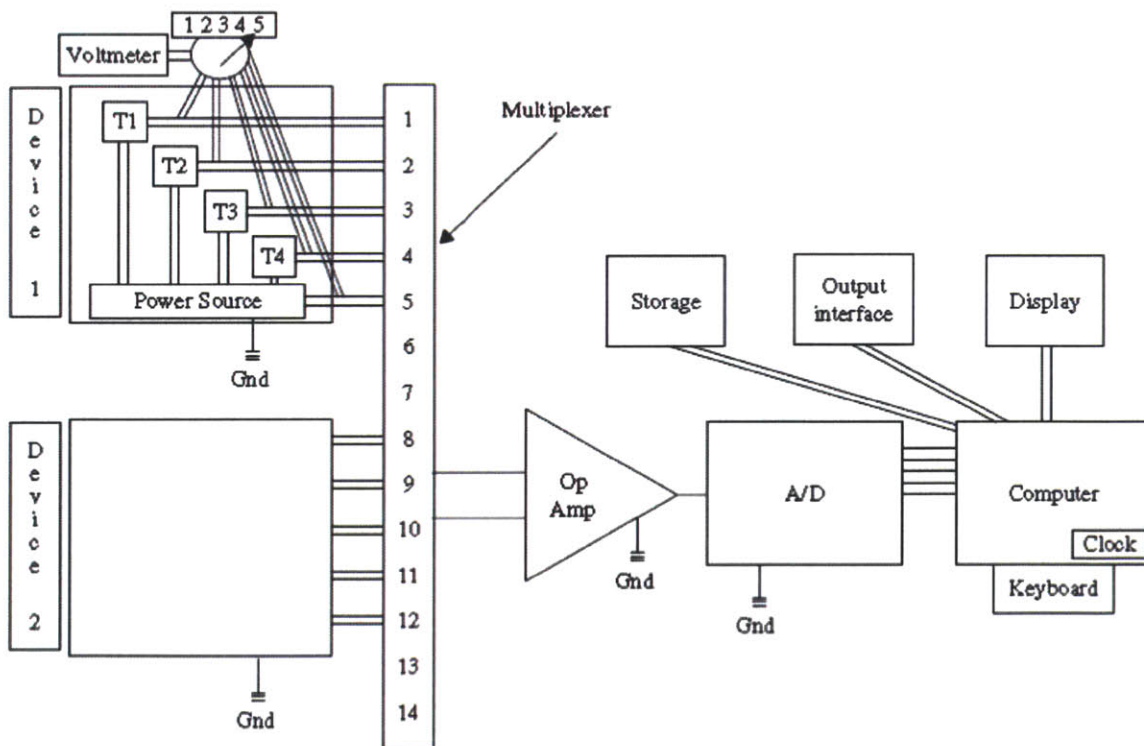
Figure 4.41: Schematic drawing of centralized data acquisition system (Germaine and Germaine, 2009)

Chapter (5)

RESULTS AND ANALYSES

5.1 Introduction

This chapter presents the results of the experimental study conducted on six different materials; four different natural soils and two clay-like materials; to investigate the relation between mode I fracture toughness, tensile strength, unit weight, and modulus of elasticity using flattened Brazilian disc (FBD) specimens. A total of 90 FBD tests were conducted on materials of different origin, mineralogy, physical and mechanical properties to investigate and characterize its fracture properties. The chapter starts with an explanation to the methodology implemented in interpretation of the experimental test results and the governing equations / correlations followed to determine and quantify the parameters of interest. Then a detailed description of the experimental results is presented for both natural soils and clay-like materials. In addition, an explanation to the failure modes of FBD specimens is presented. Afterwards, different correlations relating mode I fracture toughness and corresponding tensile strength, unit weight, and elastic modulus are presented followed by a comparison with data values reported in the literature for different soils, rocks, shale, rock-like, clay-like, and geomaterials. Finally concluding all the available data including experimental results of current research into one single equation relating fracture toughness to tensile strength.

5.2 Interpretation of the Test Results

By analyzing the data obtained from the data acquisition system and recorded during the flattened Brazilian test (FBD) until the specimen failure, one can obtain a number of relations, plots and hence parameters. During the test, data from the different transducers is recorded giving the record of the total load applied on the flattened ends using the load cell which is then converted to axial normal stress, the amount of the vertical displacement in the test setup using the linear voltage displacement (LVDT) transducer which is used as a back-up measurement and as a reference for strain measurements, and finally the actual vertical displacement within the specimen upon loading using the clip on extensometers which is converted to axial strain. It is worth noting that the displacement (strain) values computed using the LVDT were not indicative

of the actual strain of the test specimen as it included an amount of the machine displacement which yielded in an overestimated displacement/strain value. By comparing the results of the two measuring devices, it can be observed that the LVDT overestimated the displacement value by a factor of about 10 when compared to the extensometers which resulted in an underestimated modulus of elasticity value using LVDTs by a factor of 10 as well. Hence, the measured values using the extensometers were the ones taken into consideration while computing the modulus of elasticity. **Figure 5.1** illustrates an example for the difference in magnitude between the LVDT and extensometers measurements.

From the results of a single specimen one can prepare a plot of the load-displacement (stress-strain) behavior which is used to quantify the different parameters of interest; mode I fracture toughness, tensile strength, and Young's modulus of elasticity. In addition, using basic measuring tools the dimensions of the specimens and its mass can be determined which can be converted to a density value which can be used to define correlations with other computed parameters.

Using the basic concept of flattened Brazilian discs developed by Wang and Xing (1999) and the modifications developed by Wang et al. (2004), the load displacement (stress-strain) record can be used to determine the modulus of elasticity; E from the local slope of the linear section of load displacement record just before the maximum failure load. Averaged data for the back and front of the specimen from the two extensometers are used to define the vertical displacement. And to account for the effect of the central loading angle (2α) the modulus was evaluated using a modified relation as described in section 3.4 according to the following equation:

$$E = \frac{2P}{\pi \Delta wt} \left\{ (1 - \mu) - ln\left(1 + \frac{4}{sin^2 \alpha}\right) \right\} \frac{\alpha}{sin\, \alpha} \tag{5.1}$$

Where P is the resultant of the uniformly distributed force applied through the flattened ends, Δw is the vertical displacement within the specimen which was computed by averaging the readings of the two extensometers, t is the specimen thickness, D is the specimen diameter, E is the elastic modulus, sin α = 2b/D; 2b is the width of the flat end, and μ is Poisson's ratio. In the conducted research an average estimate of 0.3 was used for Poisson's ratio.

For the determination of the tensile strength, the approach adopted by Wang et al. (2004) was used. They used the load displacement record, determined the maximum load (peak load) where failure occurs to define the tensile strength and they used a shape factor, K to account for the

central angle (2α). The shape factor k was determined as per the following equation:

$$k = \frac{(\,2\cos^3\alpha + \cos\alpha + \sin\alpha/\alpha\,)^2}{8\,(\cos\alpha + \sin\alpha/\alpha\,)} * \frac{\alpha}{\sin\alpha} \tag{5.2}$$

Where α is half the central loading angle.

And the tensile strength of the tested specimen was determined as follows:

$$\sigma_t = k\,\frac{2\,P_c}{\pi D t} \tag{5.3}$$

Where, Pc is the critical load applied on the flat ends; which is the maximum load during testing determined from the load displacement record, D is the specimen diameter, t is the specimen thickness, and k is the coefficient which is dependent on the loading angle.

And finally, mode I fracture toughness was determined according to the basic general equation proposed by Wang and Xing (1999) and later modified by Wang (2004) in the following format:

$$K_{IC} = \frac{P_{min}}{\sqrt{R t}}\,\emptyset_{max} \tag{5.4}$$

Where, Pmin is the local minimum load which can be identified directly from the load displacement test record after the peak load, R and t are radius and thickness of the specimen, respectively and φ max is the maximum dimensionless stress intensity factor which; as described in section 3.7; can be determined with several methods. For this research, the method developed by Keles and Tutluoglu (2011) is used as it provides a general equation that is function of central loading angle (2α) and is not dependent on a specific value as in the work by Wang et al. (2004). Hence, the maximum stress intensity factor was determined as follows:

$$\emptyset_{max}(\alpha) = \frac{1}{43.31 - 15.63\,\exp(\cos\alpha\,)} \tag{5.5}$$

5.3 Experimental Results

As previously mentioned both natural soils and clay-like materials were used to develop an empirical relation between mode I fracture toughness and other mechanical physical properties; Young's modulus of elasticity, tensile strength, and density. In total 90 flattened Brazilian disc tests were carried out; 75 FBD tests[1] on the natural soils and 15 FBD tests on the clay-like materials. In the following sections, a summary table of the conducted experiments on each

---

[1] Not all tests are presented in this thesis; as some tests were carried out without using extensometers or conducted with a different load frame.

material is presented followed by a number of plots showing the trends and dependency between mode I fracture toughness, tensile strength, modulus of elasticity, and density. Then based on statistical analyses and further regression analyses, empirical equations and relations between the different parameters can be defined.

For the mode I fracture toughness – tensile strength correlations, five correlations were chosen from the literature to compare to this research data. Each correlation was used to back calculate the mode I fracture toughness value based on the tensile strength value obtained from the FBD test result then this K_{IC} value is compared with the value computed experimentally from the test records. The following correlations were chosen to give a wide range of comparison summarizing twenty years of research (details about each correlation are presented in Chapter 2):

- **Gunsallus and Kulhawy (1984)**

$$K_{IC} = 0.0736\,\sigma_t + 0.76 \tag{5.6}$$

- **Whittaker et al. (1992)**

$$K_{IC} = \frac{\sigma_t + 2.53}{9.35} \tag{5.7}$$

- **Harison et al. (1994)**

$$K_{IC} = 0.0706\,\sigma_t \tag{5.8}$$

- **Zhang et al. (1998)**

$$K_{IC} = \left(\frac{\sigma_t}{8.88}\right)^{1.613} \tag{5.9}$$

- **Zhang (2002)**

$$K_{IC} = 0.1453\,\sigma_t \tag{5.10}$$

For the mode I fracture toughness – modulus of elasticity, E correlation, a single correlation was found in the literature by Iqbal and Mohanty (2006) relating the modulus of elasticity E with the estimated fracture toughness value K_{IC}. This correlation was used to back calculate the mode I fracture toughness based on the modulus of elasticity value obtained from the FBD test then this K_{IC} value is compared with the experimentally obtained value.

- **Iqbal and Mohanty (2006)**

$$K_{IC}^e = 0.13\,E^{0.65} \tag{5.11}$$

Where K_{IC}^e is the estimated mode I fracture toughness value and E is Young's modulus in GPa.

5.3.1 Natural Soils

Seventy five flattened Brazilian disc specimens were prepared for four different natural soils; Bangladesh Clay, San Francisco Bay Mud, Boston Blue Clay, and Presumpscot Maine Clay. The specimens were prepared with an average diameter of 60 mm, an average thickness of 20 mm, and an average loading angle (2α) of 44 degrees.

5.3.1.1 Bangladesh Clay

Three flattened Brazilian disc Bangladesh Clay (as described in section 4.2.1.1) specimens were tested in this study; the specimens had an average diameter (D) of 57.93 mm, thickness (t) of 20.59 mm, and loading angle (2α) of 49.67 degrees. For the determination of mode I fracture toughness, K_{IC} the tests had an average maximum stress intensity factor of 0.22 and an average local minimum load succeeding the peak maximum load (defining the critical point) of 206 kg, yielding to an average K_{IC} value of 0.132 MPam$^{1/2}$.

The specimens had an average peak maximum load (load at failure) of 218.33 kg, which yielded an average tensile strength, σt value of 0.92 MPa, an average modulus of elasticity, E of 6.83 GPa, and an average density, γ of 1.75 gm/cm^3. A summary of the test results and specimen dimensions is presented in **Table 5.1**.

Figure 5.2 represents the relation between mode I fracture toughness, K_{IC} and tensile strength, σt of Bangladesh clay. With simple regression analyses the relation between the two parameters can be best represented using power trend as follows:

$$K_{IC} = 0.14566 \sigma t^{1.3039}, \text{ with a coefficient of determination } R^2 = 0.9997. \tag{5.12}$$

By comparing the experimentally computed K_{IC} and σt values and their relation with the back-calculated K_{IC} values based on tensile strength σt using the literature correlations, as shown in **Figure 5.3**, we find that the coordinates coincide perfectly with the values back-calculated using the relation developed by Zhang (2002) which is the most recent correlation covering a wider range of soils, rocks, and geomaterials.

The relation between mode I fracture toughness and modulus of elasticity, E is presented in **Figure 5.4** which shows a strong correlation and dependency between the two parameters that can be expressed using a power relation as well as follows:

$$K_{IC} = 2*10^{-05} E^{0.9859}, \text{ with a coefficient of determination } R^2 = 0.9612. \tag{5.13}$$

However, by comparing the experimentally computed K_{IC} and E values and their relation with

the back-calculated estimated K_{IC} values based on modulus of elasticity E using the correlation by Iqbal and Mohanty, (2006) as shown in **Figure 5.5**, it can be observed that the estimated fracture toughness value K_{IC}^e (literature) is overestimating the value by a factor of 3 if compared to the FBD experimental results. More tests are needed to better investigate this relation and probably more accurate means of estimating the modulus of elasticity are required.

Figures 5.6 and 5.7 show relations with the dry unit weight of the tested specimens and the mode I fracture toughness and tensile strength, respectively. From **Figure 5.6** it can be concluded that an empirical correlation between K_{IC} and γ_{dry} exists and it can be best described using a power trend as follows:

$$K_{IC} = 0.0029\ \gamma_{dry}^{6.799}, \text{ with a coefficient of determination } R^2 = 0.9257. \tag{5.14}$$

While **Figure 5.7** expresses the empirical relation between the tensile strength and dry unit weight which can statistically best described using a power trend as well as follows:

$$6t = 0.0517\ \gamma dry^{5.1291}, \text{ with a coefficient of determination } R^2 = 0.9104. \tag{5.15}$$

5.3.1.2 San Francisco Bay Mud

Eight flattened Brazilian disc San Francisco Bay Mud (as described in section 4.2.1.2) specimens were tested in the current research; the specimens had an average diameter (D) of 56.71 mm, thickness (t) of 18.45 mm, and loading angle (2α) of 43.76 degrees. For determination of mode I fracture toughness, K_{IC} the tests had an average maximum stress intensity factor of 0.27 and an average local minimum load succeeding the peak maximum load (defining the critical point) of 226.9 kg, yielding to an average K_{IC} value of 0.195MPam$^{1/2}$.

The specimens had an average peak maximum load (load at failure) of 270.27 kg, which yielded an average tensile strength, 6t value of 1.35 MPa, an average modulus of elasticity, E of 5.95 GPa, and an average density, γ of 1.58 gm/cm^3. A summary of the test results and specimen dimensions is presented in **Table 5.2**.

Figure 5.8 represents the relation between mode I fracture toughness, K_{IC} and tensile strength, 6t of San Francisco Bay Mud. With simple regression analyses the relation between the two parameters can be best represented using power trend as follows:

$$K_{IC} = 0.14026t^{0.9223}, \text{ with a coefficient of determination } R^2 = 0.8781. \tag{5.16}$$

By comparing the experimentally computed K_{IC} and 6t values and their relation with the back-calculated K_{IC} values based on tensile strength 6t using the literature correlations, as shown in **Figure 5.9**, we find that the coordinates agree to a great extent (± 15%) with the values back-

188

calculated using the relation developed by Zhang (2002) which is the most general correlation covering a wider range of soils, rocks, and geomaterials.

The relation between mode I fracture toughness and modulus of elasticity, E is presented in **Figure 5.10** which shows a strong correlation and dependency between the two parameters that can be expressed using a power relation as follows:

$K_{IC} = 2*10^{-05} E^{1.0328}$, with a coefficient of determination $R^2 = 0.6983$. (5.17)

However, by comparing the experimentally computed K_{IC} and E values and their relation with the back-calculated estimated K_{IC} values based on modulus of elasticity E using the correlation by Iqbal and Mohanty, (2006) as shown in **Figure 5.11**, it can be observed that the estimated fracture toughness value K_{IC}^e (literature) is overestimating the value by a factor of 2 if compared to the FBD experimental results. As in the case of Bangladesh Clay more accurate means of estimating the modulus of elasticity are required.

Figures 5.12 and 5.13 show relations with the dry unit weight of the tested specimens and the mode I fracture toughness and tensile strength, respectively. From both figures it can be concluded that there is no dependency between the studied parameters as the same unit weight value covers a wide range of the other studied parameter, hence, no proportionality can be concluded. It is worth noting that machining of flattened ends for all the tested materials exactly to a desired width and 2α target is difficult, and there is usually an error band of a few degrees. Considering this error band, might explain the scatter and inconsistency of the results for all the tested materials.

5.3.1.3 Boston Blue Clay

Fifteen flattened Brazilian disc Boston Blue Clay (as described in section 4.2.1.3) specimens were tested in the current research; the specimens were obtained from three different locations; MIT campus, MIT housing, and east Cambridge. A summary of the test results and specimen dimensions of each site locations is presented in **Tables 5.3, 5.4, and 5.5.** The specimens had an average diameter (D) of 60.88 mm, thickness (t) of 20.51 mm, and loading angle (2α) of 44.71 degrees. For determination of mode I fracture toughness, K_{IC} the tests had an average maximum stress intensity factor of 0.26 and an average local minimum load succeeding the peak maximum load (defining critical point) of 263.17 kg, yielding to an average K_{IC} value of 0.190 MPam$^{1/2}$.

The specimens had an average peak maximum load (load at failure) of 321.88 kg, which yielded an average tensile strength, δt value of 1.35 MPa, an average modulus of elasticity, E of 9.8 GPa,

and an average density, γ of 1.70 gm/cm^3. A summary of all the BBC test results and specimen dimensions is presented in **Table 5.6.**

Figure 5.14 represents the relation between mode I fracture toughness, K_{IC} and tensile strength, δt of Boston Blue Clay. With simple regression analyses the relation between the two parameters can be best represented using a power trend as follows:

$K_{IC} = 0.14566t^{0.9725}$, with a coefficient of determination $R^2 = 0.9048$. (5.18)

By comparing the experimentally computed K_{IC} and δt values and their relation with the back-calculated K_{IC} values based on tensile strength δt using the literature correlations, as shown in **Figure 5.15**, we find that the coordinates agree to a great extent ($\pm$ 10%) with the values back-calculated using the relation developed by Zhang (2002). In addition, it can be seen that the computed values are site dependent where specimens from the same location show greater consistency and correlation.

The relation between mode I fracture toughness and modulus of elasticity, E is presented in **Figure 5.16** which shows the scatter in the data points, hence, no statistical correlation can be concluded for this soil type. And by comparing the experimentally computed K_{IC} and E values and their relation with the back-calculated estimated K_{IC} values based on modulus of elasticity E using the correlation by Iqbal and Mohanty, (2006) as shown in **Figure 5.17**, it can be observed that the estimated fracture toughness value K_{IC}^e (literature) is overestimating the value by a factor ranging from 2 to 4; depending on the site location; if compared to the FBD experimental results. As in the case of previous soils more specimens from different sites are needed to quantify the modulus value more reliably in addition to more accurate means of estimating the modulus of elasticity are required.

Figures 5.18 and 5.19 show relations with the dry unit weight of the tested specimens and the mode I fracture toughness and tensile strength, respectively. From both figures it can be concluded that there is no dependency relation between the studied parameters as there is much scatter in the unit weight values covering a wide range of the other studied parameter, hence, no proportionality can be concluded.

5.3.1.4 Presumpscot Maine Clay

Fifteen flattened Brazilian disc Presumpscot Maine Clay (as described in section 4.2.1.4) specimens were tested in the current research; the specimens were obtained from two different locations. A summary of the test results and specimen dimensions of each site is presented in

Tables 5.7 and 5.8. The specimens had an average diameter (D) of 62.47 mm, thickness (t) of 20.08 mm, and loading angle (2α) of 41.96 degrees. For determination of mode I fracture toughness, K_{IC} the tests had an average maximum stress intensity factor of 0.29 and an average local minimum load succeeding the peak maximum load (defining critical point) of 114.55 kg, yielding an average K_{IC} value of 0.090 MPam$^{1/2}$; much lower than the previous soils.

The specimens had an average peak maximum load (load at failure) of 145.33 kg, which yielded an average tensile strength, σt value of 0.62 MPa, an average modulus of elasticity, E of 7.6 GPa, and an average density, γ of 1.76 gm/cm^3. A summary of all the Presumpscot Maine Clay test results and specimen dimensions is presented in **Table 5.9**.

Figure 5.20 represents the relation between mode I fracture toughness, K_{IC} and tensile strength, σt of Presumpscot Maine Clay. With simple regression analyses the relation between the two parameters can be best represented using power trend as follows:

$K_{IC} = 0.17256t^{1.3547}$, with a coefficient of determination $R^2 = 0.8904$.   (5.19)

By comparing the experimentally computed K_{IC} and σt values and their relation with the back-calculated K_{IC} values based on tensile strength σt using the literature correlations, as shown in **Figure 5.21**, we find that the coordinates agree to a great extent (± 15%) with the values back-calculated using the relation developed by Zhang (2002). In addition, it can be seen that the computed values are site dependent where specimens from the same location show greater consistency (narrower variation) and correlation.

The relation between mode I fracture toughness and modulus of elasticity, E is presented in **Figure 5.22** which shows the scatter in the data points, hence, no statistical correlation can be concluded for this soil type. And by comparing the experimentally computed K_{IC} and E values and their relation with the back-calculated estimated K_{IC} values based on modulus of elasticity E using the correlation by Iqbal and Mohanty, (2006) as shown in **Figure 5.23**, it can be observed that the estimated fracture toughness value K^e_{IC} (literature) is overestimating the value by a factor ranging from 3 to 5 if compared to the FBD experimental results indicating the amount of scatter and inconsistency in the Young's modulus values obtained. As in the case of previous soils more specimens from different sites are needed to quantify the modulus value more reliably in addition to more accurate means of estimating the modulus of elasticity are required.

Figures 5.24 and 5.25 show relations with the dry unit weight of the tested specimens and the mode I fracture toughness and tensile strength, respectively. From both figures it can be

191

concluded that there is no dependency relation between the studied parameters as there is much scatter in the unit weight values covering a wide range of the other studied parameter, hence, no proportionality can be concluded.

To define a relationship between mode I fracture toughness and the other computed parameters for the tested natural soils, several regression analyses with the least square method were carried out to best describe the relation. It was found that by dividing the tensile strength by the dry unit weight of the specimen, a linear relation with the facture toughness (as shown in **Figure 5.26**) can be concluded as follows:

$$K_{IC} = 0.2338 \frac{\sigma_t}{\gamma_{dry}} + 0.0053, \text{ with a coefficient of determination } R^2 = 0.9239. \quad (5.20)$$

5.3.2 Clay-like Materials

Twelve flattened Brazilian disc specimens were prepared for two clay-like semi-brittle materials; molded Gypsum and Plaster of Paris. The specimens were prepared with an average diameter of 76.22 mm, an average thickness of 25 mm, and an average loading angle (2α) of 44 degrees.

5.3.2.1 Plaster of Paris

Five flattened Brazilian disc Plaster of Paris (as described in section 4.2.2.1) specimens were tested in the current research; the specimens were prepared at powder to water mix ratio by mass of 1.75:1. The specimens had an average diameter (D) of 76.47 mm, thickness (t) of 27.51 mm, and loading angle (2α) of 47.48 degrees. For determination of mode I fracture toughness, K_{IC} the tests had an average maximum stress intensity factor of 0.23 and an average local minimum load succeeding the peak maximum load (defining critical point) of 156.74 kg, yielding an average K_{IC} value of 0.070 MPam$^{1/2}$; much lower than the natural soils.

The specimens had an average peak maximum load (load at failure) of 247.8 kg, which yielded an average tensile strength, σt value of 0.60 MPa, an average modulus of elasticity, E of 3.48 GPa, and an average density, γ of 1.09 gm/cm^3 (very light material). A summary of all the Plaster of Paris test results and specimen dimensions is presented in **Table 5.10**.

Figure 5.27 represents the relation between mode I fracture toughness, K_{IC} and tensile strength, σt of Plaster of Paris. It is worth noting, that there is significant variation for fractured specimen though they all have the same density. With simple regression analyses the relation between the two parameters can be best represented using an exponential trend as follows:

$K_{IC} = 0.0147e^{2.8266t}$, with a coefficient of determination $R^2 = 0.9678$. (5.21)

By comparing the experimentally computed K_{IC} and σ_t values and their relation with the back-calculated K_{IC} values based on tensile strength σ_t using the literature correlations, as shown in **Figure 5.28**, we find that the coordinates lie in between the correlations of Harrison et al. (1994) and Zhang (2002) and does not agree completely with any of the literature correlations. This can be attributed to the fact that the empirical correlations used for reference are obtained based on experimental studies on rocks, soils, and geomaterilas not including plaster of paris with the powder to water ratio used in the current study. The computed fracture toughness values are lower than prediction, maybe due to more brittle material behavior.

The relation between mode I fracture toughness and modulus of elasticity, E is presented in **Figure 5.29** which shows proportionality correlation and dependency between the two parameters that can be expressed using a power relation as well as follows:

$K_{IC} = 1*10^{-11} E^{2.7973}$, with a coefficient of determination $R^2 = 0.7315$. (5.22)

And by comparing the experimentally computed K_{IC} and E values and their relation with the back-calculated estimated K_{IC} values based on modulus of elasticity E using the correlation by Iqbal and Mohanty, (2006) as shown in **Figure 5.30**, it can be observed that the estimated fracture toughness value K_{IC}^e (literature) is overestimating the value by a factor ranging from 2 to 6 if compared to the FBD experimental results indicating the amount of scatter and inconsistency in the Young's modulus values obtained. Which implies that the correlation; by Iqbal and Mohanty (2006); is not suitable for estimating the modulus of elasticity – fracture toughness relationship.

Figures 5.31 and 5.32 show relations with the dry unit weight of the tested specimens and the mode I fracture toughness and tensile strength, respectively. From both figures it can be concluded that there is no direct dependency relation between the studied parameters as there is much scatter in the unit weight values covering a wide range of the other studied parameter, hence, no proportionality can be concluded.

5.3.2.2 Molded Gypsum

Five flattened Brazilian disc Molded Gypsum (as described in section 4.2.2.2) specimens were tested in the current research. The specimens had an average diameter (D) of 76.09 mm, thickness (t) of 23.44 mm, and loading angle (2α) of 41.81 degrees. For determination of mode I

fracture toughness, K_{IC} the tests had an average maximum stress intensity factor of 0.28 and an average local minimum load succeeding the peak maximum load (defining critical point) of 1838.6 kg, yielding to an average K_{IC} value of 1.141 MPam$^{1/2}$; much higher than the Plaster of Paris and the natural soils.

The specimens had an average peak maximum load (load at failure) of 2133 kg, which yielded an average tensile strength, σ_t value of 6.38 MPa (relatively high approaching the values of soft rocks and rock-like materials), an average modulus of elasticity, E of 19.20 GPa, and an average density, γ of 1.56 gm/cm^3. A summary of all the molded Gypsum test results and specimen dimensions is presented in **Table 5.11**.

Figure 5.33 represents the relation between mode I fracture toughness, K_{IC} and tensile strength, σ_t of molded Gypsum. With simple regression analyses the relation between the two parameters can be best represented using an exponential trend as follows:

$$K_{IC} = 0.237e^{\,0.24556t}, \text{ with a coefficient of determination } R^2 = 0.7859. \tag{5.23}$$

By comparing the experimentally computed K_{IC} and σ_t values and their relation with the back-calculated K_{IC} values based on tensile strength σ_t using the literature correlations, as shown in **Figure 5.34**, we find agreement to a great extent but shifted to the high side of the equation with the values back calculated using Gunsallus and Kulhawy (1984) which was conducted on eight sedimentary rocks, which implies that the fracture behavior of molded gypsum approaches the behavior of sedimentary rocks.

The relation between mode I fracture toughness and modulus of elasticity, E is presented in **Figure 5.35** which shows proportionality correlation and dependency between the two parameters that can be expressed using a power relation as follows:

$$K_{IC} = 3*10^{-7}E^{1.5349}, \text{ with a coefficient of determination } R^2 = 0.8384. \tag{5.24}$$

And by comparing the experimentally computed K_{IC} and E values and their relation with the back-calculated estimated K_{IC} values based on modulus of elasticity, E, using the correlation by Iqbal and Mohanty, (2006) as shown in **Figure 5.36**, it can be observed that the estimated fracture toughness value K^e_{IC} (literature) agrees to a great extent with the FBD experimental results indicating the suitability of the empirical correlation with the Plaster of Paris. Which implies that the behavior of Plaster of Paris resembles that of soft rocks which were under the study of Iqbal and Mohanty, (2006).

Figures 5.37 and 5.38 show relations with the dry unit weight of the tested specimens and the

mode I fracture toughness and tensile strength, respectively. From both figures it can be concluded that there is no direct dependency relation between the studied parameters as there is much scatter in the unit weight values covering a wide range of the other studied parameter, hence, no proportionality can be concluded.

5.3.3 Failure Behavior of Tested Specimens

According to Hai-yong et al. (2004), the breaking behavior of the flattened uncracked Brazilian discs is different from the solid circular Brazilian discs. For the conventional solid Brazilian disc, when the applied load reaches its maximum value the disc will break along the loading diameter, and then the load will drop down to a certain level and it will increase again as the two broken halves are not separated. The failure line is along the loading line bur it is not straight as illustrated in **Figure 5.39**.

While for the flattened Brazilian discs the behavior is dependent on the flattened area of discs, the central loading angle (2α). As previously discussed in Chapter 3 and according to the theory behind the FBD test, the first crack initiates straight from the center of the specimen when the load angle (2α) exceeds 19°. However, Hai-yong et al. (2004) observed a different experimental behavior which contradicts the FBD theory. According to their conducted experimental studies, when the loading angle is in the order of 20°, the breaking crack usually initiates at two sides of disc along the edge of flattened surface and propagates to the centre of the discs, when the curve of load versus displacement reaches the first peak. Afterwards, a diagonal crack extending from the top flattened edge propagates to reach the bottom flattened end as illustrated in **Figure 5.40**.

Hai-yong et al. (2004), also stated that when the central loading angle is greater than 30°, there are three different possible behaviors: the first one is that the breaking crack initiates at one side of the disc from the edge of the top flattened surface to the bottom separating the disc into two halves, semi-discs as shown in **Figure 5.41 (a)**, in the conducted research this behavior was commonly observed where the crack is initiated and propagated exactly at the middle center of the specimen. The second possible behavior is similar to the behavior described for the flattened Brazilian discs with 20° loading angle as shown in **Figure 5.41 (b)**. The third behavior is upon reaching the critical load value where the disc is fractured along the specimen diagonal line as shown in **Figure 5.41 (c)** (Hai-yong et al., 2004). The previously mentioned behaviors contradict and deviate from the theory of first crack initiation from the center of the specimen when the

loading angle exceeds 19 degrees, which may be attributed to equipment problems, load application problems, or material specific problems.

For the flattened Brazilian disc specimens tested in the current research, the average loading angle was greater than 19 degrees and the observed behavior in the 90 conducted tests totally agreed with the theory behind the FBD test. The first crack was straight and initiated from the center of the specimen as described in Chapter 3. The observed behavior showing straight center crack initiation is illustrated in **Figures 5.42 and 5.43** However, in a few tests the specimens showed different fracturing pattern after the first center crack initiation, where a number of diagonal cracks were observed at a later stage of the test as shown in **Figures 5.44 and 5.45**. The fractured surface of the two split halves (semi discs) of the fractured flattened Brazilian specimens is presented in **Figure 5.46**, from the figure it can be concluded that the induced fractures are tensile fractures rather than shear ones.

5.4 Correlating the Measured Parameters

To define a relationship between mode I fracture toughness and the other measured/ computed parameters; the tensile strength, the modulus of elasticity, and the unit weight for all the tested materials; natural soils and clay-like materials, several statistical regression analyses were carried out to best describe the relation. It was found that by dividing the tensile strength by the dry unit weight of the specimen, a linear relation with the facture toughness (as presented in **Figure 5.47**) can be concluded as follows:

$$K_{IC} = 0.2873 \; \frac{\sigma_t}{\gamma_{dry}} - 0.0382, \text{ with a coefficient of determination } R^2 = 0.9829. \tag{5.25}$$

Or the tensile strength of the tested material can be computed in terms of fracture toughness as follows (shown in **Figure 5.48**):

$$\sigma_t = 5.3881 \; K_{IC} + 0.2359, \text{ with a coefficient of determination } R^2 = 0.9877. \tag{5.26}$$

With further regression analyses and using the least square error method, the relation between the predicted tensile strength, σ_t and the mode I fracture toughness, K_{IC} was assumed to take an exponential function format:

$$\sigma_t \; (predicted) = a \; e^{b* \, K_{IC}} \tag{5.27}$$

Using the least square error method between the predicted tensile strength and the actual measure tensile strength, the parameter a was found equal to 0.930346 and the parameter b was found

equal to 1.621593 with sum of square error equal to 0.50. **Figure 5.49** shows the relation between the actual measured tensile strength and the predicted tensile strength (having a coefficient of determination $R^2 = 0.9133$) using the following equation:

$$\sigma_t \ (predicted) = \ 0.93 \ e^{1.622* \ K_{IC}} \tag{5.28}$$

To account for the effect of the specimen's unit weight, γ and the modulus of elasticity, E further regression analyses were carried out and a multiple power function regression was adopted and the relation between the different parameters were assumed to take the following format:

$$\sigma_t(predicted) = \ a \ \left(K_{IC}{}^b \ \right)\gamma^c \ E^d \tag{5.29}$$

Using the least square error method between the predicted tensile strength and the actual measure tensile strength, the parameter a was found equal to 2.026418, the parameter b was found equal to 0.893048, the parameter c was found equal to 0.372125, and the parameter d was found equal to zero with sum of square error equal to 0.20. Having the d parameter equal to zero implies that there is no general direct relation between the modulus of the elasticity and the remaining parameters. **Figure 5.50** shows the relation between the actual measured tensile strength and the predicted tensile strength (having a coefficient of determination $R^2 = 0.9886$) using the following equation:

$$\sigma_t(predicted) = \ 2.026 \ \left(K_{IC}{}^{0.893} \ \right)\gamma^{0.372} \ E^0 \tag{5.30}$$

5.5 Comparing with Reported Values in the Literature

In order to obtain a more general correlation that is applicable to soils, rocks, clay-like materials, rock-like materials, and geomaterials, data reported in the literature was compiled with the results from flattened Brazilian tests. By referring to tables 2.2 and 2.4, reported values of mode I fracture toughness and the corresponding tensile strength were selected (presented in **Table 5.12**) and plotted with the experimental results of the current research as shown in **Figure 5.51**. From the figure it can be observed that there is a strong proportionality correlation between the two parameters covering the wide range of material irrespective to the testing method used to obtain K_{IC} (whether ISRM suggested methods or other methods on disc specimens as covered in chapter 2) and irrespective to the testing method used to obtain σ_t (whether direct tension or bending tension or Brazilian tension method)

Considering the results of the tested natural soils and clay-like materials with the literature

197

reported values and using statistical regression analyses, the relation between mode I fracture toughness and tensile strength can be best described in the form of power relation as follows (shown in **Figure 5.52**):

$K_{IC} = 0.1482 \, \sigma t^{1.0165}$, with a coefficient of determination $R^2 = 0.9508$. (5.31)

Further data were extracted from the literature including the summary plot of Haberfield and Johnston (1989), where it is the only reference covering rocks, oil shale, clays and rock-like materials on the same plot. Experimental results from this research on the six test materials in addition to some data points from the literature (as presented in **Table 5.12**) were added to the summary plot of Haberfield and Johnston (1989) as shown in **Figure 5.53**. From the figure a strong correlation between fracture toughness and tensile strength can be concluded. However, by observing the experimental Johnstone and Melbourne Mudstone data points of Haberfield and Johnston (1989), it can be seen that there is a shift in the relation compared to other materials which required further investigation. Looking at the experimental method followed by Haberfield and Johnston (1989) to estimate the tensile strength of Johnstone and Melbourne Mudstone, they used three or four point bend tests on un-notched prismatic specimens which reportedly overestimate the tensile strength value by about 30% if compared to the indirect Brazilian disc tests (Fuenkajorn, 2011), hence, a modification to the tensile strength values of Johnstone and Melbourne Mudstone was applied to make the results comparable to the experimental results of the current research and other data from the literature. **Figures 5.54 and 5.55** show the summary plot of Haberfield and Johnston (1989) in addition to experimental results and results of Johnstone and Melbourne Mudstone modified by a reduction factor of 0.70.

Considering all the available data; the results of the tested natural soils and clay-like materials with the literature reported values and modified Johnstone and Melbourne Mudstone results, using statistical regression analyses, the relation between mode I fracture toughness and tensile strength can be best described in the form of power relation as follows (shown in **Figure 5.56**):

$K_{IC} = 0.1487 \, \sigma t^{1.0179}$, with a coefficient of determination $R^2 = 0.9651$. (5.32)

Table 5.1: Summary of Flattened Brazilian Disc Specimen Dimensions and Tests Results of Bangladesh Clay

Parameter	Specimen 1	Specimen 2	Specimen 3	Mean	St Deviation
D (mm)	57.39	57.51	58.90	57.93	0.84
t (mm)	19.94	19.74	22.09	20.59	1.31
$(2\alpha°)$	46.20	49.30	53.50	49.67	3.66
ϕmax	0.24	0.22	0.19	0.22	0.02
Pmin (kg)	217.00	217.00	184.00	206.00	19.05
K_{IC} (MPam$^{1/2}$)	0.157	0.143	0.095	0.132	0.033
Pmax (kg)	235.00	225.00	195.00	218.33	20.82
k	0.81	0.78	0.75	0.78	0.03
$6t$ (MPa)	1.06	0.99	0.72	0.92	0.18
E (GPa)	8.50	7.00	5.00	6.83	1.76
γ (gm/cm3)	1.81	1.75	1.68	1.75	0.07

Table 5.2: Summary of Flattened Brazilian Disc Specimen Dimensions and Tests Results of San Francisco Bay Mud

Parameter	Specimen 1	2	3	4	5	6	7	8	Mean	St Deviation
D (mm)	56.47	55.53	56.10	58.06	56.13	57.23	57.70	56.46	56.71	0.87
t (mm)	19.18	17.76	17.77	18.88	18.15	19.15	18.74	17.99	18.45	0.60
$(2\alpha°)$	47.52	38.92	46.17	45.82	41.75	42.52	47.52	39.87	43.76	3.43
ϕmax	0.23	0.31	0.24	0.25	0.28	0.28	0.23	0.30	0.27	0.03
Pmin	218.0	155.0	204.8	332.0	200.0	267.4	155.0	283.3	226.9	62.67
K_{IC} (MPam$^{1/2}$)	0.158	0.165	0.168	0.255	0.187	0.228	0.114	0.285	0.195	0.056
Pmax	244.6	182.4	263.7	378.0	278.2	298.0	182.6	334.79	270.27	68.37
k	0.80	0.86	0.81	0.81	0.84	0.83	0.80	0.85	0.82	0.02
$6t$ (MPa)	1.15	1.01	1.36	1.78	1.46	1.44	0.86	1.79	1.35	0.34
E (GPa)	6.00	4.70	5.00	6.50	4.80	7.50	4.50	8.60	5.95	1.49
γ (gm/cm3)	1.52	1.47	1.47	1.75	1.55	1.78	1.56	1.56	1.58	0.12

Table 5.3: Summary of Flattened Brazilian Discs Specimen Dimensions and Tests Results of Boston Blue Clay from 1st site location in Cambridge

	1st Site Location: Cambridge					
	Specimen					
Parameter	1	2	3	4	Mean	St Deviation
D (mm)	58.08	58.74	58.02	58.28	58.28	0.33
t (mm)	20.98	19.44	21.56	18.91	20.22	1.25
(2α˚)	45.00	45.50	39.30	47.00	44.20	3.38
φmax	0.25	0.25	0.31	0.24	0.26	0.03
Pmin	271.00	244.00	190.00	362.35	266.84	72.03
K_{IC} (MPam$^{1/2}$)	0.193	0.182	0.160	0.267	0.201	0.046
Pmax	315.66	351.59	226.00	400.36	323.40	73.63
k	0.18	0.81	0.86	0.80	0.66	0.32
σt (MPa)	1.35	1.59	0.98	1.85	1.44	0.37
E (G Pa)	12	12	10	8	10.5	1.91
γ (gm/cm3)	1.75	1.77	1.73	1.65	1.73	0.05

Table 5.4: Summary of Flattened Brazilian Discs Specimen Dimensions and Tests Results of Boston Blue Clay from 2nd site location: MIT Campus

	2nd Site Location: MIT Campus						
	Specimen						
Parameter	1	2	3	4	5	Mean	St Deviation
D (mm)	62.42	61.81	61.33	62.17	61.56	61.86	0.44
t (mm)	20.58	20.93	19.77	21.15	20.99	20.68	0.55
(2α˚)	43.24	47.92	41.54	43.42	45.89	44.40	2.50
φmax	0.27	0.23	0.29	0.27	0.25	0.26	0.02
Pmin	114.55	151.70	149.05	225.00	265.60	181.18	62.02
K_{IC} (MPam$^{1/2}$)	0.085	0.095	0.123	0.162	0.178	0.129	0.041
Pmax	140.00	160.00	356.24	242.94	290.47	237.93	90.06
k	0.83	0.79	0.84	0.83	0.81	0.82	0.02
σt (MPa)	0.57	0.63	1.57	0.97	1.16	0.98	0.41
E (GPa)	10.00	10.00	10.00	8.00	10.00	9.60	0.89
γ (gm/cm3)	1.72	1.64	1.76	1.74	1.73	1.72	0.05

Table 5.5: Summary of Flattened Brazilian Discs Specimen Dimensions and Tests Results of Boston Blue Clay from 3rd site location: MIT Housing

Parameter	\multicolumn{6}{c}{3rd Site Location: MIT Housing}	Mean	St Deviation
	Specimen		
	1	2	3	4	5	6	Mean	St Deviation
D (mm)	62.05	62.00	61.86	62.05	61.14	61.68	61.80	0.35
t (mm)	21.31	21.06	20.24	19.37	20.29	21.06	20.56	0.73
(2α°)	46.51	49.08	44.15	39.08	43.69	49.35	45.31	3.87
ϕmax	0.24	0.22	0.26	0.31	0.27	0.22	0.25	0.03
Pmin	300.00	400.00	480.00	333.70	250.00	210.57	329.05	98.97
K_{IC} (MPam$^{1/2}$)	0.193	0.240	0.352	0.306	0.187	0.126	0.234	0.083
Pmax	346.36	445.33	514.35	410.60	334.17	294.20	390.84	81.42
k	0.81	0.79	0.82	0.86	0.83	0.78	0.81	0.03
6t (MPa)	1.34	1.71	2.15	1.86	1.42	1.13	1.60	0.38
E (GPa)	10.00	7.00	8.00	10.00	10.00	12.00	9.50	1.76
γ (gm/cm3)	1.61	1.79	1.63	1.70	1.63	1.63	1.67	0.07

Table 5.6: Summary of all Flattened Brazilian Disc Specimen Dimensions and Tests Results of Boston Blue Clay

Parameter	Mean	St Deviation
D (mm)	60.88	1.66
t (mm)	20.51	0.80
(2α°)	44.71	3.14
ϕmax	0.26	0.03
Pmin	263.17	99.87
K_{IC} (MPam$^{1/2}$)	0.190	0.075
Pmax	321.88	101.99
k	0.78	0.17
6t (MPa)	1.35	0.45
E (GPa)	9.8	1.52
γ (gm/cm3)	1.70	0.06

Table 5.7: Summary of Flattened Brazilian Discs Specimen Dimensions and Tests Results of Presumpscot Maine Clay from 1st site location

Parameter	1st Site Location								
	Specimen							Mean	St Deviation
	1	2	3	4	5	6	7		
D (mm)	62.08	62.81	62.76	63.06	63.00	62.60	62.61	62.70	0.33
t (mm)	19.74	20.67	20.90	20.86	20.70	20.78	20.18	20.55	0.43
(2α)	42.50	43.95	33.81	36.03	37.98	43.60	40.17	39.72	3.93
φmax	0.28	0.26	0.38	0.35	0.33	0.27	0.30	0.31	0.05
Pmin	217.00	142.00	142.00	149.00	188.00	168.00	83.20	155.60	42.09
K_{Ic} (MPam$^{1/2}$)	0.173	0.102	0.146	0.141	0.166	0.122	0.070	0.131	0.036
Pmax	243.41	162.25	162.25	183.55	219.73	181.00	144.38	185.22	34.93
k	0.83	0.83	0.89	0.88	0.86	0.83	0.85	0.85	0.03
6t (MPa)	1.05	0.66	0.70	0.78	0.93	0.73	0.62	0.78	0.16
E (GPa)	9.00	8.90	11.00	7.30	7.50	7.00	10.80	8.79	1.64
γ (gm/cm3)	1.49	1.81	1.81	1.74	1.78	1.73	1.74	1.73	0.11

Table 5.8: Summary of Flattened Brazilian Discs Specimen Dimensions and Tests Results of Presumpscot Maine Clay from 2nd site location

Parameter	2nd Site Location									
	Specimen								Mean	St Deviation
	1	2	3	4	5	6	7	8		
D (mm)	61.34	61.27	62.49	62.5	62.79	61.95	62.86	62.9	62.26	0.66
t (mm)	17.91	18.20	20.56	20.3	19.92	20.15	20.39	19.9	19.67	1.02
(2α)	43.04	44.10	40.74	45.7	44.45	37.67	48.86	46.8	43.92	3.51
φmax	0.27	0.26	0.29	0.25	0.26	0.33	0.22	0.24	0.27	0.03
Pmin	89.15	108.5	71.40	60.0	90.00	70.00	80.00	60.0	78.63	16.70
K_{Ic} (MPam$^{1/2}$)	0.077	0.089	0.058	0.042	0.066	0.065	0.050	0.041	0.061	0.017
Pmax	126.23	145.1	102.7	73.00	109.7	112.3	119.1	95.16	110.42	21.47
k	0.83	0.82	0.85	0.81	0.82	0.87	0.79	0.80	0.82	0.02
6t (MPa)	0.61	0.68	0.43	0.30	0.46	0.50	0.47	0.39	0.48	0.12
E (GPa)	6.00	7.00	5.00	10.00	5.00	8.00	5.50	6.00	6.56	1.72
γ (gm/cm3)	2.01	1.98	1.65	1.76	1.69	1.75	1.73	1.76	1.79	0.13

Table 5.9: Summary of all Flattened Brazilian Disc Specimen Dimensions and Tests Results of Presumpscot Maine Clay

Parameter	Mean	St Deviation
D (mm)	62.47	0.56
t (mm)	20.08	0.90
(2α ˚)	41.96	4.18
ϕmax	0.29	0.04
Pmin	114.55	49.79
K_{IC} (MPam$^{1/2}$)	0.09	0.05
Pmax	145.33	47.39
k	0.84	0.03
6t (MPa)	0.62	0.21
E (GPa)	7.60	1.99
γ (gm/cm3)	1.76	0.12

Table 5.10: Summary of Flattened Brazilian Disc Specimen Dimensions and Tests Results of Plaster of Paris

Parameter	Specimen 1	2	3	4	5	Mean	St Deviation
D (mm)	76.01	77.63	76.57	76.18	75.96	76.47	0.69
t (mm)	27.05	28.24	27.39	27.59	27.28	27.51	0.45
(2α ˚)	44.53	48.44	48.59	47.86	48.00	47.48	1.68
ϕmax	0.26	0.23	0.23	0.23	0.23	0.23	0.01
Pmin (kg)	296.50	126.48	208.70	98.50	53.52	156.74	96.43
K_{IC} (MPam$^{1/2}$)	0.145	0.052	0.088	0.042	0.023	0.070	0.048
Pmax (kg)	365.49	250.34	358.86	187.76	76.53	247.80	121.58
k	0.82	0.79	0.79	0.80	0.79	0.80	0.01
6t (MPa)	0.93	0.57	0.86	0.45	0.19	0.60	0.30
E (GPa)	4.00	3.20	4.10	3.70	2.40	3.48	0.70
γ (gm/cm3)	1.09	1.10	1.10	1.10	1.04	1.09	0.03

Table 5.11: Summary of Flattened Brazilian Disc Specimen Dimensions and Tests Results of Molded Gypsum

Parameter	Specimen					Mean	St Deviation
	1	2	3	4	5		
D (mm)	75.85	76.50	75.74	76.53	75.82	76.09	0.39
t (mm)	23.36	23.56	23.36	23.50	23.42	23.44	0.09
$(2\alpha°)$	40.50	46.18	39.35	41.32	41.72	41.81	2.60
ϕmax	0.30	0.24	0.31	0.29	0.28	0.28	0.02
Pmin (kg)	1548.0	2014.0	2015.0	1805.0	1811.0	1838.6	192.5
K_{IC} (MPam$^{1/2}$)	1.010	1.068	1.370	1.132	1.128	1.141	0.137
Pmax (kg)	1918.85	2265.41	2267.00	2072.48	2144.43	2133.63	145.89
k	0.85	0.81	0.86	0.84	0.84	0.84	0.02
6t (MPa)	5.85	6.46	6.97	6.18	6.45	6.38	0.41
E (GPa)	18.00	17.80	21.00	19.70	19.50	19.20	1.32
γ (gm/cm3)	1.54	1.55	1.57	1.56	1.58	1.56	0.02

Table 5.12: Summary of K$_{IC}$ and σ_t values as reported in the literature

Reference	Material	K$_{IC}$ MPa.m$^{0.5}$	K$_{IC}$ MPa.mm$^{0.5}$	σ_t MPa
Haberfield and Johnston, 1989	Basalt	2.27	71.78	21.50
		2.09	66.00	22.00
Gunsallus KL, Kulhawy FH, 1990	Limestone	1.58	49.96	7.86
		0.99	31.31	5.38
		1.38	43.64	8.47
Haberfield and Johnston, 1989	Marble	1.12	35.42	5.86
		1.00	31.62	5.71
		0.95	30.00	22.00
		1.26	40.00	17.00
		1.64	52.00	15.00
		0.63	20.00	18.00
Gunsallus KL, Kulhawy FH, 1991	Sandstone	0.67	21.19	3.09
		0.56	17.71	4.01
Schmidt RA, 1977	Oil Shale	0.37	11.70	3.30
		0.38	12.00	3.00
		0.63	20.00	12.00
Haberfield and Johnston, 1989	Siltstone	0.80	25.30	2.89
	Syenite	1.55	49.02	13.20
		1.11	35.00	7.50
		1.26	40.00	12.00
		1.21	38.26	11.10
	Tuff	0.41	12.97	2.80
Bhagat, 1985	Coal	0.06	1.90	0.22
		0.27	8.54	0.93
		0.12	3.79	0.36
Haberfield and Johnston, 1989	Granite	1.72	54.39	15.60
		2.53	80.00	37.00
		0.95	30.00	5.50
		0.63	20.00	4.50
		2.61	82.54	13.70
Gunsallus KL, Kulhawy FH, 1991	Dolostone	1.66	52.49	13.30
		1.66	52.49	16.40
		1.80	56.92	12.10
		1.78	56.29	13.00
		2.47	78.11	17.00
Lee et al., 1982	Clay	0.01	0.35	0.04
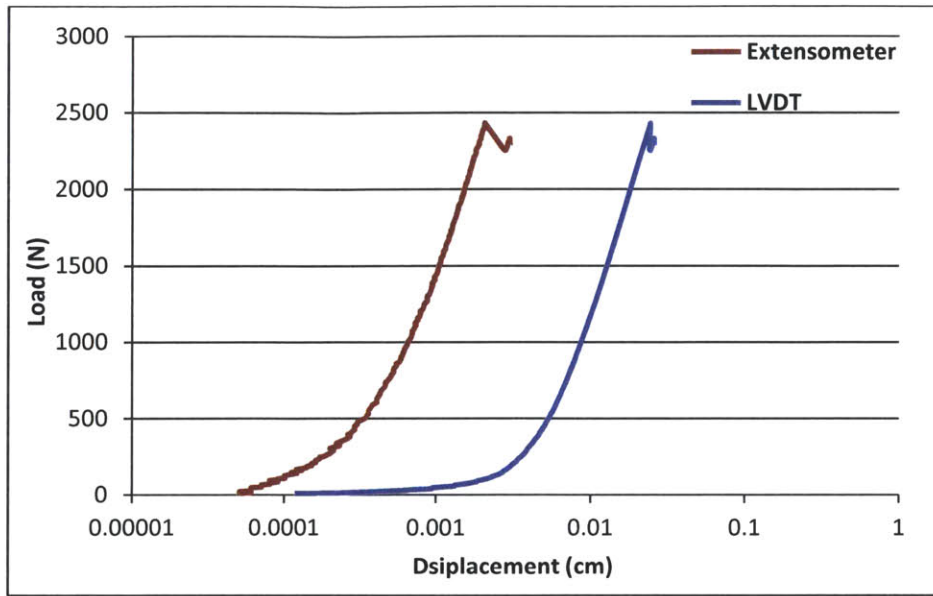
(a)
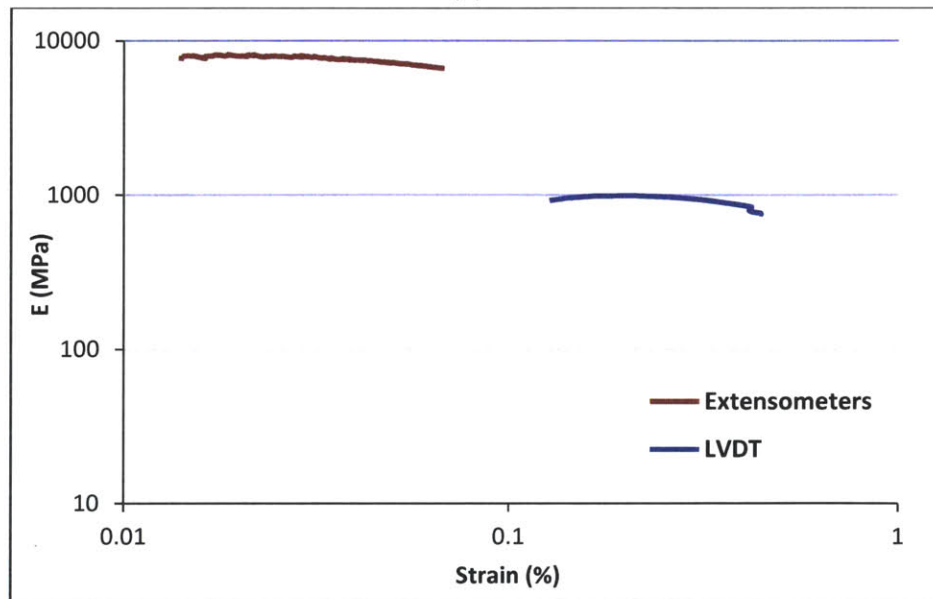
(b)

Figure 5.1: Difference between LVDT and extensometers measurements; (a) Load - displacement (b) Modulus of Elasticity - Strain
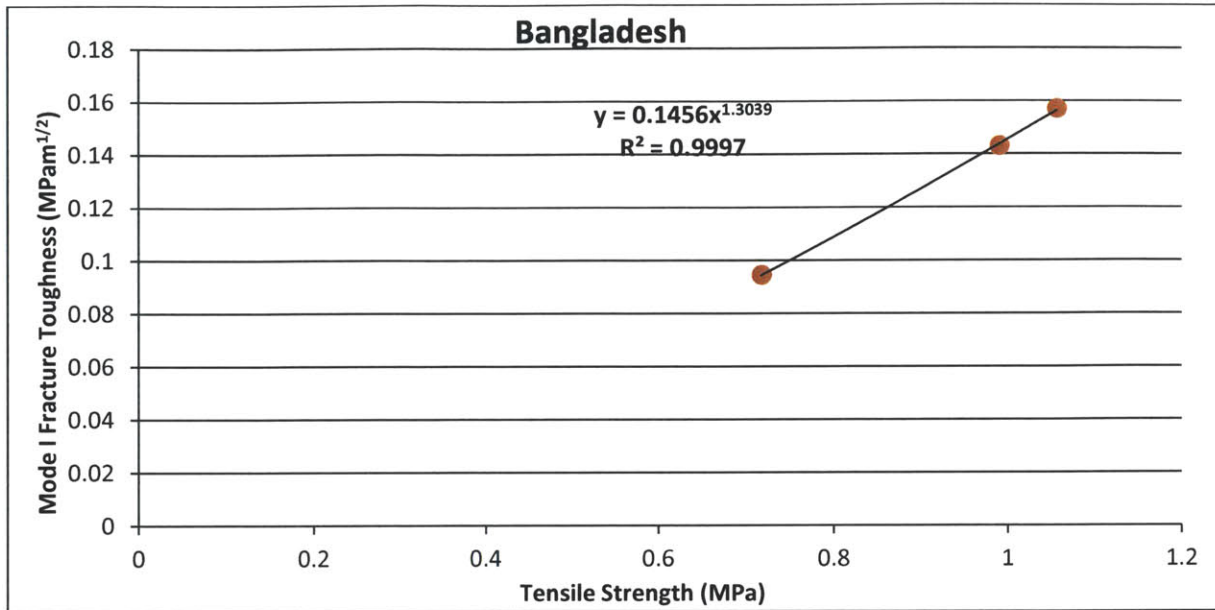
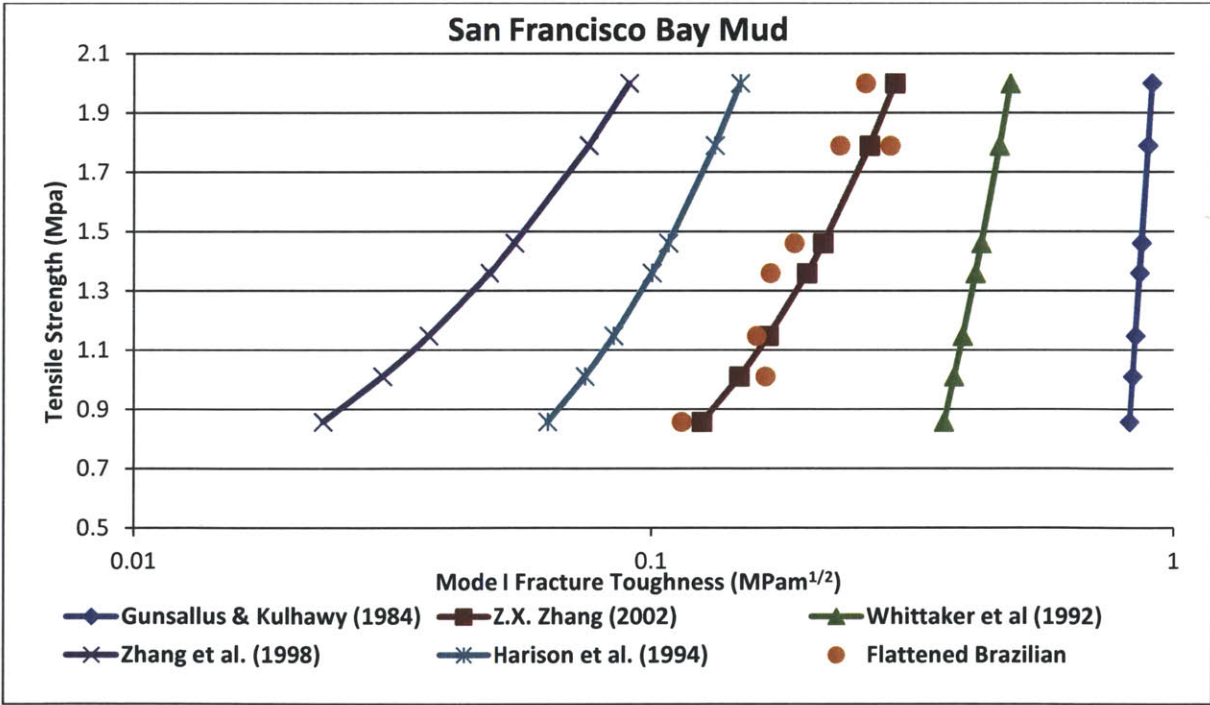**Figure 5.2: Relation between Mode I fracture toughness and tensile strength of Bangladesh Clay.**
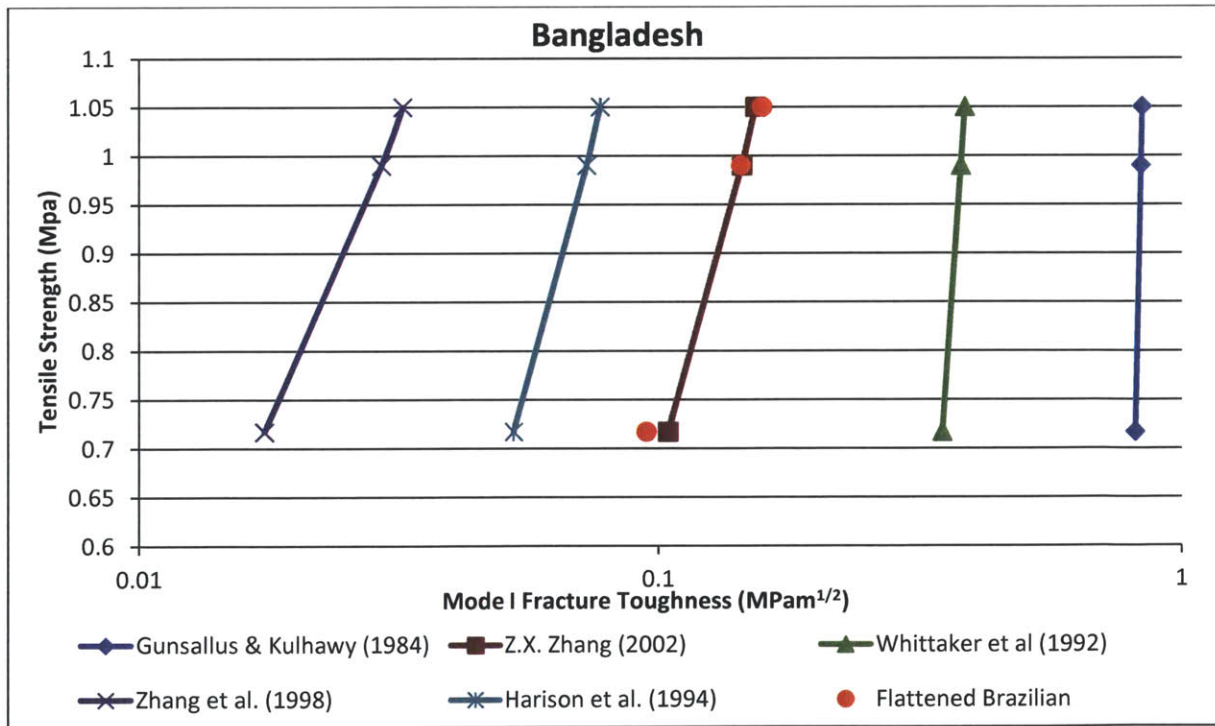
Figure 5.3: Comparing Bangladesh Clay experimental results with back-calculated K_{IC} values using tensile strength dependent literature correlations.
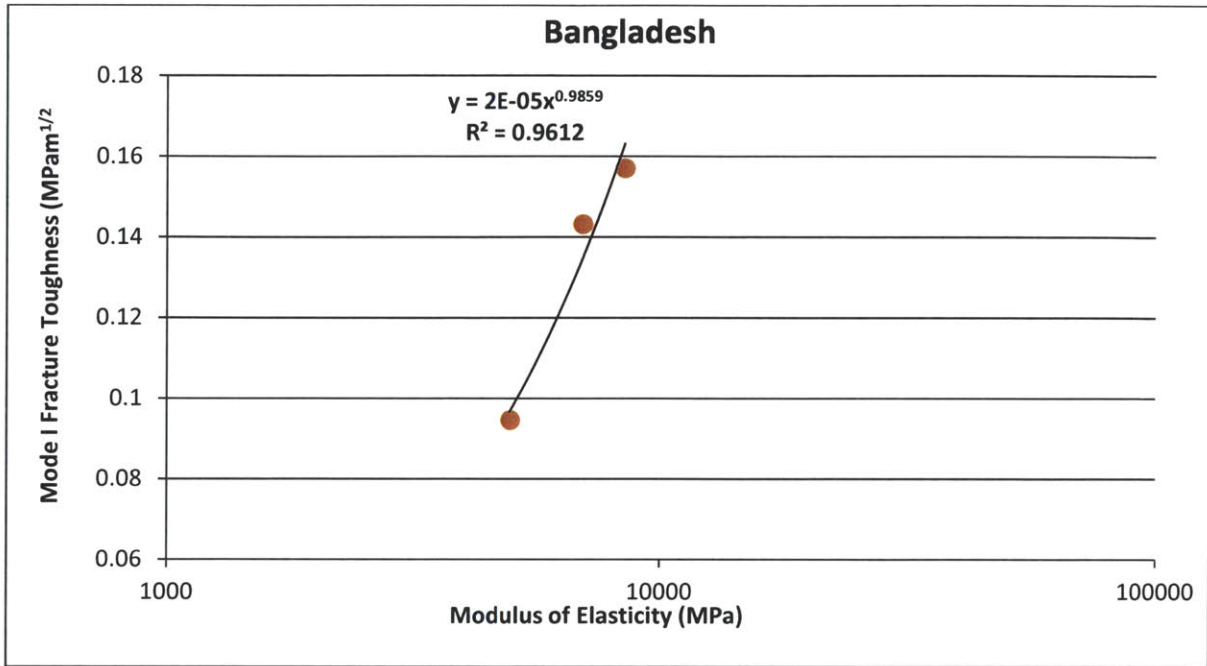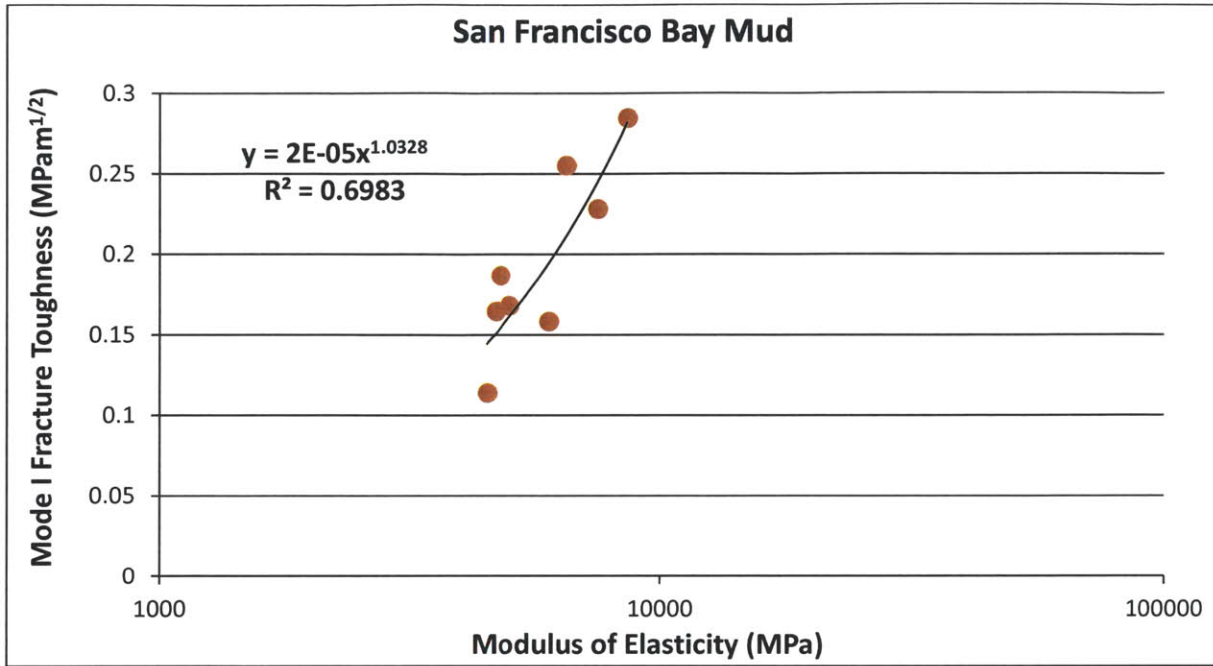
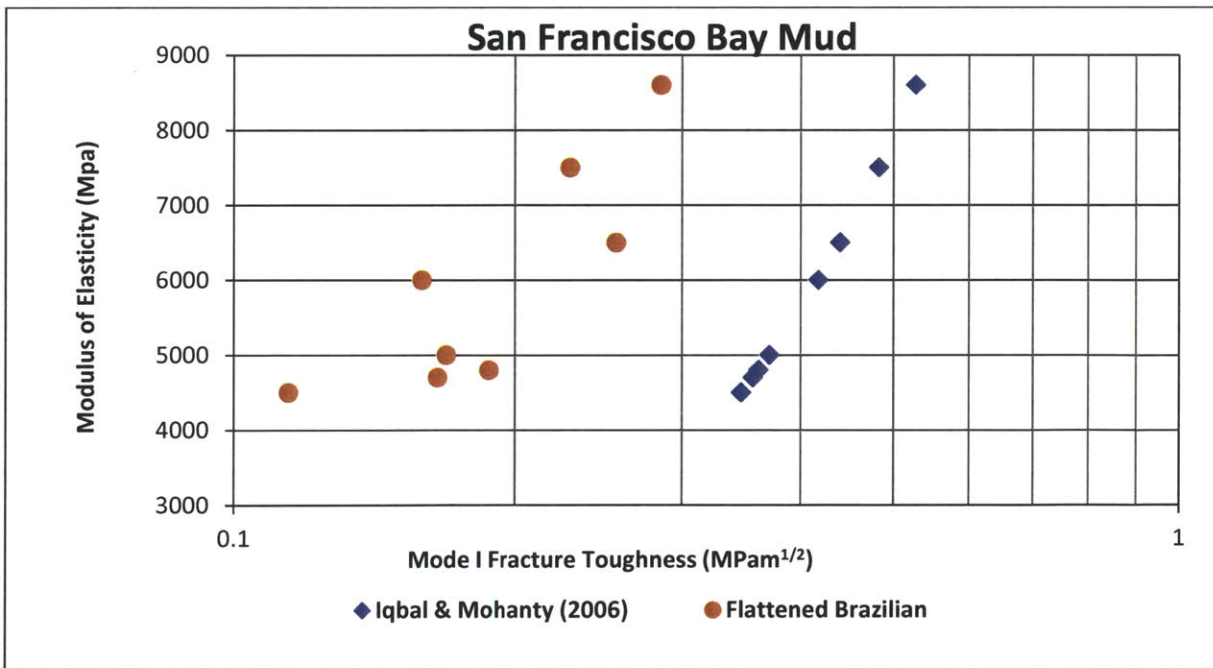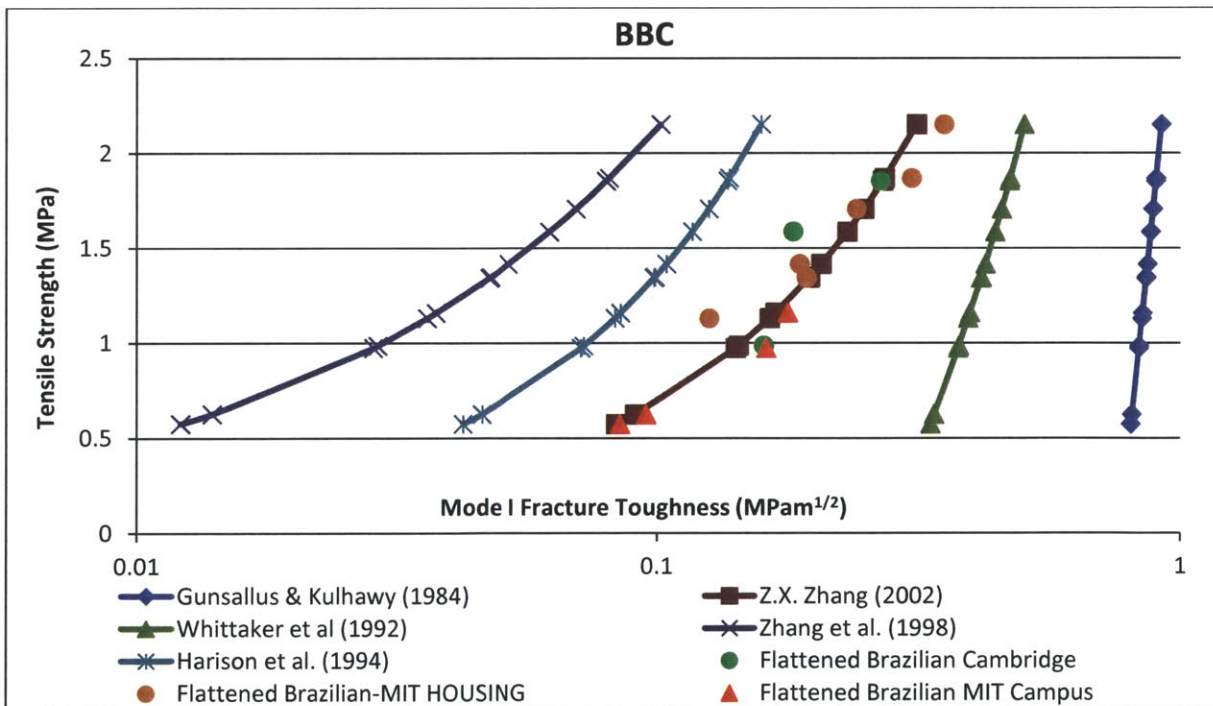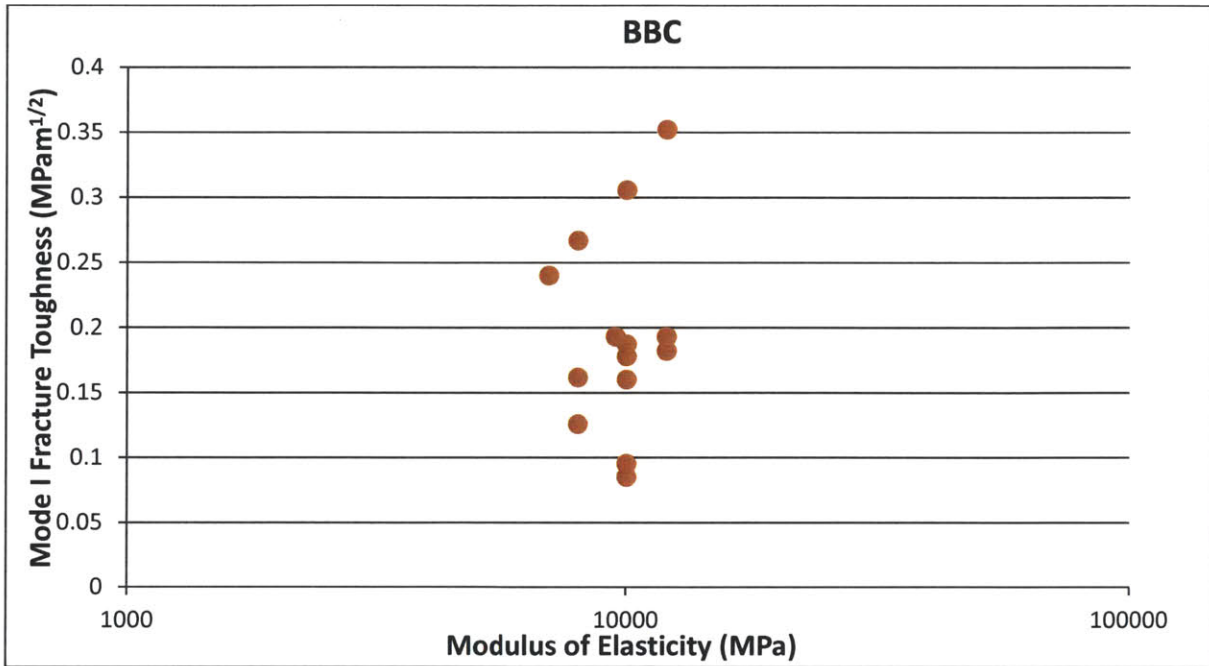**Figure 5.4: Relation between Mode I fracture toughness and modulus of elasticity of Bangladesh Clay.**
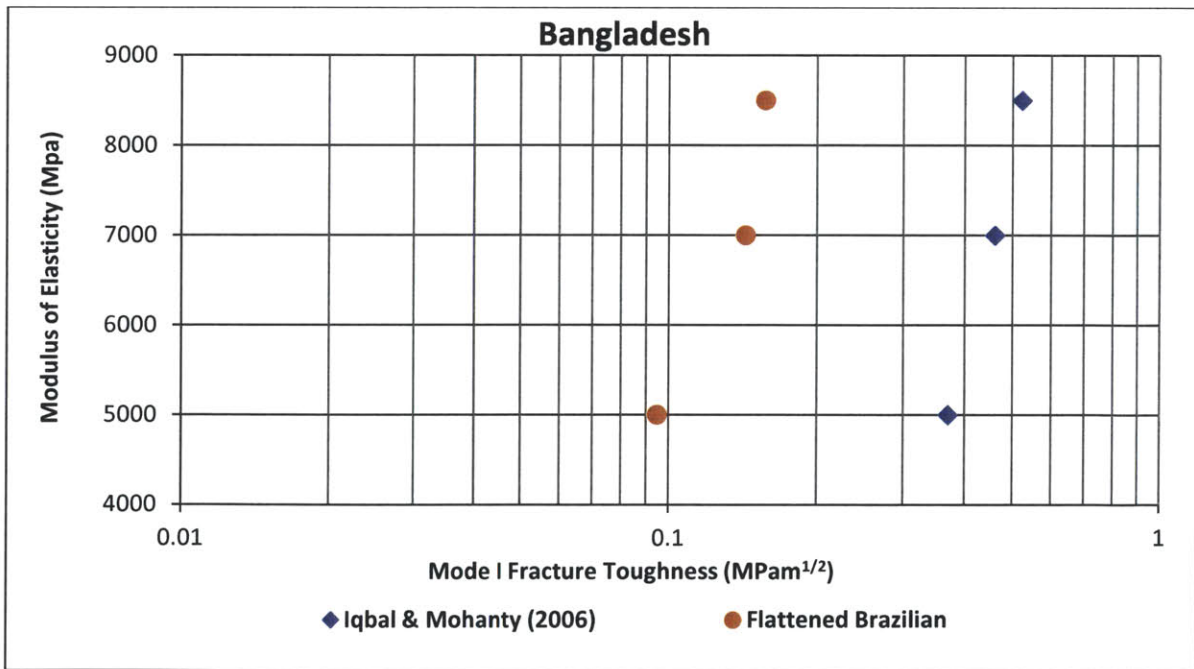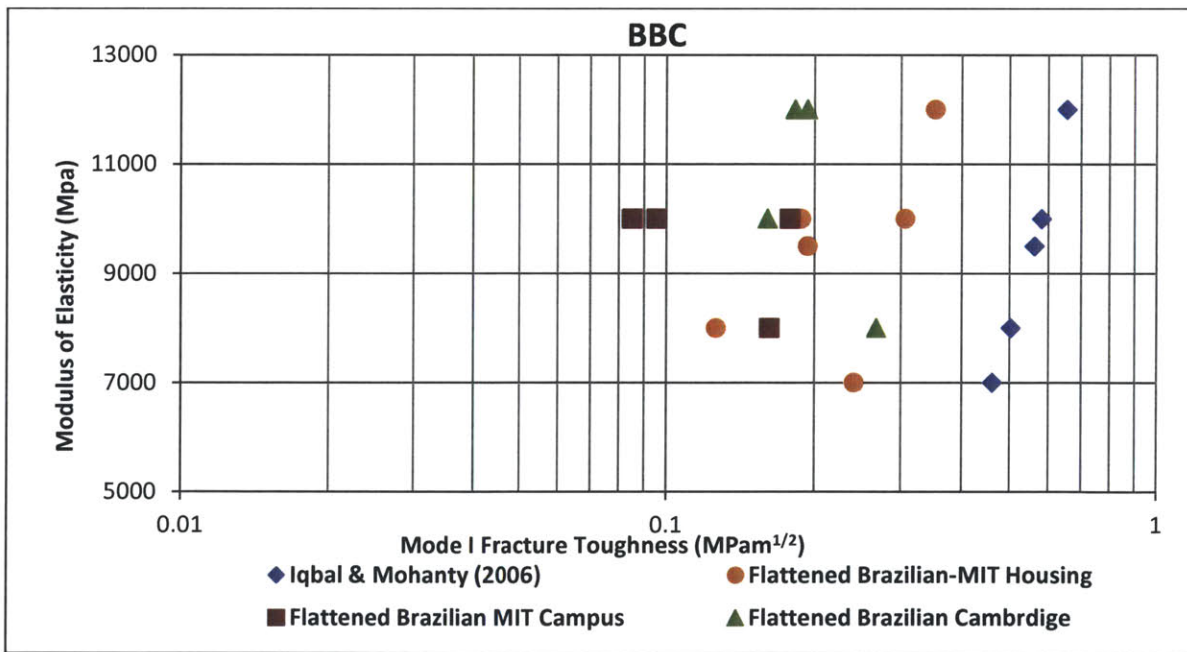

Figure 5.5: Comparing Bangladesh Clay experimental results with back-calculated K_{IC} values using modulus of elasticity dependent literature correlations.
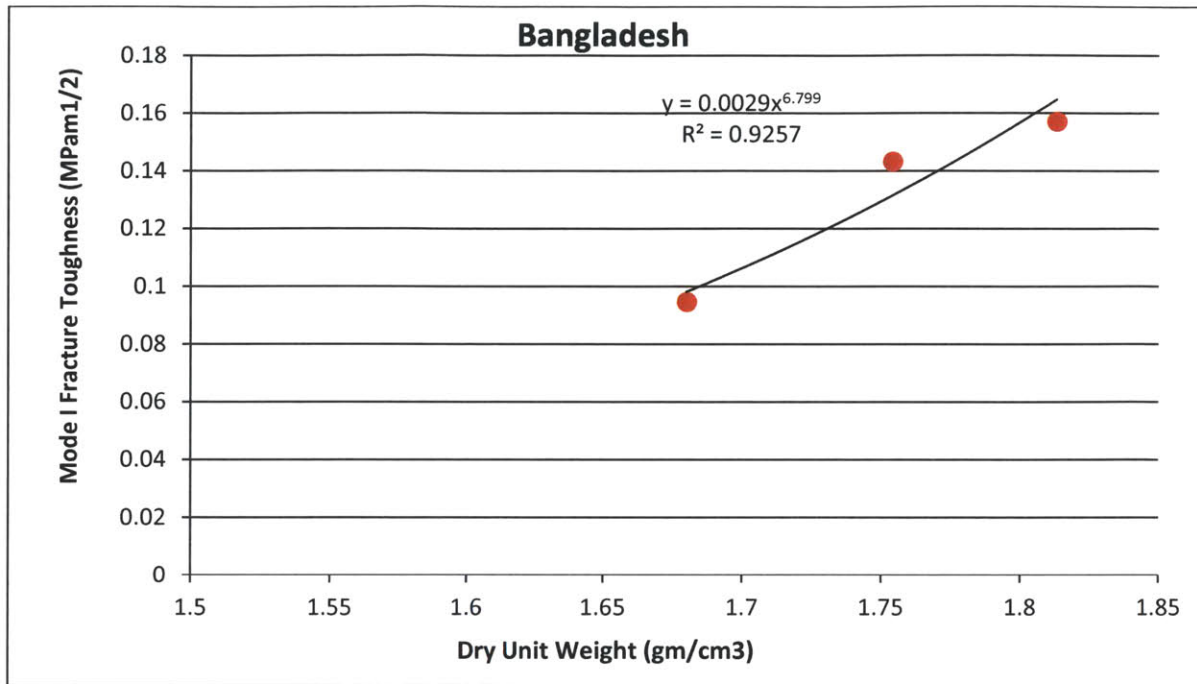
Figure 5.6: Relation between Mode I fracture toughness and dry unit weight of Bangladesh Clay.
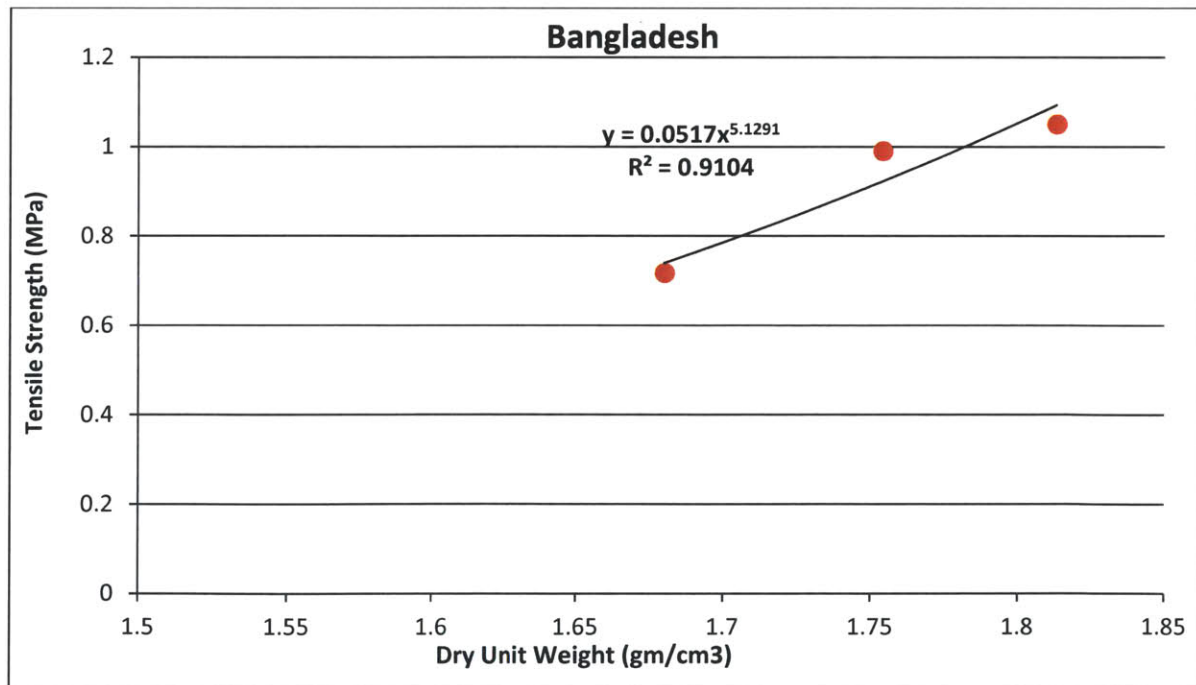
Figure 5.7: Relation between tensile strength and dry unit weight of Bangladesh Clay.
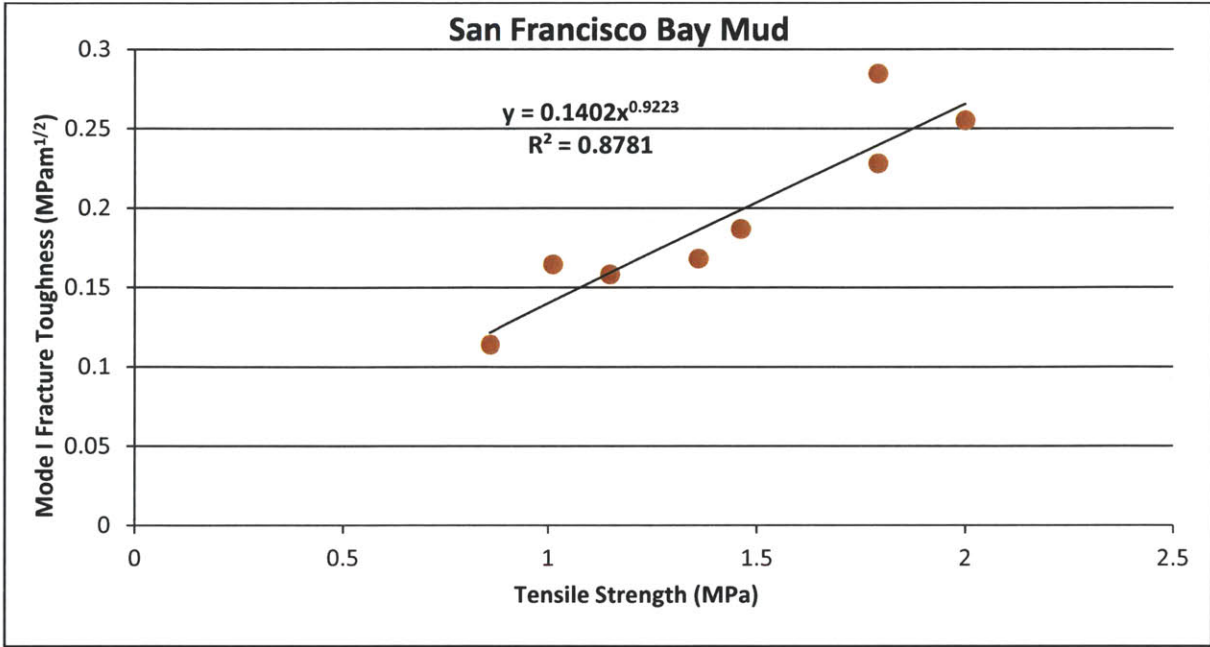
Figure 5.8: Relation between Mode I fracture toughness and tensile strength of San Francisco Bay Mud.

Figure 5.9: Comparing San Francisco Bay Mud experimental results with back-calculated K_{IC} values using tensile strength dependent literature correlations.

Figure 5.10: Relation between Mode I fracture toughness and modulus of elasticity of San Francisco Bay Mud.

Figure 5.11: Comparing San Francisco Bay Mud experimental results with back-calculated K_{IC} values using modulus of elasticity dependent literature correlations.
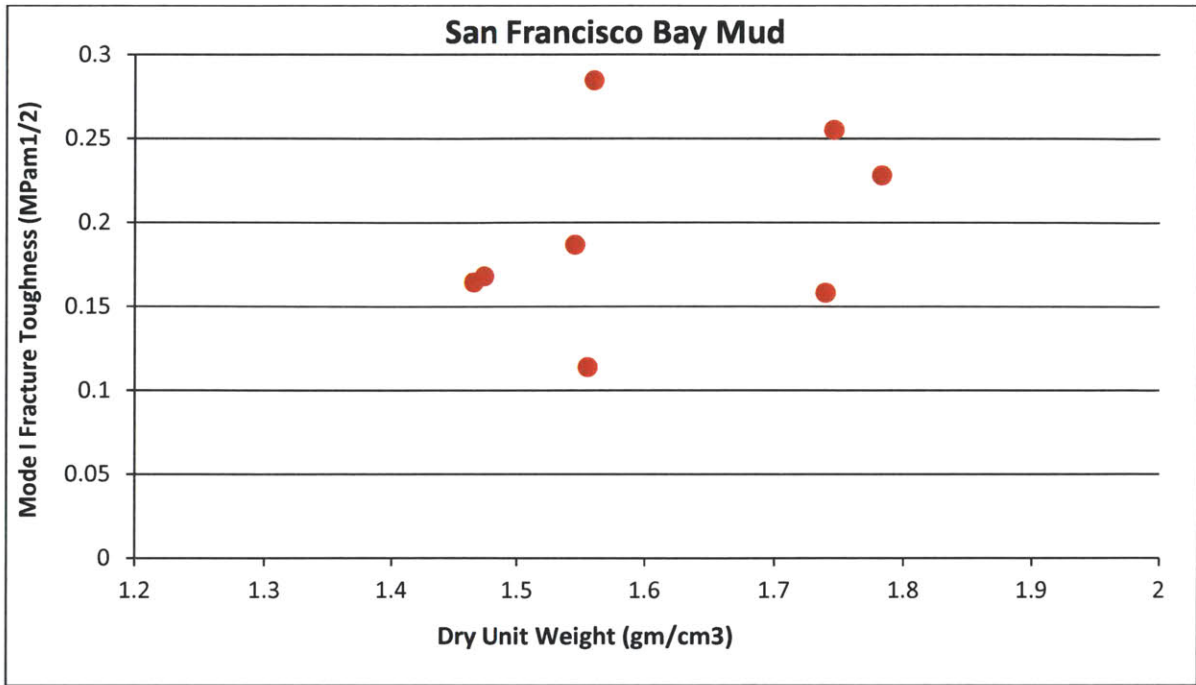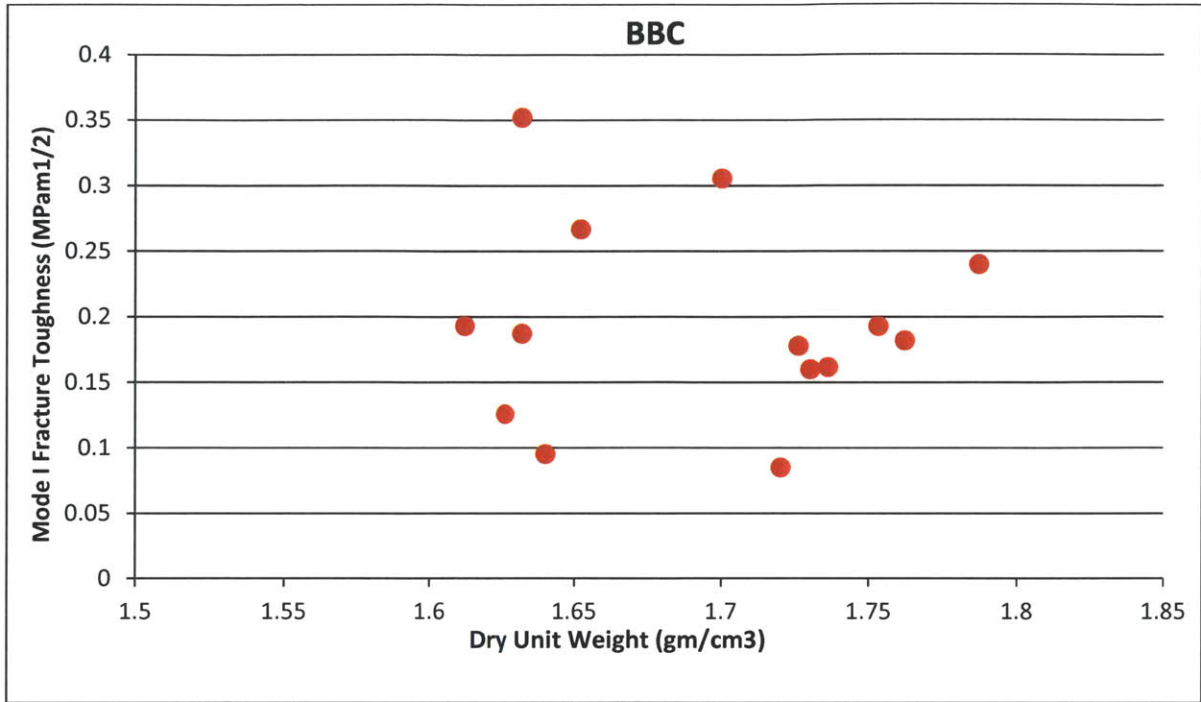
Figure 5.12: Relation between Mode I fracture toughness and dry unit weight of San Francisco Bay Mud.
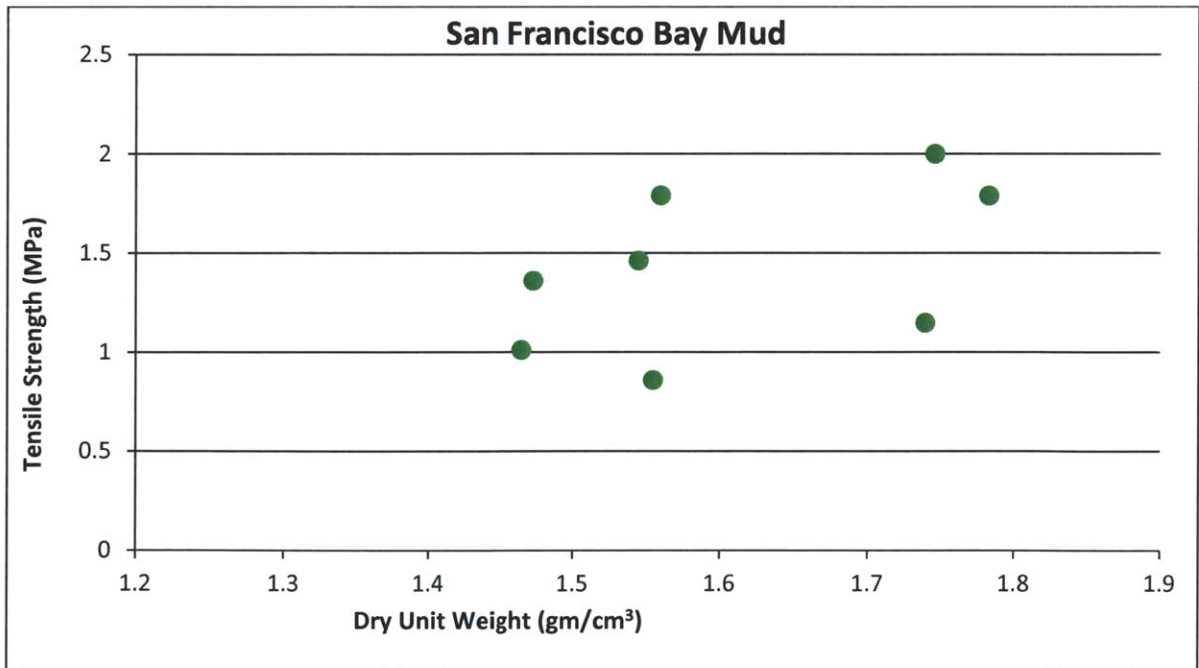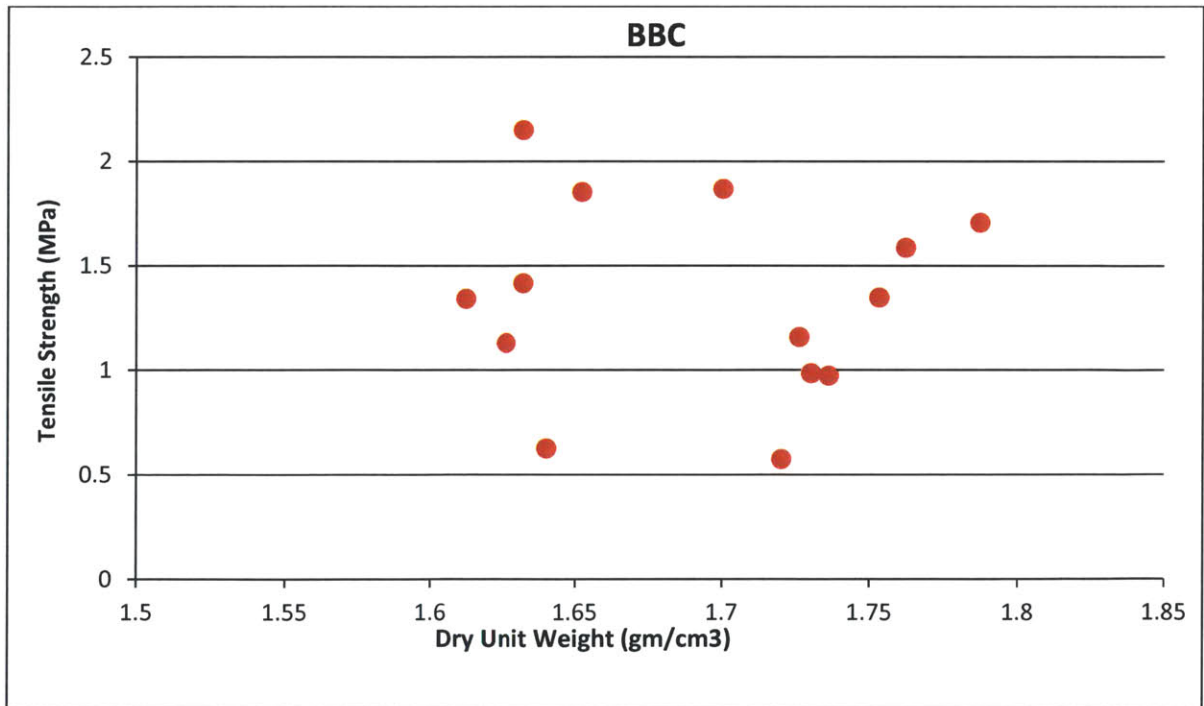

Figure 5.13: Relation between tensile strength and dry unit weight of San Francisco Bay Mud.
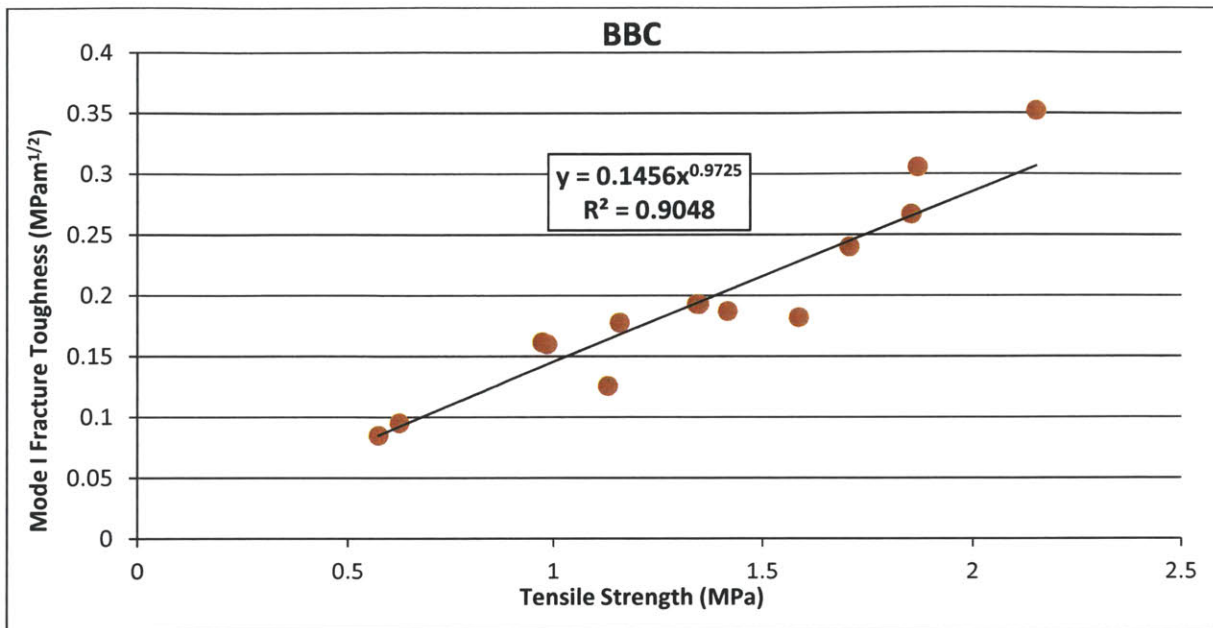
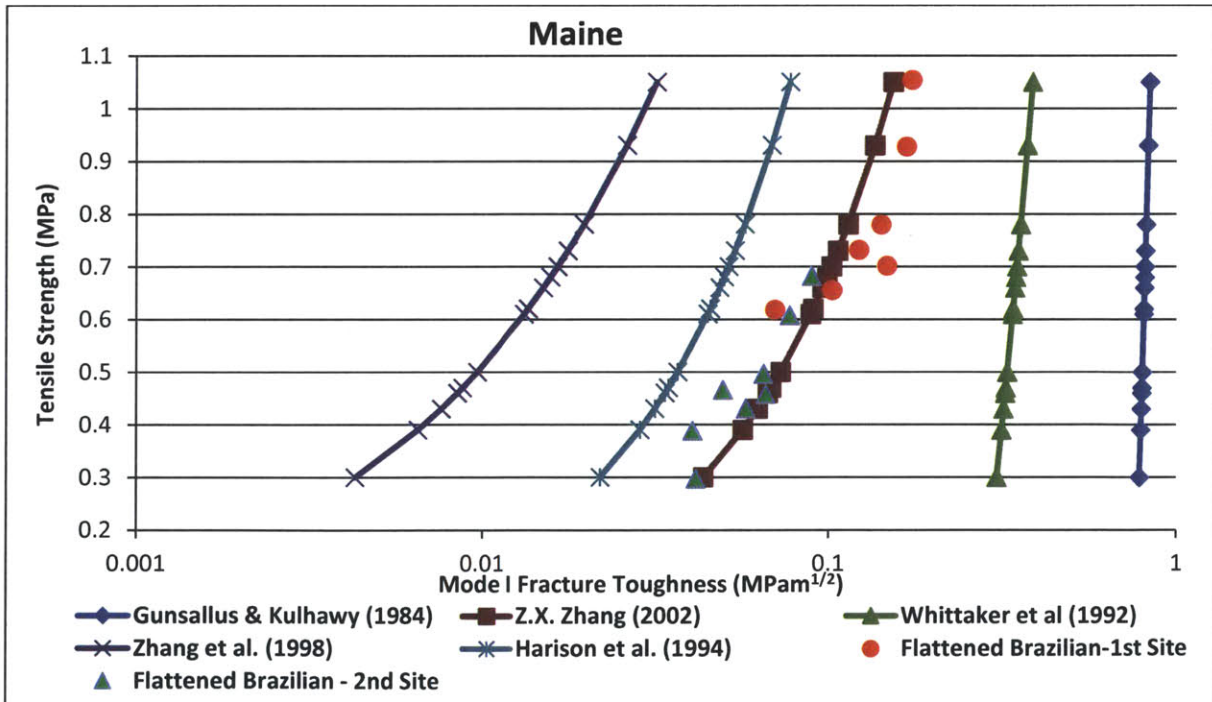**Figure 5.14: Relation between Mode I fracture toughness and tensile strength of natural Boston Blue Clay.**

Figure 5.15: Comparing Boston Blue Clay experimental results with back-calculated K_{IC} values using tensile strength dependent literature correlations.

Figure 5.16: Relation between Mode I fracture toughness and modulus of elasticity of Boston Blue Clay.

Figure 5.17: Comparing Boston Blue Clay experimental results with back-calculated K_{IC} values using modulus of elasticity dependent literature correlations.

Figure 5.18: Relation between Mode I fracture toughness and dry unit weight of Boston Blue Clay.

Figure 5.19: Relation between tensile strength and dry unit weight of Boston Blue Clay.

215
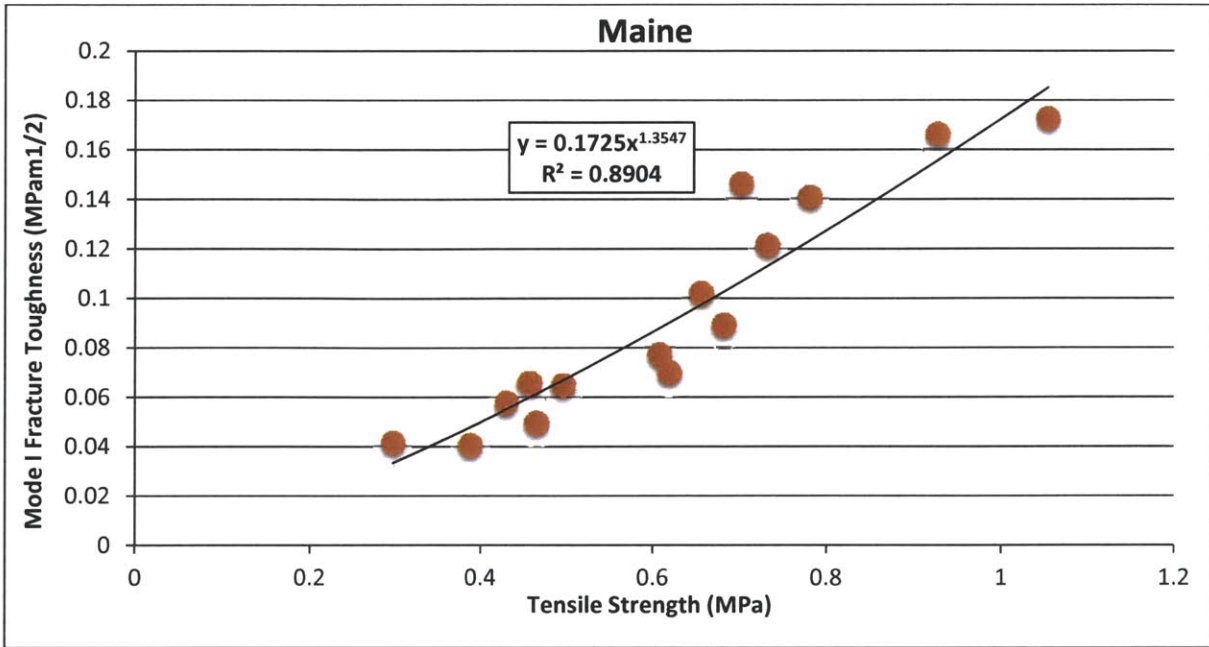
Figure 5.20: Relation between Mode I fracture toughness and tensile strength of Presumpscot Maine Clay.

Figure 5.21: Comparing Presumpscot Maine Clay experimental results with back-calculated K_{IC} values using tensile strength dependent literature correlations.
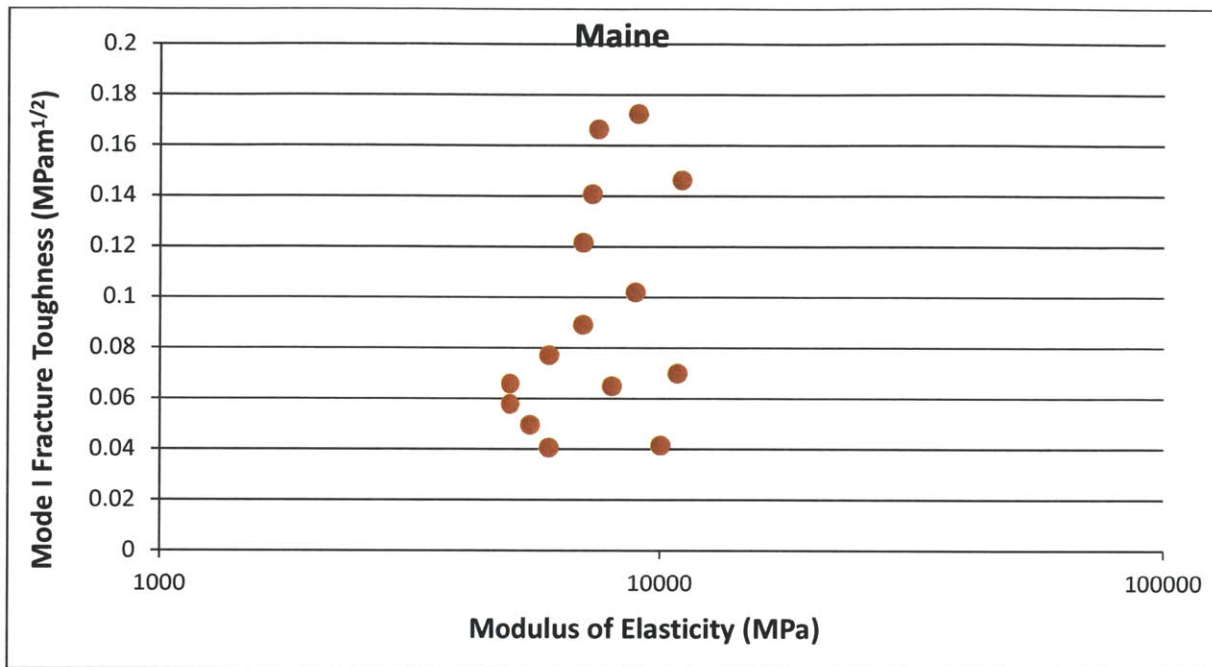
Figure 5.22: Relation between Mode I fracture toughness and modulus of elasticity of Presumpscot Maine Clay.
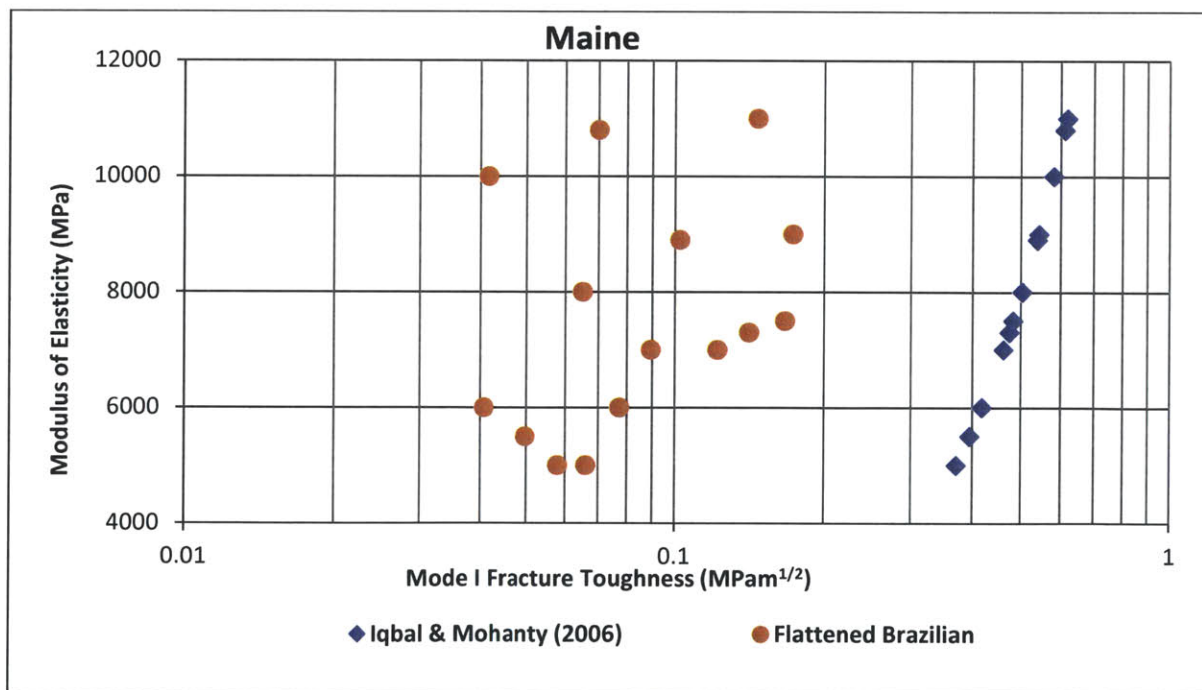

Figure 5.23: Comparing Presumpscot Maine Clay experimental results with back-calculated K_{IC} values using modulus of elasticity dependent literature correlations.
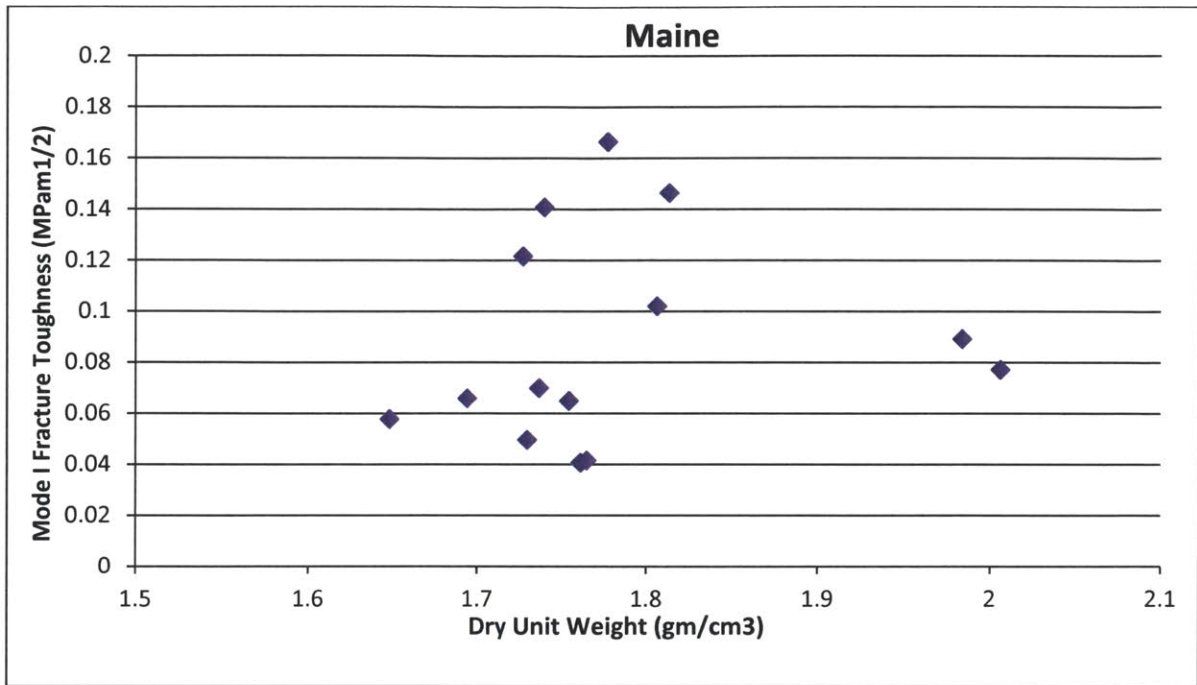
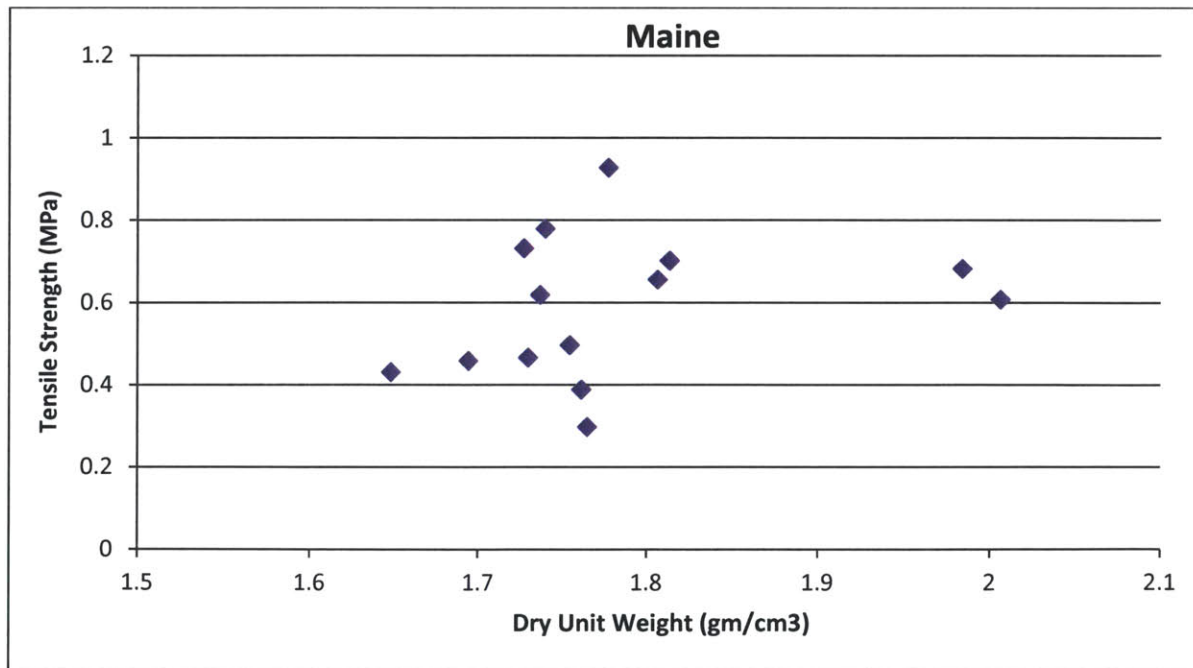**Figure 5.24: Relation between Mode I fracture toughness and dry unit weight of Presumpscot Maine Clay.**

Figure 5.25: Relation between tensile strength and dry unit weight of Presumpscot Maine Clay.
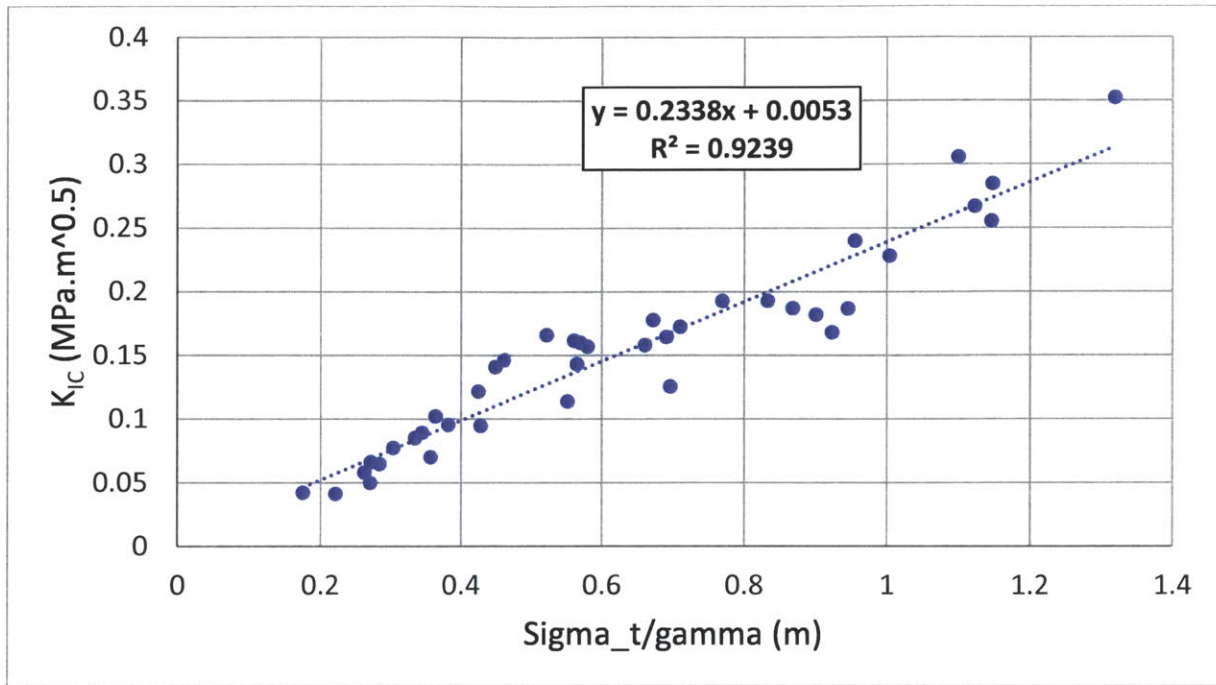
Figure 5.26: Linear relation between K_{IC} and (tensile strength/ unit weight) for the four tested natural soils.
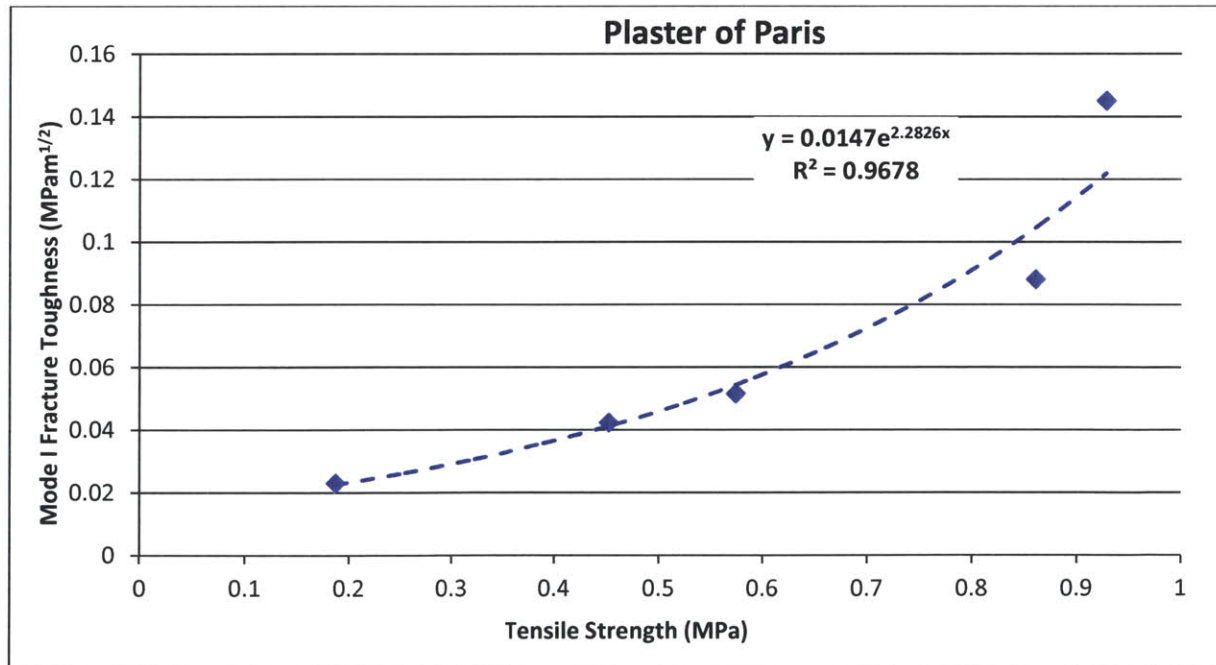

Figure 5.27: Relation between Mode I fracture toughness and tensile strength of Plaster of Paris.
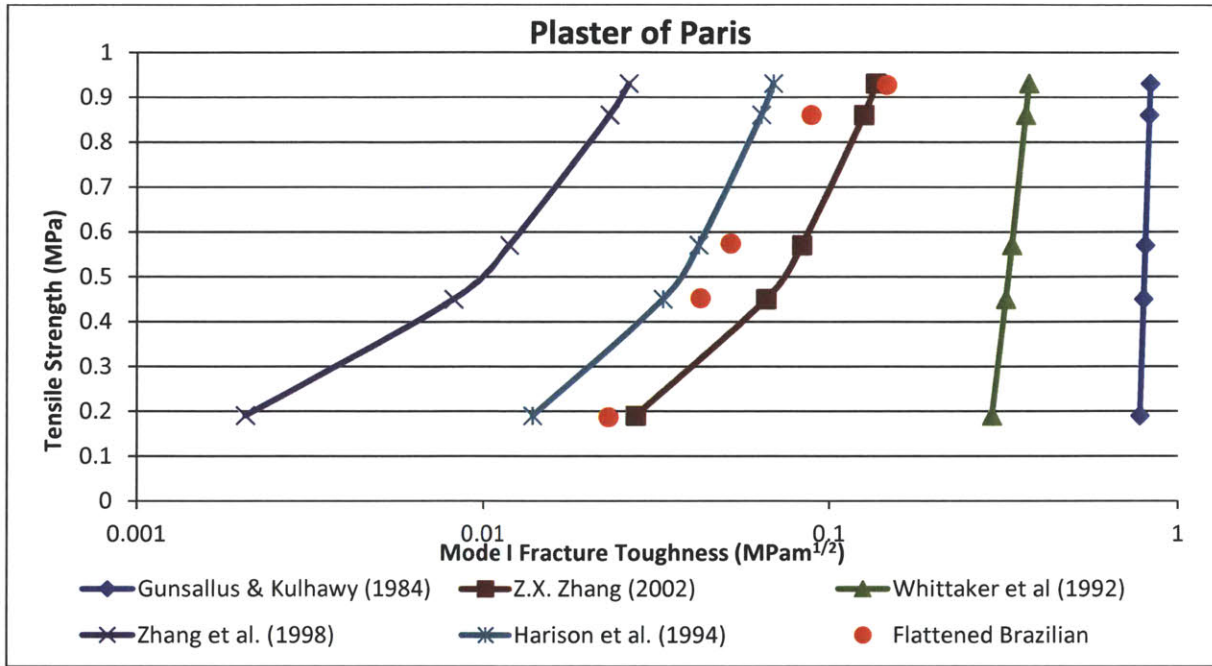
Figure 5.28: Comparing Plaster of Paris experimental results with back-calculated K_{IC} values using tensile strength dependent literature correlations.
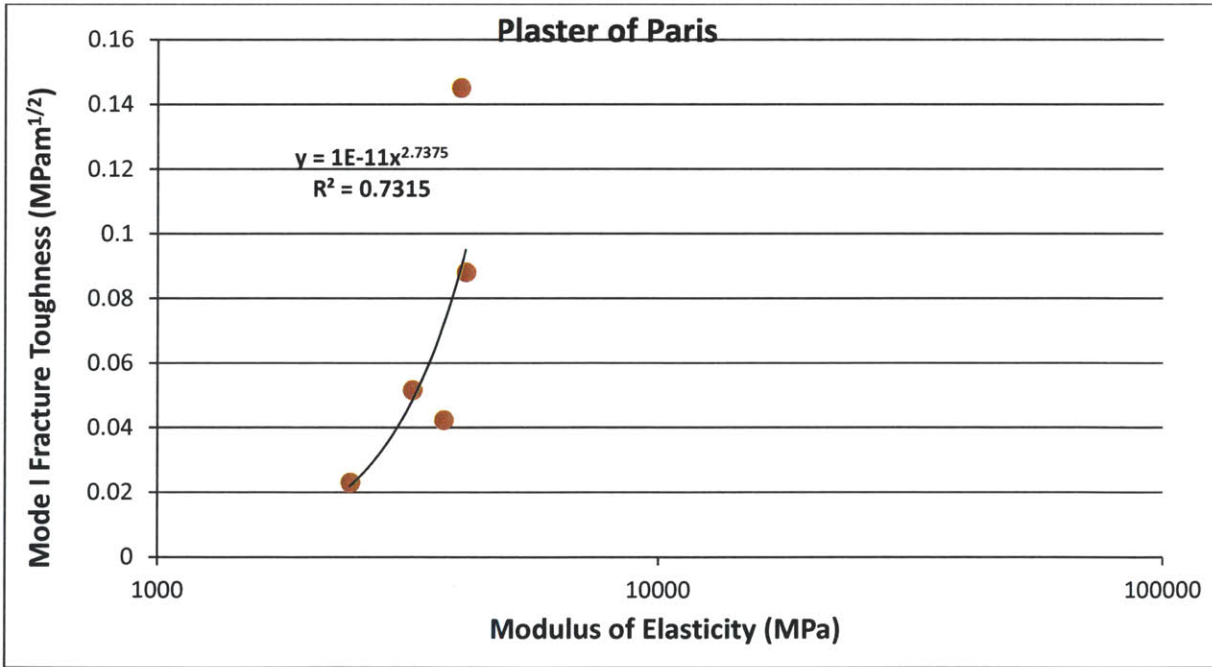

Figure 5.29: Relation between Mode I fracture toughness and modulus of elasticity of Plaster of Paris

Figure 5.30: Comparing Plaster of Paris experimental results with back-calculated K$_{IC}$ values using modulus of elasticity dependent literature correlations.

Figure 5.31: Relation between Mode I fracture toughness and dry unit weight of Plaster of Paris

Figure 5.32: Relation between tensile strength and dry unit weight of Plaster of Paris
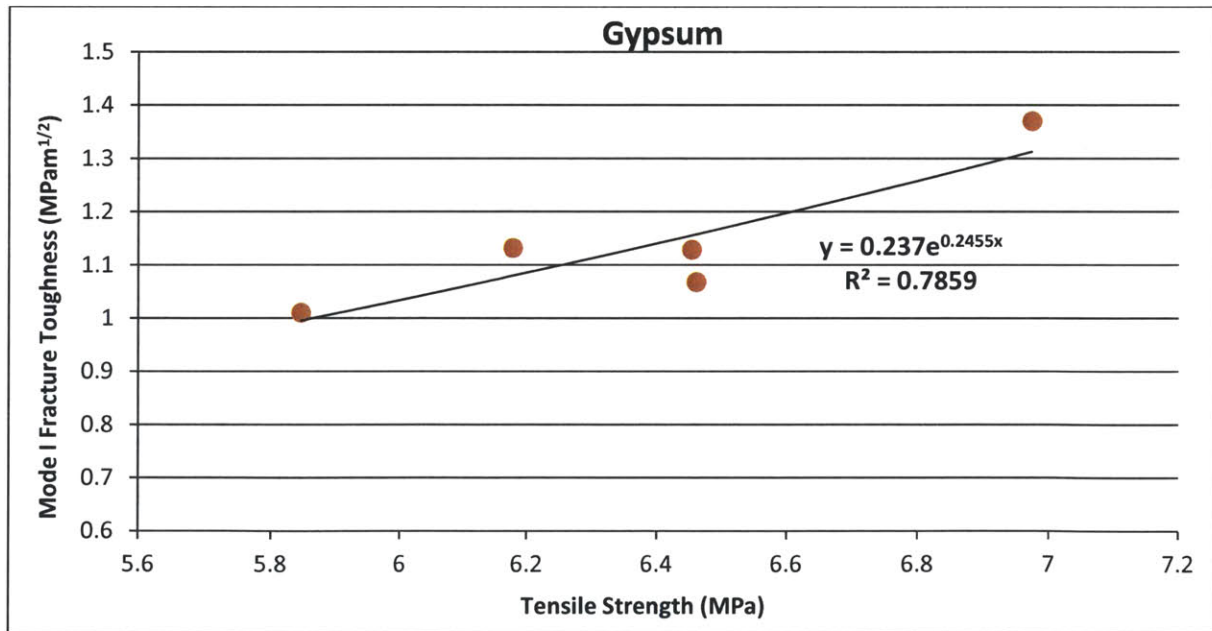
Figure 5.33: Relation between Mode I fracture toughness and tensile strength of Gypsum
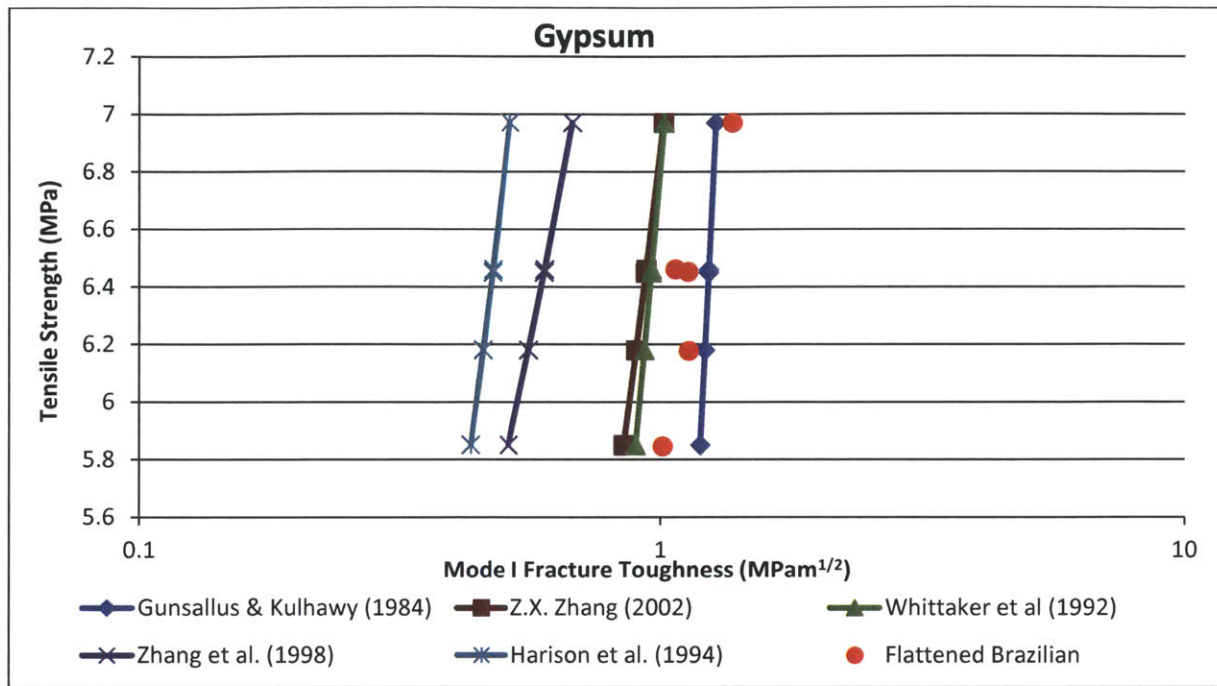
Figure 5.34: Comparing Gypsum experimental results with back-calculated K_{IC} values using tensile strength dependent literature correlations.
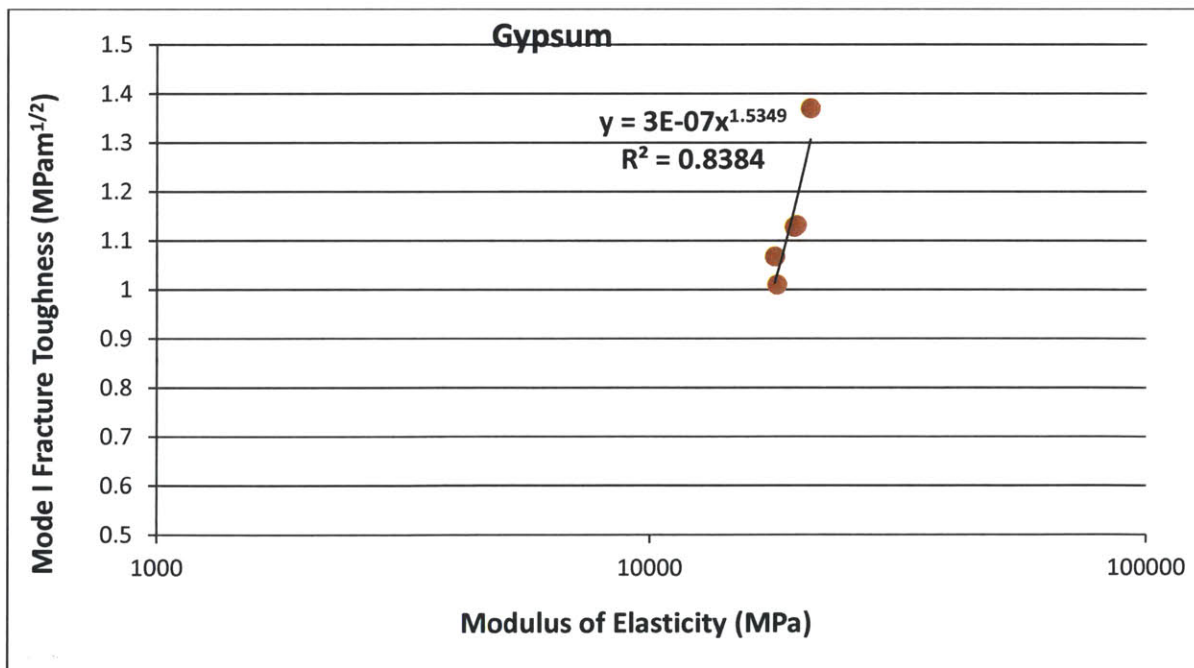
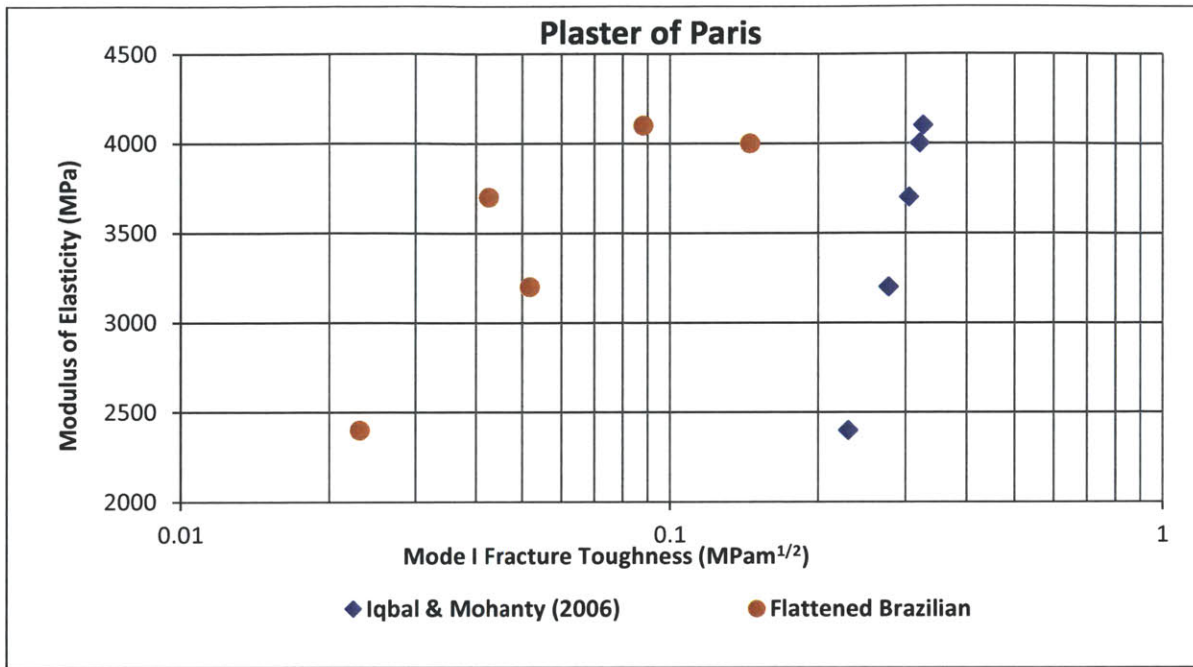**Figure 5.35: Relation between Mode I fracture toughness and modulus of elasticity of Gypsum**
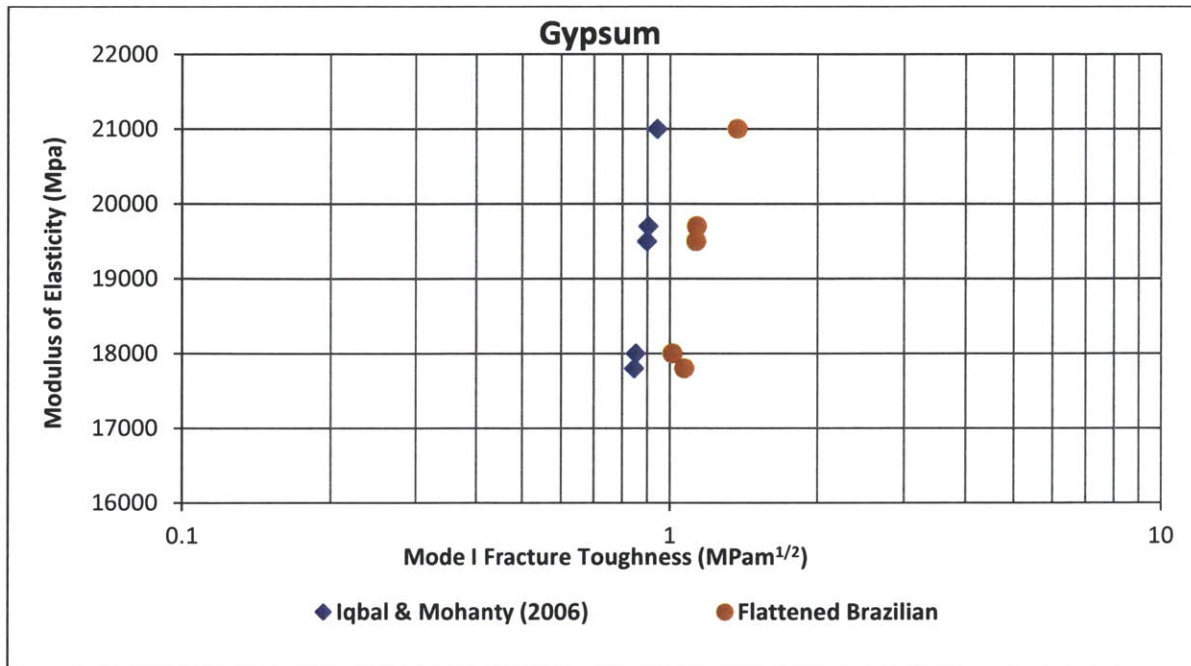
Figure 5.36: Comparing Gypsum experimental results with back-calculated K_{IC} values using modulus of elasticity dependent literature correlations.
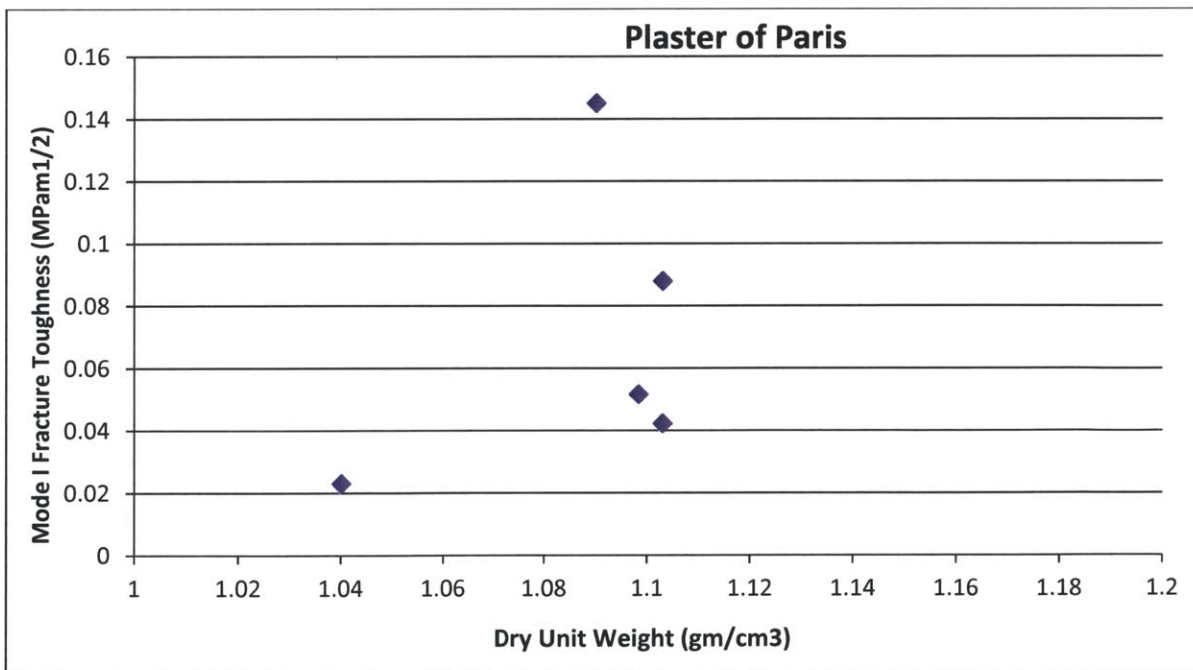

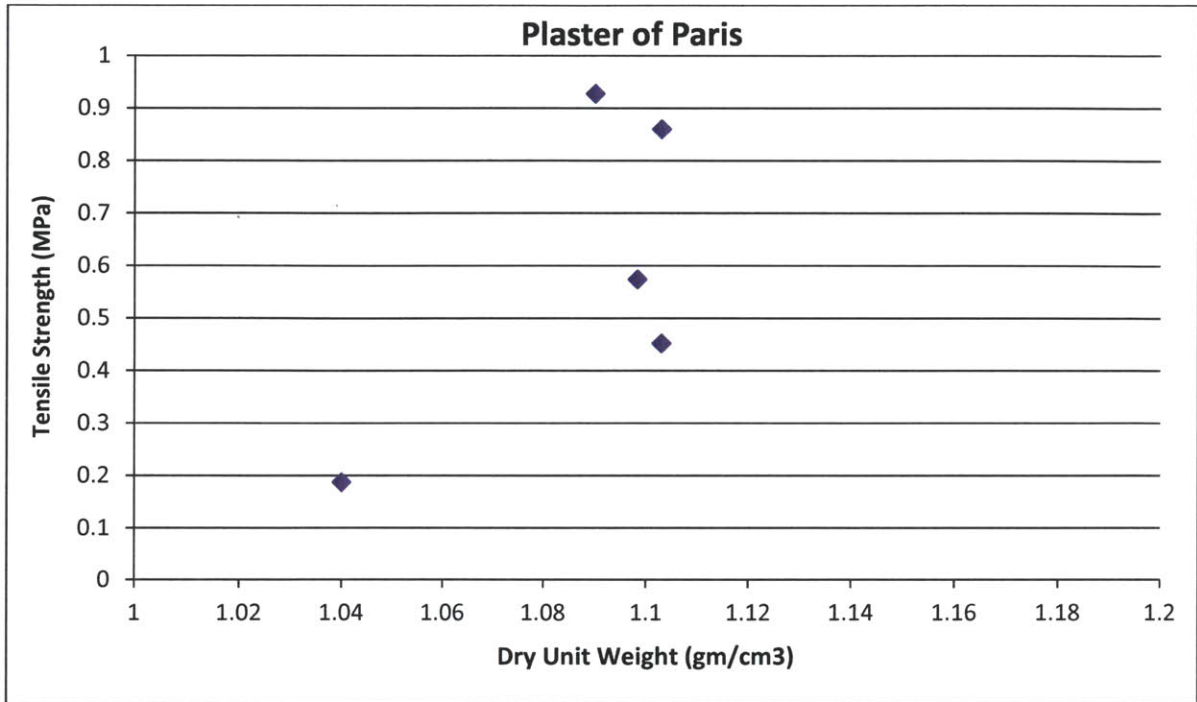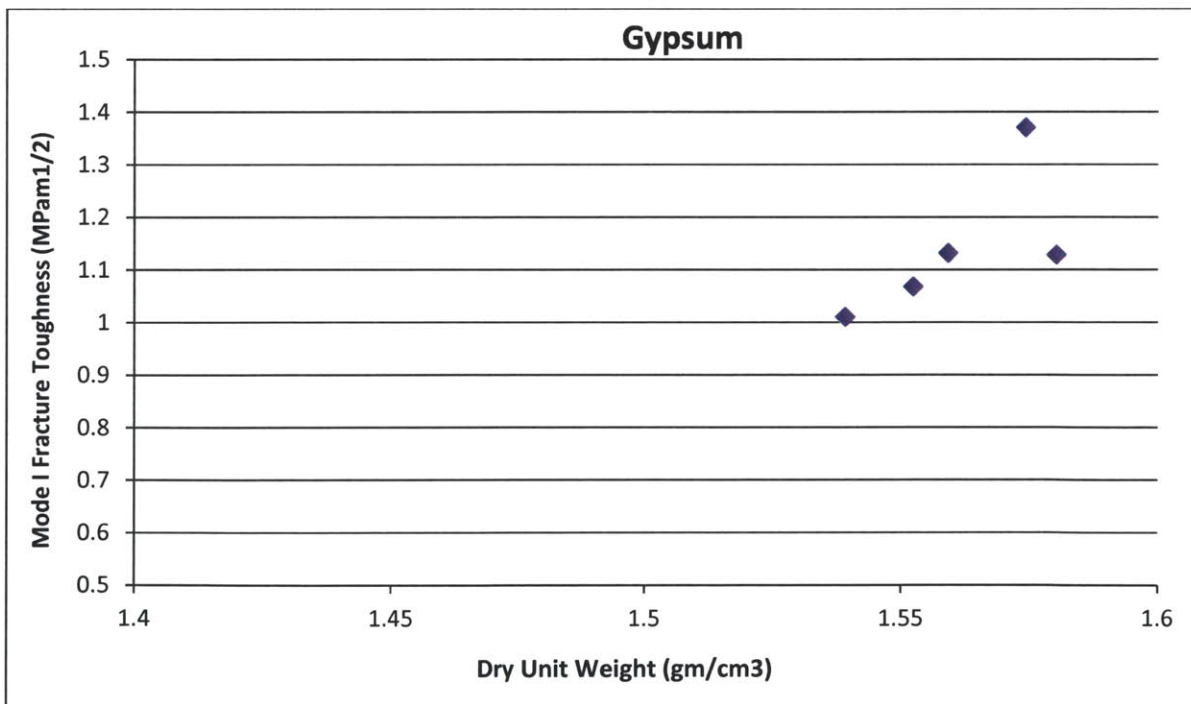**Figure 5.37: Relation between Mode I fracture toughness and dry unit weight of Gypsum**
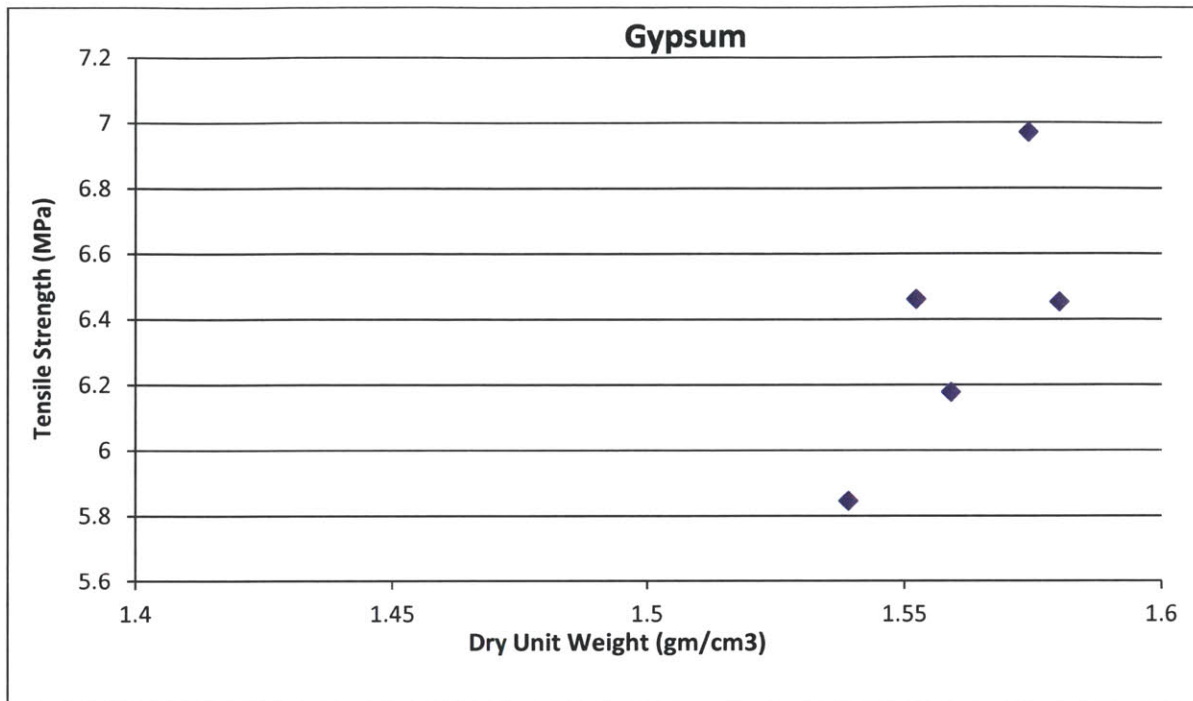
Figure 5.38: Relation between tensile strength and dry unit weight of Gypsum
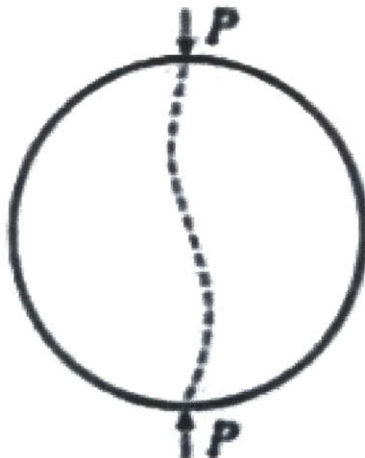
Figure 5.39: Solid Brazilian Disc behavior (Hai-yong et al., 2004)
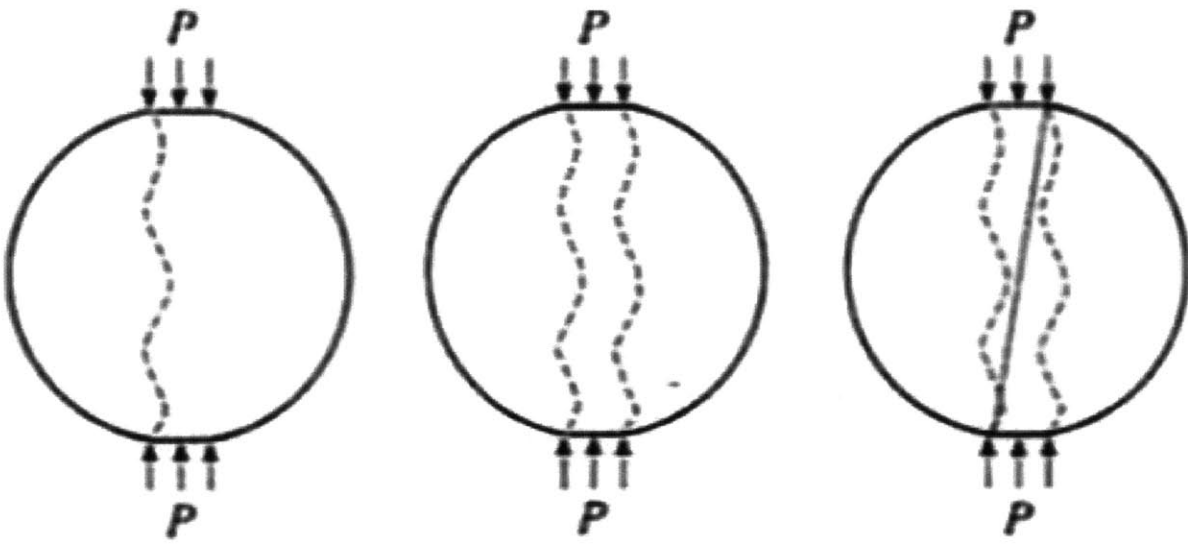
Figure 5.40: Process of flattened Brazilian disc failure with loading angle 20° (Hai-yong et al., 2004)
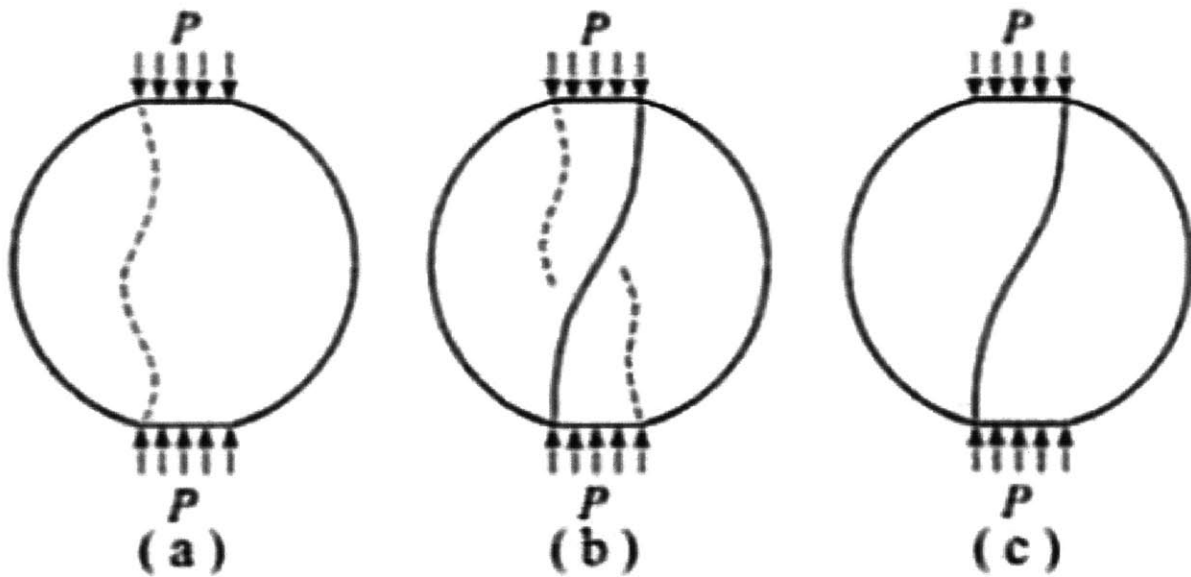
Figure 5.41: Three processes of flattened Brazilian disc failure with loading angle 30° (Hai-yong et al., 2004)
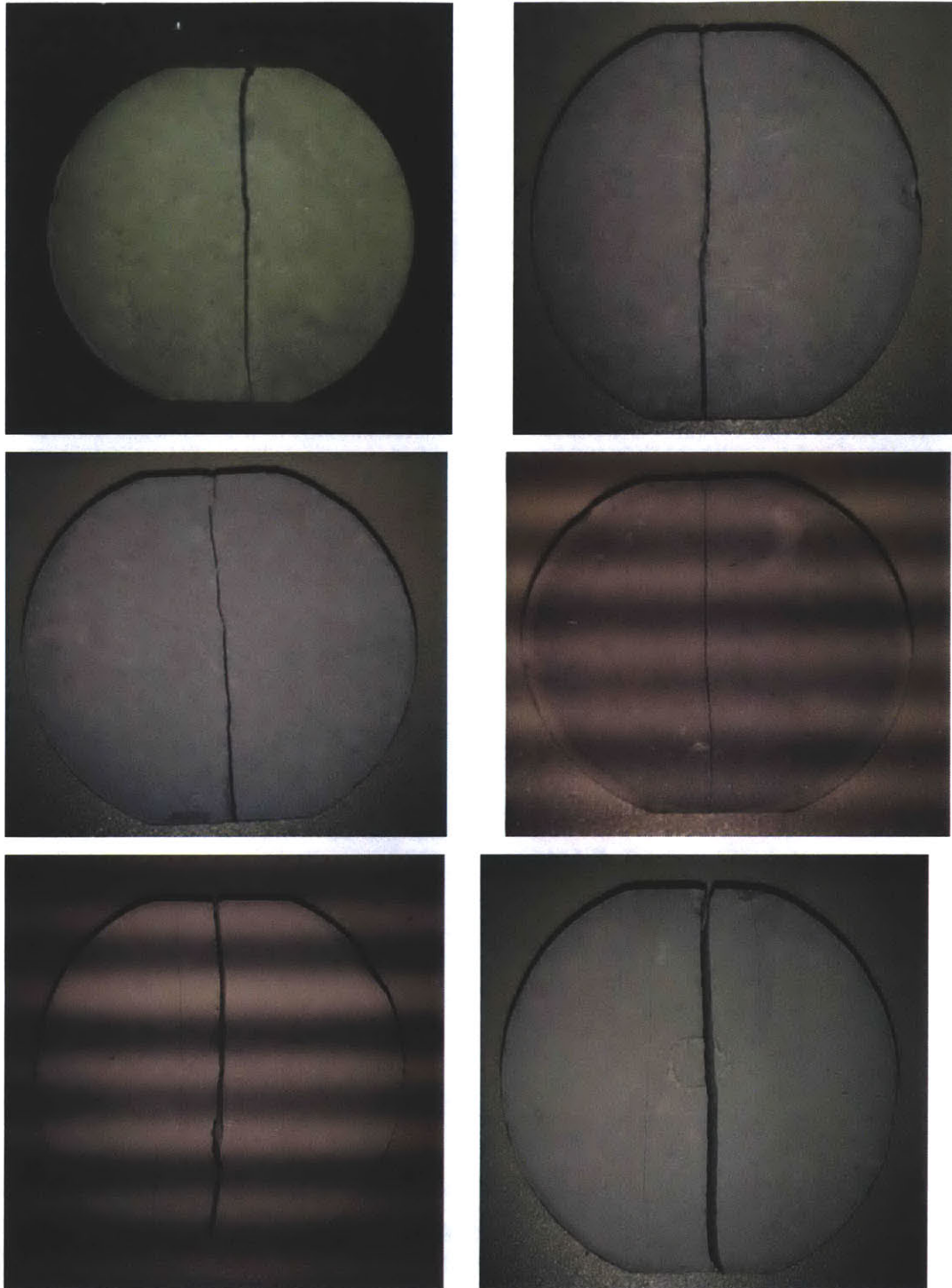
Figure 5.42: Center crack initiation in the middle of fractured flattened Brazilian discs
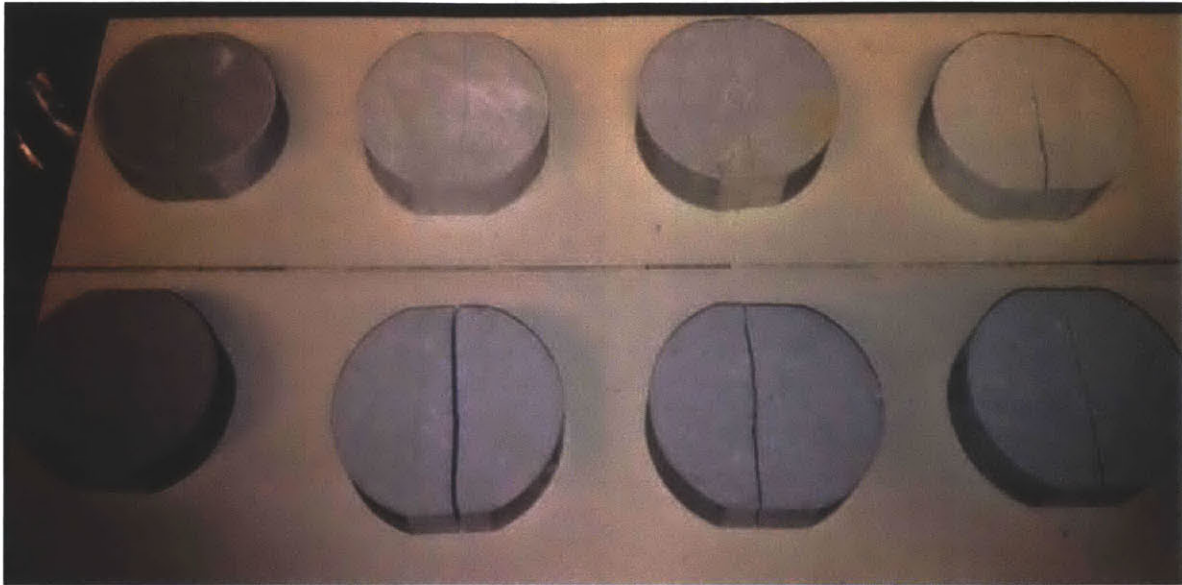
Figure 5.43: Failure pattern of fractured flattened Brazilian disc specimens
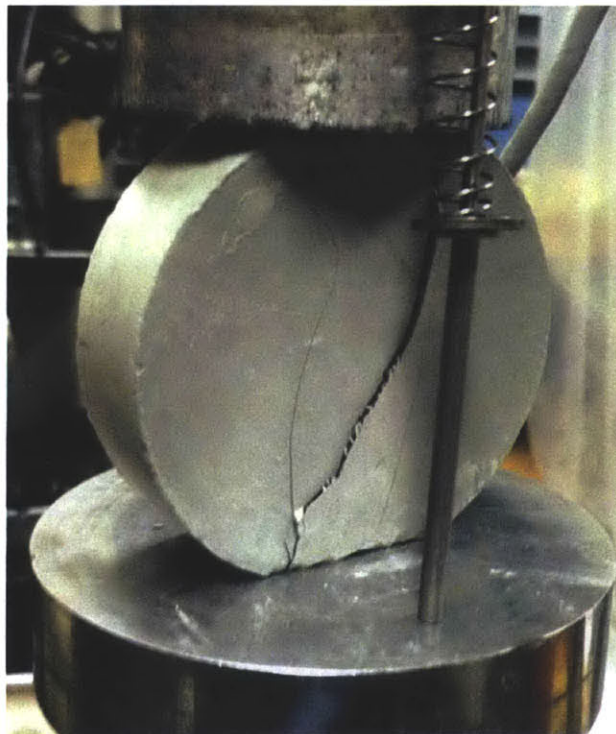
Figure 5.44: Failure pattern for fractured flattened Brazilian discs showing diagonal fracturing
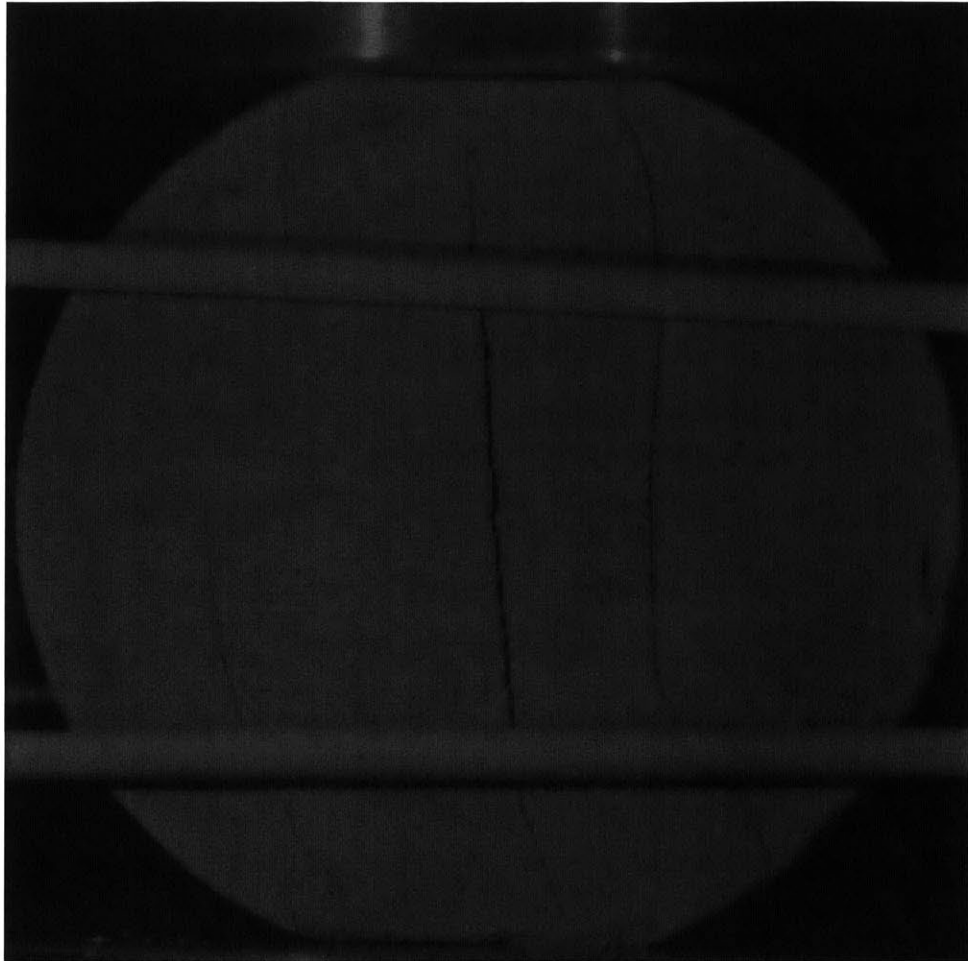
Figure 5.45: Failure pattern for fractured flattened Brazilian discs showing diagonal fracturing after center crack initiation
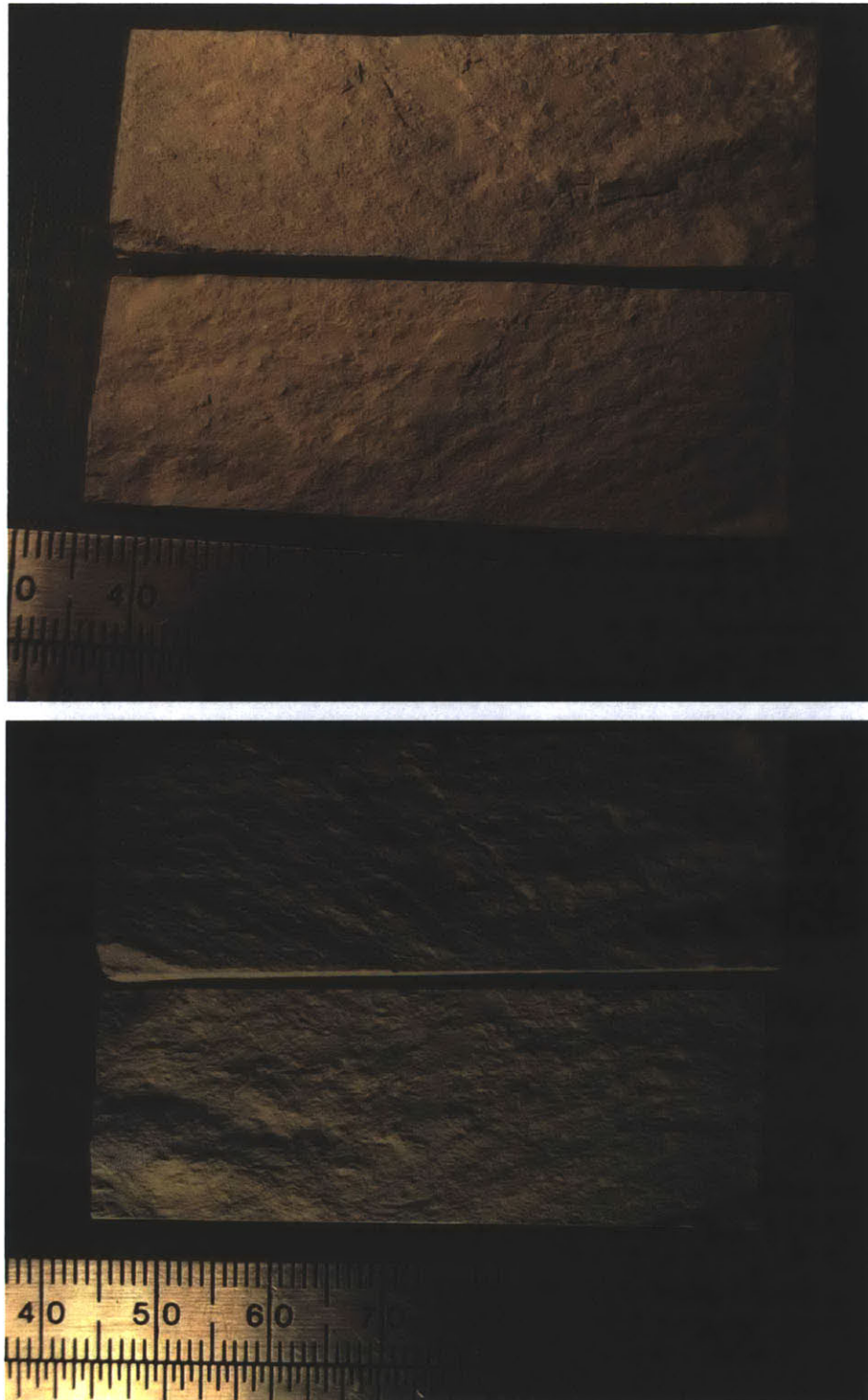
Figure 5.46: Fractured surface of the two split halves (semi discs) showing tensile fractures
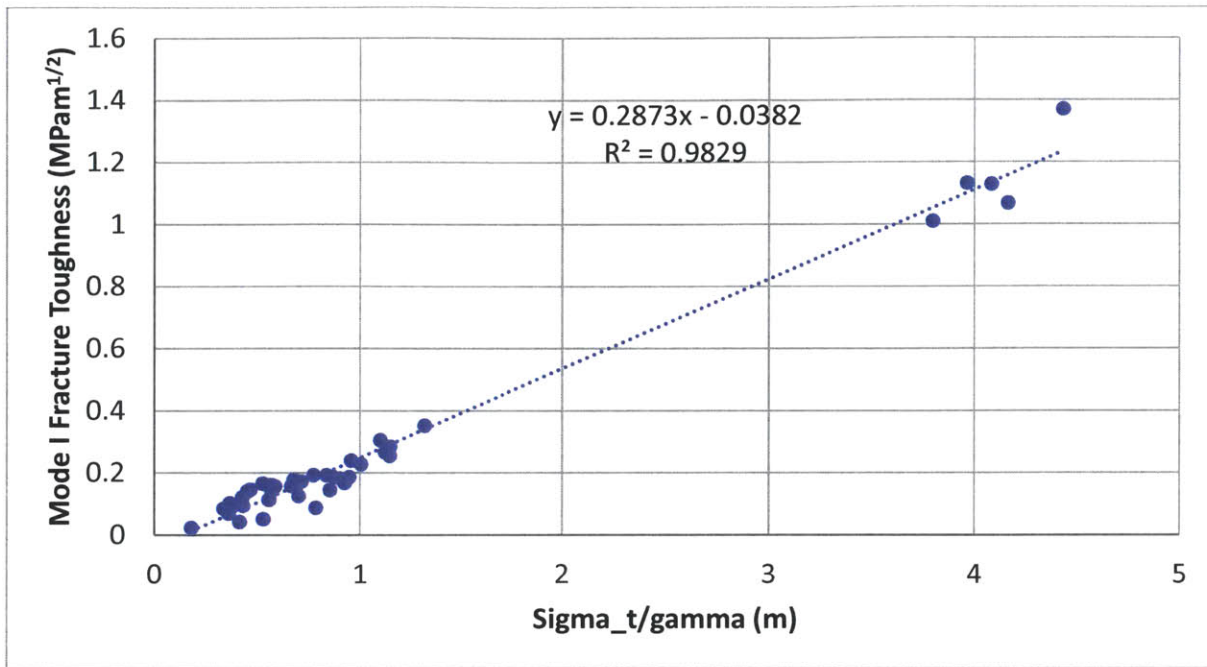
Figure 5.47: Linear relation between K_{IC} and (tensile strength/ unit weight) for the tested natural soils and clay-like materials.
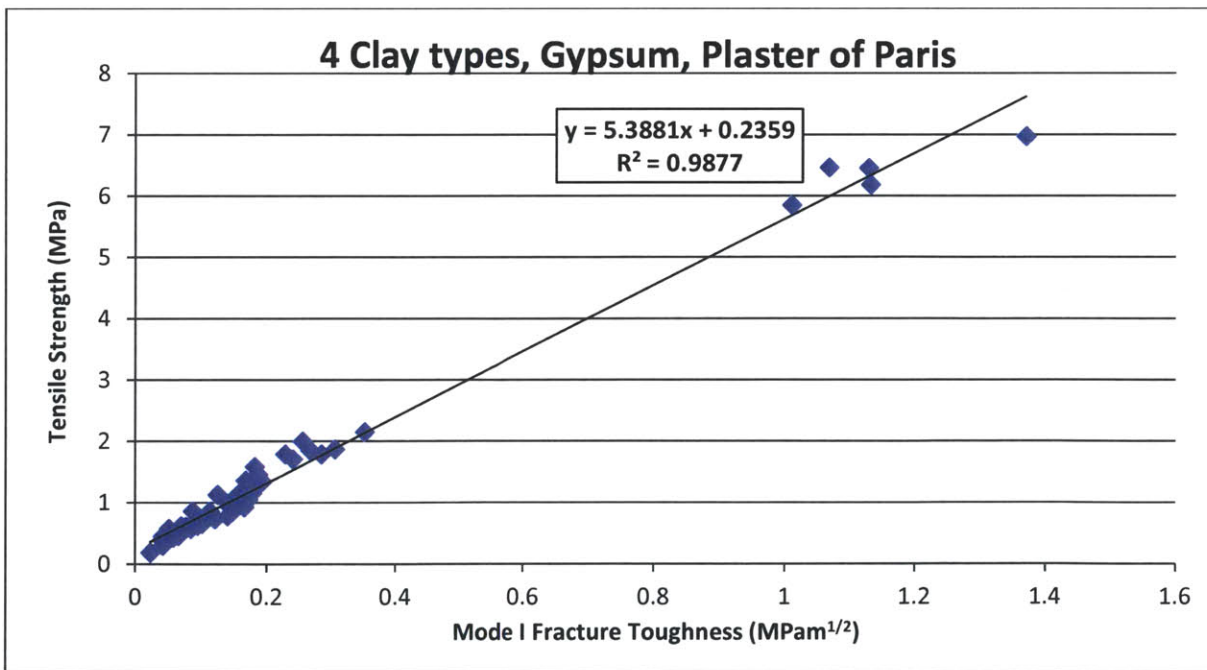
Figure 5.48: Determination of the tensile strength in terms of K_{IC} for the tested natural soils and clay-like materials.
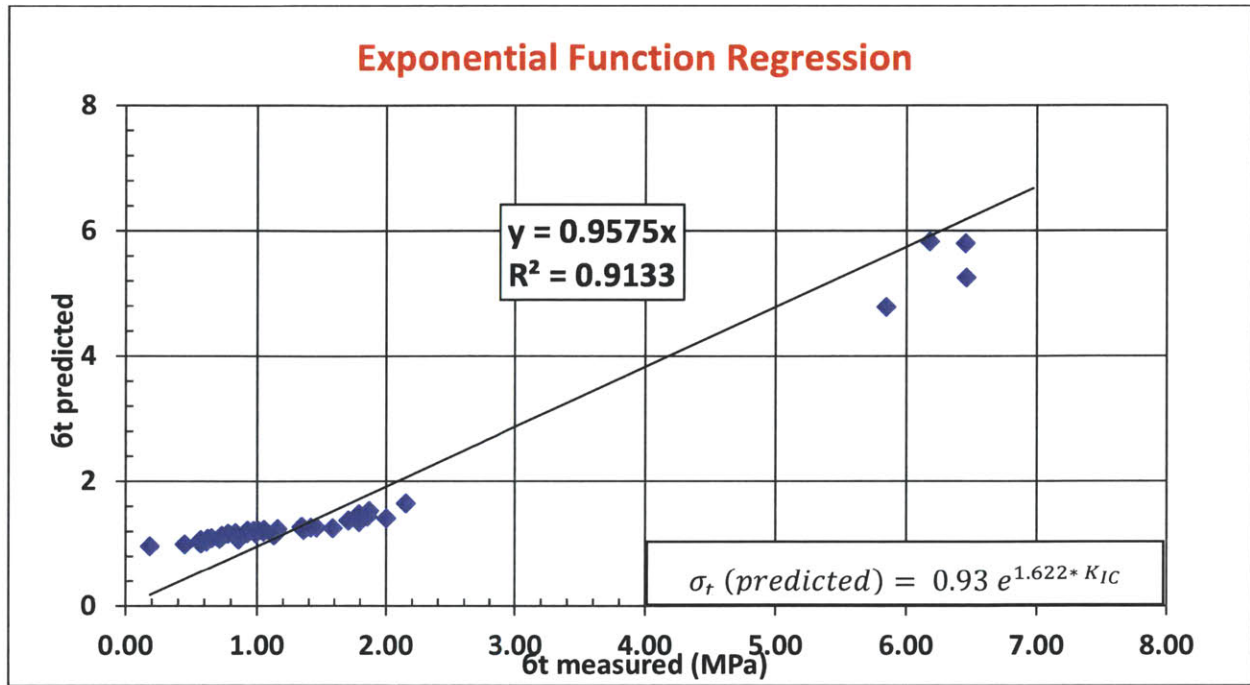
Figure 5.49: Using exponential function regression with least square error method for sigma t – K_{IC} relation for tested material.
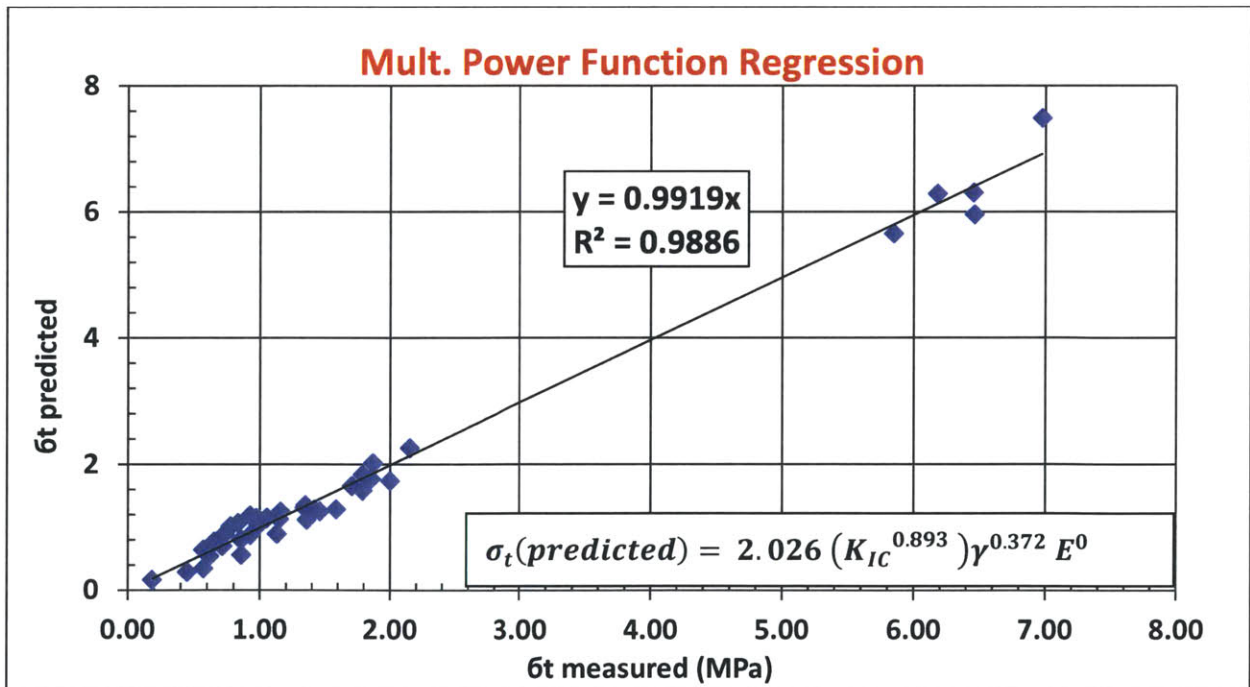
Figure 5.50: Using multiple power function regression with least square error method for sigma t – K_{IC} – unit weight – modulus of elasticity relation for tested material.

232
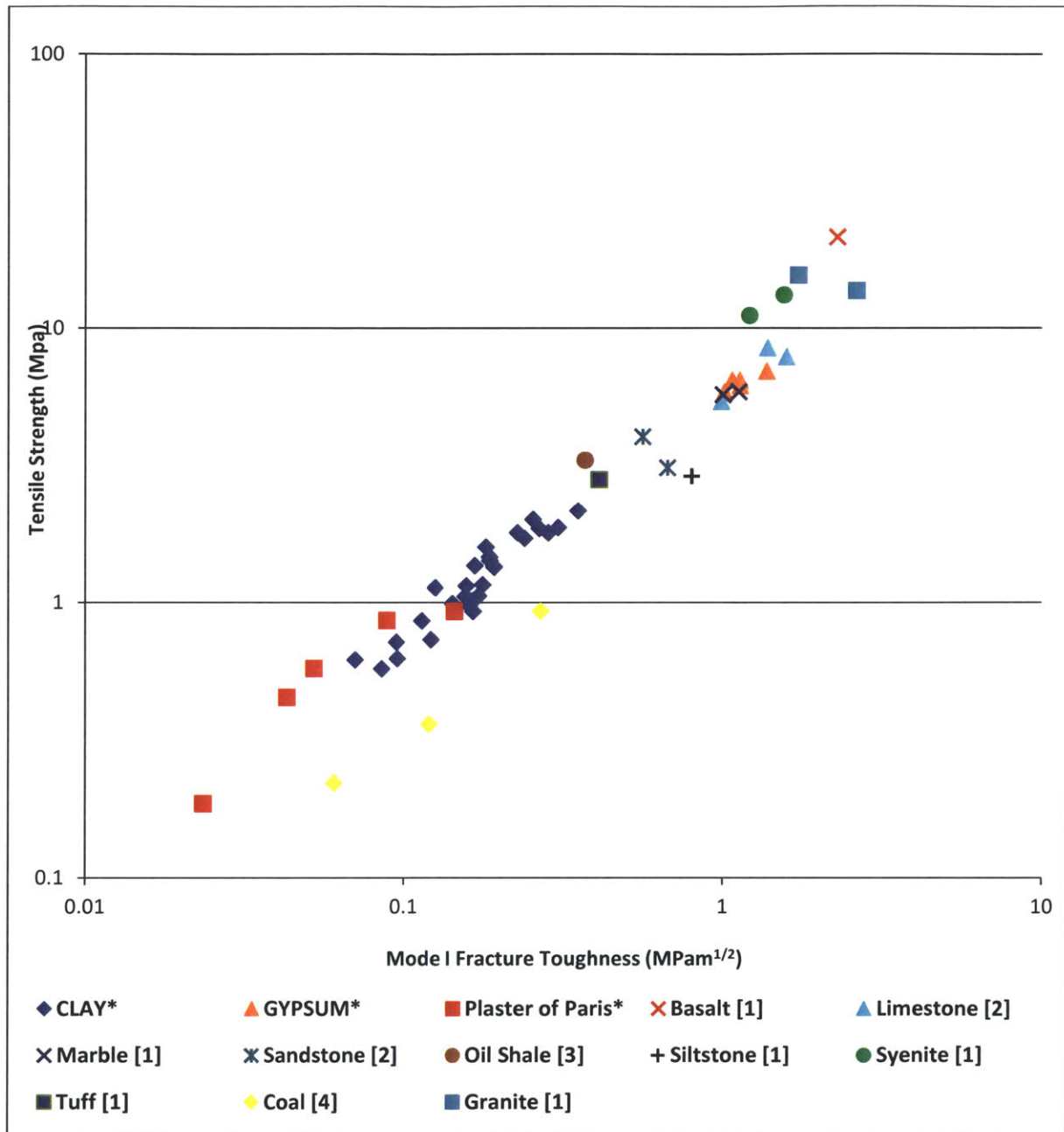
Figure 5.51: Summary of K_{IC} and σ_t values as reported in the literature in addition to experimental results for the six different tested materials

* : Current Experimental Study, [1] Haberfield and Johnston, 1989, [2] Gunsallus KL, Kulhawy FH, 1991, [3] Schmidt RA, 1977, [4] Bhagat, 1985,
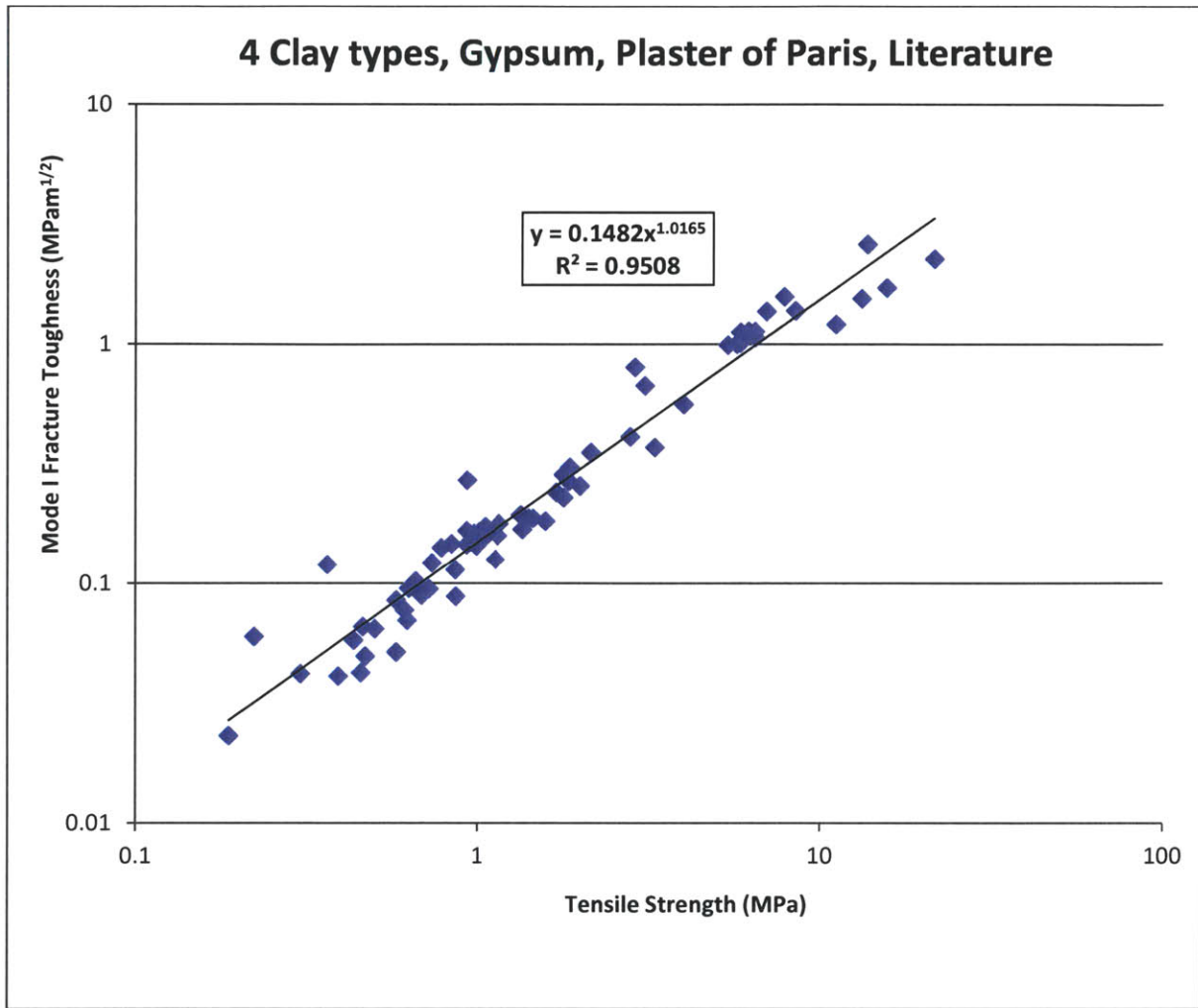
Figure 5.52: Relation between Mode I fracture toughness and tensile strength of tested material and literature data.
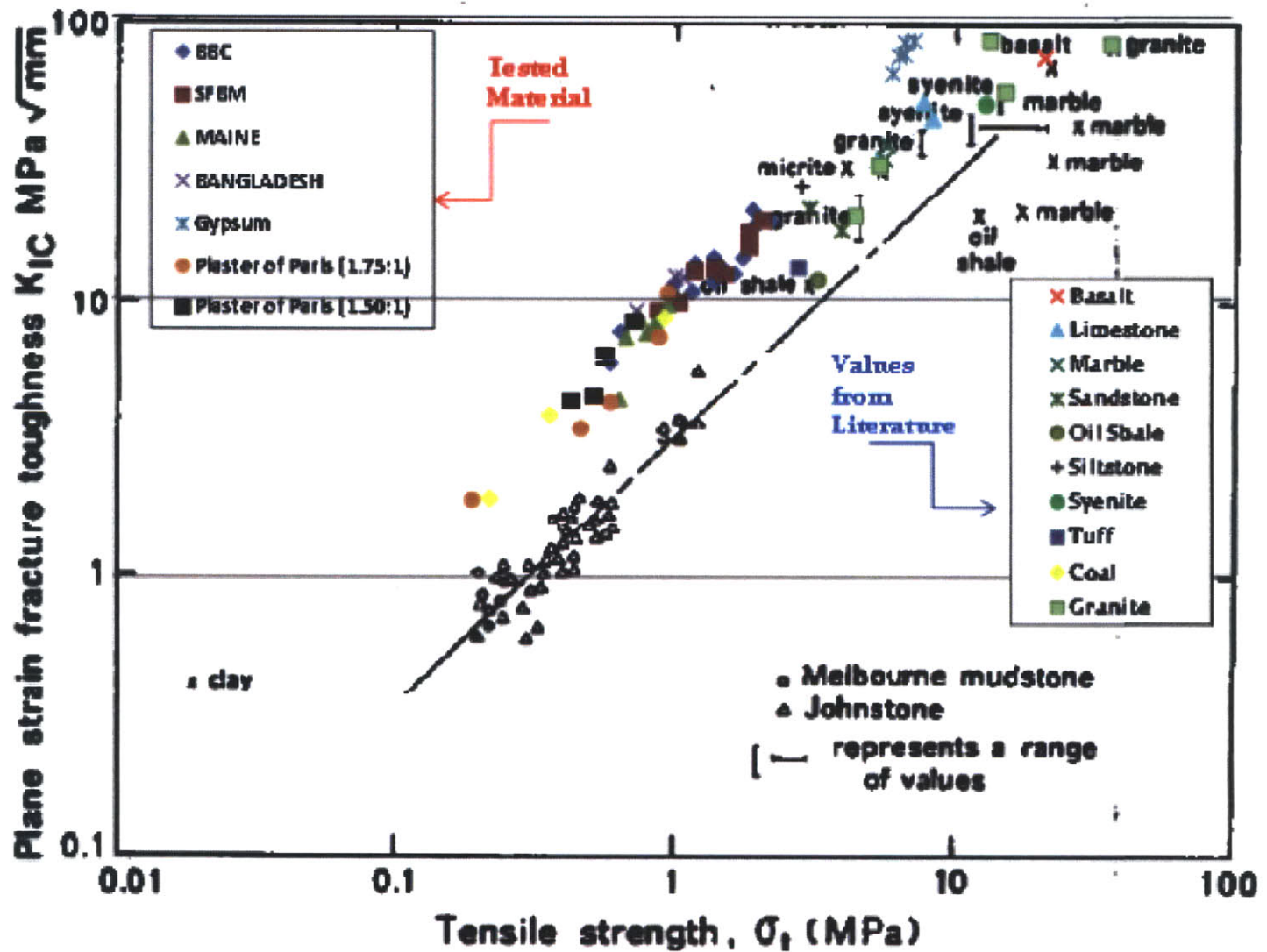
Figure 5.53: Summary of K_{IC} and σ_t values for tested materials and literature data (modified from Haberfield and Johnston, 1989)
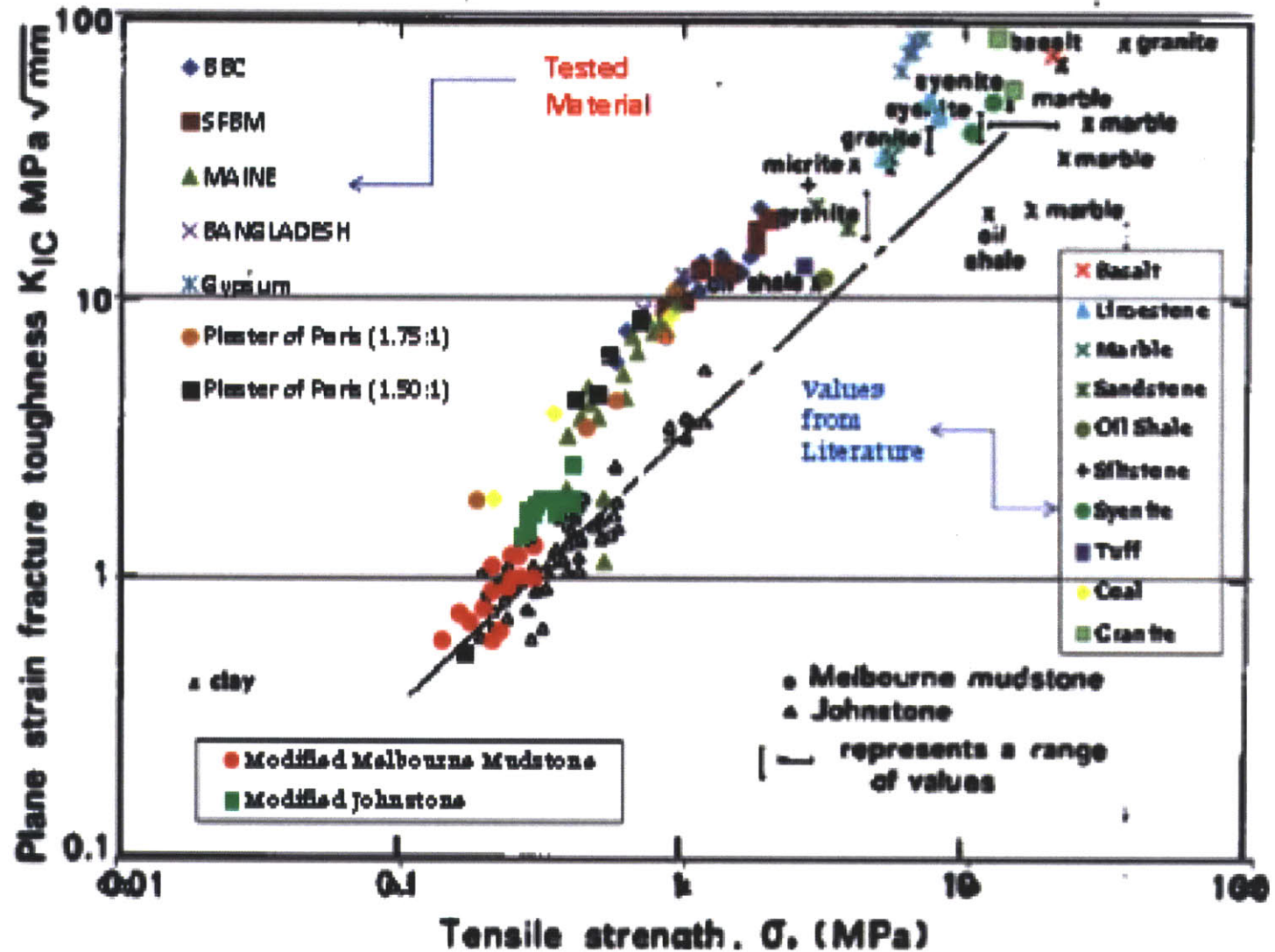
Figure 5.54: 1st Summary of K_{IC} and σ_t values for tested materials and literature data including modified Johnstone and Melbourne Mudstone (modified from Haberfield and Johnston, 1989)
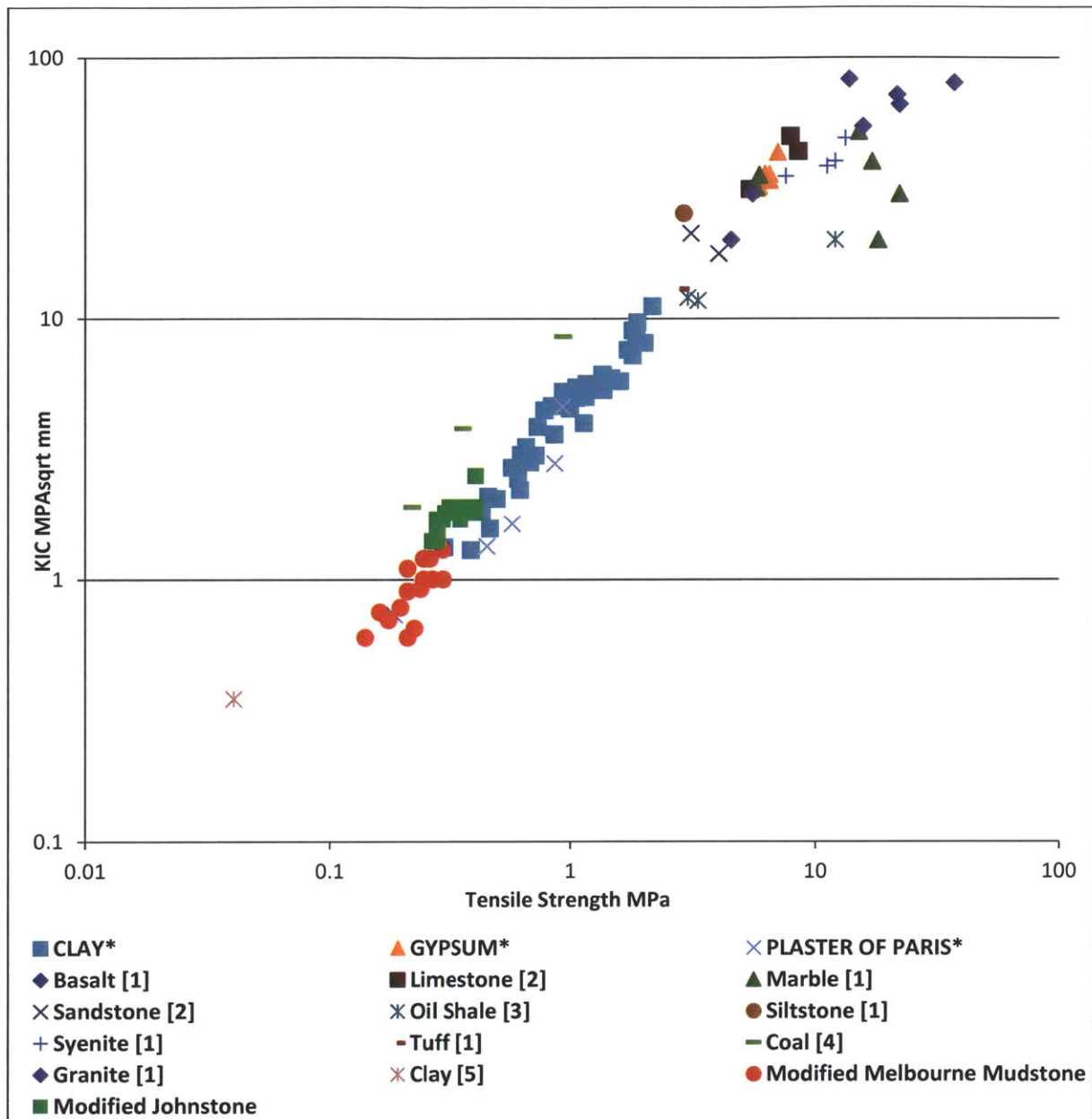
Figure 5.55: 2nd Summary of K_{IC} and σ_t values for the six different tested materials and data from the literature including modified Johnstone and Melbourne Mudstone

* : Current Experimental Study, [1] Haberfield and Johnston, 1989, [2] Gunsallus KL and Kulhawy FH, 1991, [3] Schmidt RA, 1977, [4] Bhagat, 1985, [5] Lee at al., 1982

4 Clay types, Gypsum, Plaster of Paris, Literature, Modified Melbourne Sandstone and Johnstone

$y = 0.1487x^{1.0179}$
$R^2 = 0.9651$

Mode I Fracture Toughness (MPam$^{1/2}$)

Tensile Strength (MPa)
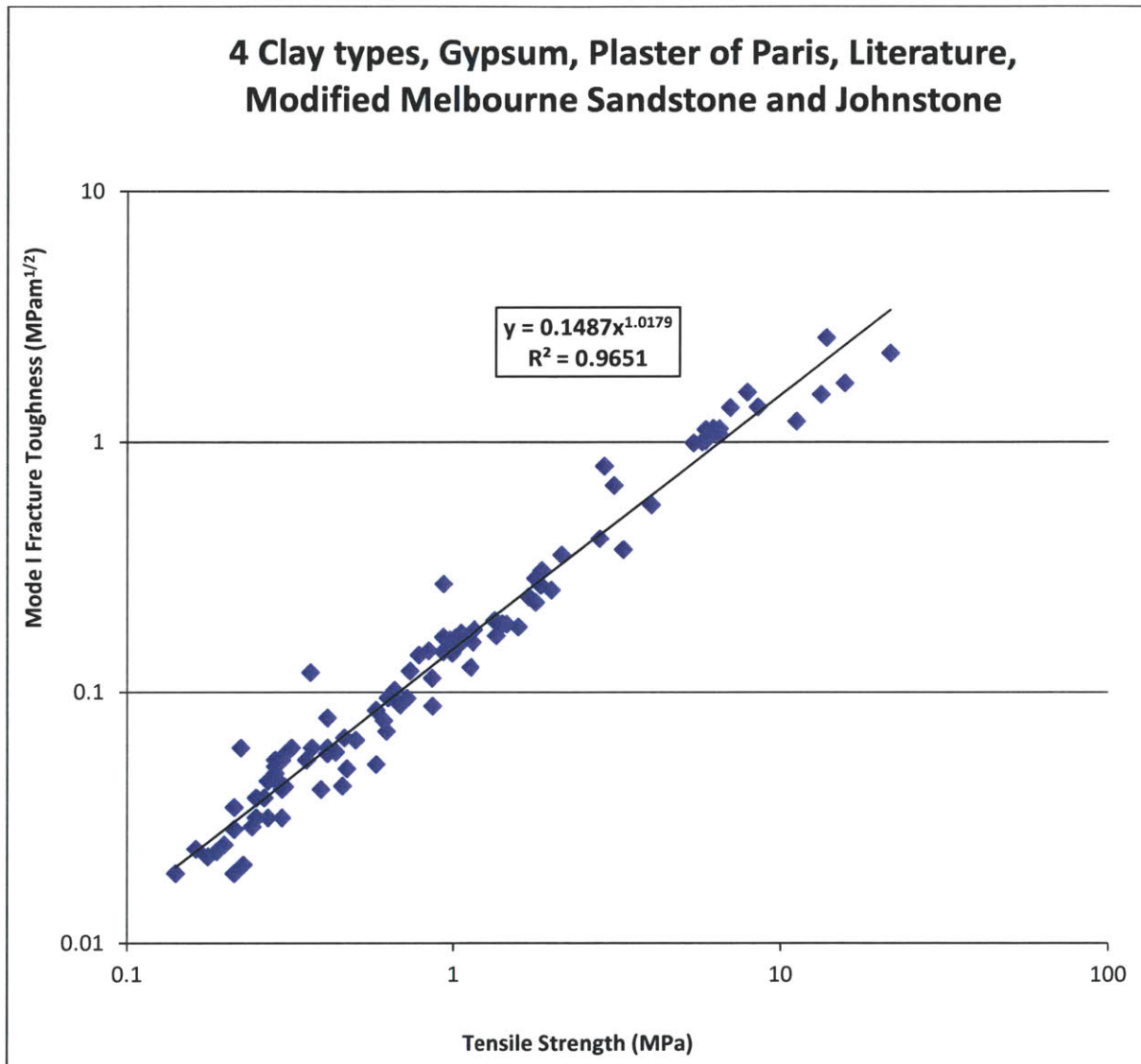
Figure 5.56: Relation between Mode I fracture toughness and tensile strength of tested material and literature data including modified Johnstone and Melbourne Mudstone

Chapter (6)

CONCLUSIONS AND RECOMMENDATIONS FOR

FURTHER RESEARCH

6.1 Introduction

Understanding the fracture properties of different mudrocks such as clays is essential to adequately model crack propagation in the oil bearing deposits to allow quantifying the needed fragmentation and resulting permeability from various bed preparation schemes that would enable cost-effective production. Optimization of bed preparation is only possible with adequate knowledge of how crack propagation takes place which, in turn, depends on how well the relevant material properties are determined.

Using simple convenient means to quantify the fracture properties of dry clays and clay-like materials is a crucial first step. This can be carried out using the flattened Brazilian disc (FBD) test which is characterized by the ease of specimen preparation, load application, and interpretation of the results. The FBD method is beneficial in quantifying three different parameters; mode I fracture toughness, tensile strength, and the elastic modulus, from a single load-displacement test record.

From the results of the 90 FBD tests conducted for this research, an empirical statistical relation between mode I fracture toughness and tensile strength is developed. This relation can be used to estimate mode I fracture toughness indirectly in case of knowing the corresponding tensile strength which can be determined using easier testing techniques if compared to fracture toughness. The developed relation is in line with trends reported in the literature for other materials tested using other approaches.

The main conclusions developed from this experimental study and recommendations for future research are presented in this chapter.

6.2 Conclusions

1. Flattened Brazilian Disc (FBD) testing is an advantageous method where three material

239

parameters; mode I fracture toughness, tensile strength, and elastic modulus; are obtained successively from only one test record.

2. Specimen preparation of the flattened Brazilian disc specimen is simpler, cheaper, and more convenient than other published fracture toughness measurement methods, where no artificial notch or crack is introduced to the flattened specimen; therefore, uncertainties due to the quality of the notch cut are avoided.

3. Testing method is convenient and easy to conduct using conventional load frame/ compressive test machine provided with diametrical load displacement measurements with no further special sophisticated machinery.

4. Load application on the flattened ends is more uniform and reliable than concentrated loading which minimizes local crushing or cracking developed by concentrated loading.

5. All fractured specimens showed center crack initiation regardless the testing material, the specimen dimensions, and the loading angle (2α).

6. Using an approximate analytical solution for the displacement of the loaded flattened end, the elastic modulus E can be determined from the slope of the section of load displacement record just preceding the maximum load.

7. Using the maximum load value in a test record with an analytical equation accounting for the shape correction of the flattened edges, the tensile strength of the specimen can be evaluated.

8. Using a simple calculation, it is convenient to determine the mode I fracture toughness using an easily identified local minimum load P_{min}; which is just subsequent to the maximum load in a test record, and the maximum value of the dimensionless stress intensity factor ϕ_{max}; obtained from an approximate equation based on numerical analyses.

9. From the test records, there appears to be strong correlation between mode I fracture toughness and tensile strength, and hence, a reasonable estimate of fracture toughness may be obtained if the tensile strength of the material is known.

10. Based on the testing data and reasonable analyses, no clear relation between mode I fracture toughness and elastic modulus was determined.

11. The relation between the unit weight and mode I fracture toughness was unclear and requires further investigation.

12. Based on the testing data and reasonable analyses, the relation between mode I fracture toughness and tensile strength for the six tested materials agrees to a great extent with

reported trends in the literature even for different fracture toughness and tensile strength testing techniques and for wider tested range of soils, rocks, geomaterials, clay-like, and rock-like materials. The overall empirical relationship considering all tested materials and trends reported in the literature can be expressed in power relation; $K_{IC} = 0.1487\,\sigma t^{1.0179}$.

6.3 Further Research Recommendations

1. For a better understanding of the flattened Brazilian disc test, the size effect of the specimen needs further investigation and clarification by varying the specimen radius, specimen thickness, their ratio, the width of the flattened edges, and the corresponding loading angle (2α).

2. Investigating the effect of temperature and specimens moisture on mode I fracture toughness by testing moist specimen at different water contents.

3. Investigating the effect of the loading rate on the development of the center cracks by varying the displacement rate in the used load frame.

4. Introducing different types of loading to the disc specimens apart from monotonic loading such as cyclic loading/ unloading conditions. In particular the specimen needs to be loaded to first crack, unloaded and reloaded to see if the crack opening load is the same as the minimum load.

5. Experimenting heat treated discs where heat treatment causes thermal cracking, hence, the mechanical properties change with temperature. In this context, soil/rock heated to different temperatures can be considered as different materials.

6. Resedimented specimens with different moisture contents should be tested in a similar manner. The advantage of using resedimented specimens is to create and test a material that can be used as a base case for fracture studies of mudrocks with common porosity, modulus and Poisson's ratio values.

7. Supplementary procedures should include taking measurements of lateral strain in compression tests that can provide indications of the onset of micro-cracking, using high speed camera for taking high speed photos of the fracturing, introducing internal flaws to resedimented specimens and testing them to investigate multi-mode fracture effects, and studying anisotropy by testing on multiple planes.

8. To obtain a more generic relation between mode I fracture toughness and tensile strength,

it is recommended to use one testing method for either fracture toughness or tensile strength or, alternatively, a quantitative conversion between the test data from different methods should be made.

9. Develop empirical relations between mode I fracture toughness and other physical mechanical parameters such as: uni-axial compressive strength, acoustic wave velocities, conductance, dynamic elastic modulus, and the clay content; to provide a feasible means of predicting fracture toughness from geo-physical logging data at a great depth.

10. Using the optical digital image correlation (DIC) technique to monitor the deformation field on the disk specimen surface during the entire compression process.

11. Introducing different types of soils, rocks, geomaterials, clay-like, and rock-like materials to cover the whole ductile-brittle behavior range.

12. Comparing the results obtained using flattened Brazilian discs with the ISRM suggested methods on same materials with same loading and placement conditions. Also, compare the results with other methods conducted on disc specimens.

13. Further numerical analyses should be performed to better quantify the maximum stress intensity factor for different loading angles (2α).

14. Investigating the effect of anisotropy in soils/rocks by studying similar specimens in different loading directions and from extracted from different orientations; parallel to bedding planes and normal to bedding planes.

15. Introducing concrete as a new testing material using FBD configuration with different specifications related to the aggregates used, aggregate percentage, additives used, and the water cement ratio.

REFERENCES

A. DINSDALE, "Pottery Science: Materials, processes and products", (Horwood, London, 1986).

Abou-Sayed, A.S. and Simonson, E.R., 1977. Fracture toughness, K1c, of triaxially-loaded Indiana Limestone. Proc. 18th US Symp. Rock Mechanics, 2A3-1 2A3-8.

Adams, Amy Lynn. *Laboratory Evaluation of the Constant Rate of Strain and Constant Head Techniques for Measurement of the Hydraulic Conductivity of Fine Grained Soils*. Thesis. Massachusetts Institute of Technology, Dept. of Civil and Environmental Engineering, 2011.

Akazawa T. International association of testing and research laboratories for materials and structures. RILEM Bull 1953; 13:13–23.

Alam, M.K., Hasan, A.K.M.S., Khan, M.R. & Whitney, J.W. 1990. *Geological Map of Bangladesh. Geological Survey of Bangladesh.*

ALKILIÇGİL, ÇİĞDEM. Development of a new method for mode 1 fracture toughness test on disc type rock specimens. Thesis. THE GRADUATE SCHOOL OF NATURAL AND APPLIED SCIENCES OF MIDDLE EAST TECHNICAL UNIVERSITY, 2006.

Al-Shayea N (2002) Comparing reservoir and outcrop specimens for mixed mode I-II fracture toughness of a limestone rock formation at various conditions. Rock Mech Rock Eng 25(4):271–297

Amarasiri, Aruna L., Susanga Costa, and Jayantha K. Kodikara. "Determination of Cohesive Properties for Mode I Fracture from Compacted Clay Beams." *Canadian Geotechnical Journal* 48.8 (2011): 1163-173.

Andreev GE (1991a) A review of the Brazilian tests for rock tensile strength determination. Part I: calculation formula. Min Sci Technol 13(3):445–456.

Andreev GE (1991b) A review of the Brazilian tests for rock tensile strength determination. Part II: contact conditions. Min Sci Technol 13(3):457–465.

ASTM (2008) D 3967-08: Standard test method for splitting tensile strength of intact rock core specimens. ASTM International, West Conshohocken, USA

ASTM C496. Standard test method for splitting tensile strength of cylindrical concrete specimens. In Annual Book of ASTM, Standards, vol. 0.042. Philadelphia: ASTM; 1984. p. 336–41.

ASTM Standard E 399, 1983. Standard test method for plane-strain fracture toughness of metallic materials. Annual Book of ASTM Standards. ASTM International, West Conshohocken, PA.

Atkinson. B.K. and Avdis, V., 1980. Fracture mechanics parameters of some rock-forming minerals determined using an indentation technique. Int. J. Rock Mech. Min. Sci. Geomech. Abstr., 17: 383 386.

Awaji H, Sato S (1978) Combined mode fracture toughness measurements by the disk test. J Eng Mater Tech Trans ASME 100:175–182

Awaji H. Diametrical compressive stress considering the Hertzian contact. J Soc Mater Sci Jpn 1987;27:336–41.

Aydin A, Basu A (2006) The use of Brazilian Test as a Quantitative Measure of Rock Weathering. Rock Mech Rock Eng 39(1): 77–85.

Backers, Tobias. *Fracture Toughness Determination and Micromechanics of Rock under Mode I and Mode II Loading*. Diss. Potsdam, 2004..

Barker LM (1977) Method for measuring plane strain fracture toughness. Eng Fract Mech 9:361–369

Bearman RA. The use of the point load test for the rapid estimation of mode 1 fracture toughness. Int J Rock Mech Min Sci 1999;36:257–63.

Berman, D.R., 1993. Characterization of the Engineering Properties of Boston Blue Clay at the MIT Campus, S.M. Thesis, Department of Civil and Environmental Engineering, MIT, Cambridge, MA, 429 p.

Bhagat, R.B., 1985. Mode I fracture toughness of coal. International Journal of Mining Engineering 3, 229–236.

Brook N. The measurement and estimation of basic rock strength. In: Hudson JA, Brown ET, Fairhurst C, Hoek E, editors. Comprehensive rock engineering principles, practice and projects, vol. 3 (Rock testing and site characterization). Oxford: Pergamon Press, 1993. p. 41–66.

Brown, G., and D. Reddish. "Experimental Relations between Rock Fracture Toughness and Density." *International Journal of Rock Mechanics and Mining Sciences* 34.1 (1997): 153-55.

C, Liu. "Elastic Constants Determination and Deformation Observation Using Brazilian Disk Geometry." *Experimental Mechanics* (2010): 1025-039.

Carneiro F, Barcellos A. International association of testing and research laboratories for materials and structures. RILEM Bull 1953;13:99–125.

Cauwellaert FV, Eckmann B. Indirect tensile test applied to anisotropic materials. Mater Struct 1994;27:54–60.

Chandler, H.W., 1984. The use of non-linear fracture mechanics to study the fracture properties of soils. Journal of Agricultural Engineering Research 29, 321–327.

Chang CI (17–19 Apr 1974) Brittle fracture and failure criteria of particulate composites. In: AIAA/ASME/SAE 15th structures, structural dynamics and materials conference. AIAA, Las Vegas

Chang, Soo-Ho, Chung-In Lee, and Seokwon Jeon. "Measurement of Rock Fracture Toughness under Modes I and II and Mixed-mode Conditions by Using Disc-type Specimens." *Engineering Geology* 66 (2002): 79-97.

Chau KT, Wong RHC. Uniaxial compressive strength and point load strength of rocks. Int J Rock Mech Min Sci 1996; 33:183–8.

Chen C-S, Pan E, Amadei B (1998) Determination of deformability and tensile strength of anisotropic rock using Brazilian tests. Int J Rock Mech Min Sci 35(1):43–61.

Chen M. and Zhang G. Q. (2004) Laboratory measurement and interpretation of the fracture toughness of formation rocks at great depth. *Journal of Petroleum Science and Engineering,* 41,221-231

Chong KP, Kuruppu MD (1984) New specimen for fracture toughness determination of rock and other materials. Int J Fract 26:R59–R62

Chou Y-C, Chen C-S (2008) Determining elastic constants of transversely isotropic rocks using Brazilian test and iterative procedure. Int J Numer Anal Meth Geomech 32(3):219–234.

Claesson J, Bohloli B (2002) Brazilian test: stress field and tensile strength of anisotropic rocks using an analytical solution. Int J Rock Mech Min Sci 39(8):991–1004.

Clausing DP (20–22 Apr 1959) Comparison of Griffith's Theory with Mohr's Failure Criteria. In: The 3rd US symposium on rock mechanics (USRMS). USRMS, Golden

Coviello A, Lagioia R, Nova R (2005) On the measurement of the tensile strength of soft rocks. Rock Mech Rock Eng 38(4): 251–273.

Cui ZD, Liu DA, An GM, Sun B, Zhou M, Cao FQ (2010) A comparison of two ISRM suggested chevron notched specimens for testing mode-I rock fracture toughness. Int J Rock Mech Min Sci 47:871–876

Donovan, James George. *Fracture Toughness Based Models for the Prediction of Power Consumption, Product Size, and Capacity of Jaw Crushers.* Diss. Virginia Polytechnic Institute and State University, 2003.

Erarslan N, Liang ZZ, Williams DJ (2011) Experimental and numerical studies on determination of indirect tensile strength of rocks. Rock Mech Rock Eng.

Erarslan N, Williams DJ (2012) Experimental, numerical and analytical studies on tensile strength of rocks. Int J Rock Mech Min Sci 49(1):21–30.

F. SINGER and S. S. SINGER, "Industrial Ceramics" (Chapman and Hall, London, 1962).

Fairbairn EMR, Ulm F-J. A tribute to Fernando L L Carneiro (1913–2001) engineer and scientist who invented the Brazilian test. Mater Struct 2002;35:195–6.

Fairhurst C (1964) On the validity of the 'Brazilian' test for brittle materials. Int J Rock Mech Min Sci 1:535-546.

Fowell RJ (1995) ISRM commission on testing methods: suggested method for determining mode 1 fracture toughness using cracked chevron notched Brazilian disc (CCNBD) specimens. Int J Rock Mech Min Sci Geomech Abstr 32(1):57–64

Fowell RJ, Xu C (1993) The cracked chevron notched Brazilian disk test-geometrical considerations for practical rock fracture toughness measurement. In: Preprint proceedings 34th US rock mechanics symposium, pp 657–660

Fowell RJ, Xu C (1994) The use of the cracked Brazilian disc geometry for rock fracture investigations. Int J Rock Mech Min Sci Geomech Abstr 31(6):571–579

Fowell RJ, Xu C, Dowd PA (2006) An update on the fracture toughness testing methods related to the cracked chevron- notched Brazilian disk (CCNBD) specimen. Pure Appl Ge- ophy 163:1047–1057

Fuenkajorn K, Klanphumeesri S (2011) Laboratory determination of direct tensile strength and deformability of intact rocks. Geotech Test J 34(1):1–6.

Germaine, J. T., & Germaine, A. V. (2009). *Geotechnical Laboratory Measurements for Engineers.* John Wiley & Sons.

Germaine, J. T. (2000, 2001, 2002, and 2005) Personal Communication.

Goodman RE (1989) Introduction to rock mechanics, 2nd edn. Wiley, New York

Griffith AA. Theory of rupture. Proceedings of the First International Congress on Applied Mechanics, Delft: 1924. p. 55–63.

Gunsallus, K.L., Kulhawy, F.H., 1984. A comparative evaluation of rock strength measures. International Journal of Rock Mechanics and Mining Science Geomechanical Abstraction 21, 233–248.

Guo, H., N. Aziz, and L. Schmidt. "Rock Fracture-toughness Determination by the Brazilian Test." *Engineering Geology* 33.3 (1993): 177-88.

Haberfield, C.M., Johnston, I.W., 1989. Relationship between fracture toughness and tensile strength for geomaterials. Proceedings of 12th International Conference of Soil Mechanics and Foundation Engineering, Rio De Janeiro, Brazil, vol. 1, pp. 47–52.

Hai-yong YU, JIN Zhi-xin, and JING Hai-he. "Mode I rock fracture toughness with different types of brazilian discs." Journal of coal science & engineering, China 10 (2004).Language: Chinese

Harison, J.A., Hardin, B.O., Mahboub, K., 1994. Fracture toughness of compacted cohesive soils using ring test. ASCE Journal of Geotechnical Engineering 120, 872–891.

Hobbs DW (1967) Rock tensile strength and its relationship to a number of alternative measures of rock strength. Int J Rock Mech Min Sci Geomech Abstr 4(1):115–127.

Hondros G (1959) The evaluation of Poisson's ratio and the modulus of materials of a low tensile resistance by the Brazilian (indirect tensile) test with particular reference to concrete. Aust J Appl Sci 10(3):243–268

Hossain, A.T.M.S., 2001. The Engineering behavior of the tropical clay soils of Dhaka, Bangladesh, unpublished Ph.D thesis, University of Durham, England, U.K.

Hossain, S.H.A.T.M., & Toll, D.G., 2006. *Geomechanical aspects of some tropical clay soils from*

Dhaka, Bangladesh. The Geological Society of London. IAEG2006 Paper number 143

House, Robert Donald. *A Comparison of the Behavior of Intact and Resedimented Boston Blue Clay (BBC).* Thesis. Massachusetts Institute of Technology, Dept. of Civil and Environmental Engineering, 2012.

Huang, J., Wang, S., 1985. An experimental investigation concerning the comprehensive fracture toughness of some brittle rocks. Int. J. Rock Mech. Mineral Sci. Geomech. Abstr. 22 (2), 99 –104.

Hudson JA, Brown ET, Rummel F. The controlled failure of rock discs and rings loaded in diametral compression. Int J Rock Mech Min Sci 1972;9:2241–8.

Iqbal MJ, Mohanty B (2006) Experimental calibration of stress intensity factors of the ISRM suggested cracked chevron- notched Brazilian disc specimen used for determination of mode-I fracture toughness. Int J Rock Mech Min Sci 43:1270–1276

Iqbal MJ, Mohanty B (2007) Experimental calibration of ISRM suggested fracture toughness measurement techniques in selected brittle rocks. Rock Mech Rock Eng 40(5):453–475

ISRM. Suggested methods for determining tensile strength of rock materials. Int J Rock Mech Min Sci Geomech Abstr 1978;15:99–103.

ISRM. Suggested methods for determining the fracture toughness of rock. Int J Rock Mech Min Sci Geomech Abstr 1988;25:71-96 [co-ordinator: F Ouchterlony].

ISRM. Suggested methods for determining the fracture toughness using cracked chevron notched Brazilian disc (CCNBD) specimen. Int J Rock Mech Min Sci 1995;32:57–64 [co-ordinator: Fowell RJ].

Jaeger JC (1967) Failure of rocks under tensile conditions. Int J Rock Mech Min Sci Geomech Abstr 4(2):219–227.

Jaeger JC, Cook NGW. Fundamentals of rock mechanics, 3rd ed. London: Chapman & Hall, 1979. p. 95–194.

Jianhong, Ye, F.Q. Wu, and J.Z. Sun. "Estimation of the Tensile Elastic Modulus Using Brazilian Disc by Applying Diametrically Opposed Concentrated Loads." *International Journal of Rock Mechanics and Mining Sciences*46.3 (2009): 568-76..

Kaklis KN, Agioutantis Z, Sarris E, Pateli A (29 June-1 July 2005) A theoretical and numerical study of discs with flat edges under diametral compression (flat Brazilian test). In: 5th GRACM international congress on computational mechanics, GRACM, Limassol

Keles, Cigdem, and Levent Tutluoglu. "Investigation of Proper Specimen Geometry for Mode I Fracture Toughness Testing with Flattened Brazilian Disc Method." *International Journal of Fracture* 169.1 (2011): 61-75.

Khan, K., Al-Shayea, N.A., 2000. Effect of specimen geometry and testing method on mixed mode I-II

fracture toughness of a limestone rock from Saudi Arabia. Rock Mechanics and Rock Engineering 33, 179–206.

Krishnan, J.C., Zhao, X.L., Zaman, M., Roegiers, J.C., 1998. Fracture toughness of a soft sandstone. International Journal of Rock Mechanics and Mining Sciences 35, 695–710.

Kuruppu MD (1997) Fracture toughness measurement using chevron notched semi-circular bend specimen. Int J Fract 86(4):L33–L38

Lajtai, E.Z. 1970. A theoretical and experimental evaluation of the Griffith theory of brittle

Lawn, B.R. and Wilshaw, R., 1975a. Review- Indentation fracture: principles and   applications. J. Mater. Sci., 10: 1049 1081.

Lawn, B.R. and Wilshaw, T.R.. 1975b. Fracture of Brittle Solids. Cambridge University Press, Cambridge.

Lawson, A.C., 1914. San Francisco Folio, U. S. Geol. Survey, Geol. Atlas, no. 193, 24 pages.

Li, Diyuan, and Louis Ngai Yuen Wong. "The Brazilian Disc Test for Rock Mechanics Applications: Review and New Insights." *Rock Mechanics and Rock Engineering* 46 (2013): 269-87.

Louderback, G.D., 1939. San Francisco Bay sediments, 6th Pacific Sci. Cong., Pr., p. 783-793.

Louderback, G.D., 1951. Geological history of San Francisco Bay, Geologic Guide Book to San Francisco Bay Counties, Calif. Div. Mines, Bull. 154.

Marjanovic, Jana. *The Study of Shear and Longitudinal Velocity Measurements of Sands and Cohesive Soils*. Thesis. Massachusetts Institute of Technology, Dept. of Civil and Environmental Engineering, 2012.

Markides CF, Pazis DN, Kourkoulis SK (2010) Closed full-field solutions for stresses and displacements in the Brazilian disk under distributed radial load. Int J Rock Mech Min Sci 47(2): 227–237.

Mellor, M. and Hawkes, 1., 1971 Measurement of tensile strength by diametral compression of disc and annuli. Eng. Geol., 5: 173 225.

Monsur, M.H., 1995. *An Introduction to The Quaternary Geology of Bangladesh*. City press and publications, Dhaka.

Morgan, Stephen Philip. *The Effect of Complex Inclusion Geometries on Fracture and Crack Coalescence Behavior in Brittle Material*. Thesis. Massachusetts Institute of Technology, Dept. of Civil and Environmental Engineering, 2011.

Nasseri MHB, Mohanty B (2008) Fracture toughness anisotropy in granitic rocks. Int J Rock Mech Min Sci 45:167–193

Nesetova and Lajtai. (1973) Fracture from compressive stress concentrations around elastic flaws, *Int J Rock Mech. Min. Sci. & Geomech. Abstr., 10*, pp. 265-284.

Neumann, Rebecca B. *The Hydrogeochemistry of Pond and Rice Field Recharge: Implications for the Arsenic Contaminated Aquifers in Bangladesh.* Diss. Massachusetts Institute of Technology, Dept. of Civil and Environmental Engineering, 2010.

Newman DA, Bennett DG (1990) The effect of specimen size and stress rate for the Brazilian test—a statistical analysis. Rock Mech Rock Eng 23(2):123–134.

Newman, J.C., 1979. Stress intensity factors and crack opening displacements for round compact specimens. NASA TM80174, Langley Research Centre, Oct.

Nguyen, H.Q., 2007. Reanalysis of the Settlement of a Levee on Soft Bay Mud. M.Sc. Thesis. MIT, 366

Nichols, J.R., Grismer, M.E., 1997. Measurement of fracture mechanics parameters in silty-clay soils. Soil Science 162, 309–322.

Nordlund E, Li C, Carlsson B. Mechanical properties of the diorite in the prototype repository at A. spo. HRL laboratory tests. International Progress Report, IPR-99-25, SKB, June 1999.

Ouchterlony F (1982) A review of fracture toughness testing of rocks. Solid Mech Arch 7:131–211

Ouchterlony, F., 1980. A new core specimen for the fracture toughness testing of rock, DS 1980:17. Swedish De tonic Res. Found. (SveDeFo), Stockholm, Sweden, 18 pp.

Satoh Y. Position and load of failure in Brazilian test, a numerical analysis by Griffith criterion. J Soc Mater Sci Jpn 1987;36:1219-24.

Schmidt RA. Fracture mechanics of oil shale unconfined fracture toughness, stress corrosion cracks, and tension test results. Proceedings of the 18thUS Symposium on Rock Mechanics, Keystone, CD, 1977. p. 2A2-1–6.

Sih, G.C., 1973. Handbook of Stress Intensity Factors for Researchers and Engineers. Institute for Fracture and Solid Mechanics, Lehigh University, Bethlehem.

Szendi-Horvath G (1980) Fracture toughness determination of brittle materials using small to extremely small specimens. Eng Fract Mech 13:955–961

Szendi-Hovrath, G.. 1982. On the fracture toughness of coal. Aust. J. Coal Min. Technol. Res., 2: 51-57.

Tada H, Paris PS, Irwin GR. The stress analysis of cracks handbook (2nd ed.). St. Louis, MO: Paris Production Inc.; 1985.

Tang T. Effect of load-distributed width on split tension of unnotched and notched cylindrical specimens. J Test Eval 1994; 22:401–9.

Thiercelin M, Roegiers JC (1986) Fracture toughness determination with the modified ring test. In: International symposium on engineering in complex rock formations, Beijing, China, pp 1–8

Timoshenko S, Goodier JN. Theory of elasticity. New York: McGraw-Hill; 1970.

Trask, P.D., and Rolston, J.W., 1965. Engineering geology of San Francisco Bay, California. Bulletin of

the Geological Society of America, Vol. 62, Sept., pp. 1079-1110.

Vargas, Albalyra. *The Mechanical Behavior of Heavily Overconsolidated Resedimented Boston Blue Clay.* Thesis. Massachusetts Institute of Technology, Dept. of Civil and Environmental Engineering, 2013.

Vekinis, G, M.F. Ashby, and P.W.R Beaumont. "Plaster of Paris as a Model Material for Brittle Porous Solids." *JOURNAL OF MATERIALS SCIENCE* 28 (1993): 3221-227.

Wang QZ. Stress intensity factors of ISRM suggested CCNBD specimen used for mode-I fracture toughness determination. Int J Rock Mech Min Sci 1998;35:977–82.

Wang QZ (2010) Formula for calculating the critical stress intensity factor in rock fracture toughness tests using cracked chevron notched Brazilian disc (CCNBD) specimens. Int J Rock Mech Min Sci Tech Note 47:1006–1011

Wang QZ, Zhang S, Xie HP (2010) Rock dynamic fracture toughness tested with holed-cracked flattened Brazilian discs diametrically impacted by SHPB and its size effect. Exp Mech 50:877–885

Wang QZ, Jia XM, Kou SQ, Zhang ZX, Lindqvist PA (2004a) The flattened Brazilian disc specimen used for testing elastic modulus, tensile strength and fracture toughness of brittle rocks: analytical and numerical results. Int J Rock Mech Min Sci 41:245–253

Wang QZ, Jia XM, Wu LZ (2004b) Wide-range stress intensity factors for the ISRM suggested method using CCNBD specimens for rock fracture toughness tests. Int J Rock Mech Min Sci Tech Note 41:709–716

Wang QZ, Wu LZ (2004) The flattened Brazilian disc specimen used for determining elastic modulus, tensile strength and fracture toughness of brittle rocks: experimental results. Int J Rock Mech Min Sci 41(3):1–5

Wang QZ, Xing L (1999) Determination of fracture toughness K_{IC} by using the flattened Brazilian disk specimen for rocks. Eng Fract Mech 64:193–201

Wang, J., J. Zhu, C. Chiu, and H. Zhang. "Experimental Study on Fracture Toughness and Tensile Strength of Clay." *Engineering Geology* 94.1-2 (2007): 65-75.

Wang, J.J., Zhu, J.G., Chiu, C.F., Chai, H.J., 2007. Experimental study on fracture behavior of silty clay. Geotechnical Testing Journal 30, 303–311.

Warren. R.,1978. Measurement of the fracture properties of brittle solids by Hertzian Indentation. Acta Metall., 26: 1759-1769.

Whittaker, B.N., Singh, R.N., Sun, G., 1992. Rock Fracture Mechanics: Principles, Design and Applications. Elsevier, Amsterdam.

Wijk G (1978) Some new theoretical aspects of indirect measurements of the tensile strength of rocks. Int J Rock Mech Min Sci Geomech Abstr 15(4):149–160.

Xu C, Fowell RJ (1994) Stress intensity factor evaluation for cracked chevron notched Brazilian disc specimens. Int J Rock Mech Min Sci 31(2):157–162

Ye J, Wu FQ, Sun JZ (2009) Estimation of the tensile elastic modulus using Brazilian disc by applying diametrically opposed concentrated loads. Int J Rock Mech Min Sci 46(3):568–576.

Yu Y, Zhang J, Zhang J (2009) A modified Brazilian disk tension tests. Int J Rock Mech Min Sci 46(2):421–425.

Yu Y. Measuring properties of rock from the site of permanent shiplock in three Gorges project. Test Report, Yangtze River Scientific Research Institute, June 2001.

Zhang ZX, Kou SQ, Jiang LG, Lindqvist PA. Effects of loading rates on rock fracture: fracture characteristics and energy partitioning. Int J Rock Mech Min Sci 2000;37(5):745–62.

Zhang S, Wang QZ (2006) Method for determination of dynamic fracture toughness of rock using holed-cracked flattened disk specimen. Chin J Geotech Eng 28(6):723–728

Zhang, Z.X. "An Empirical Relation between Mode I Fracture Toughness and the Tensile Strength of Rock." International Journal of Rock Mechanics & Mining Sciences 39 (2002): 401-06.

Zhang, Z.X., Kou, S.Q., Lindqvist, P.A., Yu, Y., 1998. The relationship between the fracture toughness and tensile strength of rock. Strength Theories: Application, Development and Prospects for 21st Century. Science Press, Beijing, pp. 215–219.

Zhao XL, Fowell RJ, Roegiers J-C, and Xu C. Discussion: Rock fracture toughness determination by the Brazilian test, by H. Guo, N.I. Aziz and L. Schmidt. Eng Geol 1993;38:181-4.

Zhenfeng, Zhao, and Chen Mian. "Relationship between Rock Fracture Toughness and Physical Properties." Petroleum Science 3.1 (2006): 56-60.